ELECTROCHEMICAL STUDIES ON SOME CARBONYL COMPOUNDS AND SUPEROXIDE IN APROTIC ORGANIC SOLVENTS

SHERMAN J. L. LAUW

2016

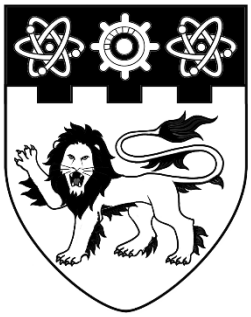

NANYANG TECHNOLOGICAL UNIVERSITY

ELECTROCHEMICAL STUDIES ON SOME CARBONYL COMPOUNDS AND SUPEROXIDE IN APROTIC ORGANIC SOLVENTS

SHERMAN JUN LIANG LAUW

SCHOOL OF PHYSICAL AND MATHEMATICAL SCIENCES

NANYANG TECHNOLOGICAL UNIVERSITY

2016

This page has been intentionally left blank

ELECTROCHEMICAL STUDIES ON SOME CARBONYL COMPOUNDS AND SUPEROXIDE IN APROTIC ORGANIC SOLVENTS

SHERMAN JUN LIANG LAUW

School of Physical and Mathematical Sciences

A thesis submitted to the Nanyang Technological University

in partial fulfilment of the requirement for the degree of

Doctor of Philosophy

2016

This page has been intentionally left blank

Acknowledgments

First and foremost, I wish to express my deepest gratitude toward Nanyang Technological University for the award of a prestigious Nanyang President's Graduate Scholarship (NPGS), the opportunity to read my postgraduate degree in this amazing institution, as well as their generous financial support for overseas conference participation.

I would also like to sincerely thank my supervisor, Prof. Richard D. Webster, for his continuous support and guidance during my Ph.D. studies. The road wasn't always smooth sailing, but his thoughtful advice and encouragement never failed to get me through this remarkable journey of constant learning and growth.

Many thanks are also owed to Prof. Philip W.H. Chan, Dr. Prasath Kothandaraman, Dr. Srinivasa R. Mothe, and Dr. Teo W.T. for their nurturing tutelage during my undergraduate studies which undoubtedly cultivated my interest and love for research.

My earnest appreciation also extends to my fellow group-mates and friends (listed in alphabetical order: Bahareh, Dejan, Diane, Gabriel, Gwen, Jazreen, Kwok Kiong, Maja, Malcolm, Novi, Raymond, Serena, Sher Li, Shu Jun, Yanni, Ya Yun, Ying Shang, and Xiuhui) for the many thought-provoking discussions, for transforming the laboratory into such a special environment, and for all the unforgettable memories we forged together. The past 4 years would certainly have not been the same without them. I would also like to take this opportunity to emphasize my gratefulness toward Joyce and Chiang Zhong, for the immeasurable amounts of hard work they put in and for the trust and confidence they placed in me.

To the many past and present CBC administration and laboratory staff (listed in alphabetical order: Ai Hua, Celine, Charlene, Ee Ling, Janice Low, Lynette, Dr. Rakesh, Selina, Si Ling, Wei Ting, Wen Wei, Yean Chin, and Yan Lin) with whom I have had the utmost

pleasure of corresponding and working with, I wish to also express my many thanks for their help in one way or another.

Last but definitely not the least, I would like to acknowledge the unwavering love and support of my family, without which this work would not have been possible.

Table of Contents

This page has been intentionally left blank

Abstract

Carbonyl compounds are an undeniably essential class of molecules. This is exemplified by their prevalence in the myriad of biologically active natural products, pharmaceutical compounds, and/or chemical reagents that we come in contact with on a daily basis. As part of their biological functions, transformations, or decomposition, many of these compounds undergo complex (and often not fully understood) electron transfer and coupled chemical reactions. For these reasons, research pertaining to this area remains relevant and is also of continued importance. Therefore, the major theme of this thesis was directed toward the examination of the redox reactions, that occur at an electrode surface, of some organic carbonyl compounds. Studies were performed by utilizing a combination of electrochemical (e.g. cyclic, linear sweep, and rotating disk voltammetry, as well as controlled potential electrolysis), spectroscopic (ATR-FTIR), and digital simulation techniques. Where possible, the exact sequence of heterogeneous electron transfer and homogeneous chemical steps that occurred were determined, and the identities of intermediate species and/or end products elucidated. In particular, this thesis focused on investigating the electrochemical behaviors of biotin (Chapter 2), cinnamaldehyde (Chapter 3), and di-(2-ethylhexyl) phthalate (Chapter 4) in aprotic organic solutions such as acetonitrile (CH_3CN), dimethyl sulfoxide (DMSO), and *N*,*N*-dimethylformamide (DMF), and under various experimental conditions including varied scan rates, temperatures, and substrate concentrations. Overall, it was found that the 3 carbonyl compounds were all electrochemically reducible at fairly large negative potentials and were generally involved in a series of follow-up chemical reactions (e.g. dimerization or decomposition) following an electron transfer step.

A second focus of this thesis was the voltammetric study of superoxide ($O_2^{\bullet-}$) and its interactions with a variety of consumable food and vitamin molecules (Chapter 5), and

structurally varied aliphatic alcohols (Chapter 6), with the aim of examining the possible scavenging reactions that take place. $O_2^{\bullet-}$ is a free radical anion of the reactive oxygen species (ROS) family which has been demonstrated to be able to lead to the undesirable modification or damage of many important biological molecules if left unchecked. Therefore, analyses of antioxidants and their reactions are highly pertinent since they constitute one of the body's main defenses against ROS; such as by scavenging free radicals like $O_2^{\bullet-}$ and thereby prevent the potential harm caused. In particular, electrochemical methods are suitable for these studies because $O_2^{\bullet-}$ can precisely be generated under mild conditions, with no by-products, while its coupled homogeneous reactions can be monitored in situ. In this thesis, examinations of the scavenging reactions of different compounds toward $O_2^{\bullet-}$ were carried out by carefully increasing the concentration of each substrate in a stepwise manner and concomitantly monitoring of the chemical reversibility of the one-electron voltammetric reduction of dioxygen (O_2) to $O_2^{\bullet-}$. This enabled the extent of radical inhibition and relative reactivities to be easily determined via measurements of the resultant oxidative peak current magnitudes (I_{pa}) on the reverse scan of CV, as well as the elucidation of the general mechanisms that were involved during the removal of electrochemically generated $O_2^{\bullet-}$. Overall, it was also found that the relative reactivities of the different compounds toward $O_2^{\bullet-}$ were strongly influenced by structural features such as the presence of acidic/labile hydrogens, conjugation in the molecule, and number of hydroxyl groups available.

Abbreviations & Symbols

ATR-FTIR	Attenuated total reflectance-Fourier transform infrared
Bu_4NPF_6	Tetrabutylammonium hexafluorophosphate
Bu_4NOH	Tetrabutylammonium hydroxide
C step	Chemical step
CA	Cinnamaldehyde
CH_3CN	Acetonitrile
CPE	Controlled potential electrolysis
CV	Cyclic voltammetry
D	Diffusion coefficient
DEHP	Di-(2-ethylhexyl) Phthalate
DMF	*N*,*N*-dimethylformamide
DMSO	Dimethyl sulfoxide
E^o	Formal potential
E_{pa}	Anodic/oxidative peak potential
E_{pc}	Cathodic/reductive peak potential
E step	Electrochemical step
Fc/Fc^+	Ferrocene/Ferrocenium redox couple
GC	Glassy carbon
h	Hour (time)
HPF_6	Hexafluorophosphoric acid
EC	Effective concentration
I_{pa}	Anodic/oxidative peak current
I_{pc}	Cathodic/reductive peak current

K	Kelvin (temperature)
k_b	Backward rate constant
K_{eq}	Equilibrium constant
k_f	Forward rate constant
k_s	Heterogeneous electron transfer rate constant
LSV	Linear Sweep Voltammetry
M	Molar (concentration)
min	Minutes (time)
mM	Millimolar (concentration)
mV	Millivolts
n	Number of moles of electrons
NMR	Nuclear magnetic resonance
$O_2^{\bullet-}$	Superoxide
RDE	Rotating disk electrode
ROS	Reactive oxygen species
s	Seconds (time)
V	Volts
α	Transfer coefficient
v	Scan rate
$\%\Delta I_{pa}$	Percentage decrease in anodic peak current
[alcohol]	Concentration of alcohol added
ΔE_p	Anodic/oxidative to cathodic/reductive peak-to-peak separation

List of Publications

1. “The Electrochemical Reduction of Biotin (Vitamin B7) and Conversion into its Ester”
Lauw, S. J. L.; Ganguly, R.; Webster, R. D. *Electrochim. Acta* **2013**, *114*, 514–520.

2. “Voltammetric Profiling of redox-active metabolites expressed by Pseudomonas aeruginosa for diagnostic purposes”
Seviour, T.; Doyle, L. E.; Lauw, S. J. L.; Hinks, J.; Rice, S. A.; Nesatyy, V. J.; Webster, R. D.; Kjelleberg, S.; Marsili, E. *ChemCommun.* **2015**, *51*, 3789–3792.

3. “Electrochemical Proton Reduction Catalysed by Selenolato-Manganese Carbonyl Complexes”
Hou, K.; Lauw, S. J. L.; Webster, R. D.; Fan, W. P. *RSC Adv.* **2015**, *5*, 39303–39309.

4. “Primary Colored Electrochromism of 1,4-Phenylenediamines”
Lauw, S. J. L.; Xu, X.; Webster, R. D. *ChemPlusChem* **2015**, *80*, 1288–1297.

5. “The Electrochemical Reduction of Carbon Dioxide (CO_2) to Methanol in the Presence of Pyridoxine (Vitamin B_6)”
Lee, J. H. Q.; Lauw, S. J. L.; Webster, R. D. *Electrochem. Commun.* **2016**, *64*, 69–73.

6. “Studies on the Electrochemical Reduction and Coupled Homogeneous Reactions of Cinnamaldehyde in Acetonitrile”
Lauw, S. J. L.; Zhong, C.; Webster, R. D. *J. Electroanal. Chem.* **2016**, *779*, 220–228.

7. “The Electrochemical Study of Vanillin in Acetonitrile”
Lee, J. H. Q.; Lauw, S. J. L.; Webster, R. D. *Electrochem. Acta* **2016**, *211*, 533–544.

8. “Sulfoxidation of alkenes and alkynes with NFSI as a radical initiator and selective oxidant”
Zhang, Y.; Wong, Z. R.; Wu, X.; Lauw S. J. L.; Huang, X.; Webster, R. D.; Chi, R. Y. *ChemCommun.* **2017**, *53*, 184–187.

9. “Trimerization of Enones under Air Enabled by NHC/ NaOtBu via a SET Radical Pathway”, Zhang, Y.; Wu, X.; Hao, L.; Wong, Z. R.; Lauw, S. J. L.; Yang, S.; Webster, R. D.; Chi, R. Y. *Org. Chem. Front.* **2017**, DOI: 10.1039/C6QO00738D.

10. “The Electrochemical Reduction of Di-(2-ethylhexyl) Phthalate (DEHP) in Acetonitrile” Lauw, S. J. L.; Lee, H. Q. J.; Tessensohn M. E.; Leong, W. Q.; Webster, R. D. *submitted*.

11. “Comparing the Relative Reactivities of Food and Vitamin Molecules Toward Electrochemically Generated Superoxide in DMF”
Lauw, S. J. L.; Yeo, Y. H. J.; Zhong, C.; Webster, R. D. *submitted*.

12. “Comparing the Relative Reactivities of Structurally Varied Alcohols Toward Electrochemically Generated Superoxide”
Lauw, S. J. L.; Zhong, C.; Lee, H. Q. J.; Webster, R. D. *in preparation*.

Chapter 1

Introduction

This page has been intentionally left blank

1.1. Organic Carbonyl Compounds

1.1.1. Background

Carbonyl compounds (aldehydes, ketones, and carboxylic acids and their derivatives) are an important class of molecules. This is exemplified by their prevalence in the plethora of biologically active natural products, pharmaceutical compounds, and chemical reagents that we come into close contact with on a regular basis. For instance, the carbonyl functionality can be found in acetaminophen (an active ingredient of an over-the-counter pain relief and fever reducing medicine), biotin (vitamin B_7), capsaicin (an active component of chili peppers), cinnamaldehyde (an active component of cinnamon spice), phthalates (plasticizer molecule), penicillin (antibiotic), and testosterone (steroid hormone) (Scheme 1.1).

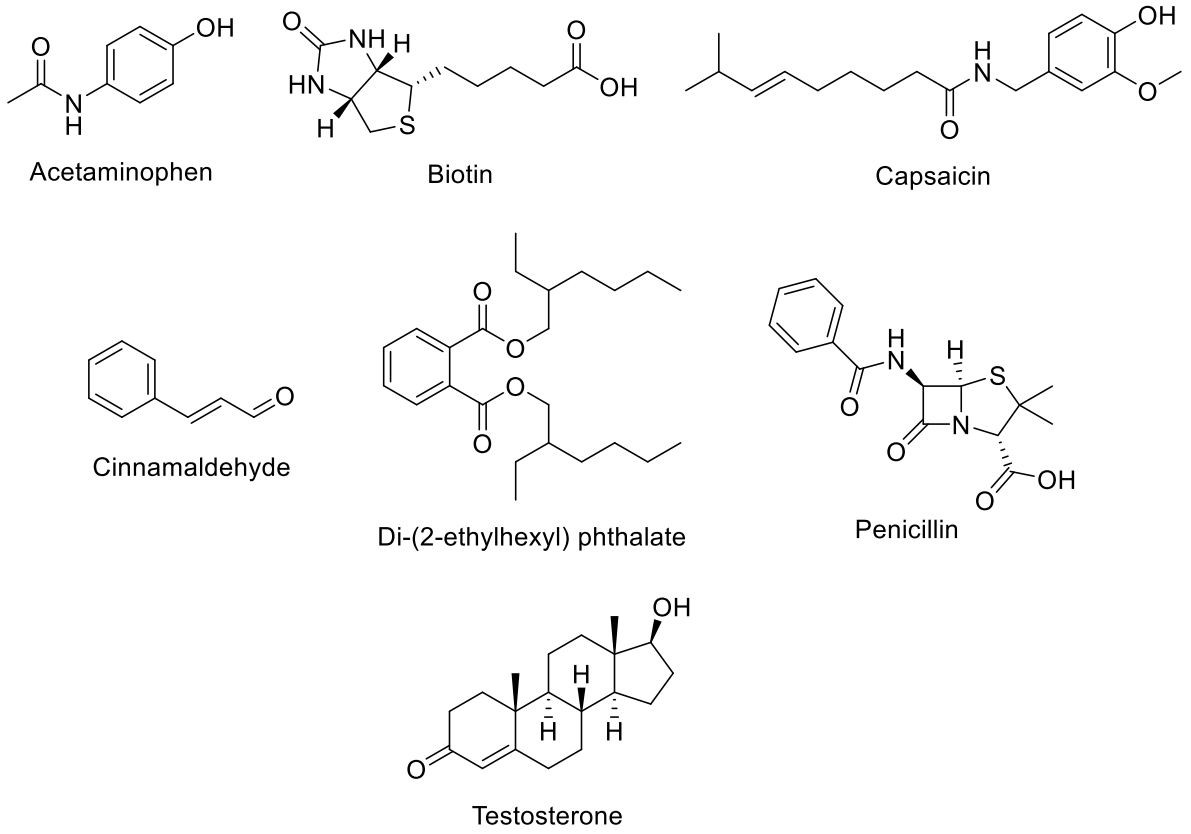

Scheme 1.1. Examples of common carbonyl group containing compounds.

1.1.2. General chemical & electrochemical reactivity of carbonyl functionalities

Within the field of synthetic chemistry, the search for reaction strategies involving more atom-economic, low cost and readily accessible substrates, wide substrate scopes, high yields, and product selectivity under mild conditions are often the main ideals that are constantly being sought after. Owing to their widespread occurrence (Scheme 1.1), it is unsurprising that the carbonyl group and its compounds are extensively studied and frequently utilized as building blocks in organic synthesis. For instance, it has been well established that most carbonyl compounds generally undergo reactions that fall into one of the following mechanistic pathways: (1) nucleophilic addition, (2) nucleophilic acyl substitution, (3) alpha substitution, and (4) carbonyl condensation, which is governed by the exact nature of the carbonyl functionality [1-4].

In comparison, in terms of electrochemical properties, the carbonyl group can be considered as an electrophore (lack of electrons) and is mostly electrochemically reducible when present in its free form (as opposed to its masked form such as in geminal diols or hemi acetals/acetals, which are electrochemically inactive). Carbonyls are typically reduced by addition of an electron to its lowest unoccupied molecular orbital (LUMO) to initially form a radical anion species, which may then be followed by other electron transfer and/or chemical reaction steps such as protonation, hydrolysis, dimerization, or others – depending on the exact structure of the rest of the molecule as well as the experimental conditions that are utilized (e.g. electrode material, pH, solvent) [5, 6].

1.1.3. Comparison between chemical & electrochemical methods

Unlike with classical chemical methods which are primarily concerned with homogenous (interaction of substances within the same phase) reactions, electrochemical techniques typically involve a combination of both homogenous and heterogeneous (reaction of species in

different phases) processes. Another disparity between the two systems stems from the different means by which the intermediate(s) and product(s) are produced. For instance, chemical approaches require the use of oxidizing or reducing agents to effect the desired redox transformation, whereas electrochemical methods utilize the electron transfer reactions that occur at an electrode/solution interface. In turn, this gives the latter technique an advantage of being able to control the driving force of the reaction through careful adjustment of the applied electrode potential, and consequently allows for the generation of highly reactive intermediates or species to be performed in a highly precise and regulated manner. Furthermore, preparative electrochemistry benefits from a simpler workup as it precludes the need for separation and treatment of products generated from the use of sensitive chemical redox reagents, although it does require the separation of the supporting electrolyte upon the completion of the electrolysis which can sometimes be difficult [7-10]. Nevertheless, the application of electrochemistry for preparative/large scales is not uncommon, with representative examples like the chloroalkali, Hall-Héroult, and Kolbe processes being conducted using electrolysis methods since the late 19^{th} century, as well as a myriad of other industrial reactions such as metal winning and refining, hydrogen production, and water electrolysis, amongst others still being utilized today [10, 11].

Regardless, it is worth highlighting that electrochemical methods frequently require sophisticated instruments and equipment (e.g. potentiostats, electrodes, and cells), which depending on the intended purpose may sometimes be difficult to obtain, necessitate highly specific or customized designs, and/or result in larger costs incurred [12-14]. Moreover, chemical transformations have also been typically shown to be superior (as compared to electrochemistry) in terms of product chemo-, regio- and/or stereo-selectivity [7-10]. Additionally, to facilitate charge transfer across the electrodes (e.g. working and counter electrodes), the solutions used for electrochemical experiments must be conducting, which mandates the use of inert electrolytes that are usually added in large excess quantities, and

solvents or buffer solutions with reasonably high dielectric constants. These reaction media are sometimes different from those often used in conventional chemical synthesis, and may possibly induce reaction pathways that diverge or are unwanted in contrast to the latter method [12-14]. Despite this, electrochemical techniques can often still be used to form intermediates and/or end-products that are similar to chemically-generated ones. More specifically, since the reactions typically start off with a neutral compound, the initial electron transfer may furnish paramagnetic species that can undergo cascades of reactions to deliver well-known species formed by chemical methods such as carbocations, carbenes, and carbanions, provided that the analyte is electrochemically active [7-10]. Nevertheless, the requirement of a redox-active species in electrochemistry can be fulfilled by the addition of electroactive pro-reagents such as redox mediators [15].

1.2. Aims & Objectives (Organic Carbonyl Compounds)

Besides supplementing conventional organic synthesis methods, electrochemical techniques are also highly valuable because it can be used as a device to study many processes such as biological, enzymatic, metabolic, and toxicity reactions, particularly if electron exchanges (such as reduction or oxidation steps) are integral to the execution of these transformations. Moreover, because electrochemical studies can be performed on the chemicals individually (after identifying and isolating the compound(s) of interest), detailed analyses of associated redox reactions can be carried out under strict laboratory conditions and in the absence of complex biological matrixes (minimizing complications that may arise due to interfering species) [16].

For instance, by using standard electrochemical procedures such as voltammetry (e.g. cyclic, linear sweep, rotating disk electrode), qualitative information regarding the thermodynamics and kinetics of the heterogeneous electron transfer step(s) and follow-up homogeneous chemical reaction(s) of many biologically-active compounds can be obtained. Moreover, when coupled together with other methods such as bulk electrolysis, spectroscopy (e.g. attenuated total reflectance Fourier transform infrared spectroscopy (ATR-FTIR) or UV-Vis spectroscopy), and digital simulation techniques, the identity and nature of associated intermediate(s) and product(s), as well as the order and number of electrons transferred can sometimes also be accurately determined [17-19]. Such information may assist in providing greater insights into the redox mechanisms of different essential substrates, and possibly unravel correlations to their biological functions and in vivo reactions [16, 20, 21].

With the above in mind, the major theme of this thesis was to conduct in-depth investigations into the electrochemical behavior and redox reactions of three carbonyl molecules: (1) biotin (vitamin B_7), (2) cinnamaldehyde (CA), and (3) di-(2-ethylhexyl)

phthalate (DEHP), which comprise of the different classes of carbonyl functionalities including carbamide and carboxylic acid, aldehyde, and ester, respectively. Detailed information regarding their background, occurrence, biological features, and/or related electroanalytical studies are given in the subsequent sections (see Sections 1.3–1.5). More importantly, because these compounds are routinely used in food or in food-related consumer products and are inevitably introduced into human biological systems, examinations of the exact redox pathways and reaction sequences of these compounds are pertinent and may be useful in providing useful information regarding their proposed biological roles, degradation, and/or toxicity.

In addition, it is noteworthy to mention that since most of the existing studies on the redox behaviors of the aforementioned compounds have been carried out by polarography in aqueous media, the experiments performed in this thesis were restricted to aprotic organic solvents (acetonitrile (CH_3CN), dimethyl sulfoxide (DMSO), and *N*,*N*-dimethylformamide (DMF)) in order to provide a complementary and/or comparison model to aqueous solutions. Aprotic solvents are also useful for electrochemical analyses due to the minimal availability of protons in such media which generally allows for less complex electrochemical phenomena. For instance, the lowered proton activities may be beneficial in minimizing the occurrence of substrate protonation even prior to the electrochemical reaction, which can affect the observed redox potentials, or serve to reduce the likelihood of coupled homogeneous reactions (e.g. protonation or hydrolysis) from taking place immediately following the electrochemical generation of transient species (e.g. radical anions). Also, this could potentially increase the stability/lifetimes of reactive intermediates and possibly enable their detection or characterization [13, 14]. Furthermore, aprotic organic solvents were utilized to provide relatively lipophilic conditions, which are more biologically relevant to the low water content environment that many of the fat-soluble molecules examined in this work might experience in vivo (such as inside of lipid membranes) [16, 20, 21].

1.3. General Introduction to Biotin (Vitamin B_7)

1.3.1. Background

Biotin (vitamin B_7) is a member of the water-soluble vitamin B complexes and an essential micronutrient which is vital in the sustenance of normal cellular functions and metabolism [22-27]. Despite the importance of this compound being recognized as early as 1927 [28], biotin was only isolated several years later in 1936 [29], and its chemical structure was only determined and synthesized in 1942 [30] and 1943 [31], respectively (Scheme 1.2).

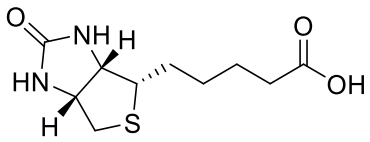

Scheme 1.2. Chemical structure of d-(+)-biotin (Vitamin B_7).

1.3.2. Biological functions of biotin

As a result of its three chiral carbon centers, there exist eight possible stereo-isomeric forms of this vitamin. However, only d-(+)-biotin is known to be biologically active. In mammals, it is well established that biotin functions as a covalently attached co-factor for five carboxylase enzymes that are found in the mitochondria and cytoplasm: acetyl-coenzyme A(CoA) carboxylases (ACC) 1 and 2; 3-methylcrotonyl-CoA carboxylase (MCC); pyruvate carboxylase (PC); and propionyl-CoA carboxylase (PCC). Collectively, these biotin-bounded enzymes catalyze key steps in metabolic pathways including amino acid catabolism, gluconeogenesis, lipogenesis, and energy transduction [22-27].

For example, both ACC1 and ACC2 catalyze the binding of bicarbonate to acetyl-CoA to produce malonyl-CoA, which is necessary for the synthesis of fatty acids and the regulation of fatty acids oxidation in the cytoplasm and mitochondria, respectively (Scheme 1.3). On the

other hand, the carboxylases MCC, PC, and PCC are all contained within the mitochondria and play key roles in catalyzing a crucial step in the metabolism of leucine, the conversion of pyruvate into oxaloacetic acid, and the metabolism of propionyl-CoA, respectively (Scheme 1.3) [22-27].

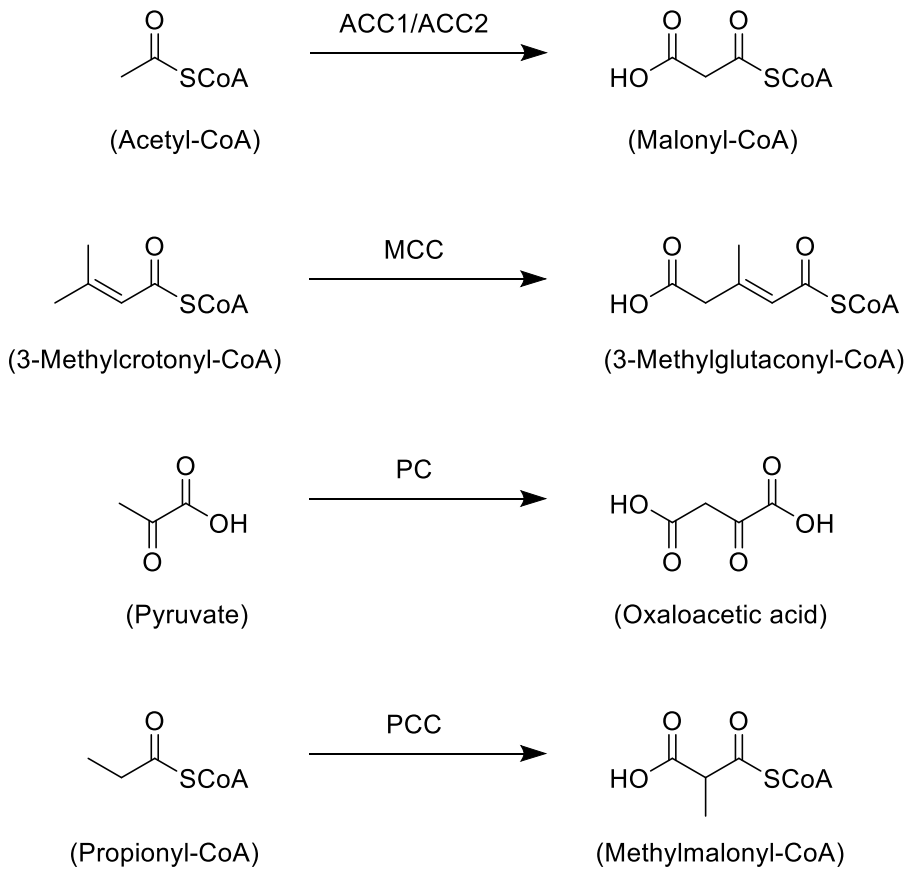

Scheme 1.3. Key carboxylation steps catalyzed by the biotin-bounded carboxylases. ACC1/ACC2: acetyl-coenzyme A(CoA) carboxylases 1 and 2; MCC: 3-methylcrotonyl-CoA carboxylase; PC: pyruvate carboxylase; and PCC: propionyl-CoA carboxylase (adapted from refs. [24, 25, 27]).

More recently, in addition to its role as a prosthetic group, the importance of biotin has also been emphasized by the discovery of its involvement in the regulation of gene expression, in cell signal signaling pathways, as well as in histone biotinylation [22-27].

1.3.3. Catabolism of biotin

The catabolism of biotin has been identified to occur via two general pathways (Scheme 1.4). In the first mechanism, biotin is catabolized by the β-oxidation of its valeric acid side chain where two carbon units are repeatedly removed to form bisnorbiotin, tetranorbiotin, and other intermediates or products associated with the β-oxidation of fatty acids (path a). In the cases of β-ketobiotin and β-ketobisnorbiotin, these compounds may also undergo a decarboxylation reaction to afford bisnorbiotin methyl ketone and tetranorbiotin methyl ketone, respectively, due to their instability [24, 25, 27, 32, 33]. A further cleavage and degradation of the heterocyclic ring in tetranorbiotin may also ensue in microorganisms [24, 25, 27, 32, 33], although this route has been demonstrated to be a relatively minor occurrence in mammals [24, 25, 27, 34]. Alternatively, in the second pathway the sulfur atom in the heterocyclic ring of biotin may be oxidized to generate biotin sulfoxide and biotin sulfone (path b). In addition, it is also possible that biotin is catabolized via a combination of both mechanisms (i.e. β-oxidation and sulfur atom oxidation) to furnish products such as bisnorbiotin sulfone [24, 25, 27, 32, 33].

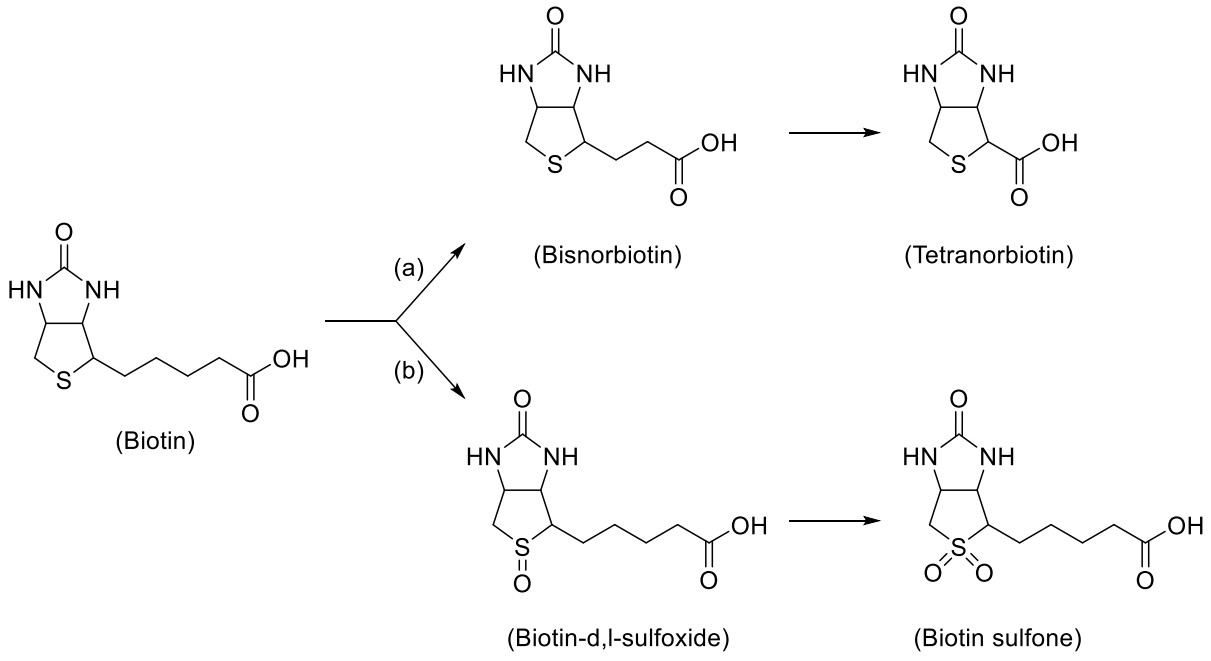

Scheme 1.4. Biotin catabolism pathways (adapted from refs. [24, 25, 27]).

1.3.4. Sources of biotin & deficiency

Although the exact amount of biotin that is required by an average adult is not precisely known, a general dosage of about 30 µg/day has been recommended [24-27]. Unfortunately, whereas plant cells and certain microorganisms are capable of producing biotin endogenously [24-27], mammals need to depend on two primary sources for this vitamin: (1) from dietary items such as dairy products, egg yolk, and organ meats [26, 33], and (2) from a bacterial source, which is the large intestine's normal microflora [35]. However, whether the latter's overall contribution to the host's nourishment is significant remains unclear [36].

Regardless, due to biotin's immense importance, it is unsurprising that a severe lack of vitamin B_7 has been demonstrated to result in a variety of clinical disorders ranging from dermatological conditions (e.g. hair loss and dermatitis) to neurological abnormalities (e.g. hallucinations and hypotonia) and retardation (e.g. growth in infants) [24-26, 37, 38]. Nevertheless, biotin deficiency is a relatively uncommon condition unless induced by malnutrition, congenital genetic disorders that affect biotin homeostasis (e.g. deficiency of Biotidinase and Holocarboxylase synthetase), or through an excessive and extended consumption of raw egg whites containing avidin, which renders biotin nutritionally inactive by binding to it with an extremely high specificity and strength [24-26, 37, 38].

1.3.5. Common applications of biotin

The extraordinary affinities that avidin and its bacterial counterpart, streptavidin, possess for biotin (dissociation constants have been estimated to be up to 10^{-15} M [39]) have formed the primary basis for a myriad of biotin related studies. For example, apart from the more conventional techniques of detecting biotin, such as via bioassays and microbiological methods, the highly specific binding of (strept)avidin to sample or labeled biotin is also routinely measured and evaluated in various chromatographic, spectroscopic, electrochemical, and/or

radiometric systems for vitamin B_7 determination [40-43]. In addition, the exceptionally strong non-covalent interactions between biotin and the aforementioned glycoproteins have also been extensively studied and exploited in numerous applications and technologies including clinical diagnostics, immunoassays, DNA hybridization assays, affinity-based separations, biosensing, targeted imaging, virus detection, and others [44-52].

1.3.6. Electroanalytical studies on biotin

In contrast, a search in literature reveals a lack of reports that describe a detailed study on the electrochemical behavior of biotin. It is to the best of our knowledge that the few existing electrochemical analyses of biotin in its free form were reported close to four decades ago, where it was ascertained by polarography that biotin undergoes a one-electron reduction at ca. -1.80 vs. SCE/V (SCE = Saturated Calomel Electrode) in DMF/water solutions [53, 54]. In these seminal work, it was also proposed that at a mercury working electrode, the electrochemical reduction of biotin was chemically irreversible, and likely followed an ECC type mechanism, where E and C represents an electrochemical and chemical step, respectively, as shown in Scheme 1.5. The carbonyl functionality on the heterocylic ring of biotin was thought to initially gain an electron leading to the formation of a radical anion intermediate, which subsequently undergoes protonation before taking part in a radical–radical coupling reaction with itself (homodimerization) to furnish a dimeric product.

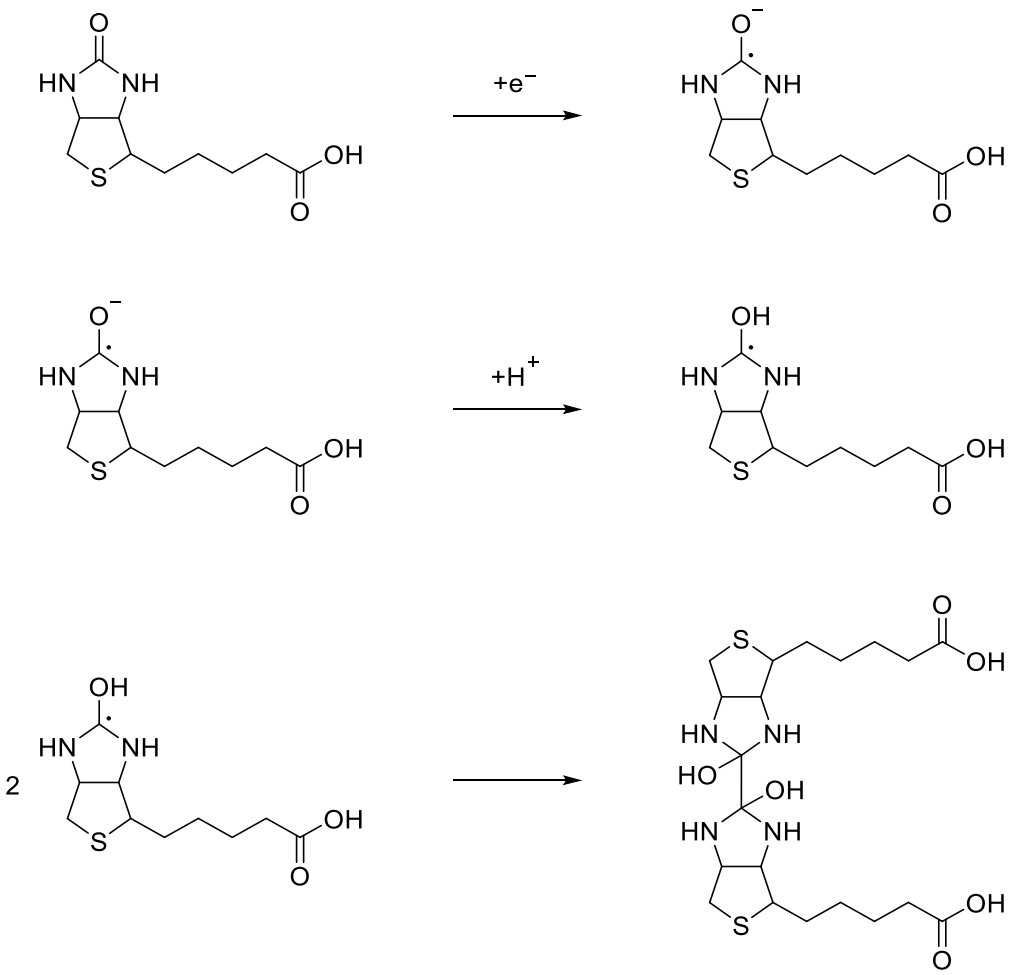

Scheme 1.5. Proposed mechanism for the electrochemical reduction of biotin (adapted from refs. [53, 54]).

In view of this, further examinations of biotin's electrochemistry at solid electrodes can be serve as a comparison and to follow up to the results previously obtained by polarography. In addition, because the final product of biotin reduction was posited to involve a change at its carbonyl functionality (at the heterocyclic ring), the use of attenuated total reflectance–Fourier transform infrared (ATR–FTIR) spectroscopy was also envisaged as a means to characterize the intermediate species and/or end-products following the electrochemical transformations.

1.4. General Introduction to Cinnamaldehyde

1.4.1. Background

Discovered and utilized by mankind since several millennia ago, cinnamon constitutes one of the oldest spices in the world besides pepper and vanilla [55-57]. Although it is at present most commonly recognized as a delectable food additive that possesses an inherently warm and aromatic flavor, cinnamon was also once traded as a precious commodity across Asia and Europe [55-57].

Commercially available cinnamon is mainly obtained from several trees that are part of the genus *cinnamomum*, of which there are ca. 250 different plant species [56-58]. The inner barks of these relatively small evergreens are first stripped off before being allowed to bake in the sun until they roll up into quills to form cinnamon sticks [56-58]. The dried barks may also be further pulverized into ground cinnamon. Regardless, the term cinnamon in fact more accurately refers to the spice that is harvested specifically from the Ceylon cinnamon tree (*cinnamomum verum* or true cinnamon), which is endemic to tropical Sri Lanka and Southern India. However, because cassia cinnamon (*cinnamomum cassia* or Chinese cinnamon) is relatively inexpensive, it is also frequently marketed as cinnamon, in spite of its widely accepted inferior taste and quality – cassia has been described to possess a comparatively spicier and more pungent flavor as well as a higher content of the hepatotoxic compound coumarin [56-58].

1.4.2. Functions and applications of cinnamaldehyde

Irrespective of its exact origins, one of the chief constituents found in the essential oils of *Cinnamomum* bark is the biologically active compound, cinnamaldehyde (Scheme 1.6) [55-60]. This α,β-unsaturated aldehyde typically exists as a yellow viscous oil, that is highly reminiscent

of the distinctive aroma and flavor associated with cinnamon and can either be isolated from natural extracts (e.g. the distillation of essential oils) [56, 57] or obtained via laboratory synthetic methods (e.g. a base catalyzed (NaOH) aldol condensation of benzaldehyde and acetaldehyde) [61, 62].

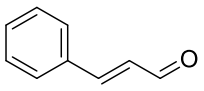

Scheme 1.6. Chemical structure of trans-cinnamaldehyde.

In addition to cinnamaldehyde's extensive role as a flavoring agent, fragrance, and additive in both the food and cosmetic industries [55, 56, 59, 60], numerous studies have also shown that this compound exhibits many desirable qualities that are valuable for unconventional applications. For example, cinnamaldehyde has been routinely demonstrated to display anticorrosion [63-65], antidiabetic [66, 67], antimicrobial [68, 69], and antitumor [70-72] properties in a plethora of studies. In light of this, it is therefore unsurprising that the vast utility and usage of cinnamaldehyde (global consumption is estimated at > 100 metric tonnes annually [59]) has also encouraged a host of research on other aspects of this natural product such as on its detection [73-75], metabolism [76], and toxicity [62, 77].

1.4.3. Electroanalytical studies on cinnamaldehyde

Nevertheless, a search in the literature reveals that there are markedly fewer reports that have focused on examining cinnamaldehyde's electrochemical behavior, and that the prevailing studies were mainly conducted in aqueous or protic media using polarography.

In these accounts, it was initially suggested that the reduction of cinnamaldehyde occurred in a similar fashion to benzaldehyde, and was restricted to only its aldehyde functionality. At low pH, this reaction was described to follow a one-electron/one-proton

transfer ($+e^-/+H^+$) to either form a dimeric diol product or undergo a further $+e^-/+H^+$ reaction at a second wave to furnish cinnamyl alcohol (Scheme 1.7). Otherwise, a direct $+2e^-/+2H^+$ reduction of cinnamaldehyde may also take place (to similarly form cinnamyl alcohol) if a medium pH is used [78-81].

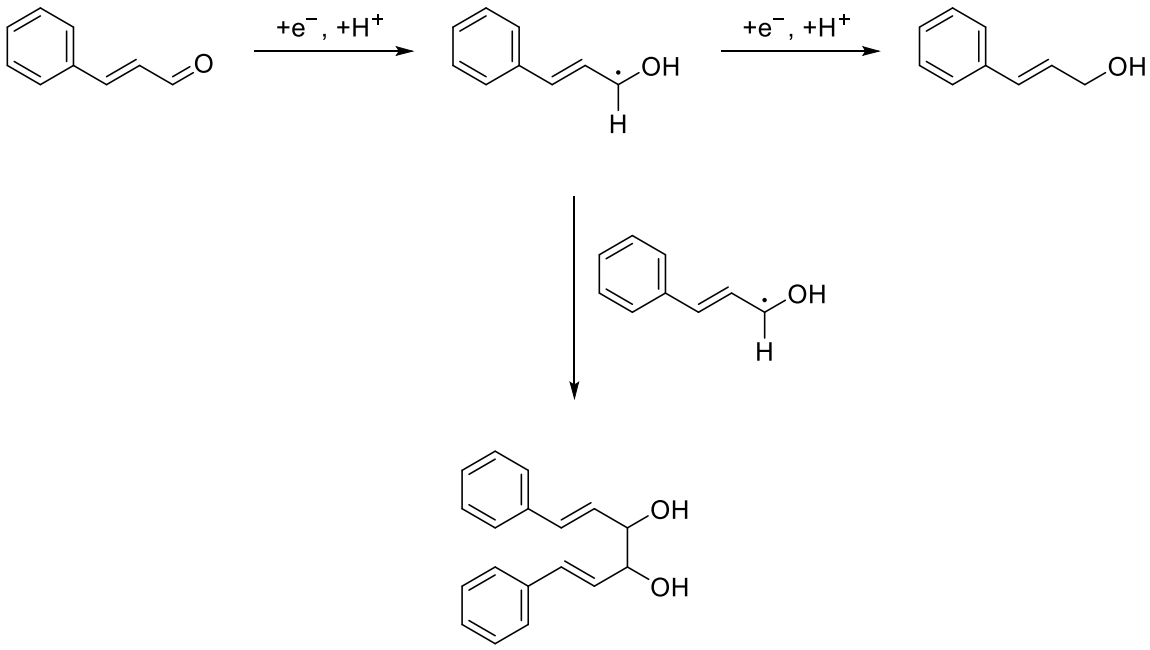

Scheme 1.7. Proposed mechanism for the electrochemical reduction of cinnamaldehyde into cinnamyl alcohol.

Nevertheless, the above premise was later refuted when it was established in subsequent reports that the first reduction step actually involves a $+2e^-/+2H^+$ process, which engages the alkene bond of the compound to produce a saturated aldehyde instead (Scheme 1.8), with slight variations to the exact electron/proton transfer sequences at low and high pH [82-86]. More specifically, it was determined that under more acidic conditions, cinnamaldehyde undergoes a CEEC ($+H^+$, $+e^-$, $+e^-$, $+H^+$) type mechanism, where E and C represent an electrochemical and chemical process, respectively. Conversely, under medium pH conditions, an ECEC ($+e^-$, $+H^+$, $+e^-$, $+H^+$) type pathway occurs instead. On the other hand, the reduction of cinnamaldehyde

under more basic conditions was described to follow a slightly different order of an EECC ($+e^-$, $+e^-$, $+H^+$, $+H^+$) sequence instead.

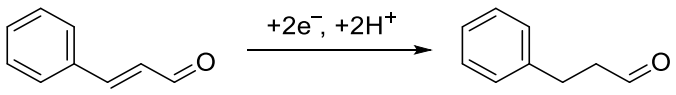

Scheme 1.8. Proposed mechanism for the electrochemical reduction of cinnamaldehyde into 3-phenylpropanal.

Regardless of the sequence of the initial $+2e^-/+2H^+$ reduction of cinnamaldehyde, a further reduction was observed following the former cathodic process, and was ascribed to an additional $+2e^-/+2H^+$ reduction of the aldehydic group to yield a saturated alcohol (Scheme 1.9) [82-86].

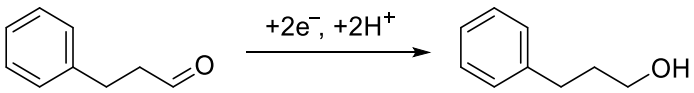

Scheme 1.9. Proposed mechanism for the electrochemical reduction of 3-phenylpropanal into 3-phenylpropan-1-ol.

In contrast, other studies have also described that the reduction involves dimerization reactions which can either furnish a mixture of dimeric products [87], couple at the aldehyde functionality to form a pinacol-type product [88], or join in a “head to tail” fashion to generate stereoisomeric tetrahydrofuranol products (Scheme 1.10) [89], depending on the composition of the test solution.

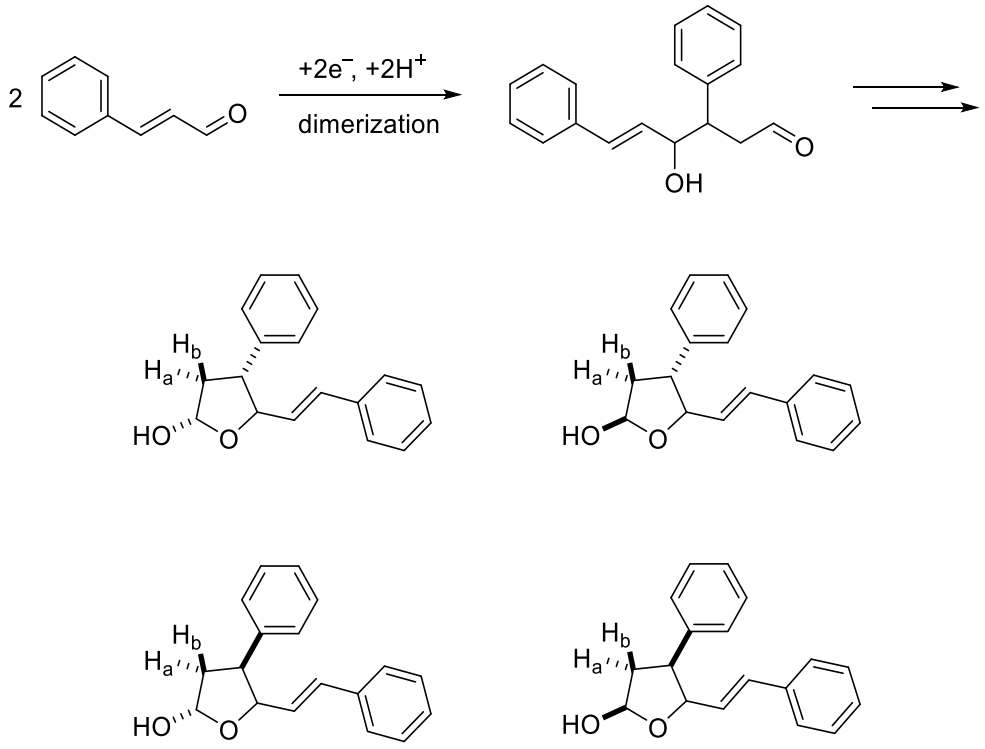

Scheme 1.10. Proposed mechanism for the electrohydrodimerization of cinnamaldehyde (adapted from ref. [89]).

Based on the above considerations, the present study was initiated to carry out a detailed examination on the electrochemistry of cinnamaldehyde in acetonitrile (CH_3CN) via voltammetric and electrolysis methods so as to provide a complementary model to existing studies that have mostly been limited to aqueous/protic systems. In addition, digital simulation techniques were used in order to facilitate a more in-depth investigation into cinnamaldehyde's electrochemical reduction and follow-up homogeneous reactions.

1.5. General Introduction to Di-(2-ethylhexyl) phthalate (DEHP)

1.5.1. Background

In recent years, phthalate esters (Scheme 1.11) have emerged as contaminants of substantial concern due to their large scale production (over several million tons annually) [90, 91], and deleterious effects toward human health and the environment [90, 92].

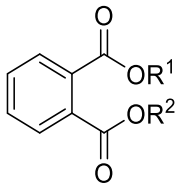

Scheme 1.11. General chemical structure of phthalate esters.

Owing to their ability to impart flexibility to polymers, these synthetic chemicals are extensively utilized as plasticizers in the manufacturing of polymeric materials (e.g. polyvinyl chloride), such as in numerous indispensable products including medical devices, food packaging, toys, clothes, cosmetics, and others [93-96]. More notably, the phthalate additives in these items are often loosely bound (not covalently bonded) to the host polymer/material and thus can easily leach into its surroundings during production, when in use, or after disposal [91, 97, 98]. As such, phthalate contamination of the environment is immensely widespread, and these molecules have been detected in a variety of matrices including soil, air, water, dust, and food [95, 99, 100]. Consequently, human exposure to phthalate esters has become highly pervasive and can occur through multiple channels including dermal absorption, inhalation, or ingestion [101-103]. For instance, it was estimated that the general intake of phthalates can amount to several hundred μg/kg of body weight/day, with children being especially susceptible to exposure [104, 105].

1.5.2. Di-(2-ethylhexyl) phthalate (DEHP)

Notably, because di-(2-ethylhexyl) phthalate (DEHP; Scheme 1.12) constitutes one of the most commonly utilized and correspondingly abundant phthalates [91, 104, 106], it is unsurprising that research into the different chemical and biological facets of this chemical remains of relevance and interest.

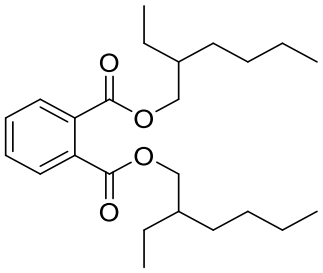

Scheme 1.12. Chemical structure of di-(2-ethylhexyl) phthalate (DEHP).

For example, one area which has led to a myriad of studies is the assessment DEHP's toxicity. In many of these reports, exposure to the aforementioned toxicant has been demonstrated to result in the manifestation of various undesirable conditions, including carcinogenicity, kidney and liver toxicity, endocrine disruption, damage to the reproductive system, and others [107-109]. Consequently, the numerous adverse health effects elicited by DEHP have consequently also led to the exploration and development of many sensitive and selective analytical techniques, which encompass biological, chromatographic, and electrochemical methods, for the efficient detection and quantification of this compound [110-113].

Another area of considerable interest is with regards to the catabolic pathways of phthalate esters such as DEHP, which have generally been described to proceed via two phases in mammals (Scheme 1.13) [104, 114-116]. In the first stage, phthalate esters generally initially undergo hydrolysis to generate phthalate monoester metabolites by the actions of unspecific

esterases and lipases. Thereafter, the shorter (lower molecular weight) phthalate monoesters are mostly excreted in the urine. In contrast, the longer (more hydrophobic) phthalates such as DEHP may undergo a further hydroxylation or oxidation of the monoester, followed by glucuronidation (often catalyzed by uridine 5'-diphosphoglucuronyl transferase) to form a variety of hydrophilic glucuronide conjugates before they are excreted in the urine and/or feces.

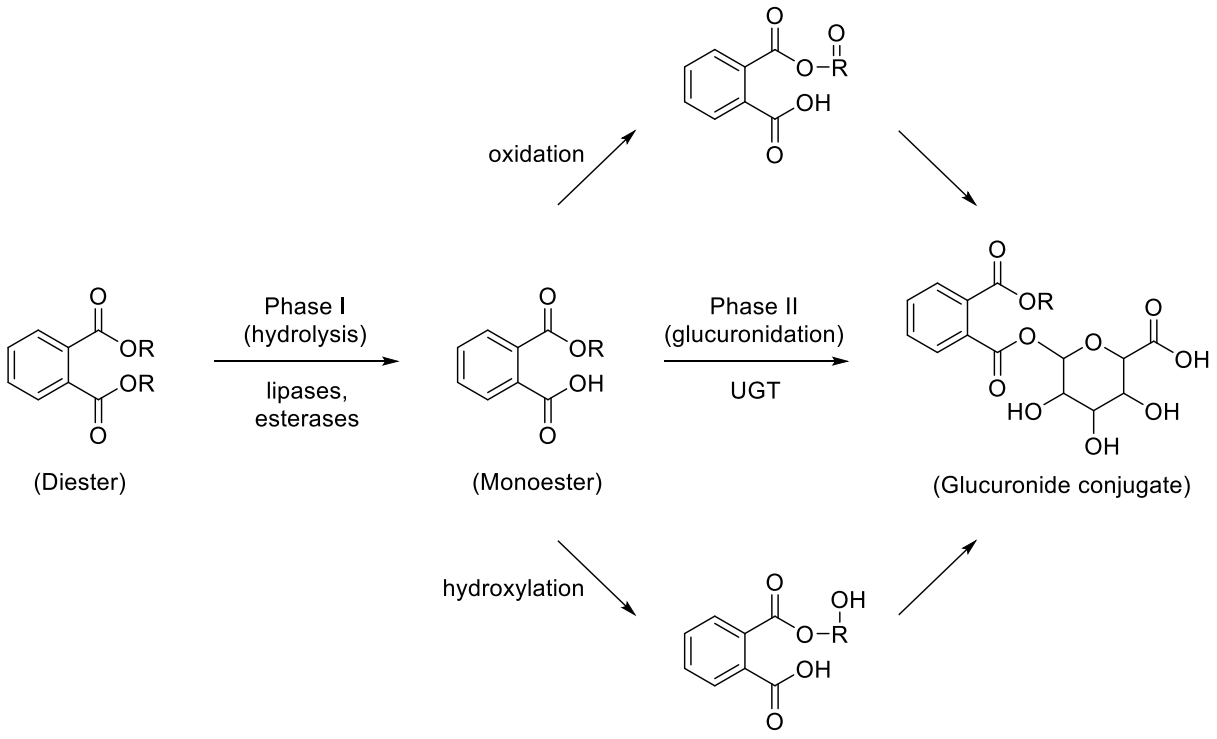

Scheme 1.13. Proposed metabolic mechanism of phthalate esters (adapted from refs. [114, 115]). UGT = uridine 5'-diphosphoglucuronyl transferase.

1.5.3. Electroanalytical studies on DEHP

To the best of our knowledge, an in-depth investigation of the electrochemical behavior of DEHP has not yet been reported, although the electrochemical reductions of benzene-based esters have been extensively studied. For instance, the electrochemical reduction of benzene monoesters has been reported to involve a one-electron transfer that generates a radical anion whose final decomposition product has led to a divergence of mechanistic viewpoint. As

outlined in Scheme 1.14, two main pathways have been proposed that differ due to the ambiguity of the bond being broken, following the formation of the highly reactive radical anion. In the first route, the oxygen alkyl bond was proposed to be cleaved to afford an acyl radical and alkoxide (Scheme 1.14; path a). Conversely, the second route involves a breakage of the carbonyl-oxygen bond to generate a carboxylate anion and alkyl radical instead (Scheme 1.14; path b). Additionally, in the case of the latter, it was also reported that the rate of bond cleavage is influenced by the stability of the alkyl radical generated [117-126].

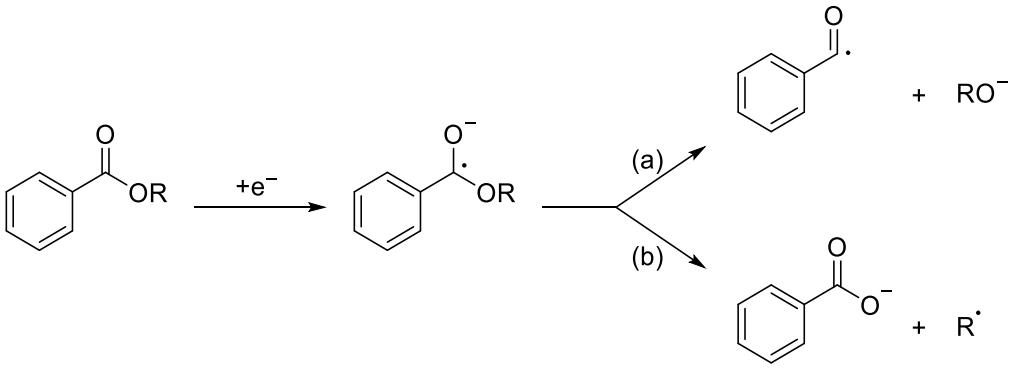

Scheme 1.14. Proposed decomposition pathways for benzene monoester radical anions.

In contrast, there exist fewer reports regarding the reduction of benzene-based diesters (ortho, meta, or para-substituted) [127-130]. In these accounts, it was shown that these compounds can be reduced by one electron at fairly large negative potentials, with some also exhibiting a second reduction step if the first process displayed some chemically reversibility at low scan rates. In a similar manner as the mechanistic pathway outlined in route (b) of Scheme 1.14, the radical anion generated after the initial one electron reduction of the benzene diesters was generally proposed to undergo a cleavage of the oxygen-alkyl bond to produce a carboxylate anion via the elimination of an alkyl radical (Scheme 1.15). Nevertheless, it was noted that the ortho-substituted benzene-based diesters were less well-explored (as compared to the meta or para-substituted isomers), and that dipropyl benzene-1,2-dicarboxylate was, to the best of our knowledge, the only example described [127, 128].

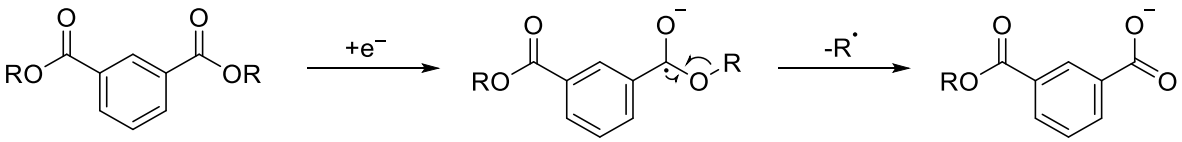

Scheme 1.15. Proposed reduction and decomposition pathway for benzene diesters.

With the aim of gathering a more thorough mechanistic understanding about the redox characteristics of DEHP, the electrochemical reduction of the aforementioned phathalate was examined in detail using cyclic voltammetry (CV) under varied scan rates, temperatures, and concentrations, as well as via controlled potential electrolysis (CPE) methods. In addition, the electrochemical data obtained from the CV experiments at varied scan rates were carefully modeled using digital simulation techniques in order to obtain information regarding the rates of the electrode reactions and their coupled chemical transformations.

1.6. Reactive Oxygen Species & Superoxide

1.6.1. Background

Free radicals are ubiquitous in biological systems and are unavoidably generated as a consequence of essential metabolic pathways (endogeneous sources), but can also arise due to external factors such as environmental stress, radiation, and reducing chemicals (exogeneous sources) [131, 132]. Generally, these by-products are unstable compounds, molecules, molecular fragments, or atoms that are comprised of one or more unpaired electrons and also possess a significant amount of reactivity. As such, a common feature amongst free radicals is their ability to react with, modify, and/or damage important biological molecules (e.g. carbohydrates, lipids, proteins, and nucleic acids), thereby leading to unwanted cell and tissue injury [133, 134].

1.6.2. Reactive oxygen species (ROS)

Although molecular oxygen/dioxygen (O_2) is by itself relatively harmless, the free radicals (and derivatives) that are derived from it form a significant class of toxicants known as the reactive oxygen species (ROS), which include radical species such as superoxide ($O_2^{\bullet -}$), hydroperoxyl radical ($HO_2^{\bullet}$), and hydroxyl radical ($HO^{\bullet}$), and non-radical species such as hydrogen peroxide (H_2O_2) and hypochlorous acid (HOCl) [135, 136].

In the human biological system, these reactive species are produced on a daily basis at approximately 5 g/day [137, 138], and are predominantly and accidentally generated during respiration processes when a small number of electrons “leak” from cellular sources like the mitochondria [139-141], as well as in metabolism reactions catalyzed by O_2 in the liver that detoxify ingested food like alcohol and drugs. Other sources of ROS also include the enzymatic transformations catalyzed by oxidases (e.g. NADPH oxidases and xanthine oxidase), which are

activated and produce ROS during normal immune response to the presence of invading foreign microorganisms [142-144]. In addition, the generation of ROS has also been shown to be essential for numerous other physiological processes occurring in the human body, such as in the control and management of cell proliferation, apoptosis, signaling, and the regulation of redox-sensitive amino acids such as protein phosphorylation [135, 136, 143, 145].

Nevertheless, although the formation of ROS embodies a part of the normal cellular metabolic processes, the dynamic modulation of ROS levels in the body is also imperative so as to prevent their excessive accumulation. This is because high concentrations can be detrimental to organisms by leading to a state known as oxidative stress, which has been implicated in a plethora of clinical conditions including aging [146-148], carcinogenesis [149-151], and inflammation [152-154]. As such, antioxidants, which can either be synthesized naturally or obtained from external avenues like food and/or supplements, are necessary in order to maintain the delicate equilibrium between the generation of ROS and the body's defense capability. Generally, antioxidants are comprised of enzymatic (e.g. superoxide dismutase/reductase, glutathione peroxidase) and non-enzymatic (e.g. tocopherol, carotenoids, flavonoids) molecules and they function via three different modes of defense, which include the suppressing of free radical formation, the scavenging of reactive species, and the repair of damages caused [135, 136, 143, 145].

1.6.3. Superoxide ($O_2^{\bullet-}$)

Within the diverse family of ROS, a prominent member is the anionic free radical, superoxide ($O_2^{\bullet-}$). This paramagnetic diatomic molecule is the singly-reduced form of O_2, and can be broadly labeled as the parent free radical species of in vivo ROS since it is one of the first activation products of molecular oxygen [135, 136, 143, 145].

As represented diagrammatically by Scheme 1.16, the mono-electronic reduction of O_2 initially results in the formation of $O_2^{\bullet-}$. Dismutation of this radical anion anion may then occur (e.g. at low pH or by the actions of superoxide dismutase (SOD)) resulting in the generation of hydrogen peroxide (H_2O_2). Alternatively, $O_2^{\bullet-}$ can also undergo a protonation reaction to afford the hydroperoxyl radical ($HO_2^{\bullet}$), or react with the radical signaling molecule, nitric oxide ($NO^{\bullet}$), to furnish peroxynitrite ($OONO^-$). The conversion of H_2O_2 into the highly reactive hydroxyl radical ($HO^{\bullet}$) is also possible in the presence of transition metals such as iron, via the Haber–Weiss mechanism (eq. 1.1 and 1.2) which comprises the Fenton reaction (eq. 1.2). Alternatively, H_2O_2 may act as substrate for myeloperoxidase (MPO) to form hypochlorous acid (HOCl), which can then further react with another molecule of H_2O_2 to generate singlet oxygen ($^1O_2$) [135, 136, 143, 145].

$$Fe^{3+} + O_2^{\bullet-} \rightarrow Fe^{2+} + O_2 \quad (1.1)$$

$$Fe^{2+} + H_2O_2 \rightarrow Fe^{3+} + OH^- + HO^{\bullet} \quad (1.2)$$

$$\text{Net reaction: } O_2^{\bullet-} + H_2O_2 \rightarrow HO^- + HO^{\bullet} + O_2 \quad (1.3)$$

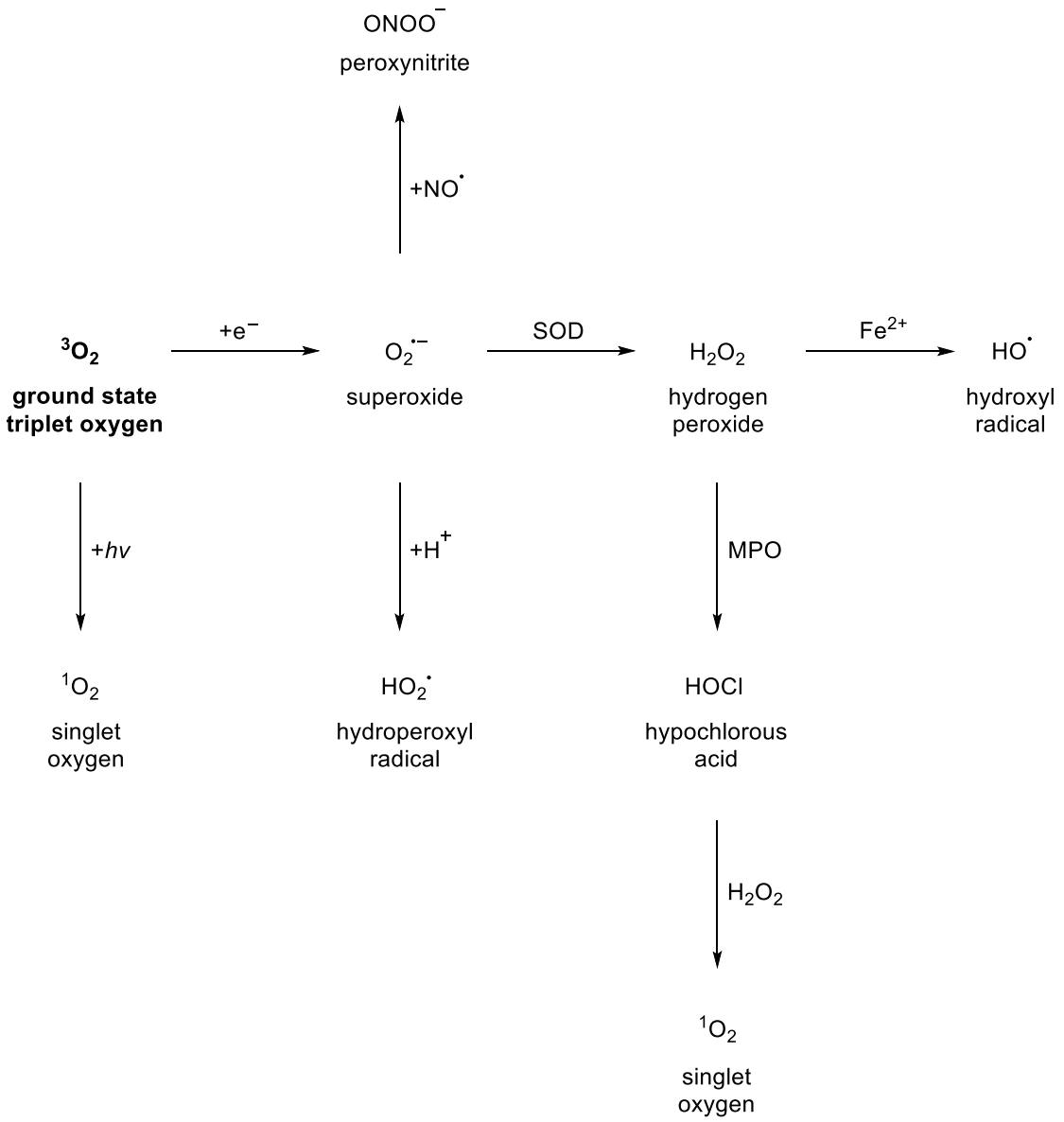

Scheme 1.16. Sequential generation of some common reactive oxygen species (ROS) from ground state triplet molecular oxygen (O_2). SOD = superoxide dismutase; MPO = myeloperoxidase. (adapted from refs. [135, 136, 143, 145]).

More importantly, although $O_2^{\bullet-}$ is most commonly associated with the elicitation of adverse health effects (e.g. aging [147, 148], carcinogenesis [150, 151, 155], and cardiovascular diseases [156, 157]), the aforementioned radical anion has also been shown to possess significant utility in various important areas such as in the synthesis of organic molecules [158-160], the destruction of hazardous chemical waste [161-163], as well as applications in metal-air batteries [164-166] – owing to its diverse and often unique chemical characteristics, which includes the ability to function as a one-electron reductant [167-169], Brønsted base/hydrogen atom abstractor [168, 170-174], or nucleophile [175-177].

In the laboratory, $O_2^{\bullet-}$ can be generated via several approaches including by biological, chemical, electrochemical, photochemical, and photocatalytic methods, in addition to the formation of $O_2^{\bullet-}$ from oxide surfaces and via the oxidation of organic compounds [140, 167, 178-181]. Amongst the abovementioned, electrochemical techniques are particularly expedient and operationally straightforward because $O_2^{\bullet-}$ can be electrochemically generated in very precise amounts, under mild conditions, and with little to no by-products in dry aprotic solutions [168, 177, 182]. In addition, $O_2^{\bullet-}$ has also been demonstrated to be relatively long-lived and easily handled in such media, while changes that occur during its reactions (such as consumption of $O_2^{\bullet-}$ or analyte) may also be monitored in situ [177]. For example, there have been a number of studies that have examined the reactions between electrochemically generated $O_2^{\bullet-}$ and various groups of natural and synthetic compounds such as flavonoids [183-187], (poly)phenols [174, 188-191], and others [176, 192-196]. More specifically, by carefully analyzing the changes in the profiles of the voltammograms obtained for O_2 reduction upon the addition of a substrate (e.g. anodic and cathodic peak current intensities), a comparison of relative reactivities across different analytes, and the elucidation of general scavenging mechanisms involved were able to be carried out in many of these accounts.

1.7. Aims & Objectives (Superoxide)

In view of the abovementioned precedent, it would be interesting to examine the interactions of electrochemically generated $O_2^{\bullet-}$ with an assorted array of food and vitamin compounds, since it is conceivable that many structurally related natural products (hydroxy-bearing or phenolic compounds) that are regularly consumed in one's diet would likewise be able to undergo similar reactions with $O_2^{\bullet-}$. Additionally, because $O_2^{\bullet-}$ has also been reported to be able to function as a one-electron reductant [167-169] or nucleophile [175-177] (besides being able to act as a Brønsted base/hydrogen atom abstractor [168, 170-174]), it was envisaged that it is possible that other classes of dietary molecules (non-hydroxy-bearing/phenolic) may likewise be able to interact with the aforementioned radical anion.

With the above in mind, the relative reactivities of different classes of compounds (food and vitamin molecules, and alcohols (Schemes 1.17–1.19) were evaluated by monitoring the decreases in the corresponding anodic peak currents (I_{pa}) in the cyclic voltammograms of the one-electron reduction of O_2, while methodically increasing the concentration of the test substrates [174, 184]. Where possible, the $O_2^{\bullet-}$ scavenging mechanisms as well as the structural features that are likely contributing to the observed reactivities (or lack thereof) are also examined. *N*,*N*-dimethylformamide (DMF) was selected as the solvent for the present work because $O_2^{\bullet-}$ has been shown to exhibit relatively long lifetimes in aprotic media [168, 197, 198], and also to provide a relatively high degree of solubility for all the compounds examined. It is important to highlight at this juncture, however, that the determination of exact antioxidant ability values is not the intent of the present study, but rather this work was initiated to provide a more common platform (i.e. the same experimental conditions) from which discussions on the chemical reactions of such compounds with electrochemically generated $O_2^{\bullet-}$ can be facilitated and possibly built upon in future studies.

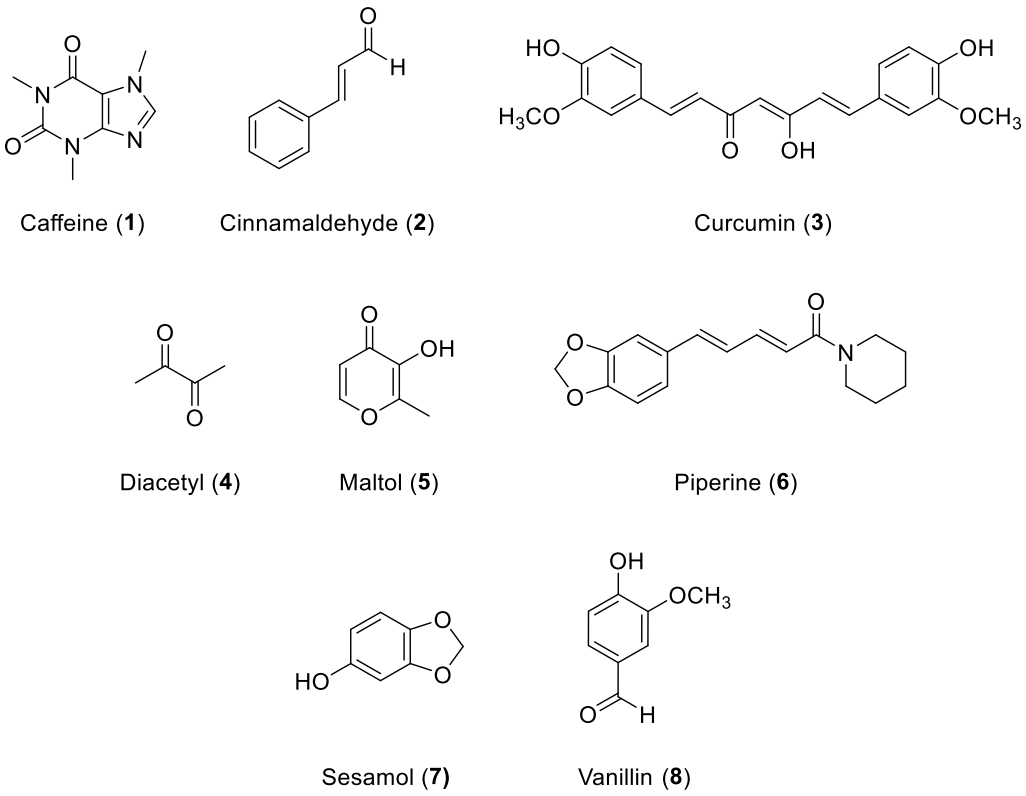

Scheme 1.17. List of food compounds examined in this study.

Vitamin A

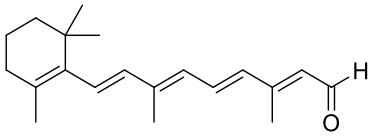

Retinal (**9**)

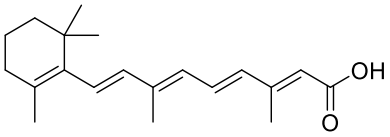

Retinoic acid (**10**)

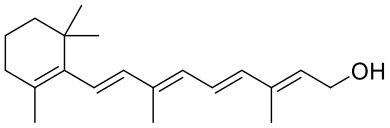

Retinol (**11**)

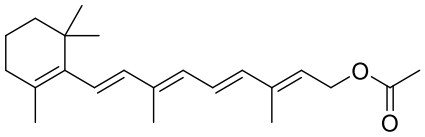

Retinyl acetate (**12**)

Vitamin B_6

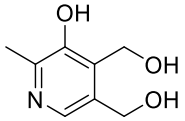

Pyridoxine (**13**)

Vitamin B_7

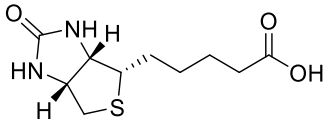

D-(+)-Biotin (**14**)

Vitamin D_2

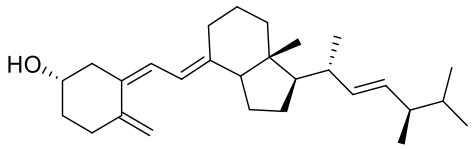

Ergocalciferol (**15**)

Vitamin D_3

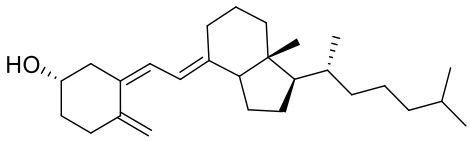

Cholecalciferol (**16**)

Vitamin E

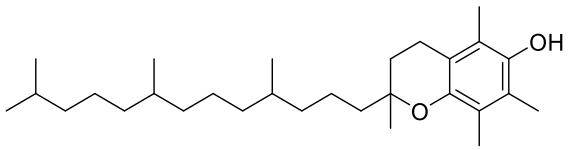

DL-α-tocopherol (**17**)

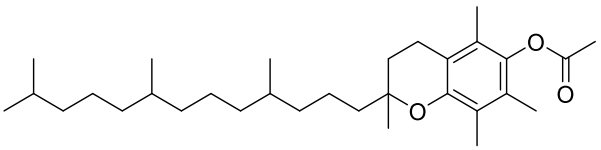

DL-α-tocopherol acetate (**18**)

Scheme 1.18. List of vitamin compounds examined in this study.

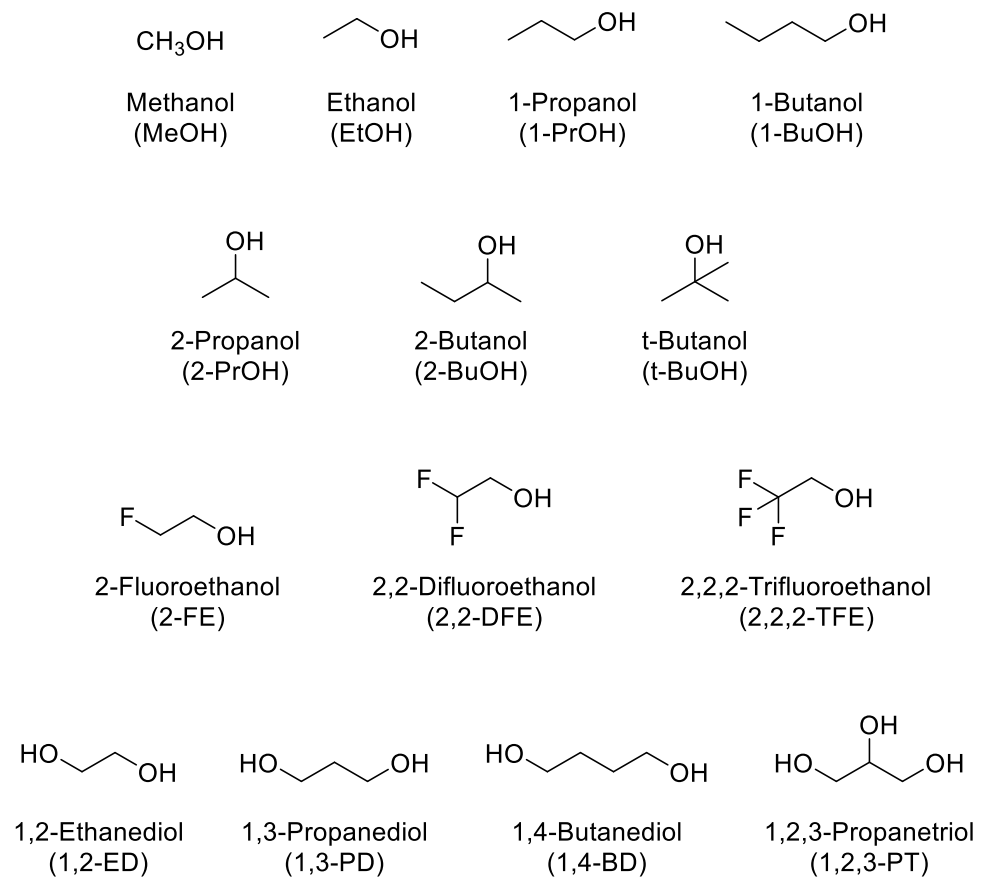

Scheme 1.19. List of alcohols examined in this study.

1.8. General Introduction to Electrochemical Techniques Used

1.8.1. General remarks

As the focus of this thesis primarily revolves around the theme of electrochemistry, the remainder of this chapter will be devoted to the description of some introductory (and pertinent) concepts regarding the electroanalytical techniques utilized in this work. Nevertheless, it should be highlighted that the theory provided herein is not fully comprehensive, and therefore the reader is strongly encouraged to consult advanced texts for a more rigorous understanding of the subject matter.

1.8.2. Voltammetry and some practical considerations

Voltammetric techniques form an important subset of electroanalytical methods in which the relationship between applied voltage and resultant current is examined during an electrochemical process. Such studies can be carried out under stationary conditions (e.g. cyclic voltammetry and linear sweep voltammetry), where diffusion is the only mode of analyte transport from the bulk solution to the electrode surface, or under stirred/hydrodynamic conditions (e.g. flow cell, rotating disk and ring disk electrode voltammetry). Regardless, these experiments are usually performed inside of an electrochemical cell which is typically comprised of three electrodes that are immersed in a solution containing the analyte(s) and a buffer or supporting electrolyte (Figure 1.1). Although, the exact design of the cell (e.g. shape, size, and material) may vary depending on the nature of the experiment, an inlet is usually also present in most electrochemical cells to allow an inert deoxygenating gas (e.g. Ar or N_2) to be passed into the solution [18, 19, 199].

The desired electrochemical reaction (oxidation or reduction) occurs at the working electrode (WE), which is frequently made up of an inert non-conducting material (e.g. PTFE)

that is fitted with a conducting circular disk (e.g. glassy carbon, gold, or platinum) at its base. Conversely, the counter/auxiliary electrode (CE) is typically a platinum or glassy carbon rod/coil which completes the current circuit by allowing the opposite reaction (as compared to the WE) to take place. Notably, the total surface area of the CE is usually similar or larger than that of the WE, so that it does not become a limiting factor in the kinetics of the electrochemical reaction. Depending on the solvent used for the electrochemical measurements, the reference electrode (RE) may be either commercially available saturated calomel or silver-silver chloride electrodes (aqueous solution) or a miniaturized half-cell, such as a silver or platinum wire in the same electrolyte-solvent as the test solution, that is separated from the exterior by a salt bridge, frit, or luggin capillary (non-aqueous solutions). Irrespective of its composition, the RE serves to provide a stable and fixed potential from which the potential at the WE can be monitored, as well as to reduce any IR (ohmic) drop across the cell since effectively no current flows between the WE and RE. IR drop (from solution resistance) is also minimized via the addition of an excess of amount of supporting electrolyte (ca. 100 equivalences), which also serves to suppress the effects of analyte migration. In general, many different solvent systems can be used for electrochemistry (aqueous, organic, protic, or aprotic), however, special attention should be paid to several factors including dielectric constant, dissolving power, useable potential and temperate range, as well as proton activity. Lastly, because the flow of current through the system is dependent on the movement of ions in solution, electrolytes are commonly inert salts with high chemical stability and discharge potential, mobility, and solubility [12, 18, 19, 199, 200].

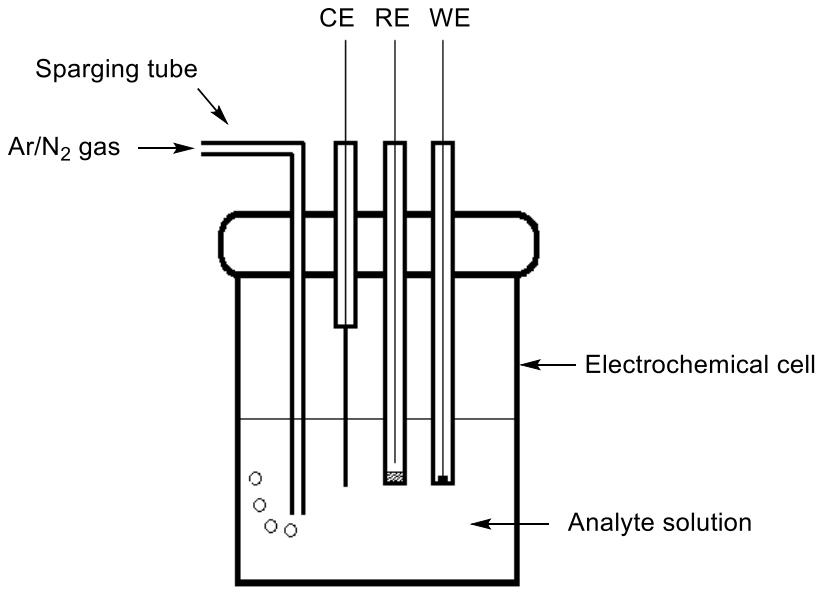

Figure 1.1. Schematic diagram of a typical three-electrode electrochemical cell set-up that is used in voltammetry.

1.8.3. Cyclic voltammetry

Cyclic voltammetry (CV) is a preeminent technique commonly used in the study of redox transformations, where the current response at the WE is recorded as the applied potential is scanned linearly. One of the main benefits of CV is the ability to conveniently perform qualitative analyses of electron transfer reactions, such as the extraction of thermodynamic and kinetic information, the observation of transient intermediates, and/or the examination of stabilities for redox species [17-19, 199].

Figure 1.2a illustrates a potential-time waveform which is representative of a typical triangular excitation signal used during a CV experiment. In this example, the applied potential is cycled linearly between 0.0 V (start and end potentials) and -1.0 V (switching potential), for the redox couple shown below (eq. 1.4).

$$Ox + e^{-} \rightleftharpoons Red \qquad (1.4)$$

Assuming that the reaction is electrochemically and chemically reversible, and that only the oxidized form of the analyte is initially present, the resultant current-potential curve (cyclic voltammogram) is given in Figure 1.2b. It can be observed that as the applied potential is swept more negatively (starting from a position where no faradaic process occurs), there is a corresponding rise in faradaic current measured due to the increasing amounts of the substrate undergoing reaction (reduction). This can be understood from the relationship between the electrode potential and the concentration of reactants present at the electrode surface, which is governed by the Nernst equation shown in eq. 1.5.

$$\mathrm{E} = \mathrm{E}^{\circ} - \frac{\mathrm{RT}}{\mathrm{nF}} \left(\ln \frac{a_{\mathrm{Red}}}{a_{\mathrm{Ox}}} \right) \tag{1.5}$$

where: E° = standard potential of the half-cell; R = ideal gas constant (8.314 J mol^{-1} K^{-1}); T = temperature (K); n = number of moles of electrons transferred in the half-cell reaction; F = Faraday's constant (96485 C mol^{-1}); and $a_{\mathrm{Ox/Red}}$ = activity of Ox/Red species.

As the scan continues further left, however, a cathodic/reduction peak current (I_{pc}) and potential (E_{pc}) is eventually reached. This is because the effects of an expanding Nernst diffusion layer begin to dominate, and the reactants are unable to be transported to the electrode surface from the bulk solution fast enough – resulting in a steady decline of the current intensity thereafter. Regardless, when the potential is varied in the opposite direction for the reverse scan, a similarly shaped anodic/oxidation peak (I_{pc}) can be observed to occur, as the reduced species (that were generated in the forward sweep of the CV) are converted back into the starting material. If the scan was halted at the switching potential (i.e. restricted to only the first half of the cycle), the measurement can be described as linear sweep voltammetry (LSV) instead [17-19, 199].

Notably, in a diffusion controlled, electrochemically reversible reaction as shown in Figure 1.2b, the peak current values are directly proportional to concentration of the analyte and the square root of the scan rate as given by Randles-Sevcik equation (eq. 1.6).

$$I_p = 0.4463nFAC\left(\frac{nFDv}{RT}\right)^{½} \quad (1.6)$$

where: I_p = peak current (A); n = number of moles of electrons transferred; F = Faraday's constant (96 485 C mol^{-1}); A = total electrode surface area (cm^2); C = concentration of analyte (mol cm^{-3}); D = diffusion coefficient of analyte (cm^2 s^{-1}); *v* = scan rate (V s^{-1}); R = ideal gas constant (8.314 J K^{-1} mol^{-1}); and T = temperature (K).

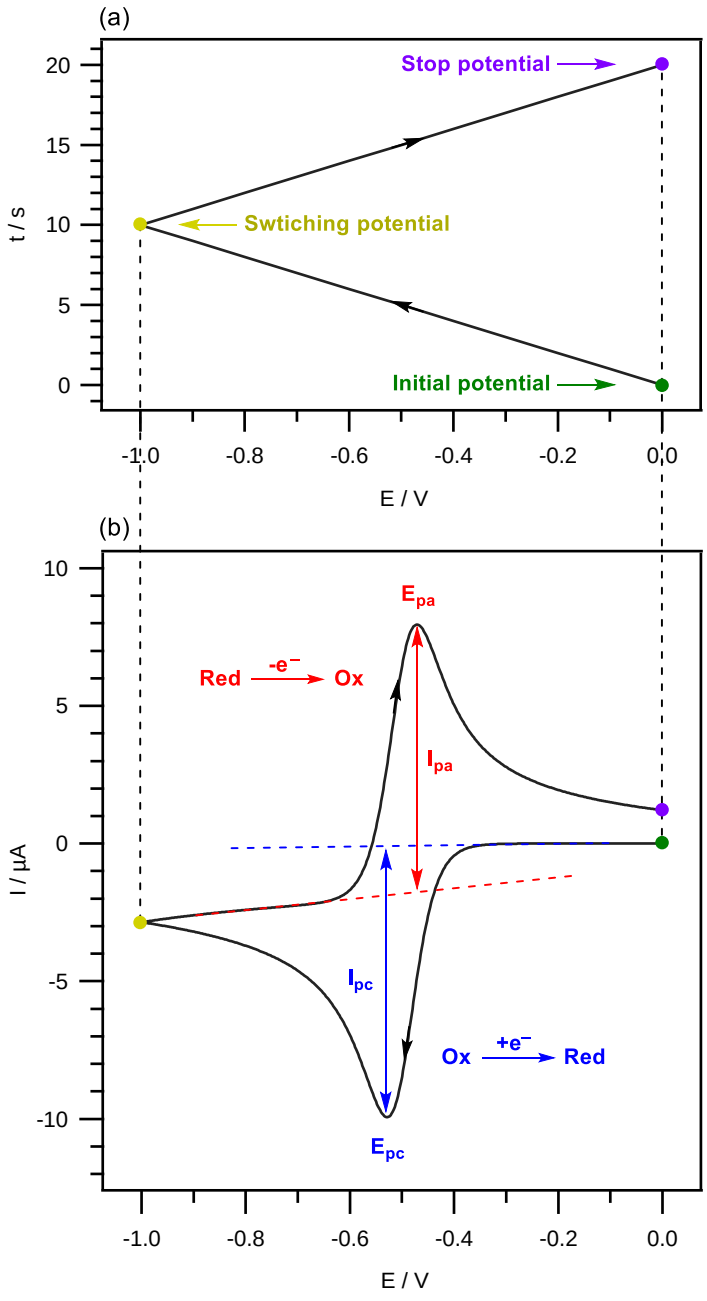

Figure 1.2. (a) Example of a triangular excitation waveform. (b) Example of a cyclic voltammogram obtained for an ideal electrochemically reversible reduction reaction. E_{pa} and I_{pa} = anodic/oxidation peak potential and current, respectively. E_{pc} and I_{pc} = cathodic/reduction peak potential and current, respectively.

1.8.4. Voltammogram conventions

There are two slightly differing standards for the representation of cyclic voltammograms. The International Union for Pure and Applied Chemistry (IUPAC) convention specifies that positive potentials and currents are to be plotted to the right and denote anodic/oxidation reactions, respectively (Figure 1.3), whereas the classical/polarographic convention depicts positive potentials to the left while using positive currents to signify cathodic/reduction processes instead (Figure 1.4). To avoid any confusion, all discussions in this thesis with regards to CV were made in accordance to the IUPAC convention [201].

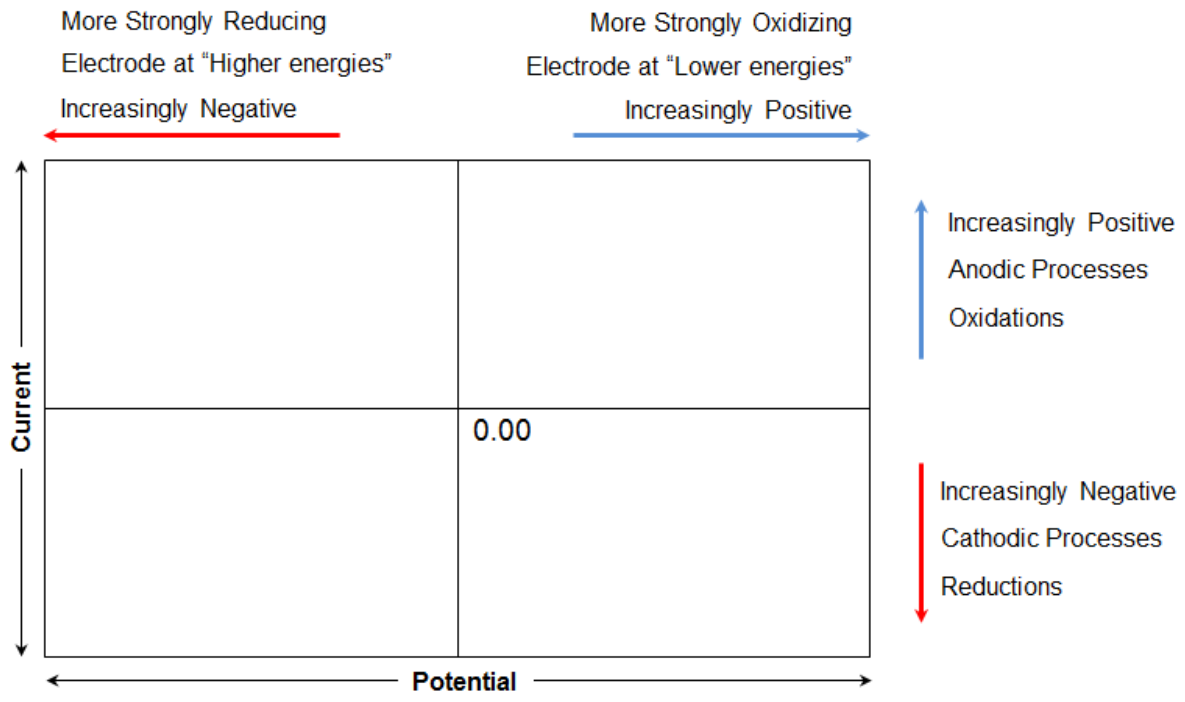

Figure 1.3. International Union for Pure and Applied Chemistry (IUPAC) voltammogram convention.

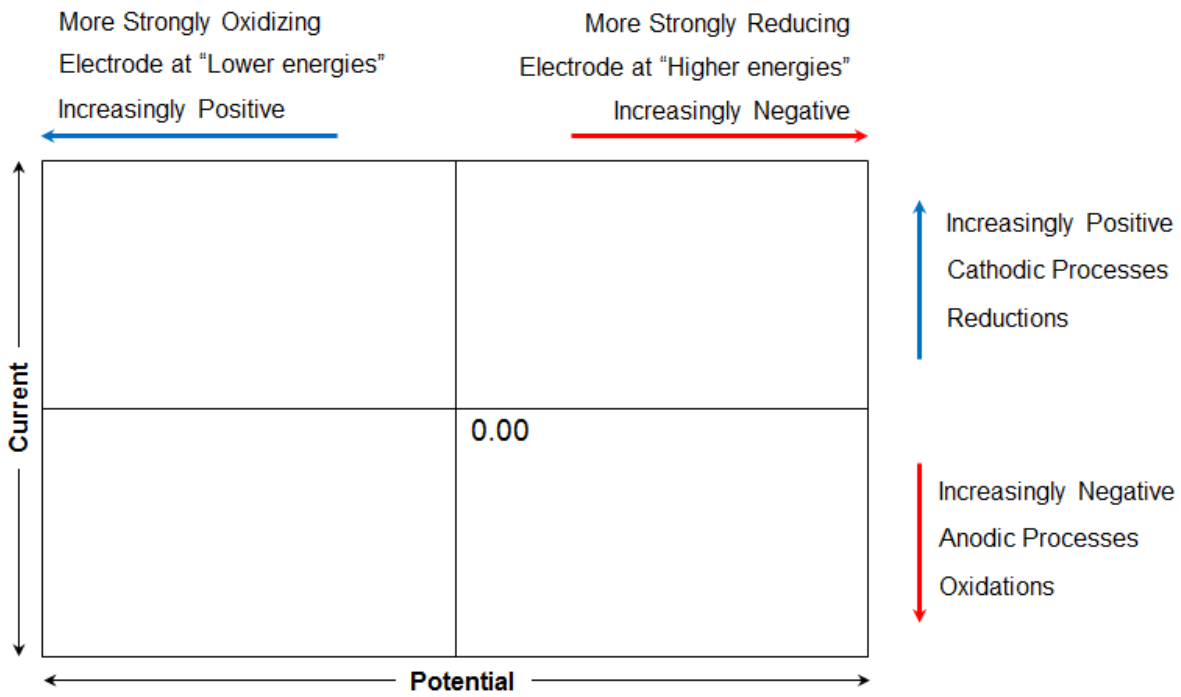

Figure 1.4. Classical/polarographic voltammogram convention.

1.8.5. Electrochemical and chemical reversibility

It is also important to highlight the distinctions between electrochemical reversibility and chemical reversibility, as these terms are frequently used (throughout this thesis) to describe the electrochemical behaviors observed.

Essentially, electrochemical reversibility relates to the rates of the heterogeneous electron transfer between the electrode surface and substrate. For example, electrochemically reversible reactions exhibit fast electron transfer rates that are not complicated by coupled reactions and follow the diagnostic parameters below. In contrast, processes that demonstrate very slow heterogeneous electron transfer rates and/or deviate from the criterion below are deemed to be electrochemically irreversible instead. Electrochemically quasi-reversible reactions fall in between the two abovementioned extremes [17-19, 199].

1. $E_{½} \approx E^{0\prime} = \frac{E_{pa} + E_{pc}}{2}$

2. $\Delta E_p = E_{pa} - E_{pc} = \frac{2.218RT}{nF} \left(\approx \frac{0.057}{n} \text{ V at 298 K}\right)$

3. $\left|\frac{I_{pa}}{I_{pc}}\right| = 1$

4. $\Delta E_{p/2} = E_{½} \pm 1.09\frac{RT}{nF} \left(\approx E_{½} \pm \frac{0028}{n} \text{V at 298 K}\right)$ (positive sign for reduction)

where: $E_{½}$, $E^{0'}$, and $E_{p/2}$ = half-wave, formal, and half-peak potentials, respectively (V); ΔE_p = anodic to cathodic peak-to-peak potential separation (V); E_{pa} and I_{pa} = anodic/oxidation peak potential (V) and current (A), respectively; E_{pc} and I_{pc} = cathodic/reduction peak potential (V) and current (A), respectively; n = number of moles of electrons; R = ideal gas constant (8.314 J K^{-1} mol^{-1}); T = temperature (K); and F = Faraday's constant (96 485 C mol^{-1}).

On the other hand, the term chemical reversibility is specifically used to refer to the stabilities (lifetimes) of the oxidized or reduced species that are generated. Consider the redox reaction in eq. 1.4. A chemically reversible reaction would be one whereby the reduced species Red is stable over the timeframe of the CV experiment (i.e. does not undergo further reaction) and can be fully converted (oxidized) back to the starting material Ox. In this scenario, the voltammogram is expected to present I_{pa} and I_{pc} values of equal magnitudes because the same amount of substrate is involved in the forward reduction and reverse oxidation reaction (Figure 1.5, black solid line). Conversely, if the reduced species were unstable (e.g. Red undergoes a follow-up irreversible chemical reaction after its formation), then the reduction reaction becomes less chemically reversible because there is a smaller amount of Red available for oxidization (back into the starting material) during the return sweep. This subsequently leads to a smaller magnitude of I_{pa}, and a I_{pa}/I_{pc} ratio that deviates from unity (Figure 1.5, green dashed line). Nevertheless, it should be noted that the chemical reversibility of a redox reaction is

sensitive to the duration of the experiment – the same system may appear to be chemically reversible when measured over a short timescale (e.g. fast scan rates) but irreversible when examined over a prolonged period (e.g. slow scan rates) [17-19, 199].

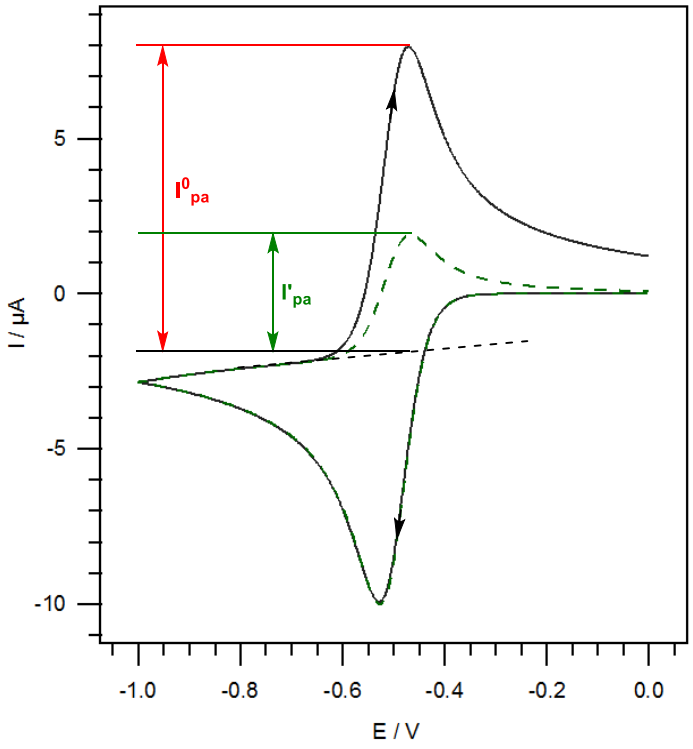

Figure 1.5. Examples of cyclic voltammograms for a (—) chemically reversible reduction process and a (- - -) reduction reaction with limited chemical reversibility. I^0_{pa} and I'_{pa}= anodic/oxidation peak current.

1.8.6. Rotating disk electrode voltammetry

Fundamentally, rotating disk electrode voltammetry (RDEV) differs from CV and LSV in a sense that these experiments are conducted under hydrodynamic conditions (forced convection through rotation of the WE) rather than in a stationary solution. As shown in Figure 1.6, the RDE is typically comprised of a planar conducting disk (e.g. glassy carbon, gold, or platinum) encapsulated inside of a cylindrical shaft made up of inert material (e.g. PTFE), that is rotated

about the axis perpendicular to the disk surface (at speeds of up to several thousand revolutions per min) [17, 18, 199].

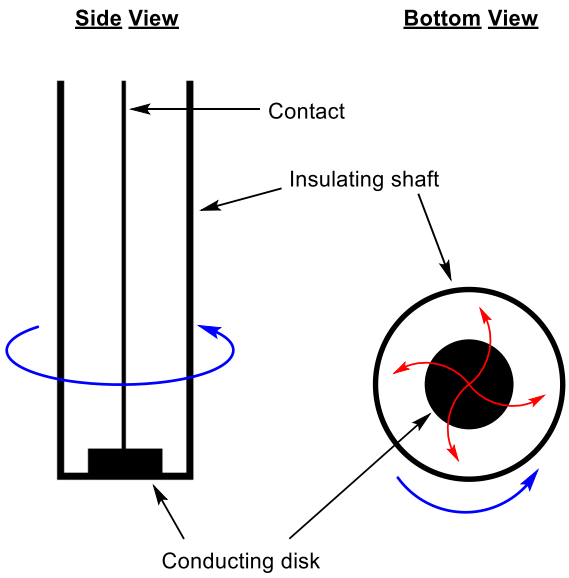

Figure 1.6. Schematic diagram of a rotating disk electrode (adapted from refs. [18, 199]).

Due to the motion of the RDE, a thin layer of fluid adjacent to the electrode surface acquires radical velocity and is dragged away continuously, with the displaced solution being replenished by an upward flow of liquid from the bulk solution. The solution which is immediately next to the electrode surface is separated into a thin stagnant layer (where diffusion is the sole mode of mass transport for the substrate to the electrode surface), and a bulk solution (where forced convection transports the analyte from the bulk region to the edge of the Nernst diffusion layer) [17, 18, 199]. The thickness of this diffusion layer (δ) is inversely proportional to the angular velocity of the electrode as given by eq. 1.7.

$$\delta = 1.61 D^{1/3} \omega^{-1/2} v^{1/6} \qquad (1.7)$$

where: D = diffusion coefficient of the analyte ($cm^2\ s^{-1}$); ω = angular rotation rate of the electrode (rad s^{-1}) (1 rpm = $2\pi/60$ rad s^{-1}); v = kinematic viscosity of the solution ($cm^2\ s^{-1}$).

Because mass transport of the analyte is no longer limited to only diffusion, in RDEV, a sigmoidal shaped current response (versus potential) is usually registered instead (Figure 1.7). In this case, the limiting (maximum) current for an electrochemically reversible system is proportional to the concentration and square root of the angular rotation velocity, as described in the Levich equation (eq. 1.8).

$$I_L = 0.62nFAD^{2/3}\omega^{1/2}v^{-1/6}C \qquad (1.8)$$

where: I_L = mass transport limiting (Levich) current (A); n = number of moles of electrons transferred, F = Faraday's constant (96 485 C mol^{-1}); A = area of the electrode (cm^2); D = diffusion coefficient of the analyte (cm^2 s^{-1}); ω = angular rotation rate of the electrode (rad s^{-1}); v = kinematic viscosity of the solution (cm^2 s^{-1}); and C = concentration of analyte (mol cm^{-3}).

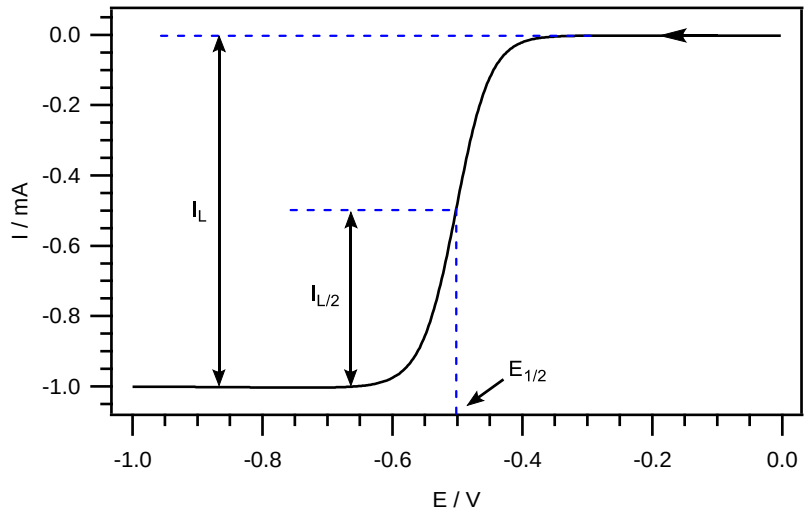

Figure 1.7. Example of a linear sweep voltammogram collected at a rotating disk electrode, for an ideal electrochemically reversible reduction reaction (such as in eq. 1.4). I_L = mass transport limiting current. $E_{½}$ = half-wave potential.

1.8.7. Bulk Controlled Potential Electrolysis

Unlike voltammetric techniques which primarily involve the study of redox reactions without effecting appreciable changes to the concentration of analyte(s) and product(s) in the bulk solution (i.e. only small perturbations are made the electrode surface), bulk/exhaustive electrolysis methods invoke significant alterations to the composition of the sample solution. As such, electrolysis techniques are generally characterized by the use of larger electrodes, currents, and/or voltages over extended durations of a few minutes to several hours. Consequently, these experiments are commonly employed for the preparative scale generation of product(s) (starting from an electroactive substrate), and/or coulometric measurements [13, 14, 17].

More specifically, in coulometric analysis (for bulk electrolysis) the amount of charge necessary for the exhaustive conversion of a known quantity of substrate is measured. This can either be performed under the conditions of a constant cell current (galvanostatic) or a constant electrode potential (potentiostatic). Notably, because the potential of the WE can provide better control over the degree of reaction for an intended redox process, the use of the constant potential electrolysis (CPE) is often more desirable. To ensure a complete analyte conversion, potentials applied during CPE experiments are typically set at slightly larger magnitudes as compared to the formal redox potential of the substrate. Thereafter, by maintaining a fixed potential at the WE, the resultant change in current over time is recorded, from which the corresponding charge values can be derived via an integration of the current-time curve (eq. 1.9). The number of moles of electrons involved in the electrode reaction can be calculated using Faraday's laws of electrolysis (eq. 1.10) [17].

$$Q = \int_0^t I \, dt \tag{1.9}$$

where: Q = charge (coulombs); I = current (A); and t = total electrolysis time (s).

$$n = Q/NF \quad (1.10)$$

where: n = number of moles of electrons transferred; Q = charge (coulombs); N = no. of moles of starting compound; and F = Faraday's constant (96 485 C mol^{-1}).

Figure 1.8 depicts a H-cell that can be used for CPE experiments, such as the one utilized in this thesis. Typically, the two segments are separated from each other by a sintered glass frit or porous membrane, which allows for a passage of ions between the anode and cathode compartments (to close the current circuit) while preventing an undesirable bulk mixing of both solutions. In addition, it is common that identically sized working and counter electrodes with large surface areas (to solution volume ratios) are used and symmetrically arranged to ensure an exhaustive conversion of the substrate can be achieved within a reasonable timeframe, whilst also facilitating an even current distribution across the system. Throughout the experiment, the solutions in both electrode compartments may also be simultaneously de-oxygenated and stirred using bubbles of inert (e.g. Ar or N_2) gas to facilitate the electrolysis [13, 14, 17].

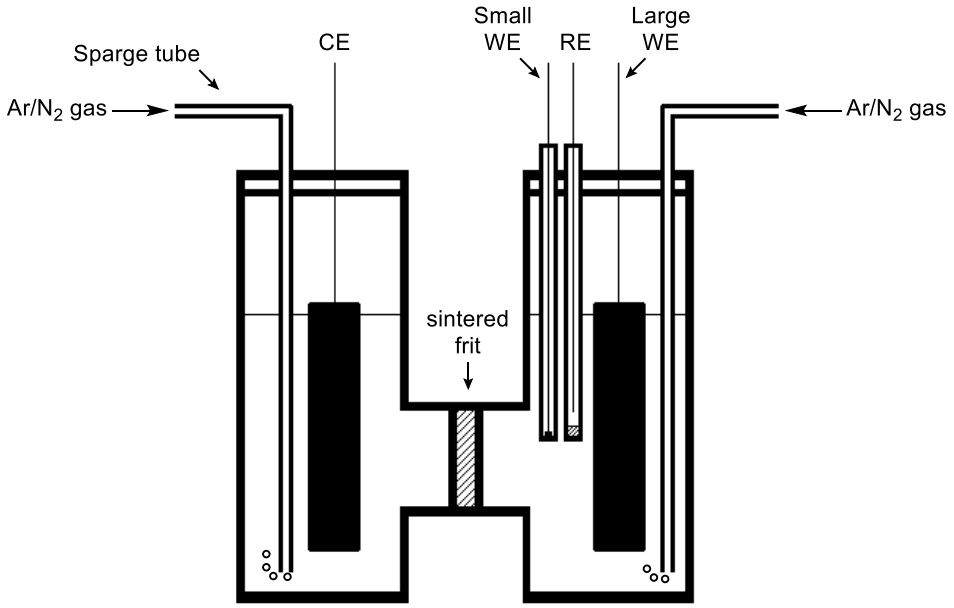

Figure 1.8. Schematic diagram of a typical H-cell set-up used in controlled potential electrolysis experiments.

1.8.8. Digital simulations

Digital simulations can be a useful tool for complementing experimental result during the study electrochemical reactions. This technique is often utilized to test the suitability of a proposed reaction mechanism against the electrochemical responses collected, explore the effects of different redox mechanisms and experimental conditions on the electrochemical behavior, and enable the extraction of quantitative information regarding the thermodynamic and kinetic parameters (e.g. heterogeneous electron transfer rates and equilibrium and forward rate constants) affiliated with the electrochemical and coupled homogeneous processes [202].

In this thesis, this was done through a systematic addition of proposed reaction steps into the software, and then comparing the initially simulated working curve against the experimental data collected. Thereafter, by means of making logical changes to the various thermodynamic and kinetic parameters (or the reaction mechanism if necessary) via a trial and error process, the fitting between both curves can be adjusted, with the match analyzed by examining the fit across prominent features of the experimental and simulated traces (e.g. peak current heights and peak potential positions). It is noteworthy to highlight that instead of simulating a set of data to fit a single cyclic voltammogram impeccably, it is usually more beneficial and essential to match a range of curves moderately. This is because a single voltammogram can sometimes be reproduced using several different mechanisms, with the use of appropriate electrochemical and kinetic values. Hence, it is important that the same set of digitally simulated parameters is able to fit an array of experimental curves obtained under different experimental conditions (e.g. varied scan rates), so as to reduce the likelihood of an inappropriate mechanism being used and increase the credibility of the results obtained [202].

1.9. References

[1] J. Clayden, N. Greeves, S. Warren, P. Wothers, Nucleophilic Addition to the Carbonyl Group, Organic Chemistry, Oxford University Press Inc., New York, US, 2001, pp. 135–150.

[2] J. Clayden, N. Greeves, S. Warren, P. Wothers, Nucleophilic Substitution at the Carbonyl (C=O) Group, Organic Chemistry, Oxford University Press Inc., New York, US, 2001, pp. 279–302.

[3] J. Clayden, N. Greeves, S. Warren, P. Wothers, Nucleophilic Substitution at C=O with Loss of Carbonyl Oxygen, Organic Chemistry, Oxford University Press Inc., New York, USA, 2001, pp. 339–358.

[4] F.A. Carey, R.J. Sundberg, Addition, Condensation and Substitution Reactions of Carbonyl Compounds, Advanced Organic Chemistry. Part A: Structure and Mechanisms, Springer Science+Business Media LLC, New York, USA, 2007, pp. 629–712.

[5] J. Grimshaw, Carbonyl Compounds, in: H. Lung, O. Hammerich (Eds.) Organic Electrochemistry, Marcel Dekker, New York, USA, 2001, pp. 411–434.

[6] J. Ludvík, Reduction of Aldehydes, Ketones, and Azomethines, in: O. Hammerich, B. Speiser (Eds.) Organic Electrochemistry, CRC Press, Boca Raton, Florida, 2016, pp. 1202–1247.

[7] N.G. Connelly, W.E. Geiger, Chemical Redox Agents for Organometallic Chemistry, Chem. Rev., 96 (1996) 877–910.

[8] H.J. Schäfer, Comparison Between Electrochemical Reactions and Chemical Oxidations and Reductions, in: H. Lung, O. Hammerich (Eds.) Organic Electrochemistry, Marcel Dekker, New York, 2001, pp. 207–221.

[9] C. Amatore, Basic Concepts, in: O. Hammerich, B. Speiser (Eds.) Organic Electrochemistry, CRC Press, Boca Raton, Florida, 2016, pp. 4–96.

[10] E.J. Horn, B.R. Rosen, P.S. Baran, Synthetic Organic Electrochemistry: An Enabling and Innately Sustainable Method, ACS Cent. Sci., 2 (2016) 302–308.

[11] H. Tanaka, M. Kuroboshi, S. Torii, Oxidation of Carboxylic Acids and Derivatives, in: O. Hammerich, B. Speiser (Eds.) Organic Electrochemistry, CRC Press, Boca Raton, Florida, 2016, pp. 1267–1307.

[12] A.J. Fry, W.E. Britton, Solvents and Supporting Electrolytes, in: P.T. Kissinger, W.R. Heineman (Eds.) Laboratory Techniques in Electroanalytical Chemistry, Marcel Dekker, New York, USA, 1996, pp. 469–485.

[13] H. Lund, Practical Problems in Electrolysis, in: H. Lung, O. Hammerich (Eds.) Organic Electrochemistry, Marcel Dekker, New York, USA, 2001, pp. 223–292.

[14] J. Jörissen, B. Speiser, Preparative Electrolysis on the Laboratory Scale, in: O. Hammerich, B. Speiser (Eds.) Organic Electrochemistry, CRC Press, Boca Raton, Florida, 2016, pp. 265–330.

[15] K. Chiba, Y. Okada, Electron Transfer–Catalyzed Reactions, in: O. Hammerich, B. Speiser (Eds.) Organic Electrochemistry, CRC Press, Boca Raton, Florida, 2016, pp. 531–555.

[16] R.D. Webster, Electrochemical Modeling of Biological Process, in: O. Hammerich, B. Speiser (Eds.) Organic Electrochemistry, CRC Press, Boca Raton, Florida, 2016, pp. 1543–1567.

[17] A.J. Bard, L.R. Faulkner, Electrochemical Methods: Fundamentals and Applications, 2nd ed., Wiley, New York, USA, 2001.

[18] J. Wang, Analytical Electrochemistry, 3rd ed., Wiley-VCH, New Jersey, 2006.

[19] O. Hammerich, B. Speiser, Techniques for Studies of Electrochemical Reactions in Solution, in: O. Hammerich, B. Speiser (Eds.) Organic Electrochemistry, CRC Press, Boca Raton, Florida, 2016, pp. 98–168.

[20] R.D. Webster, New Insights into the Oxidative Electrochemistry of Vitamin E, Acc. Chem. Res., 40 (2007) 251-257.

[21] R.D. Webster, Voltammetry of the Liposoluble Vitamins (A, D, E and K) in Organic Solvents, Chem. Rec., 12 (2012) 188–200.

[22] R.J. McMahon, Biotin in Metabolism and Molecular Biology, Annu. Rev. Nutr., 22 (2002) 221–239.

[23] L.R. McDowell, Biotin, Vitamins in Animal and Human Nutrition, Iowa State University Press, Ames, 2008, pp. 445–478.

[24] J. Zempleni, S.S.K. Wijeratne, Y.I. Hassan, Biotin, BioFactors, 35 (2009) 36–46.

[25] J. Zempleni, S.S.K. Wijeratne, T. Kuroishi, Biotin, in: J.W. Erdman Jr., I.A. Macdonald, S.H. Zeisel (Eds.) Present Knowledge in Nutrition, Wiley-Blackwell, Chichester, 2012, pp. 359–374.

[26] J.-J. Houri, P. Mougenot, F. Guyon, B. Do, Function and Effects of Biotin, in: V.R. Preedy (Ed.) B Vitamins and Folate: Chemistry, Analysis, Function and Effects, Royal Society of Chemistry, Cambridge, UK, 2013, pp. 716–733.

[27] J. Zempleni, W.K. Eng, M.P. Singh, S. Baier, Biochemistry of Biotin, in: V.R. Preedy (Ed.) B Vitamins and Folate: Chemistry, Analysis, Function and Effects, Royal Society of Chemistry, Cambridge, UK, 2013, pp. 146–157.

[28] M.A. Boas, The Effect of Desiccation upon the Nutritive Properties of Egg-white, Biochem. J., 21 (1927) 712–724.

[29] F. Kögl, B. Tönnis, Über das Bios-Problem. Darstellung von krystallisiertem Biotin aus Eigelb., Hoppe-Seyler´s Zeitschrift für Physiologische Chemie, 242 (1936) 43–73.

[30] V. du Vigneaud, D.B. Melville, K. Folkers, D.E. Wolf, R. Mozingo, J.C. Keresztesy, S.A. Harris, The Structure of Biotin: A Study of Desthiobiotin, J. Biol. Chem., 146 (1942) 475–485.

[31] S.A. Harris, Synthetic Biotin, Science, 97 (1943) 447–448.

[32] D.B. McCormick, L.D. Wright, The Metabolism of Biotin and Analogues, in: M. Florkin, E.H. Stotz (Eds.) Metabolism of Vitamins and Trace Elements, Elsevier, Amsterdam, The Netherlands, 1971, pp. 81–110.

[33] J. Zempleni, D.B. McCormick, D.M. Mock, Identification of Biotin Sulfone, Bis-Norbiotin Methyl Ketone, and Tetranorbiotin-*I*-Sulfoxide in Human Urine, Am. J. Clin. Nutr., 65 (1997) 508–511.

[34] H.M. Lee, L.D. Wright, D.B. McCormick, Metabolism of Carbonyl-labeled [14C] Biotin in The Rat, J. Nutr., 102 (1972) 1453–1464.

[35] H.M. Said, Cell and Molecular Aspects of Human Intestinal Biotin Absorption, J. Nutr., 139 (2009) 158–162.

[36] D.M. Monk, Biotin, in: M.L. Brown (Ed.) Present Knowledge in Nutrition, International Life Sciences Institute-Nutrition Foundation, Washington, DC, 1990, pp. 189–207.

[37] L. Sweetman, W.L. Nyhan, Inheritable Biotin-Treatable Disorders and Associated Phenomena, Annu. Rev. Nutr., 6 (1986) 317–343.

[38] J. Zempleni, Y.I. Hassan, S.S.K. Wijeratne, Biotin and Biotinidase Deficiency, Expert Rev. Endocrinol. Metab., 3 (2008) 715–724.

[39] N.M. Green, Avidin and Streotavidin, in: M. Wilchek (Ed.) Methods Enzymol., Academic Press, London, 1990, pp. 51–67.

[40] E. Livaniou, D. Costopoulou, I. Vassiliadou, L. Leondiadis, J.O. Nyalala, D.S. Ithakissios, G.P. Evangelatos, Analytical Techniques for Determining Biotin, J. Chromatogr. A, 881 (2000) 331–343.

[41] R. Kizek, M. Masarik, K.J. Kramer, D. Potesil, M. Bailey, J.A. Howard, B. Klejdus, R. Mikelova, V. Adam, L. Trnkova, F. Jelen, An Analysis of Avidin, Biotin and Their Interaction at Attomole Levels by Voltammetric and Chromatographic Techniques, Anal. Bioanal. Chem., 381 (2005) 1167–1178.

[42] J.-A.A. Ho, Y.-H. Lai, L.-C. Wu, S.-H. Liang, S.-L. Wong, J.-J. Liou, Analysis of Biotin (Vitamin B_7) and Folic Acid (Vitamin B_9): A Focus on Immunosensor Development with Liposomal Amplification, in: V.R. Preedy (Ed.) B Vitamins and Folate : Chemistry, Analysis, Function and Effects, Royal Society of Chemistry, Cambridge, UK, 2013, pp. 353–376.

[43] D.C. Woollard, H.E. Indyk, Biotin Analysis in Dairy Products, in: V.R. Preedy (Ed.) B Vitamins and Folate: Chemistry, Analysis, Function and Effects, Royal Society of Chemistry, Cambridge, UK, 2013, pp. 377–395.

[44] M. Masarik, R. Kizek, K.J. Kramer, S. Billova, M. Brazdova, J. Vacek, M. Bailey, F. Jelen, J.A. Howard, Application of Avidin-Biotin Technology and Adsorptive Transfer Stripping Square-Wave Voltammetry for Detection of DNA Hybridization and Avidin in Transgenic Avidin Maize, Anal. Chem., 75 (2003) 2663–2669.

[45] L. Havran, S. Billová, E. Palecek, Electroactivity of Avidin and Streptavidin. Avidin Signals at Mercury and Carbon Electrodes Respond to Biotin Binding, Electroanalysis, 16 (2004) 1139–1148.

[46] C.M. Yam, M. Deluge, D. Tang, A. Kumar, C. Cai, Preparation, Characterization, Resistance to Protein Adsorption, and Specific Avidin-Biotin Binding of Poly(Amidoamine) Dendrimers Functionalized with Oligo(Ethylene Glycol) on Gold, J. Colloid Interface Sci., 296 (2006) 118–130.

[47] A. Bonanni, M.I. Pividori, M.d. Valle, Application of the Avidin-Biotin Interaction to Immobilize DNA in the Development of Electrochemical Impedance Genosensors, Anal. Bioanal. Chem., 389 (2007) 851–861.

[48] W. Gao, H. Dong, J. Lei, H. Ji, H. Ju, Signal Amplification of Streptavidin-Horseradish Peroxidase Functionalized Carbon Nanotubes for Amperometric Detection of Attomolar DNA, Chem. Commun., 47 (2011) 5220–5222.

[49] Z. Wang, L. Liu, Y. Xu, L. Sun, G. Li, Simulation and Assay of Protein Biotinylation with Electrochemical Technique, Biosensors Bioelectron., 26 (2011) 4610–4613.

[50] S. Takahashi, K. Sato, J.-I. Anzai, Layer-By-Layer Construction of Protein Architectures through Avidin-Biotin and Lectin-Sugar Interactions for Biosensor Applications, Anal. Bioanal. Chem., 402 (2012) 1749–1758.

[51] F. Schwizer, V. Köhler, M. Dürrenberger, L. Knörr, T.R. Ward, Genetic Optimization of the Catalytic Efficiency of Artificial Imine Reductases Based on Biotin-Streptavidin Technology, ACS Catal., 3 (2013) 1752–1755.

[52] H.S. Yoon, J. Lim, S.U. Son, D.-H. Kim, I. Song, S.C. Jun, Biotin-Streptavidin Detection with a Graphene-Oxide Supported Radio-Frequency Resonator, Appl. Phys. Lett., 102 (2013) 1–4.

[53] A. Serna, J. Vera, D. Marin, Polarographic Behavior of Biotin, J. Electroanal. Chem. Interfacial Electrochem., 45 (1973) 156–159.

[54] D. Marin, J. Vera, A. Serna, Polarographic Reduction of Biotin and Its Mechanism, An. Quim., 73 (1977) 1243–1246.

[55] J. Gruenwald, J. Freder, N. Armbruester, Cinnamon and Health, Crit. Rev. Food Sci. Nutr., 50 (2010) 822–834.

[56] J. Thomas, K.M. Kuruvilla, Cinnamon, in: K.V. Peter (Ed.) Handbook of Herbs and Spices, Woodhead Publishing Limited, UK, 2012, pp. 182–196.

[57] R.K. Maheshwari, A.K. Chauhan, A. Gupta, S. Sharma, Cinnamon: An Imperative Spice For Human Comfort, Int. J. Pharm. Res. Bio-Sci., 2 (2013) 131–145.

[58] S. Shreaz, W.A. Wani, J.M. Behbehani, V. Raja, M. Irshad, M. Karched, I. Ali, W.A. Siddiqi, L.T. Hun, Cinnamaldehyde and its Derivatives, A Novel Class of Antifungal Agents, Fitoterapia, 112 (2016) 116–131.

[59] J. Cocchiara, C.S. Letizia, J. Lalko, A. Lapczynski, A.M. Api, Fragrance Material Review on Cinnamaldehyde, Food Chem. Toxicol., 43 (2005) 867–923.

[60] S. Lungarini, F. Aureli, E. Coni, Coumarin and Cinnamaldehyde in Cinnamon Marketed in Italy: A Natural Chemical Hazard?, Food Addit. Contam., Part A, 25 (2008) 1297–1305.

[61] R.G. Eilerman, Cinnamic Acid, Cinnamaldehyde, and Cinnamyl Alcohol, Kirk-Othmer Encyclopedia of Chemical Technology, Wiley, New York, USA, 2000.

[62] S. Gowder, H. Devaraj, A Review of the Nephrotoxicity of the Food Flavor Cinnamaldehyde, Curr. Bioact. Compd., 6 (2010) 106–117.

[63] A.R. Sathiya Priya, S. Muralidharan, S. Velmurugan, G. Venkatachari, Corrosion Inhibitor for the Chemical Decontamination of Primary Coolant Systems of Nuclear Power Plants, Mater. Chem. Phys., 110 (2008) 269–275.

[64] Y.G. Avdeev, Y.I. Kuznetsov, A.K. Buryak, Inhibition of Steel Corrosion by Unsaturated Aldehydes in Solutions of Mineral Acids, Corros. Sci., 69 (2013) 50–60.

[65] G. Cabello, G.P. Funkhouser, J. Cassidy, C.E. Kiser, J. Lane, A. Cuesta, CO and *trans*-Cinnamaldehyde as Corrosion Inhibitors of I825, L80-13Cr and N80 Alloys in Concentrated HCl Solutions at High Pressure and Temperature, Electrochim. Acta, 97 (2013) 1–9.

[66] P.S. Babu, S. Prabuseenivasan, S. Ignacimuthu, Cinnamaldehyde–A Potential Antidiabetic Agent, Phytomedicine, 14 (2007) 15–22.

[67] A. Sangal, Role of Cinnamon As Beneficial Antidiabetic Food Adjunt: A Review, Adv. Appl. Sci. Res., 2 (2011) 440–450.

[68] L.S.M. Ooi, Y. Li, S.-L. Kam, H. Wang, E.Y.L. Wong, V.E.C. Ooi, Antimicrobial Activities of Cinnamon Oil and Cinnamaldehyde from the Chinese Medicinal Herb *Cinnamomum cassia* Blume, Am. J. Chin. Med., 34 (2006) 511–522.

[69] N. Yossa, J. Patel, D. Macarisin, P. Millner, C. Murphy, G. Bauchan, Y.M. Lo, Antibacterial Activity of Cinnamaldehyde and Sporan against Escherichia coli O157:H7 and Salmonella, J. Food Process. Preserv., 38 (2014) 749–757.

[70] J.-H. Zhang, L.-Q. Liu, Y.-L. He, W.-J. Kong, S.-A. Huang, Cytotoxic Effect of *trans*-Cinnamaldehyde on Human Leukemia K562 Cells, Acta Pharmacol. Sin., 31 (2010) 861–866.

[71] L. Zhou, Y. Lu, G. Yang, J. Wu, Research on Tumorigenicity of Cinnamaldehyde in Melanoma Cell Lines and Its Mechanism, Tumor Biol., 35 (2014) 5717–5722.

[72] S.-H. Hong, I.A. Ismail, S.-M. Kang, D.C. Han, B.-M. Kwon, Cinnamaldehydes in Cancer Chemotherapy, Phytother. Res., 30 (2016) 754–767

[73] M.B. Gholivand, F. Ahmadi, Simultaneous Determination of trans-Cinnamaldehyde and Benzaldehyde in Different Real Samples by Differential Pulse Polarography and Study of Heat Stability of trans-Cinnamaldehyde, Anal. Lett., 41 (2008) 3324–3341.

[74] Y.-Q. Li, D.-X. Kong, H. Wu, Analysis and Evaluation of Essential Oil components of Cinnamon barks using GC–MS and FTIR spectroscopy, Ind. Crops Prod., 41 (2013) 269–278.

[75] H. Zhao, Q. Yang, Y. Xie, J. Sun, H. Tu, W. Cao, S. Wang, Simultaneous Determination of Cinnamaldehyde and Its Metabolite in Rat Tissues by Gas Chromatography–Mass Spectrometry, Biomed. Chromatogr., 29 (2015) 182–187.

[76] H. Zhao, Y. Xie, Q. Yang, Y. Cao, H. Tu, W. Cao, S. Wang, Pharmacokinetic study of cinnamaldehyde in Rats by GC–MS After Oral and Intravenous Administration, J. Pharm. Biomed. Anal., 89 (2014) 150–157.

[77] S.A. Suzi, A. El-Makawy, Could Cinnamaldehyde Be Harmful? Histological, Cytogenetical and Biochemical Studies on its Effect on Some Organs of Mice, Egypt. J. Histol., 30 (2007) 447–464.

[78] I.A. Korshunov, Z.B. Kuznetsova, L.N. Sazanova, A.S. Kirillova, Polarographic Determination of Aromatic Ketones and Aldehydes, Zavod. Lab., 16 (1950) 144– 146.

[79] C. Prévost, P. Souchay, J. Chauvelier, Comparison of the Chemical Reactivity of Ethylenic and Acetylenic Linkages, Bull. Soc. Chim. Fr., (1951) 714–724.

[80] D.M. Coulson, W.R. Crowell, Polarography of Carbonyl Compounds. I. Linear Unsaturated Conjugated Molecules J. Am. Chem. Soc., 74 (1952) 1290–1294.

[81] R.N. Schmid, E. Heilbronner, Polarographic Reduction of Aromatic Aldehydes, Helv. Chim. Acta, 37 (1954) 1453–1456.

[82] D. Barnes, P. Zuman, Polarographic Reduction of Cinnamaldehyde; Comparison with 3-Phenylpropionaldehyde and Phenylpropargylaldehyde, J. Electroanal. Chem. Interfacial Electrochem., 16 (1968) 575–582.

[83] D. Barnes, P. Zuman, Polarographic Reduction of Aldehydes and Ketones. Part 7.—Behaviour of Cinnamaldehyde at higher pH-Values., T. Faraday Soc., 65 (1969) 1681–1689.

[84] D. Barnes, P. Zuman, Polarographic Reduction of Aldehydes and Ketones. Part 6.—Behaviour of Cinnamaldehyde at lower pH-Values., T. Faraday Soc., 65 (1969) 1668–1680.

[85] P. Zuman, J. Ludvík, The Use of Controlled Potential Electrolysis with a Dropping Mercury Electrode in Elucidation of Organic Electroreduction Mechanisms, Electroanalysis, 12 (2000) 879–888.

[86] P. Zuman, Aspects of Electrochemical Behavior of Aldehydes and Ketones in Protic Media, Electroanalysis, 18 (2006) 131–140.

[87] K. Sasaki, K. Yanagisawa, N. Miura, Effect of Magnesium Ions on the Electrolytic Reduction of Cinnamaldehyde in Acetonitrile, Nippon Kagaku Kaishi, (1976) 1558–1564.

[88] L.A. Powell, R.M. Wightman, Mechanism of Electrodimerization of Retinal and Cinnamaldehyde, J. Electroanal. Chem. Interfacial Electrochem., 117 (1981) 321–333.

[89] F. Barba, J.L. de la Fuente, M. Galakhov, Electrohydrodimerization of trans-Cinnamaldehyde, Tetrahedron, 53 (1997) 5831–5838.

[90] E.S. Beach, B.R. Weeks, R. Stern, P.T. Anastas, Plastics Additives and Green Chemistry, Pure Appl. Chem., 85 (2013) 1611–1624.

[91] D.-W. Gao, Z.-D. Wen, Phthalate Esters in the Environment: A Critical Review of their Occurrence, Biodegradation, and Removal during Wastewater Treatment Processes, Sci. Total Environ., 541 (2016) 986–1001.

[92] P. Ventrice, D. Ventrice, E. Russo, G. De Sarro, Phthalates: European Regulation, Chemistry, Pharmacokinetic and Related Toxicity, Environ. Toxicol. Pharmacol., 36 (2013) 88–96.

[93] J. Sampson, D. de Korte, DEHP-Plasticised PVC: Relevance to Blood Services, Transfusion Med., 21 (2011) 73–83.

[94] R.E. Dodson, M. Nishioka, L.J. Standley, L.J. Perovich, J.G. Brody, R.A. Rudel, Endocrine Disruptors and Asthma-Associated Chemicals in Consumer Products, Environ. Health Perspect., 120 (2012) 935–943.

[95] J. Yang, Y. Li, Y. Wang, J. Ruan, J. Zhang, C. Sun, Recent Advances in Analysis of Phthalate Esters in Foods, Trends Environ. Anal. Chem., 72 (2015) 10–26.

[96] I. Al-Saleh, R. Elkhatib, Screening of Phthalate Esters in 47 Branded Perfumes, Environ. Sci. Pollut. Res., 23 (2016) 455–468.

[97] H.C. Erythropel, M. Maric, J.A. Nicell, R.L. Leask, V. Yargeau, Leaching of the Plasticizer Di(2-Ethylhexyl)Phthalate (DEHP) from Plastic Containers and the Question of Human Exposure, Appl. Microbiol. Biotechnol., 98 (2014) 9967–9981.

[98] S. Net, R. Sempéré, A. Delmont, A. Paluselli, B. Ouddane, Occurrence, Fate, Behavior and Ecotoxicological State of Phthalates in Different Environmental Matrices, Environ. Sci. Technol., 49 (2015) 4019–4035.

[99] S. Magdouli, R. Daghrir, S.K. Brar, P. Drogui, R.D. Tyagi, Di 2-Ethylhexylphtalate in the Aquatic and Terrestrial Environment: A Critical Review, J. Environ. Manage., 127 (2013) 36–49.

[100] S. Net, A. Delmont, R. Sempéré, A. Paluselli, B. Ouddane, Reliable Quantification of Phthalates in Environmental Matrices (Air, Water, Sludge, Sediment and Soil): A Review, Sci. Total Environ., 515–516 (2015) 162–180.

[101] U. Heudorf, V. Mersch-Sundermann, J. Angerer, Phthalates: Toxicology and Exposure, Int. J. Hyg. Environ. Health, 210 (2007) 623–634.

[102] T. Cirillo, R.A. Cocchieri, Phthalates in Foods, in: M. Rose, A. Fernandes (Eds.) Persistent Organic Pollutants and Toxic Metals in Foods, Woodhead Publishing Limited, Sawston, Cambridge, 2013, pp. 334–366.

[103] S. Shi, B. Zhao, Modeled Exposure Assessment via Inhalation and Dermal Pathways to Airborne Semivolatile Organic Compounds (SVOCs) in Residences, Environ. Sci. Technol., 48 (2014) 5691–5699.

[104] M. Wittassek, J. Angerer, Phthalates: Metabolism and Exposure, Int. J. Androl., 31 (2008) 131–138.

[105] M. Ejaredar, E.C. Nyanza, K.T. Eycke, D. Dewey, Phthalate Exposure and Childrens Neurodevelopment: A Systematic Review, Environ. Res., 142 (2015) 51–60.

[106] G. Latini, Monitoring Phthalate Exposure in Humans, Clin. Chim. Acta, 361 (2005) 20–29.

[107] J.A. Tickner, T. Schettler, T. Guidotti, M. McCally, M. Rossi, Health Risks Posed by Use of Di-2-Ethylhexyl Phthalate (DEHP) in PVC Medical Devices: A Critical Review, Am. J. Ind. Med., 39 (2001) 100–111.

[108] J.C. Caldwell, DEHP: Genotoxicity and Potential Carcinogenic Mechanisms—A Review, Mutat. Res., 751 (2012) 82–157.

[109] X. Li, E.F. Fang, M. Scheibye-Knudsen, H. Cui, L. Qiu, J. Li, Y. He, J. Huang, V.A. Bohr, T.B. Ng, H. Guo, Di-(2-Ethylhexyl) Phthalate Inhibits DNA Replication Leading to HyperPARylation, SIRT1 Attenuation, and Mitochondrial Dysfunction in the Testis, Sci. Rep., 4 (2014) 6434–6442.

[110] A.I. Zia, M.S.A. Rahman, S.C. Mukhopadhyay, P.-L. Yu, I.H. Al-Bahadly, C.P. Gooneratne, J. Kosel, T.-S. Liao, Technique for Rapid Detection of Phthalates in Water and Beverages, J. Food Eng., 116 (2013) 515–523.

[111] H.-B. Noh, N.G. Gurudatt, M.-S. Won, Y.-B. Shim, Analysis of Phthalate Esters in Mammalian Cell Culture Using a Microfluidic Channel Coupled with an Electrochemical Sensor, Anal. Chem., 87 (2015) 7069–7077.

[112] S. Xiong, J. Cheng, L. He, D. Cai, X. Zhang, Z. Wu, Fabrication of β-Cyclodextrin /Graphene/1,10-Diaminodecane Composite on Glassy Carbon Electrode and Impedimetric Method for Di(2-Ethylhexyl) Phthalate Determination, J. Electroanal. Chem., 743 (2015) 18–24.

[113] M. Zhang, W. Hong, X. Wu, Y. Zhang, F. Li, S.-Q. Zhao, A Highly Sensitive and Direct Competitive Enzyme-Linked Immunosorbent Assay for the Detection of Di-(2-Ethylhexyl) Phthalate (DEHP) in Infant Supplies, Anal. Methods, 7 (2015) 5441–5446.

[114] H.M. Koch, R. Preuss, J. Angerer, Di(2-Ethylhexyl)Phthalate (DEHP): Human Metabolism and Internal Exposure – An Update and Latest Results, Int. J. Androl., 29 (2006) 155–165.

[115] H. Frederiksen, N.E. Skakkebæk, A.-M. Andersson, Metabolism of Phthalates in Humans, Mol. Nutr. Food Res., 51 (2007) 899 – 911.

[116] L. Yaghjyan, N.P. Carlsson, G.L. Ghita, S.-H. Chang, Associations of Individual Characteristics and Lifestyle Factors with Metabolism of Di-2-Ethylhexyl Phthalate in NHANES 2001-2012, Environ. Res., 149 (2016) 23–31.

[117] V.G. Mairanovsky, Electro-Deprotection—Electrochemical Removal of Protecting Groups, Angew. Chem. Int. Ed., 15 (1976) 281–292.

[118] R. Seeber, F. Magno, G. Bontempelli, G.A. Mazzocchin, An Investigation on the Cathodic Behavior of Phenylbenzoate in Dimethylformamide Solution, J. Electroanal. Chem., 72 (1976) 219–228.

[119] L. Kistenbrüegger, P. Mischke, J. Voβ, G. Wiegand, Electrochemical Reduction of Organic Compounds. 1. Condensation Reactions of Acetonitrile using Electrochemically Generated Bases, Liebigs Ann. Chem., (1980) 461–471.

[120] J.H. Wagenknecht, R.D. Goodin, P.J. Kinlen, F.E. Woodard, Decomposition of Benzoate Ester Radical Anions, J. Electrochem. Soc., 131 (1984) 1559–1565.

[121] J. Masnovi, Radical Anions of Esters of Carboxylic Acids. Effects of Structure and Solvent on Unimolecular Fragmentations, J. Am. Chem. Soc., 111 (1989) 9081–9089.

[122] M. Hromadová, P. Mořkovská, L. Pospíšil, S. Giannarelli, Decomposition Reactions of Bifenox Anion Radical Involving Intramolecular Electron Transfer, J. Electroanal. Chem., 582 (2005) 156–164.

[123] K. Lam, I.E. Markó, Using Toluates as Simple and Versatile Radical Precursors, Org. Lett., 10 (2008) 2773–2776.

[124] R. Baron, N.M. Kershaw, T.J. Donohoe, R.G. Compton, Quantitative Voltammetry of the Reduction of Methyl Benzoate in THF reveals Strong Ion Pairing of the Radical Anion with Tetra-*n*-Butyl Cations, J. Phys. Org. Chem., 22 (2009) 247–253.

[125] K. Lam, I.E. Markó, Organic Electrosynthesis using Toluates as Simple and Versatile Radical Precursors, Chem. Commun., (2009) 95–97.

[126] K. Lam, I.E. Markó, Toluates: Unexpectedly Versatile Reagents, Tetrahedron, 65 (2009) 10930–10940.

[127] R.D. Webster, A.M. Bond, R.G. Compton, Voltammetric and EPR Spectroscopic Studies Associated with the Reduction of Pyridine and Benzene-Substituted n-Alkyl Esters and Thioic S-Esters in Aprotic Solvents, J. Phys. Chem., 100 (1996) 10288–10297.

[128] R.D. Webster, A.M. Bond, Electrochemical Reduction of Pyridine- and Benzene-Substituted *n*-Alkyl Esters and Thioic *S*-Esters in Acetonitrile, J. Org. Chem., 62 (1997) 1779–1787.

[129] R.D. Webster, A.M. Bond, Different Mechanisms for the Reaction of Disubstituted Aromatic Esters and Thioic *S*-Esters with Electrochemically Generated Superoxide, J. Chem. Soc., Perkin Trans. 2, (1997) 1075–1079.

[130] R.D. Webster, *In situ* Electrochemical-ATR-FTIR Spectroscopic Studies on Solution Phase Carboxylate Radical Anions, J. Chem. Soc., Perkin Trans. 2, (2002) 1882–1888.

[131] V.I. Lushchak, Free Radicals, Reactive Oxygen Species, Oxidative Stress and its Classification, Chem.-Biol. Interact., 224 (2014) 164–175.

[132] S.B. Nimse, D. Pal, Free Radicals, Natural Antioxidants, and their Reaction Mechanisms, RSC Adv., 5 (2015) 27986–28006.

[133] G. Banfi, E.L. Iorio, M.M. Corsi, Oxidative Stress, Free Radicals and Bone Remodeling, Clin. Chem. Lab. Med., 46 (2008) 1550–1555.

[134] J.M. Gebicki, Oxidative Stress, Free Radicals and Protein Peroxides, Arch. Biochem. Biophys., 595 (2016) 33–39.

[135] P. Sharma, A.B. Jha, R.S. Dubey, M. Pessarakli, Reactive Oxygen Species, Oxidative Damage, and Antioxidative Defense Mechanism in Plants under Stressful Conditions, J. Bot., 2012 (2012) 1–26.

[136] S. Bhattacharya, Reactive Oxygen Species and Cellular Defense System, in: V. Rani, U.C.S. Yadav (Eds.) Free Radicals in Human Health and Disease, Springer India, India, 2015, pp. 17–29.

[137] H. B, Antioxidants and Human Disease: A General Introduction, Nutr. Rev., 55 (1997) S44–S49.

[138] T.P. Stein, Space Flight and Oxidative Stress, Nutrition, 18 (2002) 867–871.

[139] N. Husain, A. Kumar, Reactive Oxygen Species and Natural Antioxidants: A Review, Adv. Bio Res., 3 (2012) 164–175.

[140] M. Hayyan, M.A. Hashim, I.M. AlNashef, Superoxide Ion: Generation and Chemical Implications, Chem. Rev., 116 (2016) 3029–3085.

[141] J.P. Bolaños, M.A. Moro, I. Lizasoain, A. Almeida, Mitochondria and Reactive Oxygen and Nitrogen Species in Neurological Disorders and Stroke: Therapeutic Implications, Adv. Drug Del. Rev., 61 (2009) 1299–1315.

[142] P.V. Vignais, The Superoxide-Generating NADPH Oxidase: Structural Aspects and Activation Mechanism, Cell. Mol. Life Sci., 59 (2002) 1428–1459.

[143] K. Apel, H. Hirt, Reactive Oxygen Species: Metabolism, Oxidative Stress, and Signal Transduction, Annu. Rev. Plant Biol., 55 (2004) 373–399.

[144] M. Katsuyama, K. Matsuno, C. Yabe-Nishimura, Physiological Roles of NOX/NADPH Oxidase, the Superoxide-Generating Enzyme, J. Clin. Biochem. Nutr., 50 (2012) 9–22.

[145] K. Briegera, S. Schiavone, Miller F. J. .Jr., K.-H. Krause, Reactive Oxygen Species: From Health to Disease, Swiss Med. Wkly., 142 (2012) w13659–w13672.

[146] P. Ludovico, W.C. Burhans, Reactive Oxygen Species, Ageing and the Hormesis Police, FEMS Yeast Res., 14 (2014) 33–39.

[147] M.L. Genova, G. Lenaz, The Interplay Between Respiratory Supercomplexes and ROS in Aging, Antioxid. Redox Signal., 23 (2015) 208–238.

[148] A. Sanz, Mitochondrial Reactive Oxygen Species: Do They Extend or Shorten Animal Lifespan, Biochim. Biophys. Acta, Bioenerg., 1857 (2016) 1116–1126.

[149] L.J. Marnett, Oxyradicals and DNA Damage, Carcinogenesis, 21 (2000) 361–370.

[150] M. Valko, C.J. Rhodes, J. Moncol, M. Izakovic, M. Mazur, Free Radicals, Metals and Antioxidants in Oxidative Stress-Induced Cancer, Chem.-Biol. Interact., 160 (2006) 1–40.

[151] Q. Wu, X. Ni, ROS-mediated DNA Methylation Pattern Alterations in Carcinogenesis, Curr. Drug Targets, 16 (2015) 13–19.

[152] S. Pillai, C. Oresajo, J. Hayward, Ultraviolet Radiation and Skin Aging: Roles of Reactive Oxygen species, Inflammation and Protease Activation, and Strategies for Prevention of Inflammation-Induced matrix Degradation – A Review, Int. J. Cosmetic Sci., 27 (2005) 17–34.

[153] N. Azad, Y. Rojanasakul, V. Vallyathan, Inflammation and Lung Cancer: Roles of Reactive Oxygen/Nitrogen Species, J. Toxicol. Environ. Health, Pt. B Crit. Rev., 11 (2008) 1–15.

[154] D.P. Rosanna, C. Salvatore, Reactive Oxygen Species, Inflammation and Lund Diseases, Curr. Pharm. Des., 18 (2012) 3889–3900.

[155] S. Reuter, S.C. Gupta, M.M. Chaturvedi, B.B. Aggarwal, Oxidative Stress, Inflammation, and Cancer: How Are They Linked?, Free Radical Biol. Med., 49 (2010) 1603–1616.

[156] J.Y. Jeremy, N. Shukla, S. Muzaffar, A. Handley, G.D. Angelini, Reactive Oxygen Species, Vascular Disease and Cardiovascular Surgery, Curr. Vasc. Pharmacol., 2 (2004) 229–236.

[157] P. Abrescia, P. Golino, Free Radicals and Antioxidants in Cardiovascular Diseases, Expert Rev. Cardiovasc. Ther., 3 (2005) 159–171.

[158] M.A. Casadei, S. Cesa, M. Feroci, A. Inesi, L. Rossi, F.M. Moracci, The $O_2^{\bullet-}/CO_2$ System as Mild and Safe Carboxylating Reagent. Synthesis of Organic Carbonates, Tetrahedron, 53 (1997) 167–176.

[159] M.A. Casadei, F.M. Moracci, G. Zappia, Electrogenerated Superoxide-Activated Carbon Dioxide. A New Mild and Safe Approach to Organic Carbamates, J. Org. Chem., 62 (1997) 6754–6759.

[160] P. Sethupathy, I.M. Alnashef, J.R. Monnier, M.A. Matthews, J.W. Weidner, Synthesis of Carbonyl Compounds from Alcohols Using Electrochemically Generated Superoxide Ions in RTILs, Synth. Commun., 42 (2012) 3632–3647.

[161] E.E. Kalu, R.E. White, In Situ Degradation of Polyhalogenated Aromatic Hydrocarbons by Electrochemically Generated Superoxide Ions, J. Electrochem. Soc., 138 (1991) 3656–3660.

[162] I.M. AlNashef, M.A. Matthews, J.W. Weidner, Electrochemistry: Electrochemically Generated Superoxide Ion in Ionic Liquids: Applications to Green Chemistry, in: R.D. Rogers, K.R. Seddon (Eds.) Ionic Liquids as Green Solvents. Progress and Prospects, American Chemical Society, Washington, 2003, pp. 509–525.

[163] M. Hayyan, F.S. Mjalli, M.A. Hashim, I.M. AlNashef, Generation of Superoxide Ion in Pyridinium, Morpholinium, Ammonium, and Sulfonium-Based Ionic Liquids and the Application in the Destruction of Toxic Chlorinated Phenols, Ind. Eng. Chem. Res., 51 (2012) 10546–10556.

[164] K.C. Lau, J. Lu, X. Luo, L.A. Curtiss, K. Amine, Implications of the Unpaired Spins in Li-O_2 Battery Chemistry and Electrochemistry: A Minireview, ChemPlusChem, 80 (2015) 336–343.

[165] I. Landa-Medrano, C. Li, N. Ortiz-Vitoriano, I.R. de Larramendi, J. Carrasco, T. Rojo, Sodium-Oxygen Battery: Steps Toward Reality, J. Phys. Chem. Lett., 7 (2016) 1161–1166.

[166] J. Lu, Y.J. Lee, X. Luo, K.C. Lau, M. Asadi, H.-H. Wang, S. Brombosz, J. Wen, D. Zhai, Z. Chen, D.J. Miller, Y.S. Jeong, J.-B. Park, Z.Z. Fang, B. Kumar, A. Salehi-Khojin, Y.-K. Sun,

L.A. Curtiss, K. Amine, A Lithium–Oxygen Battery Based on Lithium Superoxide, Nature, 529 (2016) 377–382.

[167] D.T. Sawyer, J.S. Valentine, How Super Is Superoxide?, Acc. Chem. Res., 14 (1981) 393–400.

[168] D. Vasudevan, H. Wendt, Electroreduction of Oxygen in Aprotic Media, J. Electroanal. Chem., 392 (1995) 69–74.

[169] J. Simonet, J.-F. Pilard, Electrogenerated Reagents, in: H. Lung, O. Hammerich (Eds.) Organic Electrochemistry, Marcel Dekker, New York, 2001, pp. 1163–1226.

[170] C.P. Andrieux, P. Hapiot, J.-M. Savéant, Mechanism of Superoxide Ion Disproportionation in Aprotic Solvents J. Am. Chem. Soc., 109 (1987) 3768–3775.

[171] D.T. Sawyer, Electrochemistry of Dioxygen, in: R.J.P. Williams (Ed.) Oxygen Chemistry, Oxford University Press, Inc., New York, 1991, pp. 27.

[172] J.-M. Savéant, Elements of Molecular and Biomolecular Electrochemistry, Wiley-Interscience, New York, 2006.

[173] C. Costentin, M. Robert, J.-M. Savéant, Acceleration of the Homogeneous and Electrochemical Reductions of Dioxygen in Aprotic Media by Ammonium Ions. Is the Driving Force a Function of NH_4^+ Concentration? What Is the Mechanism of the Reaction?, J. Phys. Chem. C, 111 (2007) 12877–12880.

[174] A. René, M.-L. Abasq, D. Hauchard, P. Hapiot, How Do Phenolic Compounds React toward Superoxide Ion? A Simple Electrochemical Method for Evaluating Antioxidant Capacity, Anal. Chem., 82 (2010) 8703–8710.

[175] W.C. Danen, R.J. Warner, The Remarkable Nucleophilicity of Superoxide Anion Radical. Rate Constants for Reaction of Superoxide Ion with Aliphatic Bromides, Tetrahedron Lett., 11 (1977) 989–992.

[176] M.J. Gibian, D.T. Sawyer, T. Ungermann, R. Tangpoonpholvivat, M.M. Morrison, Reactivity of Superoxide Ion with Carbonyl Compounds in Aprotic Solvents, J. Am. Chem. Soc., 101 (1979) 640–644.

[177] R.D. Webster, A.M. Bond, Different Mechanisms for the Reaction of Disubstituted Aromatic Esters and Thioic *S*-Esters with Electrochemically Generated Superoxide, J. Chem. Soc., Perkin Trans. 2, (1997) 1075–1079.

[178] R.A. Holroyd, B.H.J. Bielski, Photochemical Generation of Superoxide Radicals in Aqueous Solutions, J. Am. Chem. Soc., 100 (1978) 5796–5800.

[179] D. Kim, T. Oda, A. Ishimatsu, T. Muramatsu, Galacturonic Acid-Induced Increase of Superoxide Production in Red Tide Phytoplanktons *Chattonella marina* and *Heterosigma akashiwo*, Biosci., Biotechnol., Biochem., 64 (2000) 911–914.

[180] U. Stoin, A.I. Shames, I. Malka, I. Bar, Y. Sasson, In situ Generation of Superoxide Anion Radical in Aqueous Medium under Ambient Conditions, ChemPhysChem, 14 (2013) 4158–4164.

[181] A.J. Anifowose, K. Takeda, H. Sakugawa, Novel Fluorometric Method for the Determination of Production Rate and Steady-State Concentration of Photochemically Generated Superoxide Radical in Seawater Using 3',6'-(Diphenylphosphinyl)fluorescein, Anal. Chem., 87 (2015) 11998–12005.

[182] Y. Wei, X. Dang, Hu Sh., Electrochemical Properties of Superoxide Ion in Aprotic Media, Russ. J. Electrochem., 40 (2004) 400–404.

[183] J.P. Hu, M. Calomme, A. Lasure, T. De Bruyne, L. Pieters, A. Vlietinck, D.A. Vanden Berghe, Structure-Activity Relationship of Flavonoids with Superoxide Scavenging Activity, Biol. Trace Elem. Res., 47 (1995) 327–331.

[184] C. Le Bourvellec, D. Hauchard, A. Darchen, J.-L. Burgot, M.-L. Abasq, Validation of a New Method Using the Reactivity of Electrogenerated Superoxide Radical in the Antioxidant Capacity Determination of Flavonoids, Talanta, 75 (2008) 1098–1103.

[185] S. Ahmed, F. Shakeel, Antioxidant Activity Coefficient, Mechanism, and Kinetics of Different Derivatives of Flavones and Flavanones Towards Superoxide Radical, Czech J. Food Sci., 30 (2012) 153–163.

[186] E.I. Korotkova, O.A. Voronova, E.V. Dorozhko, Study of Antioxidant Properties of Flavonoids by Voltammetry, J. Solid State Electrochem., 16 (2012) 2435–2440.

[187] J.M. Dimitrić Marković, D. Milenković, D. Amić, M. Mojović, I. Pašti, Z.S. Marković, The Preferred Radical Scavenging Mechanisms of Fisetin and Baicalein Towards Oxygen-Centred Radicals in Polar Protic and Polar Aprotic Solvents, RSC Adv., 4 (2014) 32228–32236.

[188] T. Araki, H. Kitaoka, Antioxidative Properties of Probucol Estimated by the Reactivity with Superoxide and by Electrochemical Oxidation, Chem. Pharm. Bull. (Tokyo), 49 (2001) 943–947.

[189] G.K. Ziyatdinova, D.M. Gil'metdinova, G.K. Budnikov, Reactions of Superoxide Anion Radical with Antioxidants and Their Use in Voltammetry, J. Anal. Chem., 60 (2005) 49–52.

[190] G.K. Ziyatdinova, S.P. Zakharova, H.C. Budnikov, Reactions of Phenolic Antioxidants with Electrogenerated Superoxide Anion Radical and their Analytical Application, Uch. Zap. Kazan. Univ., Ser. Estestv. Nauki, 157 (2015) 129–142.

[191] T. Nakayama, B. Uno, Concerted Two-proton–coupled Electron Transfer From Catechols To Superoxide Via Hydrogen Bonds, Electrochim. Acta, 208 (2016) 304–309.

[192] M.E. Ortiz, L.J. Núñez-Vergara, J.A. Squella, Relative Reactivity of Dihydropyridine Derivatives to Electrogenerated Superoxide Ion in DMSO Solutions: A Voltammetric Approach, Pharm. Res., 20 (2003) 292–296.

[193] A.M.C. Herath, R.M. Gamini Rajapakse, V. Karunarathne, A. Wicramasinghe, Electrochemical Investigation of Superoxide Anion Scavenging Ability of 1,2,3-Triketohydrindene Hydrate in Aprotic Solvents, Electrochim. Acta, 51 (2006) 2890–2897.

[194] G. Feroci, A. Fini, Voltammetric Investigation of the Interactions Between Superoxide Ion and Some Sulfur Amino Acids, Inorg. Chim. Acta, 360 (2007) 1023–1031.

[195] Z. Ghiaba, M. Yousfi, M. Hadjadj, M. Saidi, M. Dakmouche, Study of Antioxidant Properties of Five Algerian Date (*Phoenix dactylifera* L) Cultivars by Cyclic Voltammetric Technique, Int. J. Electrochem. Sci., 9 (2014) 909–920.

[196] T. Nakayama, B. Uno, Importance of Proton-Coupled Electron Transfer from Natural Phenolic Compounds in Superoxide Scavenging, Chem. Pharm. Bull., 63 (2015) 967–973.

[197] T. Ozawa, A. Hanaki, H. Yamamoto, On A Spectrally Well-Defined and Stable Source of Superoxide Ion, O_2^-, FEBS Lett., 74 (1977) 99–102.

[198] D.T. Sawyer, G. Chiericato, Jr.,, C.T. Angells, E.J. Nanni, Jr., T. Tsuchlya, Effects of Media and Electrode Materials on the Electrochemical Reduction of Dioxygen, Anal. Chem., 54 (1982) 1720–1724.

[199] R.G. Compton, C.E. Banks, Understanding Voltammetry, 2nd ed., Imperial College Press, London (UK), 2011.

[200] T.J. Smith, K.J. Stevenson, Reference Electrodes, in: C.G. Zoski (Ed.) Handbook of Electrochemistry, Elsevier, Amsterdam, The Netherlands, 2007, pp. 73–110.

[201] M. Ciobanu, J.P. Wilburn, M.L. Krim, D.E. Cliffel, Fundamentals, in: C.G. Zoski (Ed.) Handbook of Electrochemistry, Elsevier, Amsterdam, The Netherlands, 2007, pp. 3–29.

[202] B. Speiser, Application of Digital Simulation, in: O. Hammerich, B. Speiser (Eds.) Organic Electrochemistry: Revised and Expanded, CRC Press, Boca Raton, Florida, 2016, pp. 205–227.

Chapter 2

The Electrochemical Reduction of Biotin (Vitamin B_7) and

Conversion to its Ester

This page has been intentionally left blank

2.1. Chapter Overview

In this chapter, the electrochemical behavior of biotin (vitamin B_7; Scheme 2.1) was examined in aprotic organic solvents (DMF and DMSO) using cyclic voltammetry (CV) and controlled potential electrolysis (CPE) techniques.

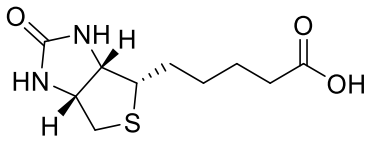

Scheme 2.1. Chemical structure of d-(+)-biotin (Vitamin B_7).

Overall, the results obtained revealed that at ca. -1.6 to -1.8 vs. $(Fc/Fc^+)/V$ (where Fc/Fc^+ = ferrocene/ferrocenium), biotin can be reduced by one electron to form its carboxylate anion and dihydrogen (H_2) via a direct discharge of the carboxylic acid functionality at a platinum (Pt) electrode surface, whereas no observable faradaic current was registered over the same potential window when using a glassy carbon (GC) electrode instead. The electrochemical reduction process appeared to be chemically reversible on the time-frame of CV ($t \leq$ seconds), but not over the extended period of CPE experiments ($t \geq$ minutes) where the conversion of biotin into its carboxylate anion was found to be chemically irreversible.

A procedure to functionalize the carboxylic acid group was also established by performing a bulk reductive electrolysis on the compound, and then reacting the electrochemically generated carboxylate anion with iodomethane (CH_3I) to afford the biotin methyl ester product in excellent yield (91%). In addition, attenuated total reflectance–Fourier transform infrared (ATR–FTIR) spectroscopy was successful in identifying several distinct and characteristic carbonyl absorbance peaks associated with the analogous forms of biotin available before electrolysis, after electrolysis, and after the methylation reaction.

2.2. Results & Discussion

2.2.1. Electrochemical reduction of biotin

Biotin was found to exhibit poor solubility in most organic solvents suitable for electrochemistry, except in the cases of the highly polar solvents DMF and DMSO. Preliminary cyclic voltammetry (CV) experiments were therefore conducted in these two solutions (Figures 2.1 and 2.2). This revealed that, at a Pt electrode, biotin displays the presence of a single reduction/cathodic process on the forward scan and a corresponding oxidation/anodic wave when the scan direction is reversed. When the electrode material was changed to glassy carbon (GC), however, no current response due to biotin was observed (Figures 2.1 and 2.2).

In DMF solutions, the cathodic peak potential (E_{pc}) associated with the reduction of biotin was found to occur at ca. -1.6 vs. (Fc/Fc^{+})/V (Figure 2.1), and at ca. -1.8 vs. (Fc/Fc^{+})/V when DMSO was used (Figure 2.2). Moderately larger and better resolved peak currents were also observed in DMF as compared DMSO. The peak current differences are partially attributable to changes in diffusion coefficients of biotin in both solvents due to different solvent viscosities. The size of the solvated molecules may also vary between the different solvents thus influencing their diffusion coefficient values.

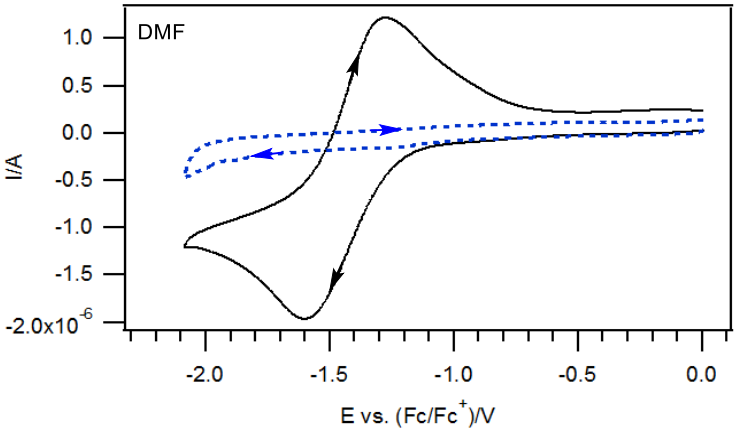

Figure 2.1. Cyclic voltammogram of 2 mM biotin and 0.2 M Bu_4NPF_6 in DMF recorded at a scan rate of 0.1 V s^{-1}. (—) 1-mm diameter planar Pt disk electrode. (- - -) 1 mm diameter planar glassy carbon disk electrode.

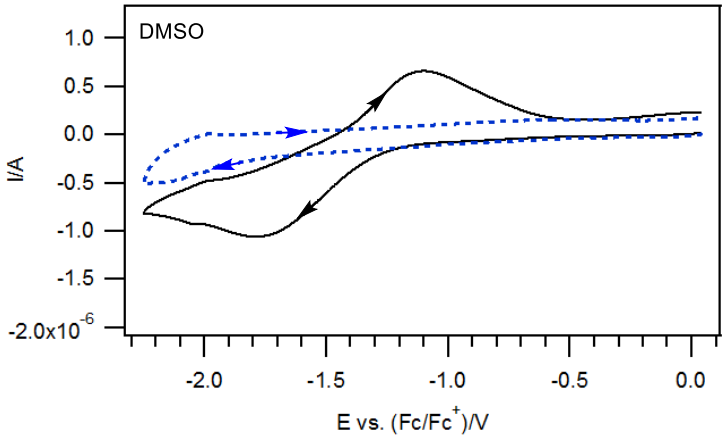

Figure 2.2. Cyclic voltammogram of 2 mM biotin and 0.2 M Bu_4NPF_6 in DMSO recorded at a scan rate of 0.1 V s^{-1}. (—) 1-mm diameter planar Pt disk electrode. (- - -) 1 mm diameter planar glassy carbon disk electrode.

In addition, it was also observed that the electrochemical reduction of biotin appeared to be chemically reversible in the sense that it gave cathodic (I_{pc}) and anodic (I_{pa}) peak current ratios of close to unity. It should be noted here that the terms chemical reversibility and irreversibility when used in conjunction with cyclic voltammetry refer to the stability of the

reduced species of the molecules on the timescales of the voltammograms ($t \leq$ seconds), and do not imply electrochemical (thermodynamic) reversibility or irreversibility with respect to the heterogeneous electron transfer step where a cathodic to anodic peak-to-peak separation (ΔE_p) value of ca. 57 mV is ideally observed for a fast one electron process. For example, the ΔE_p value that was obtained in DMF was at least several hundred mV larger than what is expected for an electrochemically reversible process; while an even larger ΔE_p value was recorded in DMSO. Since the overall voltammetric behavior obtained in DMF was simpler and well defined, the remaining discussion of biotin's electrochemistry in this chapter will be restricted to this solvent.

A large ΔE_p value obtained can sometimes arise from the effects of uncompensated solvent resistance (which was not experimentally compensated for in this study). As such, variable scan rate CV experiments were performed to further investigate this, and the respective cyclic voltammograms are shown in Figure 2.3. It was observed that as the scan rate was increased from 0.1 V s^{-1} to 20 V s^{-1}, the ΔE_p values increased substantially from ca. 350 mV to ca. 1 V, respectively. In addition, the variable scan rate data for biotin were also compared against the ΔE_p values that were obtained for the Fc/Fc^+ redox couple (which was used as a standard for an electrochemically reversible process). It can be observed that even at a relatively low scan rate of 0.1 V s^{-1}, the difference between the ΔE_p values obtained for biotin and Fc are noticeable and become significantly larger at higher scan rates (Figure 2.4). In particular, at a scan rate of 20 V s^{-1}, the ΔE_p value for biotin was ca. 1 V, whereas that for Fc was found to be only ca. 150 mV.

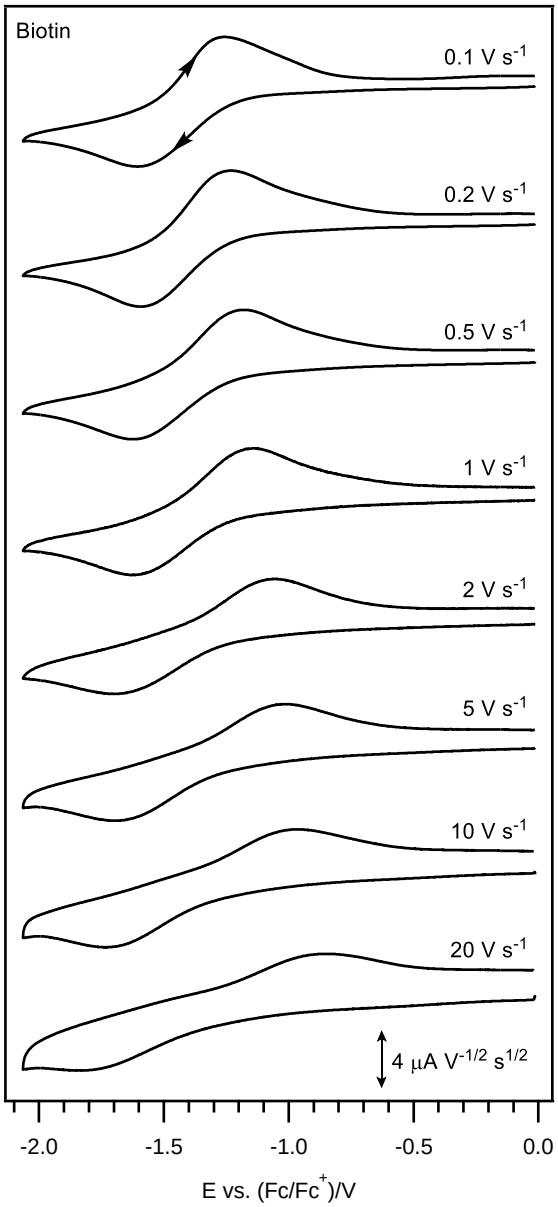

Figure 2.3. Cyclic voltammograms of 2 mM biotin in DMF containing 0.2 M Bu_4NPF_6, recorded at 295 (±2) K using a 1-mm diameter planar Pt disk electrode and at different scan rates. The current data have been normalized by multiplying against (scan rate)$^{-1/2}$.

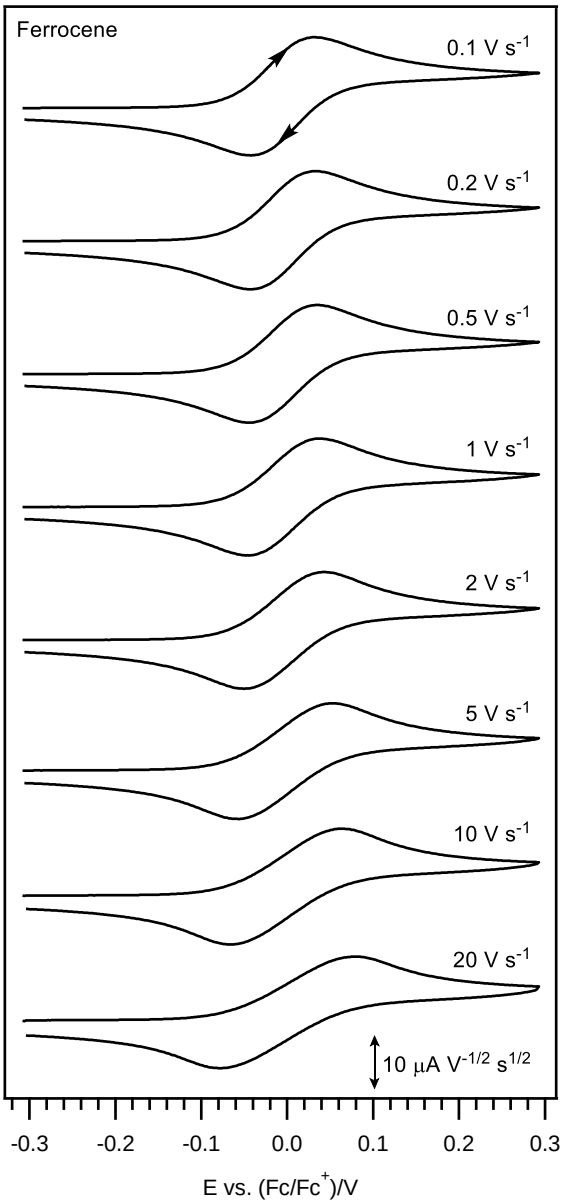

Figure 2.4. Cyclic voltammograms of 2 mM ferrocene in DMF containing 0.2 M Bu_4NPF_6, recorded at 295 (±2) K using a 1-mm diameter planar Pt disk electrode and at different scan rates. The current data have been normalized by multiplying against $(\text{scan rate})^{-1/2}$.

It is also noteworthy, that an excellent linear relationship (R^2 = 0.9892) was obtained for a plot of cathodic peak current against the square root of scan rate signifying therefore that the reduction of biotin at the Pt electrode is almost entirely diffusion (and not adsorption) controlled (Figure 2.5).

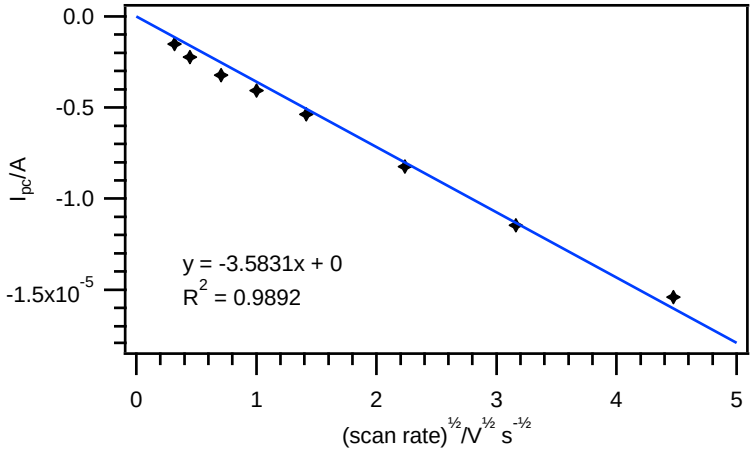

Figure 2.5. Plot of cathodic peak current vs. square root of scan rate for cyclic voltammograms of 2 mM biotin in DMF containing 0.2 M Bu_4NPF_6, recorded at 295 (±2) K using a 1-mm diameter planar Pt disk electrode at different scan rates (0.1, 0.2, 0.5, 1.0, 2.0, 5.0, 10.0, and 20.0 V s^{-1}).

More importantly, in isolation, the cyclic voltammograms shown in Figures 2.1–2.3 do not allow the direct determination of the number of electrons transferred during the electrochemical reduction of biotin and whether the heterogeneous electron transfer reactions and following homogeneous chemical reactions are chemically reversible over longer times. As such, controlled potential electrolysis (CPE) experiments were performed on biotin to more accurately determine the aforementioned points. The potential applied during these CPE experiments were ca. 150 mV more negative than the E_{pc} values obtained by CV experiments in order to ensure that a complete reduction of the starting material in the bulk solution was achieved. Cyclic voltammograms obtained at the start and at the end of the electrolysis are

shown in Figure 2.6a, along with the corresponding coulometric data for the bulk reduction in Figure 2.6b. The exhaustive reduction of biotin showed that a total of one electron was transferred per molecule (n = 1.03) after ca. 0.5 h. CV data obtained after electrolysis, on the other hand, shows the disappearance of the initial cathodic wave at ca. -1.6 vs. $(Fc/Fc^{+})/V$, indicating a complete reduction of the substrate. Concomitantly, the voltammograms revealed that the electrochemical reduction of biotin is chemically irreversible over the extended periods of CPE ($t \geq$ minutes), and also showed the presence of a new irreversible oxidation process at ca. +0.7 vs. $(Fc/Fc^{+})/V$.

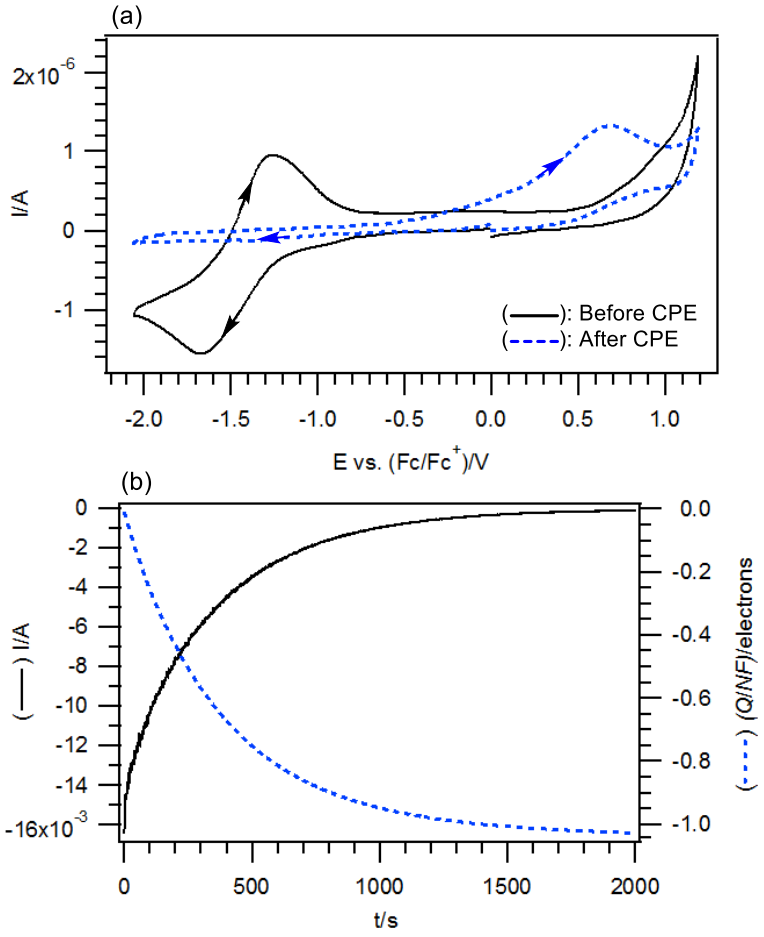

Figure 2.6. Voltammetric and coulometric data obtained during the reductive CPE of 2 mM biotin in DMF containing 0.2 M Bu_4NPF_6 at 295 (±2) K. (a) Cyclic voltammograms recorded at 0.1 V s^{-1} with a 1-mm diameter planar Pt disk electrode. (b) Current/coulometry vs. time data obtained during the reductive CPE experiment (at -1.82 vs. (Fc/Fc^+)/V). For (b), the number of electrons transferred per molecule (*Q*/*NF*) during the reductive CPE experiment was calculated from eq. 2.4.

2.2.2. Proposed redox mechanism

In the course of elucidating the redox mechanism, it can sometimes be beneficial to study model substrates with functional groups that are characteristic of the analyte, as the results obtained might provide important clues about the redox mechanism (such as the site of electroactivity). With this in mind, the compounds 2-imidazolidinoe (ethylene urea), tetrahydrothiophene (thiophane), and acetic acid were systematically investigated by CV under the present conditions.

As shown in Figure 2.7a, data obtained from the voltammetric study of ethylene urea correspondingly revealed that it is not reduced in the measured potential window that was applied for biotin (ca. 0 to -2.1 vs. $(Fc/Fc^{+})/V$). Similarly, no current response due to thiophane was observed when the aforementioned compound was studied under the same experimental conditions (Figure 2.7b). In contrast, when acetic acid was examined, a redox couple at ca. -1.7 vs. $(Fc/Fc^{+})/V$ that appeared to be highly reminiscent of biotin's voltammetric behavior was exhibited (Figure 2.7c), signaling therefore that it is likely that the carboxylic acid functionality of biotin is responsible for its observed electroactivity (but see Sections 2.2.3 and 2.2.4).

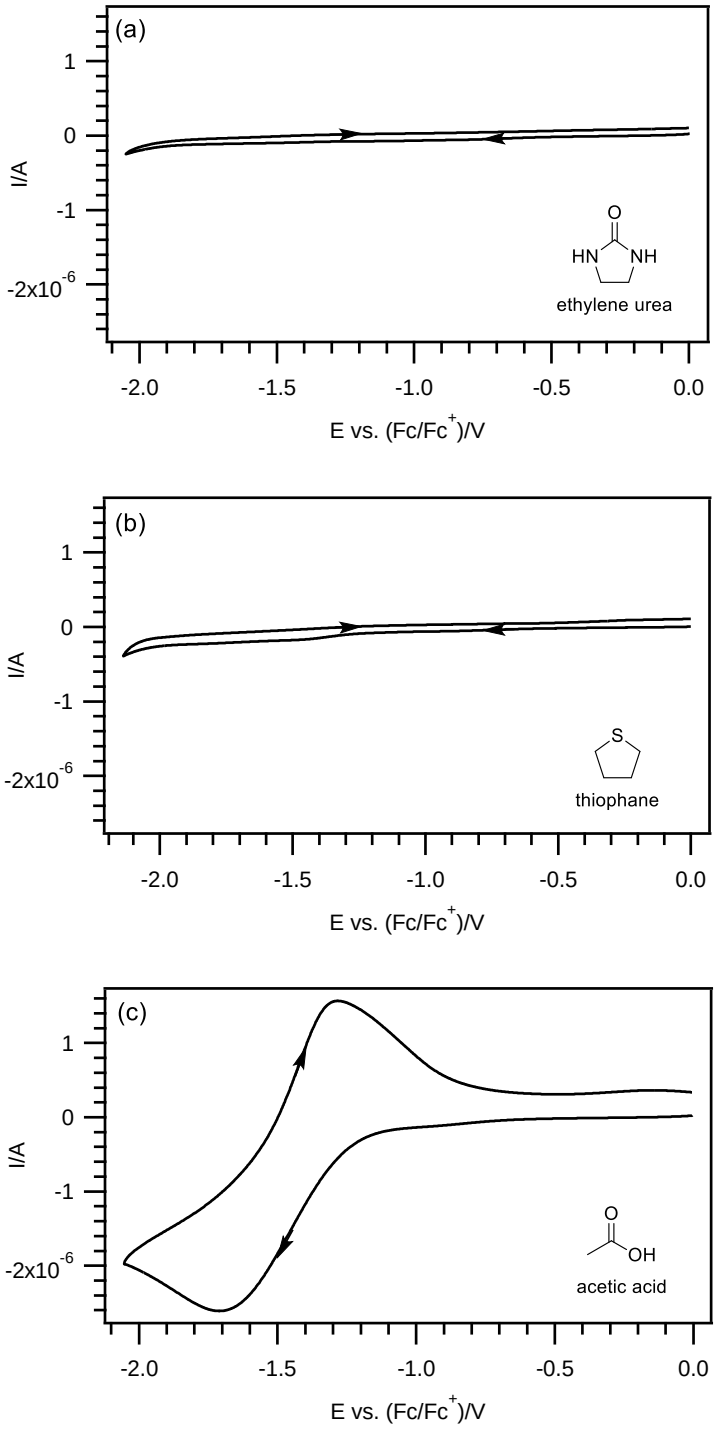

Figure 2.7. Cyclic voltammograms of 2 mM (a) ethylene urea, (b) thiophane, and (c) acetic acid in DMF containing 0.2 M Bu_4NPF_6, recorded at 295 (±2) K using a 1-mm diameter planar Pt disk electrode and a scan rate of 0.1 V s^{-1}.

On the basis of the experimental results obtained above, it is proposed that biotin is likely reduced electrochemically according to a mechanism that involves a direct discharge of the carboxylic acid at the Pt electrode surface as described below (the structure of biotin has been abbreviated as RCOOH for clarity) [1, 2]. The carboxyl group on biotin initially gains an electron leading to the generation of its conjugate base and an adsorbed hydrogen atom on the Pt surface (eq. 2.1). The importance of a catalytic surface such as Pt to support this process is underlined by the fact that no cathodic wave was observed when a glassy carbon electrode is used (Figures 2.1 and 2.2, blue dashed line). Formation of dihydrogen then occurs either through a surface dimerization of adsorbed hydrogen atoms (eq. 2.2), or when a second molecule of biotin is reduced at the electrode surface possessing a pre-existing adsorbed hydrogen atom (eq. 2.3). The oxidation of adsorbed hydrogen atoms gives rise to the anodic wave that is registered in CV when the scan direction is returned (reverse of eq. 2.1) [3]. In this study, the counter-ion for the carboxylate anion is the supporting electrolyte cation, Bu_4N^+.

$$RCOOH + Pt + e^- \rightleftharpoons RCOO^- + Pt\text{–}H_{(ads)} \quad (2.1)$$

$$2\ Pt\text{–}H_{(ads)} \rightarrow H_2 + 2\ Pt \quad (2.2)$$

$$RCOOH + Pt\text{–}H_{(ads)} + e^- \rightarrow RCOO^- + H_2 + Pt \quad (2.3)$$

2.2.3. Reaction with iodomethane

Further to the electrochemical reduction of biotin and generation of its carboxylate, it was envisaged that this anion would be susceptible to trapping with an appropriate electrophile. It was found that after a bulk reduction of biotin, the addition of 1.5 molar equivalence of iodomethane (CH_3I) into the working electrode compartment's solution afforded biotin methyl ester in a high yield of 91% (Scheme 2.2).

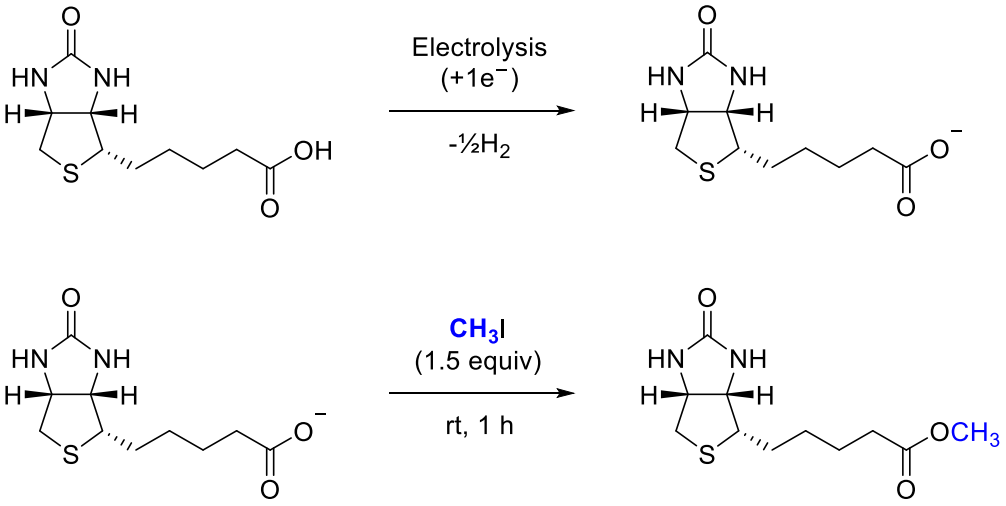

Scheme 2.2. Electrochemical reduction of biotin and reaction of its carboxylate anion with iodomethane.

In addition, during the course of isolating the methylated product from the reaction mixture, the supporting electrolyte (Bu_4NPF_6) was also recovered in near quantitative yield. The structure of biotin methyl ester was confirmed on the basis of NMR, HRMS, and by X-ray crystallography as illustrated in Figure 2.8, with the crystallographic data (i.e. unit cell dimensions, space group, Z) appearing to be in good agreement with a literature precedent [4]. Notably, this result also lends weight to the mechanism put forth in eq. 2.1−2.3, that the reduction of biotin (under the present conditions) involves its carboxylic acid groups rather than the urea/thiophane rings.

Conventional approaches to esterify biotin's carboxyl group have typically required long reaction times, elaborate procedures, or the use of equimolar or excess amounts of harsh reagents [5-11] – potentially leading to the formation of undesirable by-products or resulting in poor substrate scope tolerance for the electrophilic counterpart. Hence, this encouraging result provides both a form of validation for the proposed mechanism, and also presents an alternative route to conveniently functionalize biotin at its carboxylic acid group.

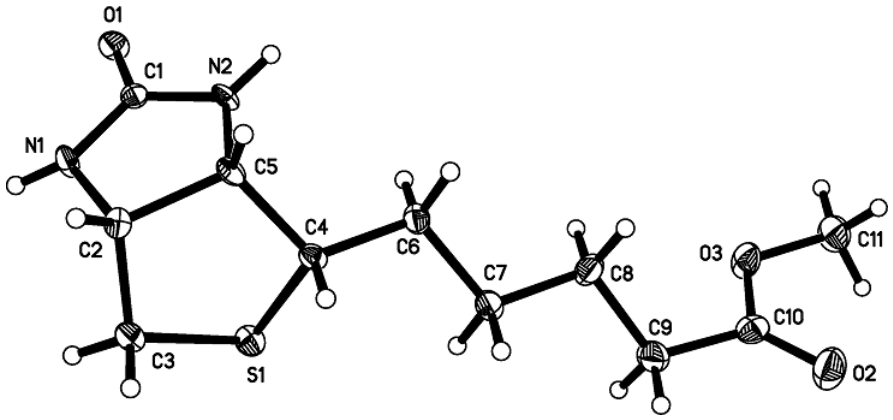

Figure 2.8. ORTEP drawing of biotin methyl ester with thermal ellipsoids at 50% probability levels.

2.2.4. ATR–FTIR spectroscopy

Work from our laboratories had previously reported the utilization of FTIR spectroscopy with an ATR probe for the in situ characterization of carbonyl and carboxylate functional groups during the bulk reductive CPE of pyridine- and benzene-based diesters [12]. Hence, it was thought that this technique might similarly offer a suitable and valuable means to study the different carbonyl and carboxylate containing species that are likely to be present before and after the CPE of biotin, and after methylation of its carboxylate anion (Scheme 2.2).

Preliminary ATR–FTIR experiments revealed that DMF absorbs strongly at ca. 1800–1600 cm^{-1}. As such, subsequent experiments were switched to using DMSO instead with the aim of minimizing the obscuring of peaks of interest due to biotin which are also expected to fall within the same mid-infrared (carbonyl) region. In addition, DMSO was observed to dissolve biotin more readily, especially in the substantially higher concentration of 50 mM (as compared to the 2 mM concentrations that were used for the electrochemical measurements) that is required such that acceptably intense absorbance bands and high signal-to-noise ratios can be obtained within a reasonable time frame.

Figure 2.9 shows the ATR–FTIR spectra obtained before reductive CPE, after reductive CPE, and after the methylation of 50 mM biotin in DMSO containing 0.2 M Bu_4NPF_6 from 1950 to 650 cm^{-1}. The spectra were background subtracted to remove the peaks associated with the solvent and supporting electrolyte for easier interpretation of the data.

Prior to the commencement of the electrolysis of biotin, the recorded spectrum displayed the presence of a sharp and intense absorbance peak at 1708 cm^{-1} that is likely due to an overlapping of the C=O stretches of biotin's carboxylic acid group and carbamide group. A relatively less intense peak is also observed at 1264 cm^{-1} which is assigned to a C(=O)–OH stretch of the carboxylic acid moiety.

After the exhaustive reduction of biotin, the sharp band that was previously at 1708 cm^{-1} diminished in intensity and width by ca. 25%, and shifted in wavenumbers very slightly to 1706 cm^{-1}. More notably, however, the C–O stretching absorbance at 1264 cm^{-1} disappeared and two new absorbance bands appeared at 1582 and 1380 cm^{-1}. These new absorbances are attributable to the asymmetric and symmetric stretching (at 1582 and 1380 cm^{-1}, respectively) of the electrochemically generated carboxylate anion, and it is in accordance with expectation that they should appear at a lower wavenumber due to a greater single bond character in the C=O bond arising from the possibility of resonance forms within the carboxylate anion. In order to maintain charge neutrality as the bulk electrochemical reduction of biotin proceeds, the supporting electrolyte ions must transverse between the two compartments in the electrolysis cell. Thus, the strong negative absorbance peaks that occurred at ca. 850 cm^{-1} are due to the PF_6^- anions being lost from the working electrode compartment and migrating into the auxiliary electrode compartment of the CPE cell.

Following the methylation of the carboxylate anion with 1.5 molar equivalence of iodomethane, the ATR–FTIR spectrum similarly displayed a sharp and intense peak that is

likely due to the C=O stretching of the carbamide functionality at 1706 cm^{-1}. Conversely, the two absorbance bands associated with the asymmetric and symmetric stretches of the carboxylate anion (at 1582 and 1380 cm^{-1}, respectively) disappeared and a new medium intensity absorbance band was shown at 1734 cm^{-1} which is attributable to the contribution of the C=O stretching of the ester group in the newly formed biotin methyl ester. Two relatively less intense absorbances likely corresponding to the C–O stretches for the $C(=O)–OCH_3$ and $O–CH_3$ vibrations were also observed at 1253 cm^{-1} and 1177 cm^{-1}, respectively. Since the same solution was used for the ATR–FTIR measurements of the biotin carboxylate anion as well as the methylation reaction to form biotin methyl ester, the negative absorbance peaks that occurred at ca. 850 cm^{-1} (due to the loss of PF_6^- anions) are similarly observed here.

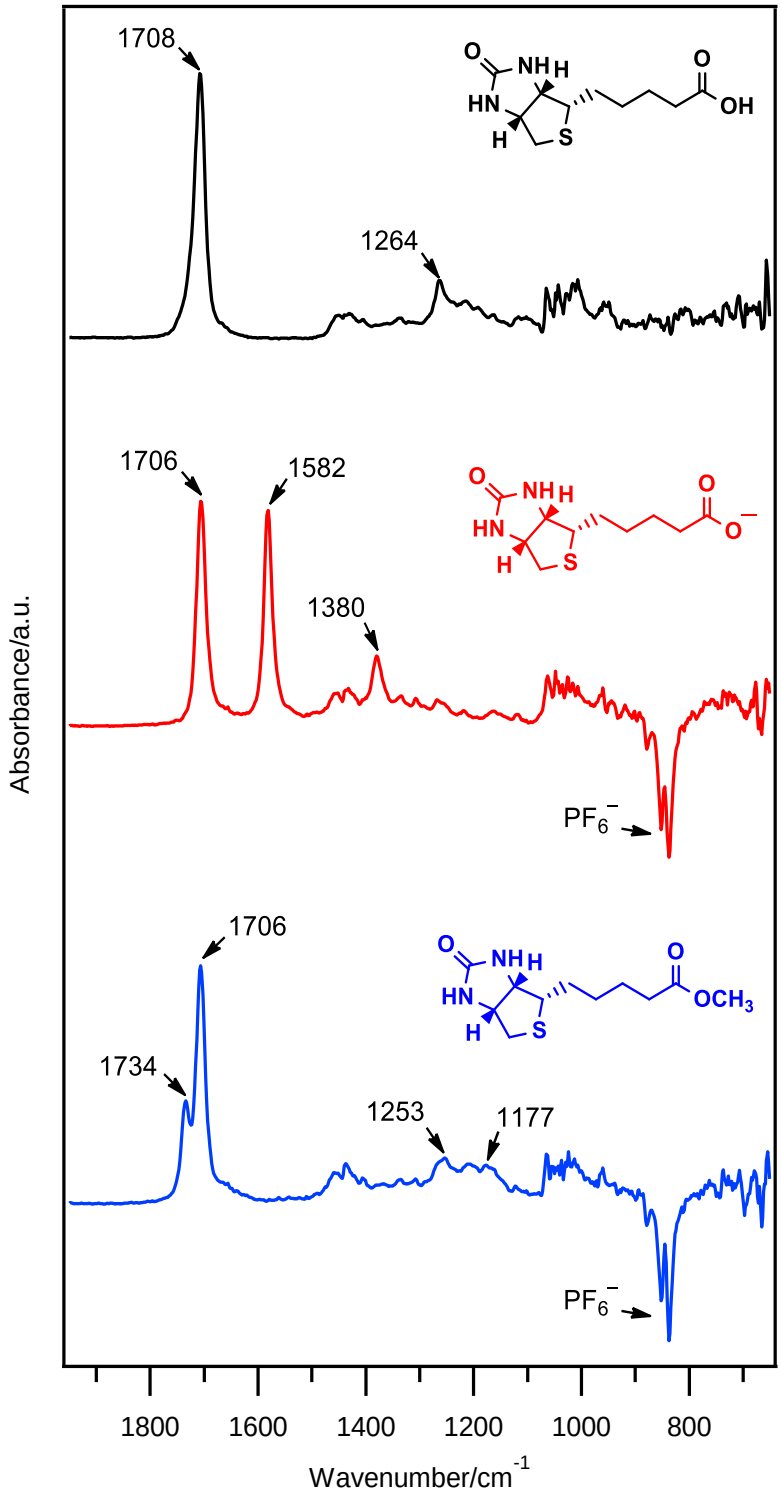

Figure 2.9. ATR-FTIR spectra of 50 mM biotin in DMSO with 0.2 M Bu_4NPF_6 recorded before CPE (top graph); after CPE at -1.95 vs. (Fc/Fc^+)/V (middle graph); and after CPE and reaction with 1.5 molar equivalence of iodomethane for 1 h (bottom graph). All spectra are background (DMSO with 0.2 M Bu_4NPF_6) subtracted.

2.3. Conclusion

In summary, CV and reductive CPE experiments have established that at a Pt electrode, biotin undergoes a one electron reduction in DMF and DMSO solutions, at ca. -1.6 to -1.8 vs. $(Fc/Fc^{+})/V$ to generate its carboxylate anion and dihydrogen. Mechanistically, the electrochemical reduction is believed to occur via a direct discharge of the carboxylic acid on the Pt electrode surface. On the CV time-scale ($t \leq$ seconds), the electrochemical reduction of biotin appears to be chemically reversible in the sense that similarly sized forward and reverse peaks are detected, albeit with wide cathodic to anodic peak-to-peak spacing due to relatively slow heterogeneous electron transfer. On the CPE time-scale ($t \geq$ minutes), however, the reduction process was found to be chemically irreversible resulting in the formation of biotin carboxylate anion. Subsequent to the bulk reductive electrolysis of biotin, the carboxylate anion was efficiently trapped with iodomethane (91% yield), thus highlighting a possible strategy to functionalize biotin's carboxylic acid group. The different forms of biotin present before CPE, after CPE, and after methylation were also examined via ATR–FTIR spectroscopy, and were found to display several distinct and characteristic carbonyl absorbance peaks.

2.4. Materials & Methods

2.4.1. General remarks

Unless otherwise specified, all chemicals and reagents were purchased from commercial sources and used as received. ^{1}H and ^{13}C NMR spectra were recorded on a Bruker Avance 500 (AV 500) spectrometer equipped with Ultra-shield Plus 500 MHz magnet with BBI probe (5mm). Chemical shifts (parts per million) were recorded with tetramethylsilane (TMS) as the internal reference standard. Multiplicities are given as follows: s (singlet), d (doublet), t (triplet), q (quartet), m (multiplet), dd (doublet of a doublet). The number of protons (*n*) for a given resonance is indicated by *n*H and coupling constants are reported as a *J* value in Hertz (Hz). High resolution mass spectra (HRMS) were obtained using a Waters Q-Tof Premier Mass Spectrometer equipped with Waters Acquity UPLC.

2.4.2. Chemicals & reagents

D-(+)-Biotin (98+%) was purchased from Alfa-Aesar, 2-imidazolidinone (97%) and trifluoroacetic acid (>99%) from Tokyo Chemical Industry Co., Ltd., acetic acid (AR grade) from Sinopharm Chemical Reagent Co., Ltd., and tetrahydrothiophene/thiophane (99%) and iodomethane (99%) from Sigma-Aldrich. All solvents used were of ACS grade/purity. *N*,*N*-dimethylformamide (DMF) and dimethyl sulfoxide (DMSO) were obtained from Tedia, methanol (MeOH) from Anaqua Chemicals Supply, and dichloromethane (DCM) from Merck. The supporting electrolyte tetrabutylammonium hexafluorophosphate (Bu_4NPF_6) was prepared following a standard procedure by reacting equal molar amounts of a 40% aqueous solution of Bu_4NOH (Alfa-Aesar) with a 65% aqueous solution of HPF_6 (Alfa-Aesar), washing the precipitate with hot water, recrystallizing three times from hot ethanol, and then drying under vacuum for 6 h at 413 K.

2.4.3. Voltammetry experiments

Cyclic voltammetry experiments were conducted with a computer-controlled Metrohm Autolab PGSTAT302N potentiostat using a three electrode system. Working electrodes were 1-mm diameter planar platinum and glassy carbon disks (eDAQ Pty Ltd), used in conjunction with a platinum auxiliary/counter electrode (Metrohm) and a silver wire miniature reference electrode (eDAQ Pty Ltd) connected to the test solution via a salt bridge (containing 0.5 M Bu_4NPF_6 in CH_3CN). Prior to each scan, the solutions used for voltammetric analysis were de-oxygenated by purging with high purity argon gas, and the working electrodes were cleaned by polishing with alumina oxide (grain size 0.3 μm) slurry on a Buehler Ultra-pad polishing cloth, rinsing with ultrapure water, acetone, and then dried. In accordance with IUPAC recommendations, accurate potentials were also obtained by using ferrocene as an internal standard, which was added to the test solution at the end of the measurements. All voltammetric experiments were conducted at 295 (±2) K in a Faraday cage.

2.4.4. Controlled potential electrolysis experiments

Bulk electrolysis experiments were performed in a two-compartment controlled potential electrolysis cell divided by a sintered glass frit with a porosity no. 5 (1.0–1.7 μm). Identically sized platinum meshes were used as the working and auxiliary electrodes and symmetrically arranged with respect to each other with a silver wire reference electrode (isolated via a salt bridge containing 0.5 M Bu_4NPF_6 in CH_3CN) that was positioned to within 2 mm of the surface of the working electrode. The volumes of the solutions in both electrode compartments were approximately 25 mL each and simultaneously de-oxygenated and stirred using bubbles of argon gas. All electrolysis experiments were conducted at 295 (±2) K. The number of electrons transferred during the bulk electrolysis process was calculated from:

$$n = Q/NF \quad (2.4)$$

where: n = number of moles of electrons transferred; Q = charge (coulombs); N = no. of moles of starting compound; and F = Faraday's constant (96 485 C mol^{-1}).

2.4.5. Procedure for the reaction of biotin carboxylate with iodomethane

Following a preparative scale electrochemical reduction of biotin (0.5 mmol, 122 mg) in DMF (25 mL), iodomethane (0.75 mmol, 46.7 μL) was added to the working electrode compartment's solution and stirred for one hour at room temperature, under a nitrogen atmosphere. On completion, the solvent was removed from the reaction mixture by using a high vacuum rotary evaporator and then leaving to dry further in vacuo overnight. Analytical thin layer chromatography was performed using pre-coated silica gel plates and visualization was achieved by staining with $KMNO_4$. Purification by flash column chromatograph over silica gel (eluent used: DCM/MeOH = 15:1) recovered the supporting electrolyte (Bu_4NPF_6), and afforded biotin methyl ester as a white solid; 91% yield; m.p. 158−159 °C; ^{1}H NMR ($CDCl_3$+CD_3OD, 500 MHz) δ: 4.53−4.51 (m, 1H), 4.34−4.32 (m, 1H), 3.68 (s, 3H), 3.24−3.18 (m, 1H), 2.94 (dd, J = 5, 13 Hz, 1H), 2.75 (d, J = 13 Hz, 1H), 2.37 (t, J = 7.3 Hz, 2H), 1.76−1.62 (m, 4H), 1.50−1.45 (m, 2H); ^{13}C NMR ($CDCl_3$+CD_3OD, 125 MHz) δ: 175.3, 165.1, 62.6, 60.8, 56.2, 51.9, 40.7, 34.2, 29.0, 28.7, 25.2; HRMS (ESI) calcd. for $C_{11}H_{19}N_2O_3S$ $[M + H]^+$: 259.1116, found: 259.1121.

2.4.6. ATR–FTIR experiments

Fourier transform infrared (FTIR) spectra were obtained using a Mettler Toledo ReactIR™ IC10 with a silicon composite attenuated total reflectance (ATR) probe inserted into DMSO solutions containing ca. 50 mM of the analyte and 0.2 M Bu_4NPF_6. Background spectra were obtained by using DMSO solutions containing only 0.2 M Bu_4NPF_6. For consistency, the spectroscopic measurements conducted during the different stages (i.e. before CPE, after CPE,

and after methylation) were performed using the same batch of the test solution. Each reported spectrum represents a total of 256 scans recorded at a resolution of 4 cm^{-1}. All spectroscopic experiments were conducted at 295 (±2) K.

2.5. References

[1] S.E. Treimer, D.H. Evans, Electrochemical Reduction of Acids in Dimethyl Sulfoxide. CE Mechanisms and Beyond, J. Electroanal. Chem., 449 (1998) 39–48.

[2] S.E. Treimer, D.H. Evans, Electrochemical Reduction of Acids in Dimethyl Sulfoxide. Comparison of Weak C–H, N–H and O–H Acids, J. Electroanal. Chem., 455 (1998) 19–27.

[3] Y. Meng, S. Norman, C. Hardacre, R.G. Compton, The Electroreduction of Benzoic Acid: Voltammetric Observation of Adsorbed Hydrogen at a Platinum Microelectrode in Room Temperature Ionic Liquids, Phys. Chem. Chem. Phys., 15 (2013) 2031–2036.

[4] G.T. Detitta, R. Parthasarathyt, R.H. Blessing, W. Stallings, Carboxybiotin Translocation Mechanisms Suggested by Diffraction Studies of Biotin and Its Vitamers, Proceedings of the Academy of Natural Sciences, 77 (1980) 333–337.

[5] R.W. Dixon, R.J. Radmer, B. Kuhn, P.A. Kollman, J. Yang, C. Raposo, C.S. Wilcox, L.A. Klumb, P.S. Stayton, C. Behnke, I. Le Trong, R. Stenkamp, Theoretical and Experimental Studies of Biotin Analogues That Bind Almost as Tightly to Streptavidin as Biotin, J. Org. Chem., 67 (2002) 1827–1837.

[6] C. Inard, E. Fourcade, R. Baron, D. Tovar, L. Chaisemartin, C. Blonski, J.-C. Faye, Syntheses of Functionalized Biotin N-1' Derivatives: New Tools for the Control of Gene Expression with Small Molecules, Bioconj. Chem., 17 (2006) 1030–1035.

[7] L. Tao, J. Geng, G. Chen, Y. Xu, V. Ladmiral, G. Mantovania, D.M. Haddleton, Bioconjugation of Biotinylated PAMAM Dendrons to Avidin, Chem. Commun., (2007) 3441–3443.

[8] Y. Li, A.R. Chase, P.F. Slivka, C.T. Baggett, T.X. Zhao, H. Yin, Design, Synthesis, and Evaluation of Biotinylated Opioid Derivatives as Novel Probes to Study Opioid Pharmacology, Bioconj. Chem., 19 (2008) 2585–2589.

[9] J.C. Iglesias-Sánchez, D.S. María, R.M. Claramunt, J. Elguero, Molecular Recognition Studies on Naphthyridine Derivatives, Molecules, 15 (2010) 1213–1222.

[10] L.-Q. Ying, B.P. Branchaud, Design of a Reversible Biotin Analog and Applications in Protein Labeling, Detection, and Isolation, Chem. Commun., 47 (2011) 8593–8595.

[11] S. Arumugam, S.V. Orski, J. Locklin, V.V. Popik, Photoreactive Polymer Brushes for High-Density Patterned Surface Derivatization Using a Diels-Alder Photoclick Reaction, J. Am. Chem. Soc., 134 (2012) 179–182.

[12] R.D. Webster, In situ Electrochemical-ATR-FTIR Spectroscopic Studies on Solution Phase Carboxylate Radical Anions, J. Chem. Soc., Perkin Trans. 2, (2002).

Chapter 3

The Electrochemical Reduction of Cinnamaldehyde in Acetonitrile

This page has been intentionally left blank

3.1. Chapter Overview

In this chapter, an in-depth investigation on the redox reactions of cinnamaldehyde (Scheme 3.1) in acetonitrile (CH_3CN) was carried out through the use of cyclic, linear sweep, and rotating disk electrode voltammetry in conjunction with controlled potential electrolysis and digital simulations.

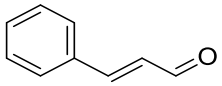

Scheme 3.1. Chemical structure of trans-cinnamaldehyde.

Generally, it was found that cinnamaldehyde displays a similar reduction behavior to retinal (an aldehyde form of vitamin A), and can be reduced by two consecutive one-electron processes to initially form its radical anion ($E_{pc} \approx$ -1.95 vs. (Fc/Fc^+)/V, where E_{pc} refers to the cathodic/reductive peak potential and Fc/Fc^+ = ferrocene/ferrocenium), and then its dianion ($E_{pc} \approx$ -2.50 vs. (Fc/Fc^+)/V). Both reduction processes had limited chemically reversibility even when examined at relatively fast scan rates and low temperatures. Voltammetry and electrolysis experiments revealed that the electrochemical reduction critically depends on the amount of cinnamaldehyde used. At high concentrations, the radical anions have a propensity to undergo a heterodimerization reaction with the starting material to form a radical anionic dimer which could be voltammetrically detected at fast scan rates. The experimental data also indicated a number of other homogeneous reactions involving the reduced species (radical anion and dianion) which were modeled by digital simulations to determine the electrochemical and kinetic parameters affiliated with all of the heterogeneous electron transfer and homogeneous reaction steps.

3.2. Results & Discussion

3.2.1. Electrochemical reduction of cinnamaldehyde in acetonitrile

It had previously been reported that retinal (R), a form of vitamin A with some structural resemblances to cinnamaldehyde (unsaturated aldehyde), can be electrochemically reduced by two sequential one-electron steps into its radical anion ($R^{\bullet -}$) and dianion (R^{2-}) in CH_3CN [1, 2]. At a glassy carbon (GC) electrode, and using a scan rate of 0.1 V s^{-1}, retinal exhibits the presence of two successive reduction/cathodic processes (waves 1 and 2) at ca. -1.82 and -2.15 vs. (Fc/Fc^+)/V, respectively (Figure 3.1a). Although both cathodic reactions display a corresponding oxidative peak in the return sweep of the CV (waves 3 and 4), they are only moderately chemically reversible since the anodic/oxidative to cathodic/reductive peak current ratios (I_{pa}/I_{pc}) for both redox couples are << 1. Nonetheless, halting the forward potential scan to allow only a single reduction to occur improves the chemical reversibility of the first process, as depicted by the more pronounced size of wave 4.

Preliminary CV scans of cinnamaldehyde under the same conditions disclosed some similarities to the voltammetric behavior of retinal. On the forward scan, cinnamaldehyde likewise presents two successive cathodic processes (waves I and II) at ca. -1.95 and -2.50 vs. (Fc/Fc^+)/V, respectively (Figure 3.1b). Conversely, it was found that considerably smaller corresponding anodic currents (waves III and IV) were measured when the scan direction was reversed; especially for wave IV. Moreover, a restriction of the scan's potential range did not appear to benefit the chemical reversibility of the first reduction step.

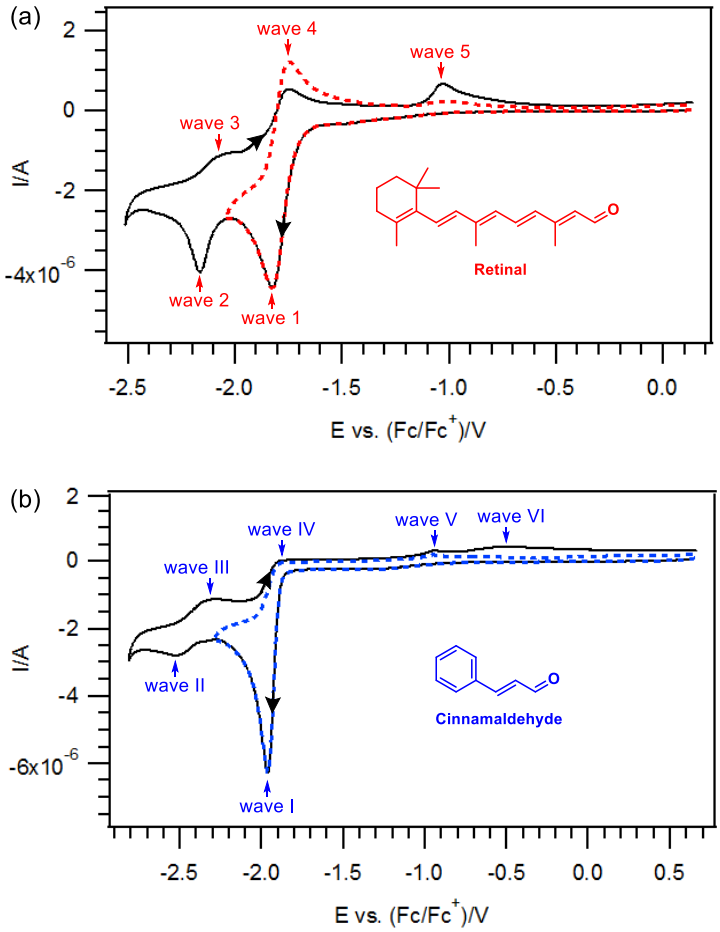

Figure 3.1. Cyclic voltammograms of 2 mM (a) retinal and (b) cinnamaldehyde in CH_3CN containing 0.2 M Bu_4NPF_6, recorded at 295 (±2) K using a 1-mm diameter planar GC disk electrode at 0.1 V s^{-1}. (a) (—) Switching potential ≈ -2.51 vs. (Fc/Fc^+)/V. (- - -) Switching potential ≈ -2.04 vs. (Fc/Fc^+)/V. (b) (—) Switching potential ≈ -2.81 vs. (Fc/Fc^+)/V. (- - -) Switching potential ≈ -2.29 vs. (Fc/Fc^+)/V.

3.2.2. Cyclic voltammetry at varied scan rates

To further investigate the electrochemical reduction of cinnamaldehyde, CV experiments were next conducted at varied scan rates (Figure 3.2). Overall, it was observed that waves III and IV did not grow substantially despite the use of relatively fast scan rates, indicating that the reduced species are scarcely converted back into the starting materials. Therefore, it is reasonable to assume that the reduced forms of cinnamaldehyde are highly reactive/unstable and do not

survive over the timeframes of the CV experiments (≤ seconds). This premise is also attested to by the commensurately smaller magnitudes of wave II relative to wave I at slower rates, indicating that there are fewer molecules able to undergo a second reduction step. This can be rationalized by the larger amount of time available at lower scan rates for the reduced species (formed after the first reduction) to undergo other homogeneous reactions before it is reduced again. In other words, as the scan rate is increased, the homogeneous reactions of the initially formed radical anion are outrun; hence, wave II (which is related to the reduction of the radical anion) is able to increase in magnitude as compared to wave I at faster scan rates.

During the voltammetric reduction of retinal, a third and separate anodic process (wave 5) was also recorded at more positive potentials on the return scan (ca. -1.03 vs. $(Fc/Fc^{+})/V$), and is associated with the oxidation of secondary products formed after the reductions (Figure 3.1a and Figure A3.1 in the appendix) [1]. In a similar vein, two oxidation processes (waves V and VI) were also detected at ca. -0.95 and -0.65 vs. $(Fc/Fc^{+})/V$, respectively, after first reducing cinnamaldehyde, and became more prominent at faster scan rates (Figure 3.2). Thus, it is conceivable that these subsidiary waves are likewise associated with the oxidation of secondary products generated after cinnamaldehyde's reduction. More importantly, because waves V and VI are registered in the voltammogram even if the scan range was limited to only the first cathodic process (wave I), it can be inferred that the ancillary products stem from the reactions of the singly reduced form of cinnamaldehyde, and not its dianion. Nevertheless, these molecules are relatively short-lived since waves V and VI are barely detected at lower scan rates. It is also possible that other accessory products are formed after both reductions, but either do not fall within the potential window of CH_3CN (using a GC electrode) or are not redox active.

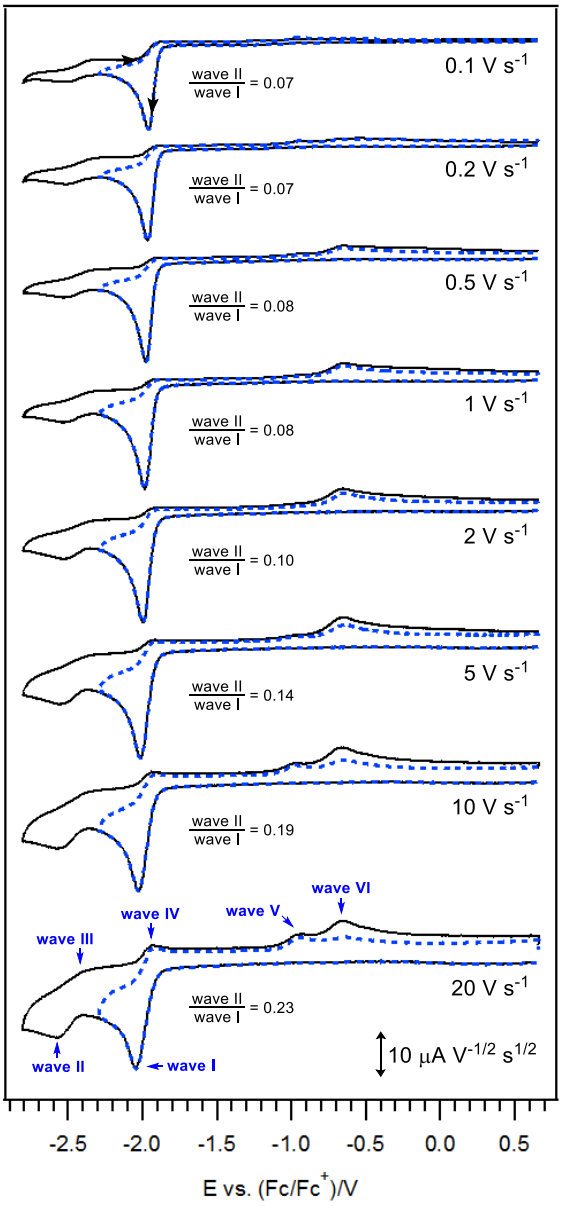

Figure 3.2. Cyclic voltammograms of 2 mM cinnamaldehyde in CH_3CN containing 0.2 M Bu_4NPF_6, recorded at 295 (±2) K using a 1-mm diameter planar GC disk electrode and at different scan rates. (—) Switching potential ≈ -2.80 vs. (Fc/Fc^+)/V. (- - -) Switching potential ≈ -2.29 vs. (Fc/Fc^+)/V. The current data have been normalized by multiplying against (scan rate)$^{-1/2}$.

For a diffusion controlled electrochemically reversible process, the *Randles–Sevcik* equation [3] states that the peak current (I_p /A) should be proportional to the square root of the scan rate (v /V s^{-1}),

$$I_p = (2.686 \times 10^5)n^{3/2}ACD^{1/2}v^{1/2} \quad (3.1)$$

where: n = number of moles of electrons transferred; A = area of the electrode (cm^2); and C = concentration of the analyte (mol cm^{-3}); and D = diffusion coefficient (cm^2 s^{-1}).

As Figure 3.3 illustrates, a plot of the I_p^{red} (wave I) against the square root of scan rate afforded an excellent linear relationship. On this basis, it can be surmised that the electrochemical reduction of cinnamaldehyde in this study is primarily diffusion controlled. However, it is worth highlighting that it has been found that the proportionality of I_p to $n^{3/2}$ is mostly valid for concurrent multi-charge transfer processes, and thus it may be more accurate for $n^{3/2}$ to be replaced by n when describing the more common reactions which show sequential electron transfer [4]. Regardless, assuming n = 1 for the first reduction step (wave I) (see section 3.2.5), it can be calculated (using eq. 3.1 and the gradient of the linear plot in Figure 3.3) that $D = 3.04 \times 10^{-5}$ cm^2 s^{-1} for cinnamaldehyde under the present conditions, which is close to the values obtained subsequently (sections 3.2.5 and 3.2.7).

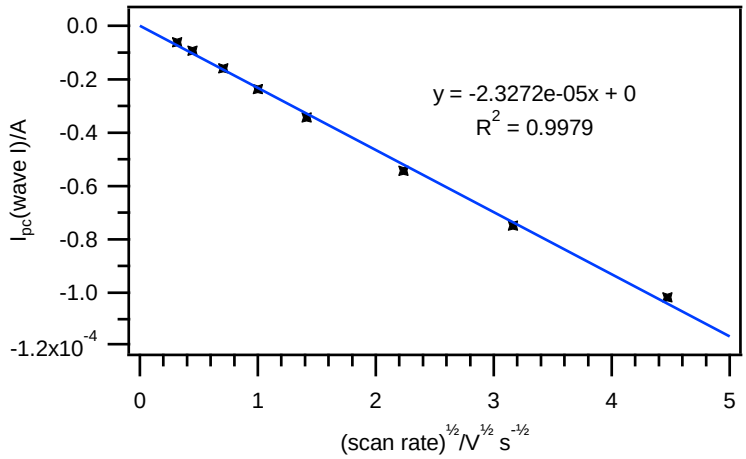

Figure 3.3. Plot of cathodic peak current (wave I) vs. square root of scan rate for cyclic voltammograms of 2 mM cinnamaldehyde in CH_3CN containing 0.2 M Bu_4NPF_6, recorded at 295 (±2) K using a 1-mm diameter planar GC disk electrode at different scan rates (0.1, 0.2, 0.5, 1.0, 2.0, 5.0, 10.0, and 20.0 V s^{-1}).

3.2.3. Cyclic voltammetry at varied temperatures

CV experiments were also performed at lowered temperatures. However, the chemical reversibility of cinnamaldehyde's electrochemical reduction did not improve appreciably, signifying that decreased temperatures do not significantly aid in stabilizing the reduced forms (Figure 3.4). For instance, the reverse oxidation peaks (waves III and IV) remained small even at a relatively low temperature of 243 K and a high scan rate of 20 V s^{-1} (Figure A3.2 in the appendix). Nonetheless, it was observed that wave VI appeared to be more distinct at temperatures < 273 K, suggesting that the secondary product responsible for this process survives somewhat better in colder environments.

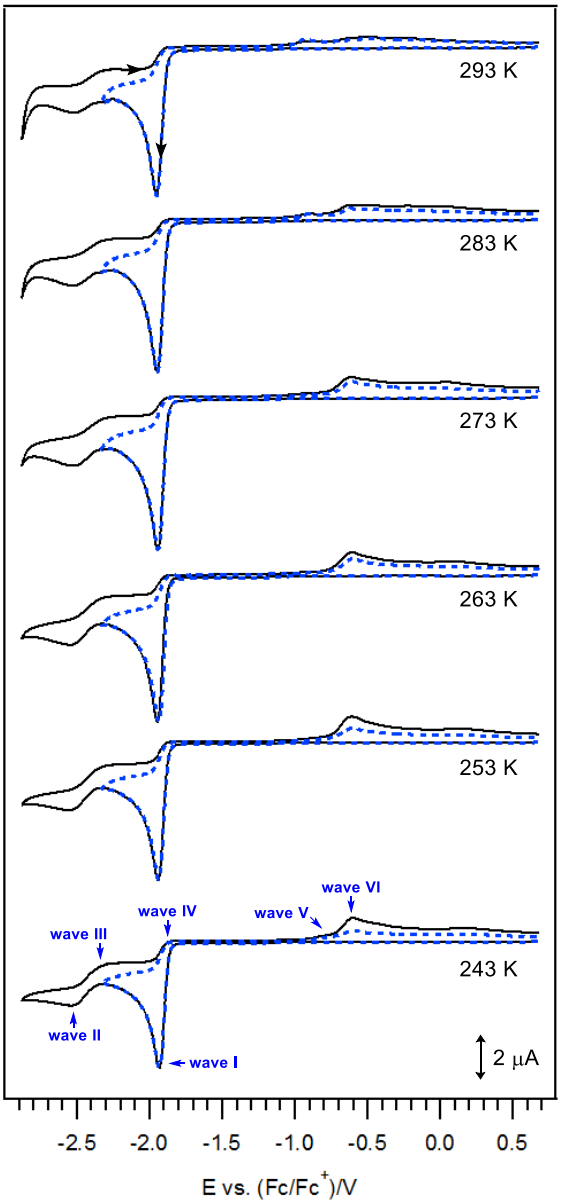

Figure 3.4. Cyclic voltammograms of 2 mM cinnamaldehyde in CH_3CN containing 0.2 M Bu_4NPF_6, recorded using a 1-mm diameter planar GC disk electrode, at 0.1 V s^{-1}, and at different temperatures. (—) Switching potential ≈ -2.88 vs. (Fc/Fc^+)/V. (- - -) Switching potential ≈ -2.33 vs. (Fc/Fc^+)/V.

3.2.4. Cyclic Voltammetry at varied concentrations

In order to assess the effects of starting material concentration on the reduction mechanism, CV experiments were subsequently carried out using different concentrations of cinnamaldehyde (Figure 3.5). This showed that as the initial concentration of cinnamaldehyde used is increased, wave II decreases in size relative to the wave I, indicating that with increasing concentration of analyte, fewer molecules are able to undergo the second reduction.

There have been a number of studies that have reported on the reversible dimerization of the radical anions of aromatic compounds produced by electrochemical methods [1, 5-11]. These dimers were described as more difficult to oxidize than their monomers, which is consistent with the secondary anodic processes (waves V and VI) appearing at ca. several hundred mV more positive than the anodic peak potential (E_{pa}) of the radical anion (wave IV). As such, it can be inferred that the reduction of cinnamaldehyde also likely entails a similar dimerization/coupling reaction. After cinnamaldehyde is reduced at the wave I, two of the reduced forms and/or the starting material can react together, causing fewer radical anions to be available for a second reduction. Since the reactants would be present in greater quantities at higher concentrations, the dimerization reaction(s) would be favored under such conditions, thereby drastically impeding the occurrence of a second reduction and concomitantly leading to the diminished size of wave II as compared to wave I at larger concentrations.

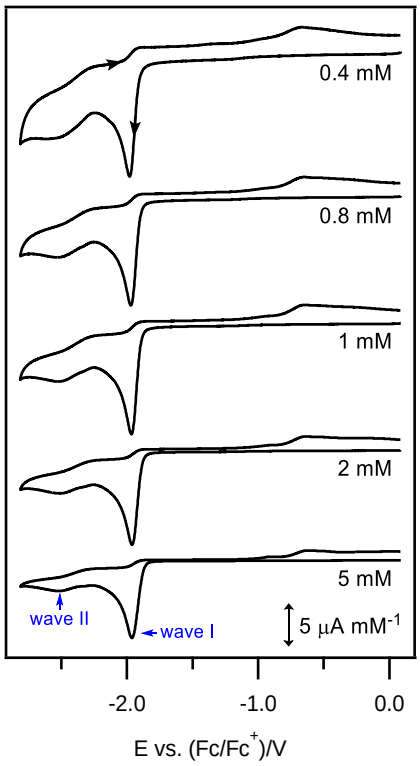

Figure 3.5. Cyclic voltammograms of different concentrations of cinnamaldehyde, in CH_3CN solutions containing 0.2 M Bu_4NPF_6, recorded at 295 (±2) K using a 1-mm diameter planar GC disk electrode at 0.5 V s^{-1}. The current data have been normalized by multiplying by $(concentration)^{-1}$.

3.2.5. Voltammetry at a rotating disk electrode

Results from the preceding sections have established that the singly reduced form of cinnamaldehyde undergoes other homogeneous (e.g. dimerization) reactions in tandem with its electrochemical production. To study this interaction in greater detail, rotating disk electrode (RDE) voltammetry was employed to investigate cinnamaldehyde's redox behavior under hydrodynamic conditions [12]. More specifically, it was envisaged that the continuous supply of fresh reactants to the electrode surface (when using a RDE) would allow for the consecutive reductions of cinnamaldehyde to be carried out without the interferences of the homogeneous reactions of its reduced form. The RDE experiments were all performed at a scan rate of 0.02

V s^{-1}, at which the noise level was minimal. Moreover, the utilization of a slower sweep also provides more time for the reductions to attain a steady state response.

To serve as a comparison, linear sweep voltammograms (no rotation) were first recorded of cinnamaldehyde at varied scan rates. In general, they agreed with earlier findings and revealed a more aggravated decline in wave II relative to wave I at lower scan rates; such that at 0.02 V s^{-1} (the scan rate used for the RDE experiments), wave II appeared almost indistinguishable from the background (Figure 3.6a). In contrast, the RDE voltammograms display marked increments in current intensities for the second reduction process (wave II), even at a relative low rotation speed of 500 rpm, denoting that more of the radical anions are capable of undergoing a second reduction (Figure 3.6b).

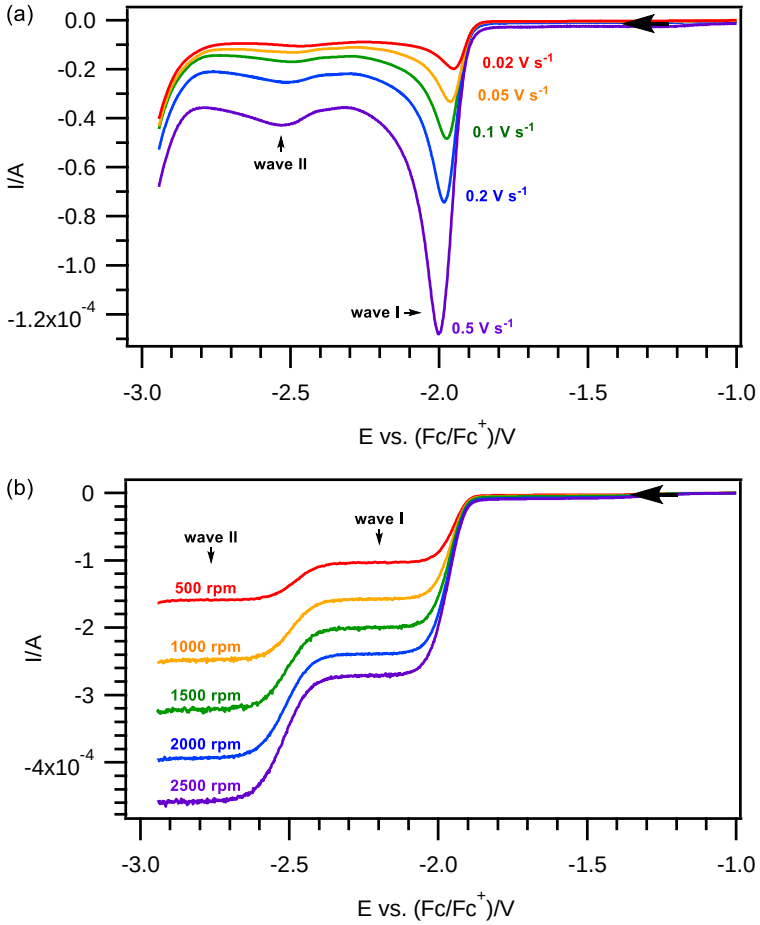

Figure 3.6. Linear sweep voltammograms of 2 mM cinnamaldehyde in CH_3CN containing 0.2 M Bu_4NPF_6, recorded at 295 (±2) K (a) using a 3-mm diameter planar GC disk electrode and at different scan rates, (b) using a 3-mm diameter planar GC rotating disk electrode, at 0.02 V s^{-1}, and at different rotation speeds.

The general reversible wave equation [13] is used to test for reversibility under steady state conditions for a hydrodynamic voltammogram and can be expressed as,

$$E = E_{½} \pm \frac{RT}{nF} \ln \frac{I_d - I}{I} \qquad (3.2)$$

where: E = potential (V); $E_{½}$ = half-wave potential (V); n = number of moles of electrons transferred, I_d = limiting current (A); I = current for a fixed sampling time τ (A); and ± = positive for reductions. For an electrochemically reversible system, a plot of E against log[(I_d–I)/I]

would yield a linear relationship with a slope of 58.2/n mV at 293 K. Experimental values measured for wave I at the five rotation speeds were arranged into logarithm form, $\log[(I_d–I)/I]$, and then plotted with E using the linear least squares method to give straight line graphs.

A representative example is given in Figure 3.7. The slope obtained for the graph (wave I at 1500 rpm) was ca. 62.6 mV, translating to a value that is close to 1 for n. Consonant results were also calculated for the other four rotation rates (Figures A3.3-A3.6 in the appendix), supporting that a total of one-electron is transferred during the first reduction process (wave I).

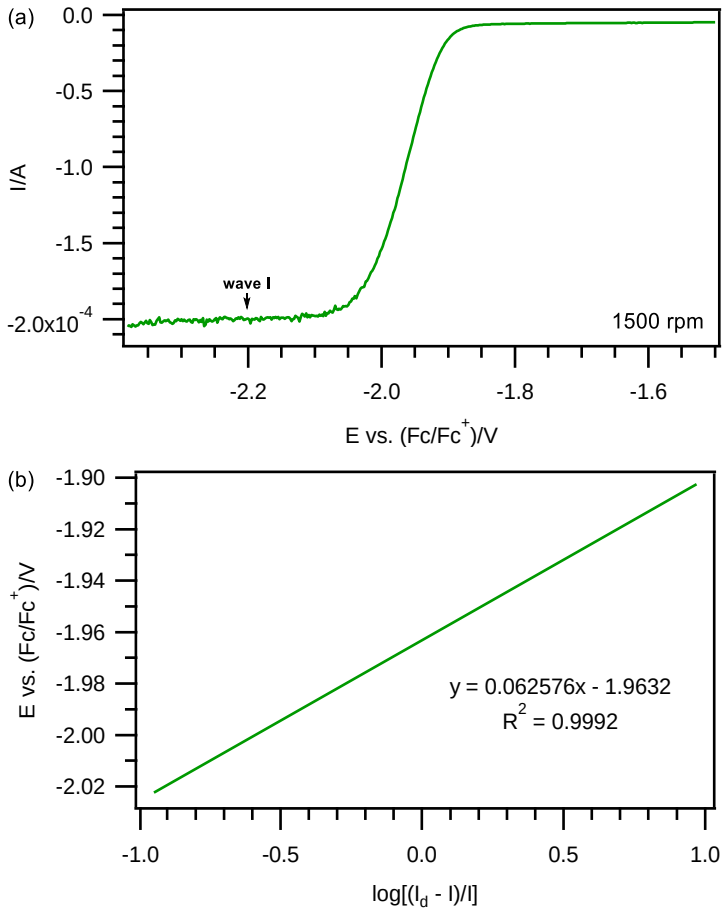

Figure 3.7. Wave slope analysis of steady state voltammogram. (a) Linear sweep voltammograms of 2 mM cinnamaldehyde in CH_3CN containing 0.2 M Bu_4NPF_6, recorded at 295 (±2) K using a 3-mm diameter planar GC rotating disk electrode, at 0.02 V s^{-1}, and at 1500 rpm. (b) Plot of E vs. $\log[(I_d – I)/I]$ using the experimental data from (a).

According to the Levich equation [13], the limiting current should be proportional to the concentration and square root of the angular rotation speed, for an electrochemical system where mass transport is the only determinant of the rate of the half-reaction.

$$I_L = 0.62nFAD^{2/3}\omega^{1/2}v^{-1/6}C \qquad (3.3)$$

where: I_L = mass transport limiting (Levich) current (A); n = number of moles of electrons transferred; F = Faraday's constant (96 485 C mol^{-1}); A = area of the electrode (cm^2); D = diffusion coefficient of the analyte (cm^2 s^{-1}); ω = angular rotation rate of the electrode (rad s^{-1}); v = kinematic viscosity of the solution (5.22×10^{-3} cm^2 s^{-1} at 293 K [14]); and C = concentration of the analyte (mol cm^{-3}). As shown in Figure 3.8 below, using the linear plot of I_L (wave I) versus $\omega^{1/2}$ (gradient = -1.57×10^{-5} A $rad^{-1/2}$ $s^{1/2}$), a diffusion coefficient of 2.15×10^{-5} cm^2 s^{-1} was derived for cinnamaldehyde under the present conditions, which is close to the value obtained previously (section 3.2.2) and by digital simulations of the CV data.

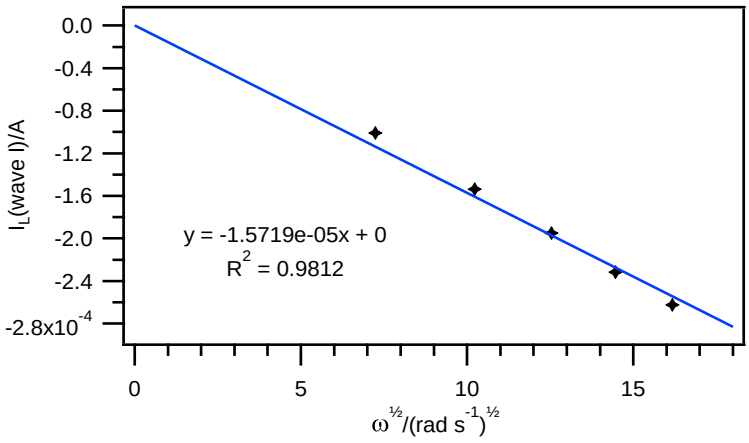

Figure 3.8. Levich (I_L(wave I) vs. $\omega^{1/2}$) plot of 2 mM cinnamaldehyde in CH_3CN containing 0.2 M Bu_4NPF_6 recorded at 295 (±2) K using a 3-mm diameter planar GC rotating disk electrode.

3.2.6. Bulk controlled potential electrolysis

Controlled potential electrolysis (CPE) experiments were conducted to gain additional insights about the intermediates and long-term reduction products (≥ minutes), as well as confirm the number of electrons transferred during the reductions. The potentials applied during the CPE experiments were ca. 0.15 V more negative than the respective cathodic peak potentials (E_{pc}) obtained by CV so as to ensure that a full conversion of analyte was accomplished.

The coulometric data collected from the reductive electrolysis (of 2 mM cinnamaldehyde) at an applied potential just past wave I are illustrated in Figure 3.9 along with the respective cyclic voltammograms acquired before and after the CPE. Verification of an exhaustive analyte reduction can be achieved from the complete disappearance of waves I and II in the latter voltammogram (Figure 3.9a, blue dashed line).

Using eq. 3.5, the bulk reduction of cinnamaldehyde (at -2.13 vs. $(Fc/Fc^{+})/V$) was calculated to involve a total of ca. 0.71 electrons transferred; which is less than the expected value of 1. Matching results were obtained when the experiments were repeated twice (Figures A3.7 and A3.8 in the appendix), while only ca. 1.51 electrons were transferred when the CPE was carried out at a potential past the second reduction step (wave II), which is less than the expected value of 2 (Figure A3.9 in the appendix). While analysis of the initial state of charge might be able to provide a value of n that is closer to 1 for the first reduction step [13], the electrolysis results obtained over a prolonged period are also useful as they illustrate that the singly reduced form of cinnamaldehyde probably undergoes a heterodimerization (radical-substrate coupling) reaction with the starting material after its formation, thereby resulting in the less than one-electron count observed. More interestingly, electrolysis experiments at larger cinnamaldehyde concentrations exhibited a trend of less number of electrons transferred as the initial concentration used is increased – only 0.46 and 0.39 electrons were transferred at 10 mM

and 30 mM concentrations, respectively (Figures A3.10 and A3.11 in the appendix), and is consistent with prior observations for the varied concentration CV experiments, where it was discerned that the reduction is highly sensitive to the analyte concentration used.

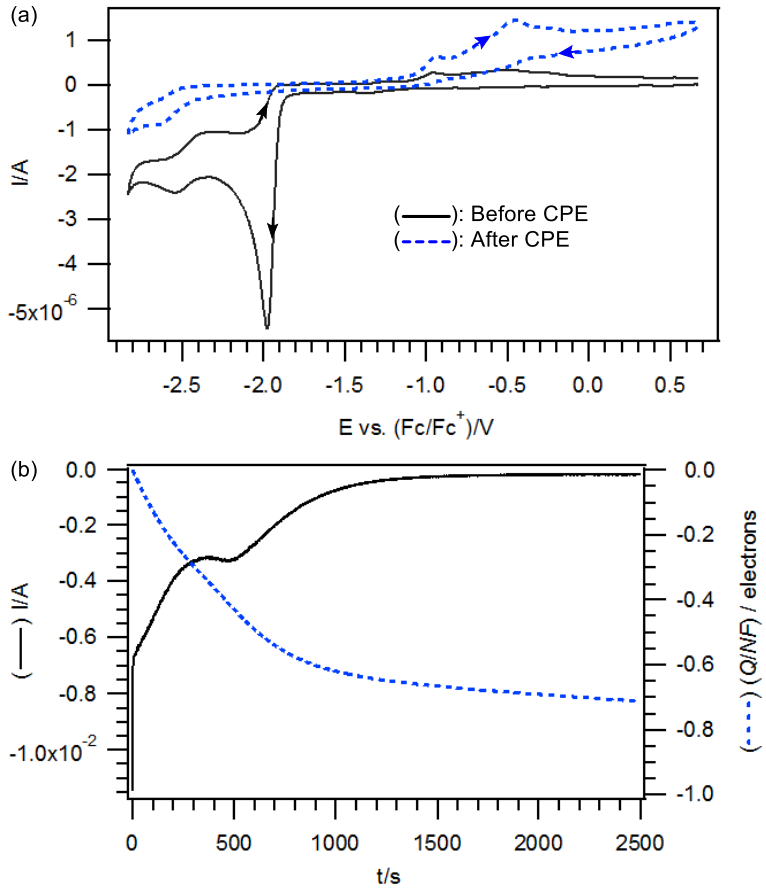

Figure 3.9. Voltammetric and coulometric data obtained during the reductive CPE (wave I) of 2 mM cinnamaldehyde in CH_3CN containing 0.2 M Bu_4NPF_6 at 295 (±2) K. (a) Cyclic voltammograms recorded at 0.1 V s^{-1} with a 1-mm diameter planar GC disk electrode. (b) Current/coulometry vs. time data obtained during the reductive CPE (at -2.13 vs. (Fc/Fc^+)/V).

Thin layer chromatography (TLC) analysis of the one-electron electrolyzed solutions at synthetic scale (100 mg) unveiled numerous products that were very difficult to separate and purify by preparative column chromatography. Nevertheless, ^1H and ^{13}C NMR analysis on the crude reaction mixture showed a complete disappearance of the aldehyde group, and therefore

shows a dissimilar pattern to aqueous systems where earlier reports found that the initial reduction of cinnamaldehyde is restricted to just the hydrogenation of its alkene group [15-18]. Unfortunately, similar to the CV experiments where it was found that the secondary products (such as the radical anion dimer) survive poorly even over short periods (≤ seconds), we were unable to obtain spectroscopic evidence for the existence of the dimer over synthetic timescales (minutes to hours). It is presumable, therefore, that the dimers only exist as transient intermediates/species, which is common in such reversible dimerization reactions [1, 5-11].

3.2.7. Digital simulations & proposed mechanism

It was postulated that the one-electron reduction of retinal is followed by a homodimerization (radical-radical coupling) reaction between two of its radical anions [1].

$$R^{\bullet -} + R^{\bullet -} \rightleftharpoons R_2^{2-} \qquad (3.4)$$

However, while an identical coupling reaction between the radical anions of cinnamaldehyde cannot be ruled out at this juncture, this must not be the only scenario since the electrolysis results at different concentrations ($n << 1$) seem to imply that a reaction between the radical anions and the starting material (cinnamaldehyde) is also happening. That is, when the concentration of cinnamaldehyde used is high, there is a greater chance that the radical anions can readily react with and consume the starting material. This in turn leads to a dwindling amount of analyte balanced in the bulk solution for further reduction and correspondingly a less than expected number of electrons transferred during the CPE experiments. In comparison, reductive electrolysis of retinal at its first cathodic process (wave 1) gave a value of very close to 1 even at high concentrations (20 mM) [1]. Furthermore, the detection of two ancillary oxidation processes (waves V and VI) on the return scans of fast rate CV also lends weight to the fact that there are probably two different secondary products formed.

With the above information at hand, digital simulations of the CV data at variable scan rates were executed to decipher the most appropriate mechanism involved in the electrochemical reduction of cinnamaldehyde. The CV scans were performed over two potential windows: the first range was sufficiently negative to bring about the two successive one-electron reduction processes, while the second range was restricted to only the first reduction step. The diffusion coefficient of cinnamaldehyde was first determined from the cathodic peak current of the first process (wave I), while the diffusion coefficient values of the other species (e.g. anions and dimers) were shrunk by up to 30% to account for their larger sizes and/or stronger electrolyte and solvent interactions which will hinder their mobility in solution. The simulation studies were then carried out by a trial and error process, and by systematically expanding the reaction steps in the reduction pathway (using one set of parameters over all scan rates) until the simulated voltammograms most closely matched the experimental data. This fitting procedure was done by eye rather than by an automated define error minimization process.

Overlays of the simulated and experimental graphs at various scan rates are represented in Figure 3.10 and generally show a relatively close fitting. The slight deviations between the simulated and experimental graphs might be partly attributable to background effects originating from the solvent or electrolyte, as well as trace impurities present in the test solutions which are not easily compensated for in the simulations. A stepwise illustration of the proposed mechanism is outlined in Scheme 3.2, while the data (electrochemical and kinetic parameters) obtained from digitally simulating the entire mechanism are given in Tables 3.1 and 3.2, respectively. The mechanism portrayed is dependent on the applied and switching potentials, with partially different pathways prevailing for the one- and two-electron reductions.

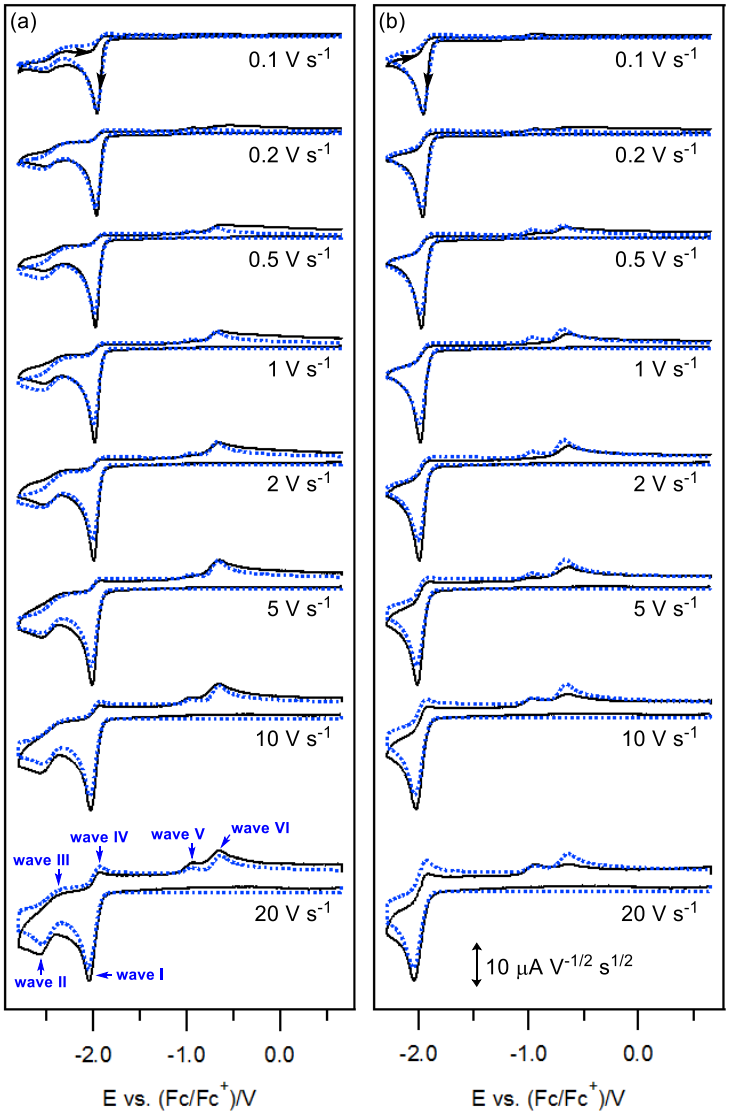

Figure 3.10. (—) Experimental cyclic voltammograms of 2 mM cinnamaldehyde in CH_3CN containing 0.2 M Bu_4NPF_6, recorded at 295 (±2) K using a 1-mm diameter planar GC disk electrode and at different scan rates. (••••) Simulated voltammograms generated according to mechanism in Scheme 3.2, and parameters in Tables 3.1 & 3.2. (a) Switching potential ≈ -2.80 vs. (Fc/Fc^+)/V. (b) Switching potential ≈ -2.29 vs. (Fc/Fc^+)/V. The current data have been normalized by multiplying against $(\text{scan rate})^{-1/2}$.

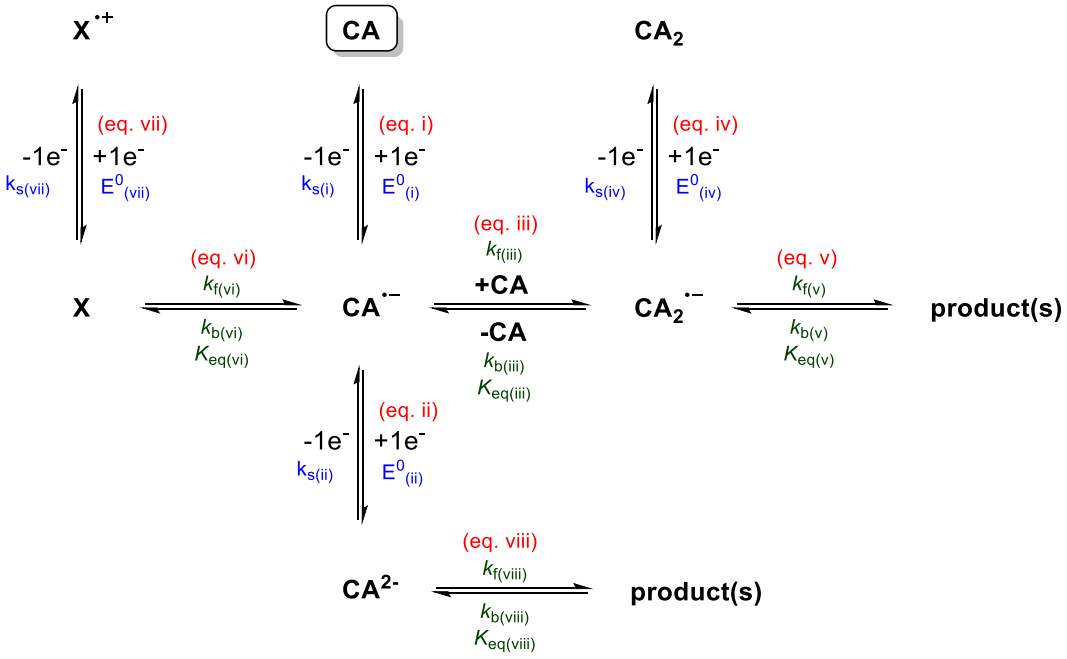

Scheme 3.2. Proposed mechanism for the electrochemical reduction of cinnamaldehyde (CA) in CH_3CN. The exact charge on $X/X^{\bullet+}$ is not precisely known.

As the applied potential is varied toward suitably negative values (wave I), a one-electron reduction of cinnamaldehyde into its radical anion is initially induced (eq. i in Scheme 3.2 and Tables 3.1 and 3.2). Thereafter, the radical anion can further accept a one-electron to form its dianion if the potential is scanned even more negatively past wave II (eq. ii). Voltammetry and electrolysis experiments have shown that the radical anions undergo at least two differing homogeneous reactions which directly accompany cinnamaldehyde's first heterogeneous electron transfer step. For example, it was ascertained by CPE that the radical anions can react with the starting material (cinnamaldehyde) to produce an expected radical anion dimer (eq. iii). As discussed previously, this dimeric species would be oxidizable (eq. iv) at potentials of a few hundred mV more positive than its constituents [1, 5-11] and is tentatively assigned to wave V. It is worth mentioning that the equilibrium and forward rate constants (K_{eq} = 5.0 x 10^6 and k_f = 3.3 x 10^4) obtained for this reaction are very large (eq. iii), and is in line with expectations since the CV experiments all expressed dissimilar peak heights between

waves I and II. Essentially, the considerably smaller magnitude of wave II relative to wave I at slower scan rates and heightened concentrations can be explained by the decreased number of radical anions that are able to undergo a second reduction due to their inclination to undergo the coupling reaction instead. Notwithstanding, this species is probably susceptible to a downstream reaction (e.g. decomposition or hydrolysis) and is short-lived (eq. v) since the radical anion dimer (wave V) can only be detected at fast scan rates (≥ 10 V s^{-1}). Therefore, the equilibrium and forward rate constants associated with eq. v are assigned to be relatively small in magnitude ($K_{eq} = 1.6 \times 10^{2}$ and $k_f = 8.0 \times 10^{-1}$) such that they can be outrun at high scan rates.

Apart from the abovementioned heterodimerization process (between the radical anions and cinnamaldehyde) a competing homogeneous reaction is necessitated by the presence of a second ancillary oxidation (wave VI) that was recorded in CV (eq. vii). In this case, it is possible that the radical anions form a presently unidentified, redox active compound X via protonation, decomposition, and/or other reaction(s) (e.g. homodimerization reaction [1, 19, 20]) (eq. vi). Akin to the behavior recorded for wave V, wave VI is only voltammetrically observable at high scan rates, and thus the associated equilibrium and forward rate constants are similarly relatively small in values ($K_{eq} = 1.6 \times 10^{-2}$ and $k_f = 1.2 \times 10^{0}$). Notably, as the radical anion formed after the initial one-electron reduction of cinnamaldehyde has been demonstrated to exhibit limited chemical reversibility, the equilibrium and forward rate constants associated with its coupled homogeneous reactions (eq. iii and vi) would be in favor of the formation of the products ($CA_2^{\bullet -}$ and X), thereby resulting in less species available for conversion back into the starting material.

Lastly, because only limited chemical reversibility was observed for both reduction reactions of cinnamaldehyde (even at fast scan rates and low temperatures) it is also plausible that the dianion partakes in a fast homogeneous reaction(s) subsequent to its formation (e.g.

decomposition; similar to retinal [1]) and has relatively high equilibrium and forward rate constants (K_{eq} = 5.0 x 10^4 and k_f = 8.0 x 10^4) (eq. viii).

Table 3.1. Electrochemical parameters[a] obtained by digital simulations of CV data[b] for the reaction mechanism given in Scheme 3.2.

Electrochemical Parameters	eq. i	eq. ii	eq. iv	eq. vii
E^0 (V)	-1.98	-2.42	-1.00	-0.72
D (cm^2 s^{-1})	3.0 x 10^{-5}	2.7 x 10^{-5}	2.1 x 10^{-5}	2.1 x 10^{-5}
k_s (cm s^{-1})	0.30	0.03	0.14	0.06

[a]D = diffusion coefficient of the oxidized form, E^0 = formal potential vs. (Fc/Fc^+), k_s = heterogeneous electron transfer rate constant. Charge transfer coefficients (α) were assumed as 0.5. [b]CV data were recorded at 295 (±2) K using a 1-mm diameter planar GC disk electrode for solutions of 2 mM cinnamaldehyde and 0.2 M Bu_4NPF_6 in CH_3CN.

Table 3.2. Equilibrium and rate constants[a] obtained by digital simulations of CV data[b] for the reaction mechanism given in Scheme 3.2.

Kinetic Parameters	eq. iii	eq. v	eq. vi	eq. viii
K_{eq}	5.0 x 10^6	1.6 x 10^2	1.6 x 10^{-2}	5.0 x 10^4
k_f	3.3 x 10^4	8.0 x 10^{-1}	1.2 x 10^0	8.0 x 10^4
k_b	6.6 x 10^{-3}	5.0 x 10^{-3}	7.5 x 10^0	1.6 x 10^0

[a]K_{eq} = equilibrium constant, k_f = forward rate constant, k_b = backward rate constant. k_f and k_b have units of s^{-1} and L mol^{-1} s^{-1} for the first- and second-order reactions, respectively. [b]CV data were recorded at 295 (±2) K using a 1-mm diameter planar GC disk electrode for solutions of 2 mM cinnamaldehyde and 0.2 M Bu_4NPF_6 in CH_3CN.

3.3. Conclusion

The results gathered from the voltammetric and electrolytic responses of cinnamaldehyde in CH_3CN have shown that at moderately large negative potentials, the aforementioned compound can undergo two one-electron transfer reactions in succession to generate its radical anion and dianion. It was established that the reduction processes are strongly influenced by the concentration of cinnamaldehyde used due to existence of several accompanying homogeneous reactions that take place after the electrochemical generation of the anions (radical anion and dianion). In particular, it was elucidated that the use of high cinnamaldehyde concentrations encourages a heterodimerization reaction between the radical anions and starting material to form a dimeric species that could be observed voltammetrically at high scan rates. NMR analysis of the one-electron electrolyzed solutions of cinnamaldehyde in CH_3CN also suggested that the reduction does not follow the exact mechanistic pathways involved in aqueous systems (examined by polarography) but, instead, probably also involves its aldehyde (rather than only the alkene) functionality from the onset of the first electron uptake. Finally, through careful interpretation of the experimental data, a mechanism for the electrochemical reduction of cinnamaldehyde was proposed and modeled by digital simulations (showing a good fit) to determine all the associated electrochemical and kinetic parameters.

3.4. Materials & Methods

3.4.1. Chemicals & reagents

Unless otherwise specified, all chemicals and reagents were purchased from commercial sources and used as received. trans-Cinnamaldehyde (98+%) was obtained from Alfa-Aesar. Acetonitrile (HPLC grade) was purchased from Anhui Fulltime Solvents & Reagents Co., Ltd., ethanol (ACS grade) and diethyl ether (ACS grade) from Merck, and *N*,*N*-dimethylformamide (HPLC grade) from VWR. The supporting electrolyte tetrabutylammonium hexafluorophosphate (Bu_4NPF_6) was prepared by reacting equal molar amounts of a 40% aqueous solution of Bu_4NOH (Alfa-Aesar) with a 65% aqueous solution of HPF_6 (Alfa-Aesar), washing the precipitate with hot water, recrystallizing three times from hot ethanol, and then drying in vacuo at 413 K for 6 h.

3.4.2. Voltammetry experiments

Voltammetric experiments were conducted with a computer-controlled Metrohm Autolab PGSTAT302N potentiostat using a three electrode system.

For cyclic voltammetry experiments, working electrodes were 1-mm diameter planar glassy carbon (GC) disks (eDAQ Pty Ltd), used in conjunction with a platinum wire auxiliary/counter electrode (Metrohm) and a silver wire miniature reference electrode (eDAQ Pty Ltd) that is connected to the test solution via a salt bridge containing 0.5 M Bu_4NPF_6 in CH_3CN. Variable temperature cyclic voltammetric experiments were carried out in a Metrohm jacketed glass cell and the temperatures controlled by a Julabo FP89-HL ultralow refrigerated ethanol circulating bath. Rotating disk electrode voltammetry experiments were done using a Metrohm Autolab RDE-2 rotator and a 3-mm diameter planar glassy carbon electrode (Metrohm), in conjunction with the aforementioned instrumentation.

Prior to each voltammetric scan, all solutions used were de-oxygenated by purging with high purity argon gas. The working electrodes were cleaned by polishing with alumina oxide (grain size 0.3 μm) slurry on a Buehler Ultra-pad polishing cloth, rinsing with ultrapure water, acetone, and then dried. Accurate potentials were obtained by using ferrocene as an internal standard, which was added to the test solution at the end of the experiments.

3.4.3. Controlled potential electrolysis experiments

Electrolysis experiments were conducted in a two-compartment electrolysis cell separated by a sintered glass frit with a porosity no. 5 (1.0–1.7 μm). Identically sized GC cylinders were used as the working and auxiliary electrodes and symmetrically arranged with respect to each other with a silver wire reference electrode, isolated via a salt bridge containing 0.5 M Bu_4NPF_6 in CH_3CN, that was positioned to within 2 mm of the surface of the working electrode. The solutions in both electrode compartments were 25 mL each and simultaneously de-oxygenated and stirred using bubbles of argon gas. The number of electrons transferred during the bulk electrolysis process was calculated from

$$n = Q/NF \tag{3.5}$$

where: n = number of moles of electrons transferred; Q = charge (coulombs); N = no. of moles of starting compound; and F = Faraday's constant (96 485 C mol^{-1}).

3.4.4. NMR analysis of electrolyzed solution

^1H and ^{13}C NMR spectra were measured on a Bruker Avance 500 (500 MHz) NMR spectrometer. Chemical shifts (ppm) were recorded using tetramethylsilane (TMS, 0.00 ppm) as the internal reference standard and referenced to CD_3CN, the solvent used. CD_3CN was acquired from the Cambridge Isotope Laboratories Inc. The electrolyte (Bu_4NPF_6) was removed prior to NMR analysis of the one-electron electrolyzed solutions of cinnamaldehyde

by first evaporating CH_3CN under reduced pressure, dissolving the crude electrolyte-products in a mixture of DMF/water (5:3 ratio), extracting with diethyl ether, washing the organic layer with brine, and drying over anhydrous sodium sulphate [21].

3.4.5. Digital Simulations

Digital simulation modeling of the CV data was performed using a DigiElch electrochemical simulation software package (DigiElch 7) purchased from Gamry Instruments.

3.5. References

[1] Y.S. Tan, Y. Yue, R.D. Webster, Competing Hydrogen-Bonding, Decomposition, and Reversible Dimerization Mechanisms during the One- and Two-Electron Electrochemical Reduction of Retinal (Vitamin A), J. Phys. Chem. B, 114 (2013) 9371–9379.

[2] Y.S. Tan, D. Urbančok, R.D. Webster, Contrasting Voltammetric Behavior of Different Forms of Vitamin A in Aprotic Organic Solvents, J. Phys. Chem. B, 118 (2014) 8591–8600.

[3] J. Wang, Analytical Electrochemistry, 3rd ed., Wiley-VCH, New Jersey, 2006.

[4] K. Aoki, Is Voltammetric Current Proportional to the Number of Transferred Electrons for Multi-Charged Ions or to 3/2 Power of the Number?, Electroanalysis, 17 (2005) 1379–1383.

[5] O. Hammerich, V.D. Parker, Kinetics and Mechanisms of Reactions of Organic Cation Radicals in Solution Adv. Phys. Org. Chem., 20 (1984) 55–189.

[6] C. Amatore, D. Garreau, M. Hammi, J. Pinson, J.M. Savéant, Kinetic Analysis of Reversible Electrodimerization Reactions by the Combined Use of Double Potential Step Chronoamperometry and Linear Sweep Voltammetry: Application to the Reduction of 9-Cyanoanthracene, J. Electroanal. Chem. Interfacial Electrochem., 184 (1985) 1–24.

[7] R.D. Webster, EPR and Voltammetric Evidence for the Reversible Dimerization of Anion Radicals of Aromatic *meta*-Substituted Diesters and Dithioic *S,S'*-Diesters, J. Chem. Soc., Perkin Trans. 2, (1999) 263–269.

[8] V. Mazine, J. Heinze, Dimerization of Electrochemically Generated Radical Ions under High Pressure, J. Phys. Chem. A, 108 (2004) 230–235.

[9] N.A. Macías-Ruvalcaba, G.A.N. Felton, D.H. Evans, Contrasting Behavior in the Reduction of 1,2-Acenaphthylenedione and 1,2-Aceanthrylenedione. Two Types of Reversible Dimerization of Anion Radicals, J. Phys. Chem. C, 113 (2009) 338–345.

[10] K. Haubner, J. Tarábek, F. Ziegs, V. Lukeš, E. Jaehne, L. Dunsch, Charged States of α,ω-Dicyano β,β'-Dibutylquaterthiophene as Studied by in Situ ESR UV-Vis NIR Spectroelectrochemistry, J. Phys. Chem. A, 114 (2010) 11545–11551.

[11] N.A. Macías-Ruvalcaba, D.H. Evans, Association Reactions of the Anion Radicals of Some Hydroxyquinones: Evidence for Formation of π- and σ-Dimers as Well as a Neutral-Anion Radical Complex, J. Phys. Chem. C, 114 (2010) 1285–1292.

[12] R.G. Compton, C.E. Banks, Understanding Voltammetry, 2nd ed., Imperial College Press, London (UK), 2011.

[13] A.J. Bard, L.R. Faulkner, Electrochemical Methods: Fundamentals and Applications, 2nd ed., Wiley, New York, USA, 2001.

[14] B. Garcia, J.C. Ortega, Excess Viscosity η^{E}, Excess Volume V^{E}, and Excess Free Energy of Activation ΔG^{*E} at 283, 293, 303, 313, and 323 K for Mixtures of Acetonitrile and Alkyl Benzoates, J. Chem. Eng. Data, 33 (1988) 200–204.

[15] D. Barnes, P. Zuman, Polarographic Reduction of Cinnamaldehyde; Comparison with 3-Phenylpropionaldehyde and Phenylpropargylaldehyde, J. Electroanal. Chem. Interfacial Electrochem., 16 (1968) 575–582.

[16] D. Barnes, P. Zuman, Polarographic Reduction of Aldehydes and Ketones. Part 7.—Behaviour of Cinnamaldehyde at higher pH-Values., T. Faraday Soc., 65 (1969) 1681–1689.

[17] D. Barnes, P. Zuman, Polarographic Reduction of Aldehydes and Ketones. Part 6.—Behaviour of Cinnamaldehyde at lower pH-Values., T. Faraday Soc., 65 (1969) 1668–1680.

[18] P. Zuman, Aspects of Electrochemical Behavior of Aldehydes and Ketones in Protic Media, Electroanalysis, 18 (2006) 131–140.

[19] L.A. Powell, R.M. Wightman, Mechanism of Electrodimerization of Retinal and Cinnamaldehyde, J. Electroanal. Chem. Interfacial Electrochem., 117 (1981) 321–333.

[20] F. Barba, J.L. de la Fuente, M. Galakhov, Electrohydrodimerization of trans-Cinnamaldehyde, Tetrahedron, 53 (1997) 5831–5838.

[21] R.D. Webster, A.M. Bond, T. Schmidt, Electrochemical Reduction of Some 2,6-disubstituted Pyridine-Based Esters and Thioic S-esters in Acetonitrile, J. Chem. Soc., Perkin Trans. 2, (1995) 1365–1374.

This page has been intentionally left blank

Chapter 4

The Electrochemical Reduction of Di-(2-ethylhexyl) Phthalate (DEHP) in Acetonitrile

This page has been intentionally left blank

4.1. Chapter Overview

The redox behavior of the extensively utilized plasticizer and toxicant, di-(2-ethylhexyl) phthalate (DEHP; Scheme 4.1), was studied in detail in acetonitrile (CH_3CN) solutions using cyclic voltammetry (at varied scan rates, temperatures, and concentrations) and controlled potential electrolysis techniques.

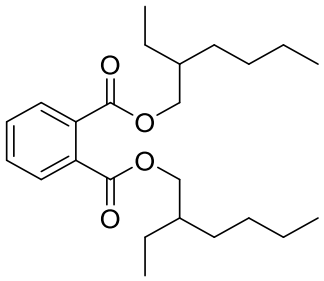

Scheme 4.1. Chemical structure of di-(2-ethylhexyl) phthalate (DEHP).

Overall, DEHP was found to be reducible by two one-electron steps at moderately large negative potentials to first form its radical anion ($E_{pc} \approx$ -2.47 vs. (Fc/Fc^+)/V, where E_{pc} refers to the cathodic/reductive peak potential and Fc/Fc^+ = ferrocene/ferrocenium), and to the dianion ($E_{pc} \approx$ -2.65 vs. (Fc/Fc^+)/V). The results obtained also revealed that the cathodic reactions were only moderately chemically reversible, even when measured at high scan rates or lowered temperatures, as the reduced forms of DEHP were involved in a number of chemical transformations (such as dimerization and decomposition) following their generation. Based on the voltammetric and electrolytic responses gathered, a mechanism was proposed for the electrochemical reduction of DEHP, and the heterogeneous electron transfer and homogeneous reaction steps were all modeled by digital simulation techniques in order to determine the associated thermodynamic and kinetic parameters.

4.2. Results & Discussion

4.2.1. Electrochemical reduction of DEHP in acetonitrile

DEHP is a highly lipophilic molecule with an estimated partition coefficient (log K_{ow}) value of 7.6 [1-3]. Hence, the present study was conducted in the aprotic organic solvent acetonitrile (CH_3CN) in order to provide reasonably good solubility for the compound, as well as to more closely simulate the relatively low moisture environment of the hydrophobic sites within biological systems that DEHP may reside in.

Using a glassy carbon (GC) electrode and a scan rate of 0.1 V s^{-1}, DEHP was found to display two successive reduction/cathodic peaks (E_{pc}) on the forward scan at ca. -2.47 and -2.65 vs. (Fc/Fc^+)/V (waves 1 and 2, respectively), and two corresponding oxidation/anodic peaks (E_{pa}) at ca. -2.55 and -2.37 vs. (Fc/Fc^+)/V when the scan direction was reversed (waves 3 and 4, respectively) (Figure 4.1). It can be noted from the voltammogram, however, that both reductions only possessed a modest degree of chemical reversibility as their oxidative (I_{pa}) to reductive (I_{pc}) peak current ratios were both < 1. Furthermore, this notion is also supported by the detection of an additional anodic process at ca. -1.25 vs. (Fc/Fc^+)/V (wave 5), which is likely associable with the oxidation of a secondary product resulting from the homogeneous reactions of the reduced species.

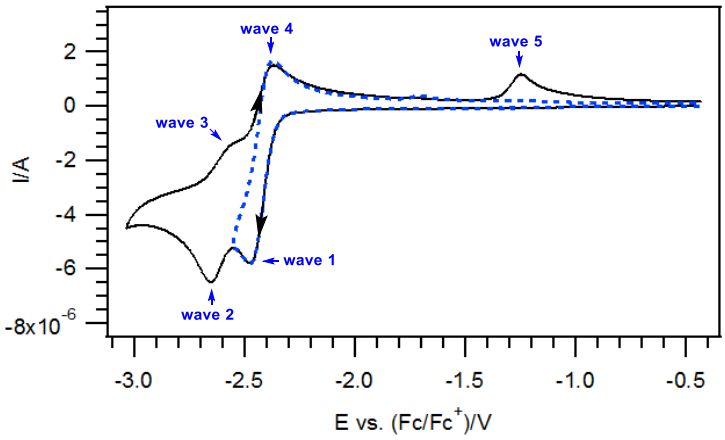

Figure 4.1. Cyclic voltammograms of 2 mM DEHP in CH_3CN containing 0.2 M Bu_4NPF_6, recorded at 295 (±2) K using a 1-mm diameter planar GC disk electrode and at a scan rate of 0.1 V s^{-1}. (—) Switching potential ≈ -3.03 vs. (Fc/Fc^+)/V. (- - -) Switching potential ≈ -2.55 vs. (Fc/Fc^+)/V.

4.2.2. Cyclic voltammetry at varied scan rates

CV analyses employing variable sweep rates were subsequently conducted with the aim of examining the dependence of voltammetric scan rate on DEHP's redox behavior. As shown in Figure 4.2, the use of higher scan rates generally benefited the chemical reversibility of the first cathodic process, particularly when examined in a restricted potential window that allowed only the initial electron transfer step to occur (wave 1), as evidenced by the more distinct size of wave 4 (Figure 4.2, dashed lines). This can be rationalized by the decreased amounts of time available for the singly reduced species to undergo other homogeneous reactions over the smaller potential window and at higher scan rates; hence, wave 4 (which is related to the oxidation of the radical anion) increases in intensity due to the greater availability of the reduced species to be converted back into the starting material.

In contrast, however, the use of faster sweep rates (up to 20 V s^{-1}) did not appear to elicit significant improvements in the magnitudes of waves 3 and 4 over the wider scan range

encompassing both reduction steps (waves 1 and 2) (Figure 4.2, solid line). As such, it is likely that the doubly reduced form of DEHP is comparatively more reactive/unstable and consequently unable to survive over the timeframes of the CV measurements (≤ seconds). More interestingly, it was determined that the use of higher scan rates led to a decrease in the magnitude of wave 5 while concomitantly increasing the presence of a new anodic peak (wave 6) at less positive potentials (ca. -1.62 vs. $(Fc/Fc^{+})/V$). As these oxidation waves are only observed after the reduction transformations of DEHP, it is conceivable that these ancillary processes emanate from the oxidation reactions of secondary products that are formed after the reduction reactions (waves 1 or 2) [4]. Nevertheless, it is also possible that other auxiliary products are formed after both reductions, but are neither redox active nor fall within the potential window of CH_3CN (using a GC electrode).

A plot of I_{pc} (wave 1) against the square root of scan rate was also performed and is given in Figure 4.3. Based on the excellent linear relationship obtained ($R^2 = 0.9988$), it can be inferred that the electrochemical reduction of DEHP under the present conditions is primarily diffusion controlled.

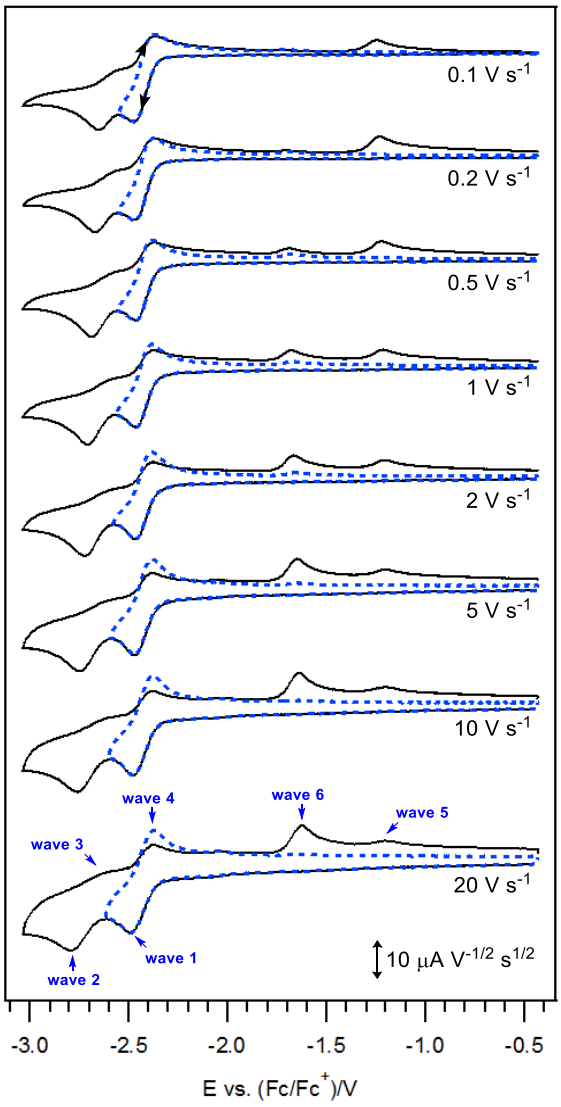

Figure 4.2. Cyclic voltammograms of 2 mM DEHP in CH_3CN containing 0.2 M Bu_4NPF_6, recorded at 295 (±2) K using a 1-mm diameter planar GC disk electrode and at different scan rates. (—) Switching potential ≈ -3.03 vs. (Fc/Fc^+)/V. (- - -) Switching potential ≈ -2.55 to 2.62 vs. (Fc/Fc^+)/V. The current data have been normalized by multiplying against $(\text{scan rate})^{-1/2}$.

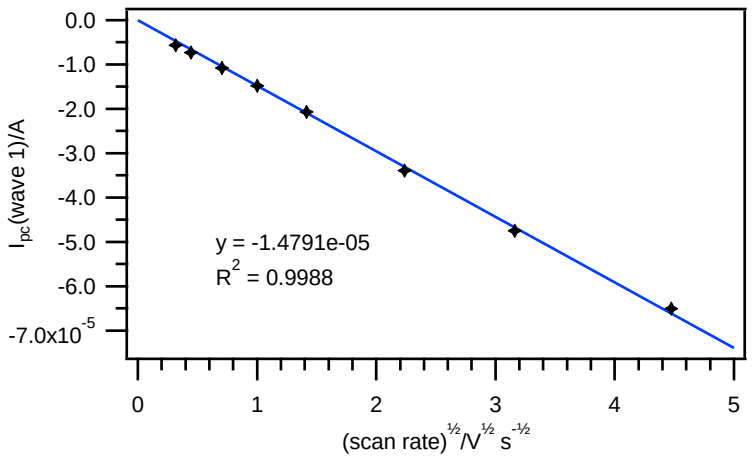

Figure 4.3. Plot of cathodic peak current (wave 1) vs. square root of scan rate for cyclic voltammograms of 2 mM DEHP in CH_3CN containing 0.2 M Bu_4NPF_6, recorded at 295 (±2) K using a 1-mm diameter planar GC disk electrode and at different scan rates (0.1, 0.2, 0.5, 1.0, 2.0, 5.0, 10.0, and 20.0 V s^{-1}).

4.2.3. Cyclic voltammetry at varied temperatures

Besides the use of fast scan rates, lowered temperatures can sometimes also aid in the capture of transient species by extending their lifetimes and consequently provide additional information on the electrode reactions involved [5]. Hence, variable temperature CV experiments of between 293-243 K were carried out so as to further investigate the electrochemical behavior of DEHP (Figure 4.4). Akin to the results obtained during the varied scan rates experiment (Figure 4.2), it was found that the chemical reversibility of the cathode reactions did not improve appreciably at lower temperatures unless the scan was scan direction was reversed before the onset of the second reduction process. Additionally, it was also observed that the progressive decrease in temperatures similarly resulted in a diminishment in the peak current intensity of wave 5 alongside an increment in the peak current magnitude of wave 6. As such, it is apparent that the anodic reaction occurring in wave 6 must arise from an intermediate that is relatively short-lived or highly reactive since wave 6 can only be detected

at higher scan rates or lower temperatures. On the other hand, the species that is responsible for wave 5 can be reasoned to stem from a more stable, long-term product whose formation is promoted at lower scan rates or higher temperatures.

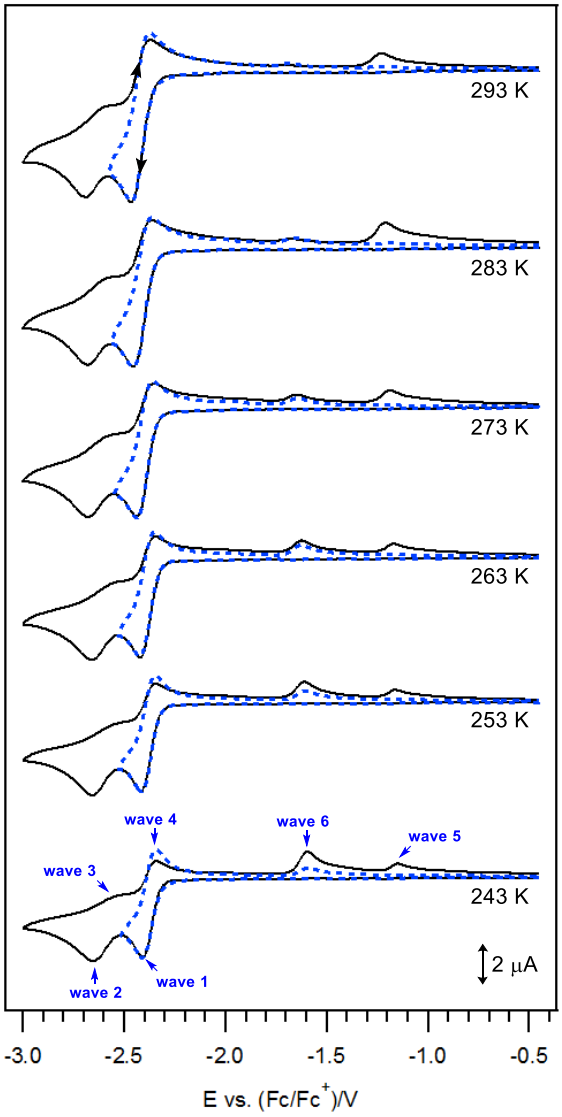

Figure 4.4. Cyclic voltammograms of 2 mM DEHP in CH_3CN containing 0.2 M Bu_4NPF_6, recorded using a 1-mm diameter planar GC disk electrode, at a scan rate of 0.1 V s^{-1}, and at different temperatures. (—) Switching potential ≈ -3.00 vs. (Fc/Fc^+)/V. (- - -) Switching potential ≈ -2.55 vs. (Fc/Fc^+)/V.

4.2.4. Cyclic voltammetry at varied concentrations

In a separate study investigating the voltammetric reduction of aromatic diesters, it was posited that the reversible dimerization of electro-generated radical anions (formed after the one-electron reduction of the analyte) takes place as a secondary process, and that the resultant dianion dimers then undergo subsequent anodic reactions at potentials which are more positive than their corresponding parent radical anions [4, 6-12].

Taking the above into consideration, it was rationalized that a similar coupling reaction could be ensuing from the electrochemical reduction of DEHP based upon the voltammetric appearances of waves 5 and 6, which were both found to occur at considerably more positive potentials than wave 4. As such, CV measurements at increasing concentrations of DEHP were next investigated to distinguish between the two anodic processes since the dimer formation reaction would be favored at larger concentrations (due to the presence of greater amounts of reactants), and thereby lead to a corresponding increase in magnitude of the electrochemical oxidation wave associated with the dianion dimer. Moreover, as waves 5 and 6 exhibited contrasting voltammetric behaviors during the variation of scan rates and temperature (Figures 4.2 and 4.4), it is logical that only one of these two ancillary oxidation reactions should involve the dimer. As Figure 4.5 illustrates, the use of an increasing concentration of the starting material (DEHP) from 1-20 mM gave a corresponding increase in the size of wave 5 and an accompanying decrease in the magnitude of wave 6. On the basis of these results, therefore, it stands to reason that wave 5 is likely due to the oxidation of the dianion dimer as opposed to wave 6.

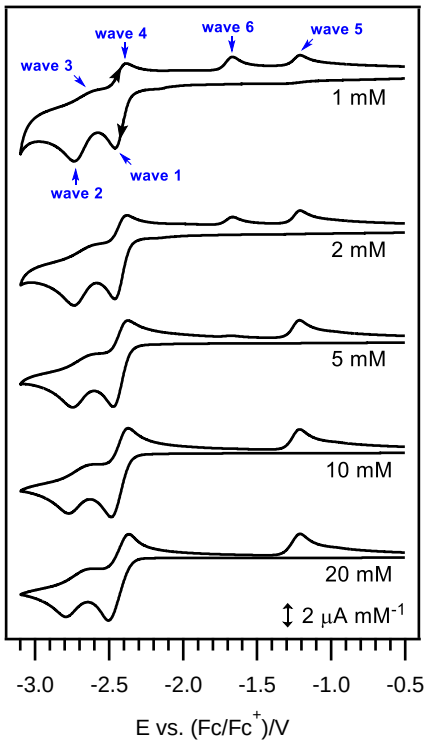

Figure 4.5. Cyclic voltammograms of different concentrations of DEHP, in CH_3CN containing 0.2 M Bu_4NPF_6, recorded at 295 (±2) K using a 1-mm diameter planar GC disk electrode and at 0.5 V s^{-1}. The current data have been normalized by multiplying by $(concentration)^{-1}$.

4.2.5. Controlled potential electrolysis

With the CV results at hand, controlled potential electrolysis (CPE) experiments were next carried out to determine the number of electrons involved in the reduction processes, as well as extract information regarding the lifetimes of the reduced products over longer time domains (≥ minutes). In these experiments, the electrode potential was held at 100 mV more negative than the E_{pc} value obtained by CV in order to ensure a complete reduction of the substrate is achieved. The coulometric data acquired during the bulk electrolysis of DEHP at a potential that is sufficiently negative to allow only the first reduction process (wave 1) to occur is recorded in Figure 4.6, together with the cyclic voltammograms that were measured before and

after the reductive electrolysis. An exhaustive conversion of the analyte was verified by the observation of a nearly zero current value in the coulometric graph (Figure 4.6b, dotted line).

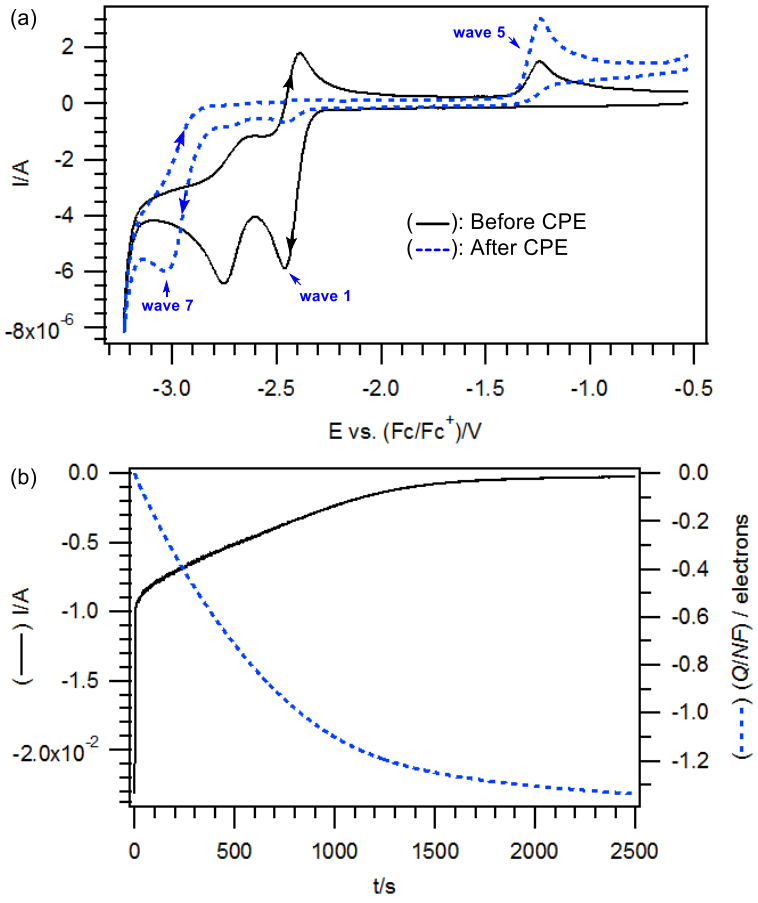

Figure 4.6. Voltammetric and coulometric data obtained during the reductive CPE (wave 1) of 2 mM DEHP in CH_3CN containing 0.2 M Bu_4NPF_6 at 295 (±2) K. (a) Cyclic voltammograms recorded at 0.1 V s^{-1} with a 1-mm diameter planar GC disk electrode. (b) Current/coulometry vs. time data obtained during the reductive CPE (at -2.56 vs. $(Fc/Fc^+)/V$).

Using eq. 4.1, the initial reduction process (wave 1) was calculated to involve approximately one mole of electrons (n = 1.3). In addition, it was found that a more pronounced wave 5 was registered in the voltammogram collected after the reductive CPE, along with a new reduction peak at ca. -3.00 vs. $(Fc/Fc^+)/V$ (wave 7) (Figure 4.6a, dotted line). The presence of wave 5 after the prolong period of electrolysis further affirms the relatively high stability of

the species giving rise to this anodic peak, which was likewise observed when low scan rates and higher temperatures were employed (Figures 4.2 and 4.4). Conversely, the appearance of wave 7 is likely attributable to the presence of a carboxylic anion end-product that is generated following the one-electron reduction of DEHP as previously reported for aromatic diesters (see section 4.2.6) [13-16].

4.2.6. Digital simulations & proposed mechanism

To gain additional insights into the mechanism and reaction rates associated with the multistep processes that occurred during the electrochemical reduction of DEHP, digital simulations of the experimental data were performed over the range of scan rates recorded in Figure 4.2, with the same set of reaction parameters used for all the scan rates examined. The simulated voltammograms were generated over two potential ranges; one which allowed only the first one-electron reduction to occur and another which extended to the second cathodic process.

The diffusion coefficient of DEHP was first determined from the cathodic peak current of the first process (wave 1), thereafter, the corresponding diffusion coefficients of the other species (e.g. radical anions, dianions, dimer) were reduced by up to 30% to account for their greater sizes and/or stronger interactions with the solvent and electrolyte that will lead to slower mobilities in solution. Modeled according to the mechanism outlined in Scheme 4.2, the simulation studies were next performed using a trial and error method, and by systemically modifying the reaction steps until the electrochemical and chemical parameters gave a reasonable fit between the experimental and simulated data. This fitting process was conducted by eye instead of an automated define error minimization method. The electrochemical and kinetic parameters associated with the different heterogeneous and their follow-up homogeneous reactions are summarized in Tables 4.1 and 4.2, respectively, with an overlay of the simulated and experimental voltammograms shown in Figure 4.7. Generally, a comparison

of the simulated and experimental graphs over the various scan rates examined revealed a relatively good fit apart from slight variations that are partially ascribable to background interferences that can arise from multiple sources such as the reagents used (e.g. solvent, electrolyte) or trace impurities that may be present in the sample solution, which are difficult to compensate for during the modeling study.

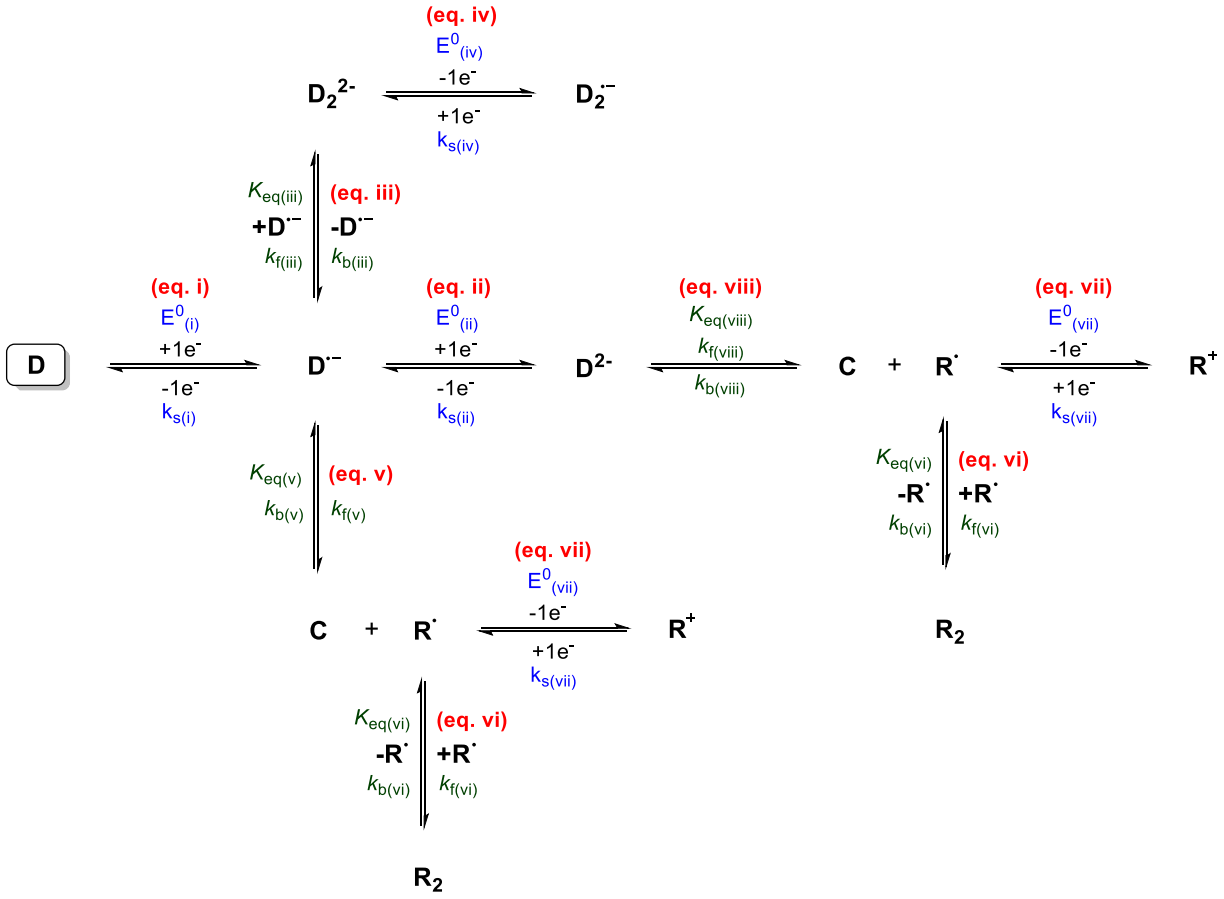

Scheme 4.2. Proposed mechanism for the electrochemical reduction of DEHP (D). C and R• represent final products of the reaction, the carboxylate anion of DEHP and the alkyl radical of the ester functionality, respectively.

Table 4.1. Electrochemical parameters[a] obtained by digital simulations of CV data[b] for the reaction mechanism given in Scheme 4.2.

Electrochemical Parameters[b]	**eq. i**	**eq. ii**	**eq. iv**	**eq. vii**
E^0 (V)	-2.48	-2.61	-1.28	-1.68
D ($cm^2\ s^{-1}$)	1.80×10^{-5}	1.63×10^{-5}	1.26×10^{-5}	1.26×10^{-5}
k_s ($cm\ s^{-1}$)	0.50	0.05	0.1	0.1

[a]D = diffusion coefficient of the oxidized form, E^0 = formal potential vs. (Fc/Fc^+), k_s = heterogeneous electron transfer rate constant. Charge transfer coefficients (α) were assumed as 0.5. [b]CV data were recorded at 295 (±2) K using a 1-mm diameter planar GC disk electrode for solutions of 2 mM DEHP and 0.2 M Bu_4NPF_6 in CH_3CN.

Table 4.2. Equilibrium and rate constants[a] obtained by digital simulations of CV data[b] for the reaction mechanism given in Scheme 4.2.

Kinetic Parameters[c]	**eq. iii**	**eq. v**	**eq. vi**	**eq. viii**
K_{eq}	2.0×10^{7}	1.1×10^{-2}	1.0×10^{5}	8.0×10^{-2}
k_f	1.2×10^{5}	8.0×10^{3}	2.0×10^{1}	1.2×10^{3}
k_b	6.0×10^{-3}	7.3×10^{5}	2.0×10^{-4}	1.5×10^{4}

[a]K_{eq} = equilibrium constant, k_f = forward rate constant, k_b = backward rate constant. k_f and k_b have units of s^{-1} and L $mol^{-1}\ s^{-1}$ for the first- and second-order reactions, respectively. [b]CV data were recorded at 295 (±2) K using a 1-mm diameter planar GC disk electrode for solutions of 2 mM DEHP and 0.2 M Bu_4NPF_6 in CH_3CN.

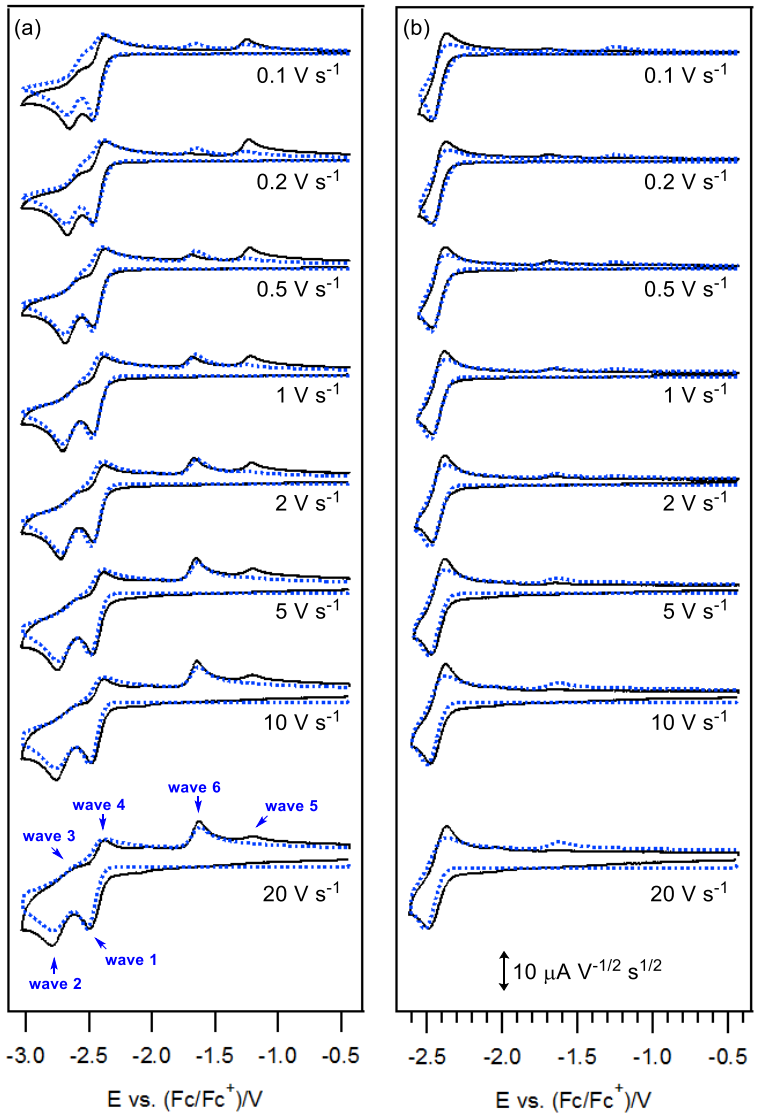

Figure 4.7. (—) Experimental cyclic voltammograms of 2 mM DEHP in CH_3CN containing 0.2 M Bu_4NPF_6, recorded at 295 (±2) K using a 1-mm diameter planar GC disk electrode and at different scan rates. (••••) Simulated voltammograms generated according to mechanism shown in Scheme 4.2, and parameters in Tables 4.1 & 4.2. (a) Switching potential ≈ -3.03 vs. (Fc/Fc^+)/V. (b) Switching potential ≈ -2.55 to 2.62 vs. (Fc/Fc^+)/V. The current data have been normalized by multiplying against $(\text{scan rate})^{-1/2}$.

Overall, it is proposed that the voltammetric reduction of DEHP involves two stepwise one-electron cathodic reactions, giving rise to the observation of the two successive cathodic processes waves 1 and 2 (eq. i and ii). The radical anions which are formed after the initial one-electron reduction can then undergo a coupling reaction with one another to produce a dianionic dimer product (eq. iii) [4]. The presence of the dimer is corroborated by the increase in the size of wave 5 measured (eq. iv) as the concentration of the starting material (DEHP) used is increased (Figure 4.5). It is noteworthy, however, that while a homodimerization (radical-radical coupling) reaction is outlined in the current scheme, another route occurring via a heterodimerization (radical-substrate coupling) process cannot be completely ruled out as it is very difficult to voltammetrically distinguish between these two pathways. Regardless, a competing process which involves the cleavage of an oxygen alkyl [C(O)O–R] bond within the DEHP radical anion to generate an alkyl (2-ethylhexyl) radical and a long-term carboxylic anion product (which was observed during the reduction of other aromatic diesters [13-16]) is also postulated (eq. v) (Scheme 4.3.).

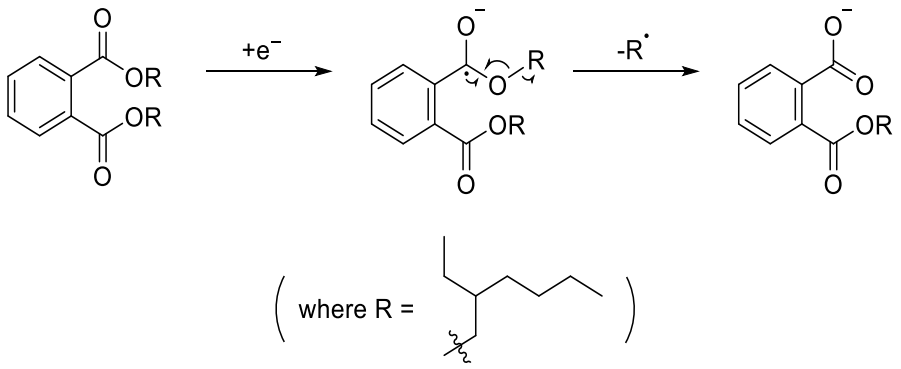

Scheme 4.3. Proposed mechanism for the cleavage of the oxygen alkyl [C(O)O–R] bond within the DEHP radical anion.

As discussed previously, the intermediate involved in wave 6 must be chemically unstable and since it can only be voltammetrically detected at fast scan rates or low temperatures. With this in mind, wave 6 is possibly attributable to the oxidation of the

aforementioned alkyl radicals, which are expected to be high reactive and relatively short-lived. Although the presence of the alkyl radicals was not voltammetrically detected in previous work dealing with aromatic diesters having primary alkyl functionalities [13-16], the oxidation of the 2-ethylhexyl radicals in the present study is likely made possible by its comparatively large and bulky alkyl substituents which can stabilize both the radical and resultant cation (generated after the oxidation process at wave 6). For instance, it is possible that the primary alkyl radical formed after the cleavage of the [C(O)O–R] bond (Scheme 4.3) is able undergo a 1,2-rearrangement reaction to form a more stable tertiary radical species that is relatively long-lived (i.e. detectable by CV at fast scan rates). The importance and relevance of the structural nature of the alkyl substituent was also emphasized by a previous proposal that the rate of the unimolecular cleavage reaction is affected by the stability of the radical formed from the alkyl fragments of benzene esters [17, 18].

At low scan rates, the alkyl radicals would be expected to possess sufficient time to undergo a homodimerization reaction to form a saturated hydrocarbon compound (eq. vi). At high sweep rates, however, the aforementioned coupling reaction can be outrun, allowing the oxidation of alkyl radical to occur instead (eq. vii), and thus give rise to an increase in peak current magnitude of wave 6 as the scan rates are increased. It is worth mentioning that although a radical-radical coupling is proposed (eq. vi), it is also possible that a hydrogen atom transfer reaction is also occurring between the alkyl radical and the solvent/electrolyte/moisture which likewise furnishes a saturated alkyl product (RH). More importantly, although the equilibrium constant associated with the coupling reaction (eq. vi) is assigned to be relatively large (K_{eq} = 1.0 x 10^5), the corresponding forward rate constant is considerably smaller magnitude (k_f = 2.0 x 10^1) such that it can be eluded at high scan rates. In doing so, at slow scan rates, the coupled chemical reactions such as the dimerization of the singly reduced form of DEHP (eq. iii) and

coupling reactions of the alkyl radicals (eq. vi) are able to proceed, thereby leading to the more prominent size of wave 5 and a minimal detection of wave 6.

Noteworthily, owing to the modest chemical reversibility exhibited by the first electron transfer step of DEHP and its pronounced improvement during the restricted potential range at high scan rates (Figure 4.2), the equilibrium constant associated with the cleavage of the oxygen alkyl [C(O)O–R] bond (eq. v) was allocated to be less than one (K_{eq} = 1.1 x 10^{-2}). In this regard, although the aforementioned equilibrium constant appears relatively small in magnitude, the bond breakage reaction (eq. v) can be expected to still predominantly proceed in the forward direction due to the presence of a follow-up dimerization reaction between the resultant alkyl radicals (eq. vi). Lastly, it is also conceivable that a similar oxygen alkyl [C(O)O–R] bond cleavage reaction can take place at the ester functionalities of the doubly reduced form of DEHP (D^{2-}) to generate a corresponding dicarboxylate anion and two alkyl radicals due to the symmetrical nature of the DEHP molecule (eq. viii) [13-16].

4.3. Conclusion

In summary, CV and CPE analyses of DEHP in CH_3CN have established that this compound can undergo two consecutive one-electron transfer steps to generate its radical anion and dianion at large negative potentials. The cathodic processes only exhibited limited chemical reversibility, however, as the reduced forms of DEHP were susceptible to several homogeneous reactions following their electro-generation. For instance, it was established that the radical anion of DEHP undergoes either a homodimerization reaction to produce a dianion dimer, or an oxygen alkyl [C(O)O–R] bond cleavage at its ester functionality to produce a carboxylate anion and 2-ethylhexyl radical. In addition, it was found that the use of lower scan rates and higher concentrations favored the voltammetric detection of the dianion dimer, whereas the employment of higher scan rates and lower concentrations enabled the observation of the alkyl radicals instead. Based on the electrochemical observations attained from the preceding sections, a mechanism for the electrochemical reduction of DEHP has been proposed and modeled by digital simulations to obtain information regarding the related electrochemical and kinetic parameters.

4.4. Materials & Methods

4.4.1. Chemicals & reagents

Unless otherwise stated, all chemicals and reagents were purchased from commercial sources and used as received. DEHP (98%) and acetonitrile (CH_3CN, HPLC grade) were obtained from Alfa-Aesar and Anhui Fulltime Solvents & Reagents Co., Ltd. respectively. The supporting electrolyte, tetrabutylammonium hexafluorophosphate (Bu_4NPF_6), was prepared by reacting equal molar amounts of a 65% aqueous solution of HPF_6 (Alfa-Aesar) and a 40% aqueous solution of Bu_4NOH (Alfa-Aesar), washing the resulting precipitate with hot water, recrystallizing three times from hot ethanol, and then drying in vacuo at 413 K for 6 h.

4.4.2. Cyclic voltammetry experiments

Cyclic voltammetry (CV) measurements were carried out with a computer-controlled Metrohm Autolab PGSTAT302N potentiostat using a three electrode system. The working electrodes were 1-mm diameter planar glassy carbon (GC) disks (eDAQ Pty Ltd), used together with a platinum (Pt) wire auxiliary/counter electrode (Metrohm) and a silver (Ag) wire miniature reference electrode (eDAQ Pty Ltd) that was connected to the sample solution via a salt bridge containing 0.5 M Bu_4NPF_6 in CH_3CN. Variable temperature CV experiments were performed using a Metrohm jacketed glass cell, with the temperatures controlled by a Julabo FP89-HL ultralow refrigerated ethanol circulating bath. Before each voltammetric analysis, all test solutions were de-oxygenated by purging with high purity argon gas and the working electrode was cleaned by polishing with alumina oxide (grain size 0.3 μm) slurry on a Buehler Ultra-pad polishing cloth, rinsing with ultrapure water, followed by acetone, and then dried. At the end of the experiments, accurate potentials were obtained by adding ferrocene (Fc) as an internal standard. All CV experiments were conducted inside of a Faraday cage.

4.4.3. Controlled potential electrolysis experiments

Controlled potential electrolysis (CPE) experiments were performed in a two-compartment electrolysis cell separated by a sintered glass frit with a porosity no. 5 (1.0–1.7 μm). Two identically sized GC cylinders were used as the working and counter electrodes and were placed symmetrically with respect to each other, with the abovementioned Ag wire reference electrode positioned to within 2 mm of the surface of the working electrode. The solutions in both electrode compartments were 25 mL each and simultaneously de-oxygenated and stirred using bubbles of high purity argon gas. The number of electrons involved in the bulk electrolysis process was calculated from:

$$n = Q/NF \quad (4.1)$$

where: n = number of moles of electrons transferred; Q = charge (coulombs); N = no. of moles of starting compound; and F = Faraday's constant (96 485 C mol^{-1}).

4.4.4. Digital simulations

Digital simulation modeling of the CV graphs at varied scan rates was carried out using a DigiElch electrochemical simulation software package (DigiElch 7) acquired from Gamry Instruments.

4.5. References

[1] J. De Bruijn, F. Busser, W. Seinen, J. Hermens, Determination of Octanol/Water Partition Coefficients for Hydrophobic Organic Chemicals with the "Slow-Stirring" Method, Environ. Toxicol. Chem., 8 (1989) 499–512.

[2] S. Gutiérrez, C. Fernández, B.I. Escher, J.V. Tarazona, A New Hazard Index of Complex Mixtures Integrates Bioconcentration and Toxicity to Refine the Environmental Risk Assessment of Effluents, Environ. Int., 34 (2008) 773–781.

[3] H. Noorizadeh, S. Sajjadifar, A. Farmany, S. Sobhanardakani, Prediction of Octanol-Water Partition Coefficients of Organic Chemicals by QSAR Models, Toxicol. Environ. Chem., 95 (2013) 1267–1278.

[4] Y.S. Tan, Y. Yue, R.D. Webster, Competing Hydrogen-Bonding, Decomposition, and Reversible Dimerization Mechanisms during the One- and Two-Electron Electrochemical Reduction of Retinal (Vitamin A), J. Phys. Chem. B, 114 (2013) 9371–9379.

[5] A.J. Fry, W.E. Britton, Solvents and Supporting Electrolytes, in: P.T. Kissinger, W.R. Heineman (Eds.) Laboratory Techniques in Electroanalytical Chemistry, Marcel Dekker, New York, USA, 1996, pp. 469–485.

[6] O. Hammerich, V.D. Parker, Kinetics and Mechanisms of Reactions of Organic Cation Radicals in Solution Adv. Phys. Org. Chem., 20 (1984) 55–189.

[7] C. Amatore, D. Garreau, M. Hammi, J. Pinson, J.M. Savéant, Kinetic Analysis of Reversible Electrodimerization Reactions by the Combined Use of Double Potential Step Chronoamperometry and Linear Sweep Voltammetry: Application to the Reduction of 9-Cyanoanthracene, J. Electroanal. Chem. Interfacial Electrochem., 184 (1985) 1–24.

[8] R.D. Webster, EPR and Voltammetric Evidence for the Reversible Dimerization of Anion Radicals of Aromatic *meta*-Substituted Diesters and Dithioic *S,S'*-Diesters, J. Chem. Soc., Perkin Trans. 2, (1999) 263–269.

[9] V. Mazine, J. Heinze, Dimerization of Electrochemically Generated Radical Ions under High Pressure, J. Phys. Chem. A, 108 (2004) 230–235.

[10] N.A. Macías-Ruvalcaba, G.A.N. Felton, D.H. Evans, Contrasting Behavior in the Reduction of 1,2-Acenaphthylenedione and 1,2-Aceanthrylenedione. Two Types of Reversible Dimerization of Anion Radicals, J. Phys. Chem. C, 113 (2009) 338–345.

[11] K. Haubner, J. Tarábek, F. Ziegs, V. Lukeš, E. Jaehne, L. Dunsch, Charged States of α,*ω*-Dicyano *β,β'*-Dibutylquaterthiophene as Studied by in Situ ESR UV-Vis NIR Spectroelectrochemistry, J. Phys. Chem. A, 114 (2010) 11545–11551.

[12] N.A. Macías-Ruvalcaba, D.H. Evans, Association Reactions of the Anion Radicals of Some Hydroxyquinones: Evidence for Formation of π- and σ-Dimers as Well as a Neutral-Anion Radical Complex, J. Phys. Chem. C, 114 (2010) 1285–1292.

[13] R.D. Webster, A.M. Bond, R.G. Compton, Voltammetric and EPR Spectroscopic Studies Associated with the Reduction of Pyridine and Benzene-Substituted n-Alkyl Esters and Thioic S-Esters in Aprotic Solvents, J. Phys. Chem., 100 (1996) 10288–10297.

[14] R.D. Webster, A.M. Bond, Electrochemical Reduction of Pyridine- and Benzene-Substituted *n*-Alkyl Esters and Thioic *S*-Esters in Acetonitrile, J. Org. Chem., 62 (1997) 1779–1787.

[15] R.D. Webster, A.M. Bond, Different Mechanisms for the Reaction of Disubstituted Aromatic Esters and Thioic *S*-Esters with Electrochemically Generated Superoxide, J. Chem. Soc., Perkin Trans. 2, (1997) 1075–1079.

[16] R.D. Webster, *In situ* Electrochemical-ATR-FTIR Spectroscopic Studies on Solution Phase Carboxylate Radical Anions, J. Chem. Soc., Perkin Trans. 2, (2002) 1882–1888.

[17] J.H. Wagenknecht, R.D. Goodin, P.J. Kinlen, F.E. Woodard, Decomposition of Benzoate Ester Radical Anions, J. Electrochem. Soc., 131 (1984) 1559–1565.

[18] J. Masnovi, Radical Anions of Esters of Carboxylic Acids. Effects of Structure and Solvent on Unimolecular Fragmentations, J. Am. Chem. Soc., 111 (1989) 9081–9089.

This page has been intentionally left blank

Chapter 5

Comparing the Relative Reactivities of Food and Vitamin Molecules Toward Electrochemically Generated Superoxide

This page has been intentionally left blank

5.1. Chapter Overview

In this chapter, the relative reactivities of 18 food and vitamin molecules (Schemes 5.1 and 5.2, respectively) toward electrochemically generated superoxide ($O_2^{\bullet-}$) were investigated in *N*,*N*-dimethylformamide (DMF) using cyclic voltammetry (CV). The quenching of $O_2^{\bullet-}$ was measured by monitoring the decreases in the anodic peak currents (I_{pa}) of the reverse peaks after the one-electron reduction of molecular oxygen/dioxygen (O_2) while systematically increasing the concentration of the test substrates. The reactivity each compound was then approximated and compared using effective concentration indexes, EC_{10} and EC_{50}, which represent the amount of compound required to reduce the concentration of the electrochemically generated $O_2^{\bullet-}$ by 10 % and 50 %, respectively, under the present conditions. Where possible, the likely mechanisms that are involved in the scavenging of $O_2^{\bullet-}$ are also discussed.

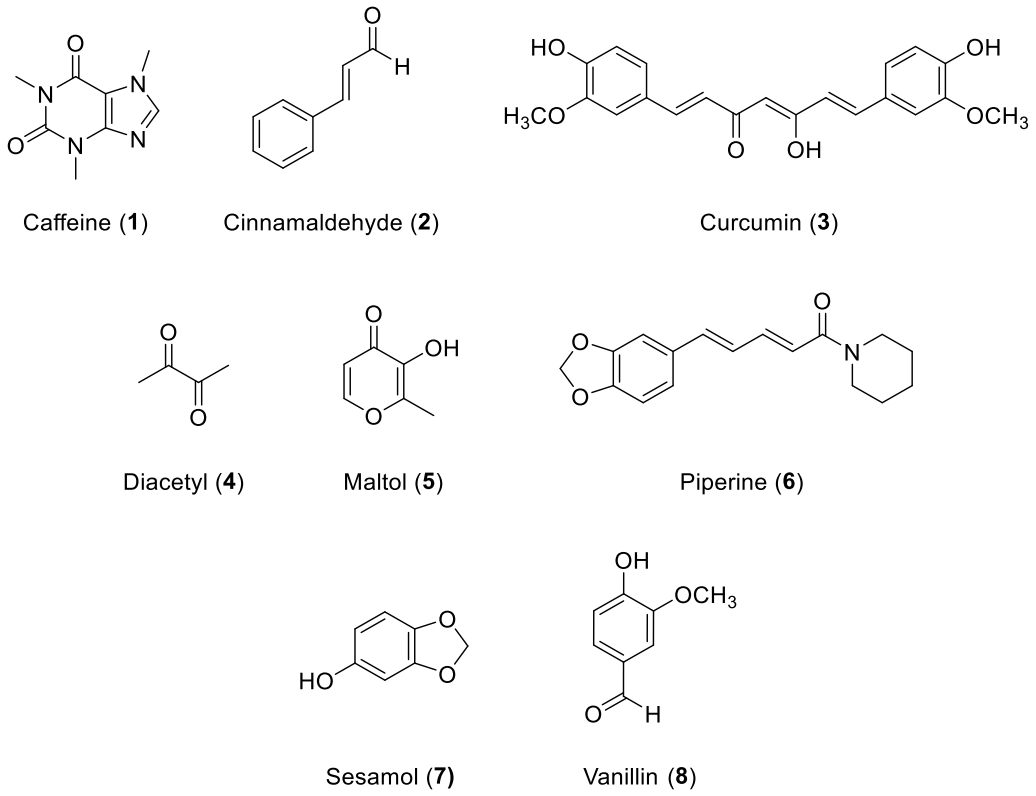

Scheme 5.1. List of food compounds examined in this study.

Vitamin A

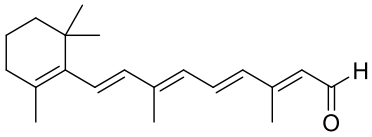

Retinal (**9**)

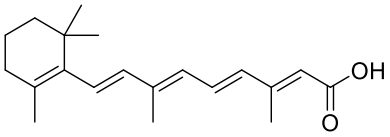

Retinoic acid (**10**)

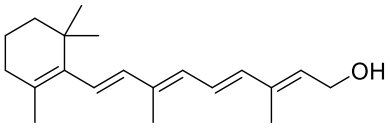

Retinol (**11**)

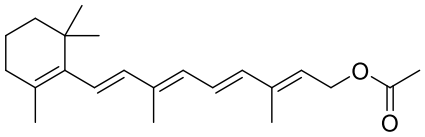

Retinyl acetate (**12**)

Vitamin B_6

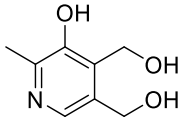

Pyridoxine (**13**)

Vitamin B_7

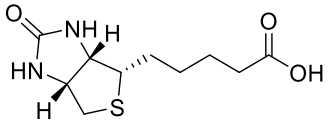

D-(+)-Biotin (**14**)

Vitamin D_2

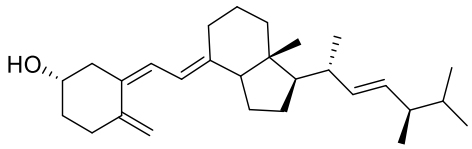

Ergocalciferol (**15**)

Vitamin D_3

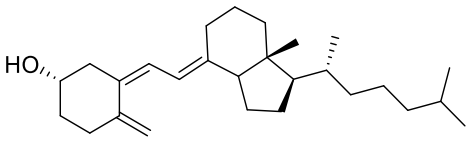

Cholecalciferol (**16**)

Vitamin E

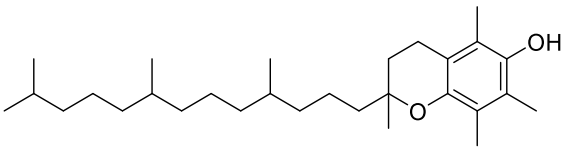

DL-α-tocopherol (**17**)

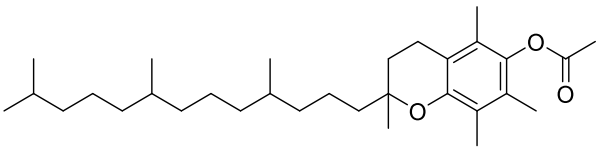

DL-α-tocopherol acetate (**18**)

Scheme 5.2. List of vitamin compounds examined in this study.

5.2. Results & Discussion

5.2.1. Electrochemical reduction of molecular oxygen (O_2)

Amongst the various approaches that have been employed to generate $O_2^{\bullet-}$ (e.g. biological, chemical, photochemical [1-5]), electrochemical techniques have been demonstrated to be highly precise and accessible as only mild conditions are required and little to no by-products are produced [6-8].

More specifically, in many dry aprotic organic solvents such as DMF, O_2 can be voltammetrically reduced by two sequential one-electron transfer steps to first form $O_2^{\bullet-}$, and then its dianion (O_2^{2-}) according to eq. 5.1 and 5.2.

$$O_2 + e^- \rightleftharpoons O_2^{\bullet-} \quad (5.1)$$

$$O_2^{\bullet-} + e^- \rightleftharpoons O_2^{2-} \quad (5.2)$$

Figure 5.1 depicts a typical cyclic voltammogram that was collected (using a 1-mm diameter planar GC disk electrode) for the initial one-electron reduction of O_2 in dry, air saturated DMF. Even at a scan rate of 0.1 V s^{-1}, it can be observed that the first heterogeneous electron transfer process (eq. 5.1) appears to be chemically reversible in the sense that an anodic/oxidation (I_{pa}) to cathodic/reduction (I_{pc}) peak current ratio of close to unity was obtained. Essentially, this iterates the relatively high stability of the electrochemically generated $O_2^{\bullet-}$ under the present conditions (in the timeframe of the CV), and that the singly reduced species ($O_2^{\bullet-}$) can be fully transformed back into the starting material (O_2) following its formation. In contrast, however, the further one-electron reduction of $O_2^{\bullet-}$ (eq. 5.2) appears to be chemically irreversible as no corresponding anodic wave is detected on the return sweep of the CV scan (Figure A5.1 in the appendix). Nevertheless, since the second reduction process does not occur in the vicinity of $O_2^{\bullet-}$ production, the generation of the dianionic species (O_2^{2-}) will not be considered in this

study. In addition, it is in line with expectations that no noticeable redox couples were recorded over the same potential window after the solution was deoxygenated by purging with argon gas (Figure A5.1, dashed line).

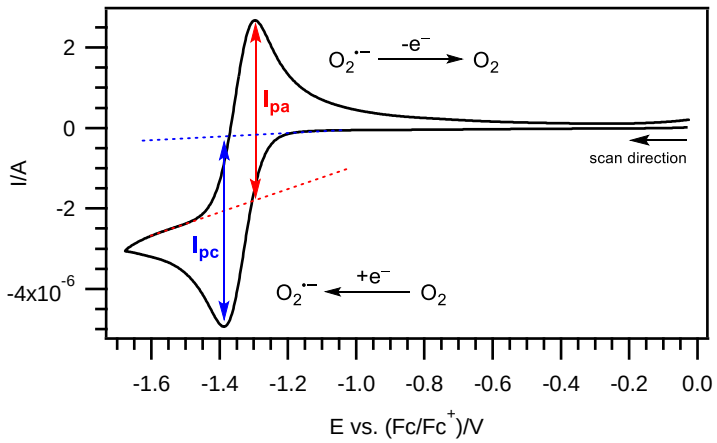

Figure 5.1. Cyclic voltammogram of the one-electron reduction of O_2 in dry, air saturated DMF containing 0.1 M Bu_4NPF_6, recorded using a 1-mm diameter planar GC disk electrode and a scan rate of 0.1 V s^{-1}. I_{pa}: Anodic peak current. I_{pc}: Cathodic peak current.

Despite the apparent stability of $O_2^{\bullet-}$, it is well-documented that the one-electron electrochemical reduction of O_2 (into $O_2^{\bullet-}$) is sensitive to the presence of trace protic impurities/substances such as moisture, as $O_2^{\bullet-}$ readily acts a Brønsted base toward proton donors, and subsequently undergoes a disproportionation reaction to form hydrogen peroxide (H_2O_2) and O_2 (eq. 5.3 and 5.4) [6, 9]. Alternatively, $O_2^{\bullet-}$ may also interact with some compounds as a H-atom abstractor, one-electron reductant, or nucleophile [2, 6, 8, 10]. Regardless, the irreversible removal of $O_2^{\bullet-}$ in either case (after it is first electrochemically generated on the forward scan of the CV) would lead to a resultant decrease in the magnitude of I_{pa} (as there will be less $O_2^{\bullet-}$ molecules available for the reverse oxidation reaction), which can be monitored voltammetrically as an indication of $O_2^{\bullet-}$ reaction.

$$O_2^{\bullet-} + H^+ \rightleftharpoons HO_2^{\bullet} \qquad (5.3)$$

$$2\ HO_2^{\bullet} \rightarrow H_2O_2 + O_2 \qquad (5.4)$$

Therefore, in order to minimize the unwanted reactions of $O_2^{\bullet-}$ with water, dry DMF was used as the aprotic organic solvent in this work. DMF was also selected due to its ability to dissolve many types of compounds (Schemes 5.1 and 5.2) in high concentrations (≥ 50 mM).

5.2.2. Electrochemical reduction of O_2 in the presence of food and vitamin compounds

Since the electrochemical signals of the compounds examined (Schemes 5.1 and 5.2) can potentially interfere with the subsequent measurements, it is crucial these substances are not redox active within the potential window employed for the one-electron reduction of O_2 (i.e. between -1.70 to -0.05 vs. (Fc/Fc^+)/V). As such, the voltammetric behaviors of the 18 food and vitamin compounds were first studied in the absence of O_2, and were all found to be suitable for use as they were electrochemically inactive within the test range (Figures A5.2–A5.19 in the appendix).

At the start of each experiment, a cyclic voltammogram of the one-electron reduction of O_2 was first collected in dry, air saturated DMF solution containing 0.1 M Bu_4NPF_6 in order to capture the initial voltammetric currents. Thereafter, the voltammograms were recorded in the presence of incremental concentrations of the different test substrates so as to investigate their respective scavenging abilities. As discussed in the preceding section, and assuming that the analyte of interest is capable of reacting with $O_2^{\bullet-}$, the I_{pa} (and consequently the chemical reversibility) of the cyclic voltammograms will be expected to decrease after the compounds are added (Figure 5.2). This decrease in current intensity is proportional to the amount of $O_2^{\bullet-}$ that has reacted and, thus, provides a relative measure of each substrate's reactivity. In general, a large decrease in I_{pa} at a fixed substrate concentration can be accredited to a larger amount of $O_2^{\bullet-}$ being scavenged, while a small decrease in I_{pa} would imply that little reaction with $O_2^{\bullet-}$ has taken place [11, 12]. In addition, it is worth highlighting at this juncture that the increments

in concentrations of several compounds also led to an increase in the I_{pc} magnitudes observed. This is attributable to the reaction mechanism involved and is elaborated on in greater detail in section 5.2.4.

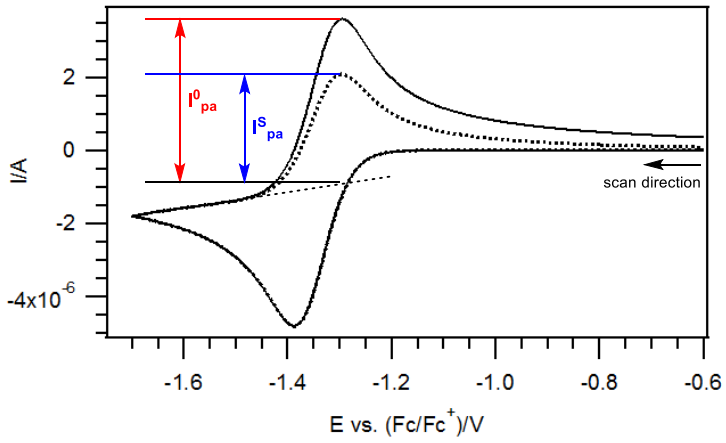

Figure 5.2. Digitally simulated cyclic voltammograms of the one-electron reduction of O_2 in dry, air saturated DMF containing 0.1 M Bu_4NPF_6, at a 1-mm diameter planar GC disk electrode, a scan rate of 0.1 V s^{-1}, and in the (—) absence and (·····) presence of a typical food or vitamin compound. I^0_{pa}: Initial anodic peak current in the absence of any analyte. I^S_{pa}: Anodic peak current after addition of the analyte.

Figure 5.3 depicts four representative examples in which a series of cyclic voltammograms for the reduction of O_2 were registered for different substrate and concentrations. It is evident from the scans that increasing amounts of maltol (**5**), retinyl acetate (**12**), and dl-α-tocopherol (**17**) all led to concomitant decreases in the sizes of I_{pa} (Figures 5.3a–5.3c), signifying therefore that the electrochemically generated $O_2^{\bullet-}$ is being consumed in their presence; albeit at different rates. Conversely, it can be surmised from the graphs in Figure 5.3d that caffeine (**1**) possesses a markedly poorer reactivity toward $O_2^{\bullet-}$ (under the present conditions), as the compound did not appear to significantly alter the voltammetric profile of O_2 reduction even at a relatively high concentration of 50 mM. Similar experiments were also

carried out for the remaining 14 substrates and their associated cyclic voltammograms are provided in the appendix (Figures A5.20–A5.37). The reduction of O_2 in the presence of certain compounds also led to the detection of additional voltammetric oxidation peaks at more positive potentials when the scan direction was reversed, as shown for maltol (**5**) and dl-α-tocopherol (**17**) in Figures 5.3a and 5.3c, respectively. These additional oxidation peaks are likely associated with electroactive products formed via the reaction of the starting materials with $O_2^{\bullet-}$. For example, the anodic waves that are observed at ca. −0.9 V vs. (Fc/Fc^+) on the reverse scan of Figure 5.3c are probably attributable to the oxidation of a phenolate anion product [13, 14] that is formed after dl-α-tocopherol undergoes reaction with $O_2^{\bullet-}$ (see section 5.2.4).

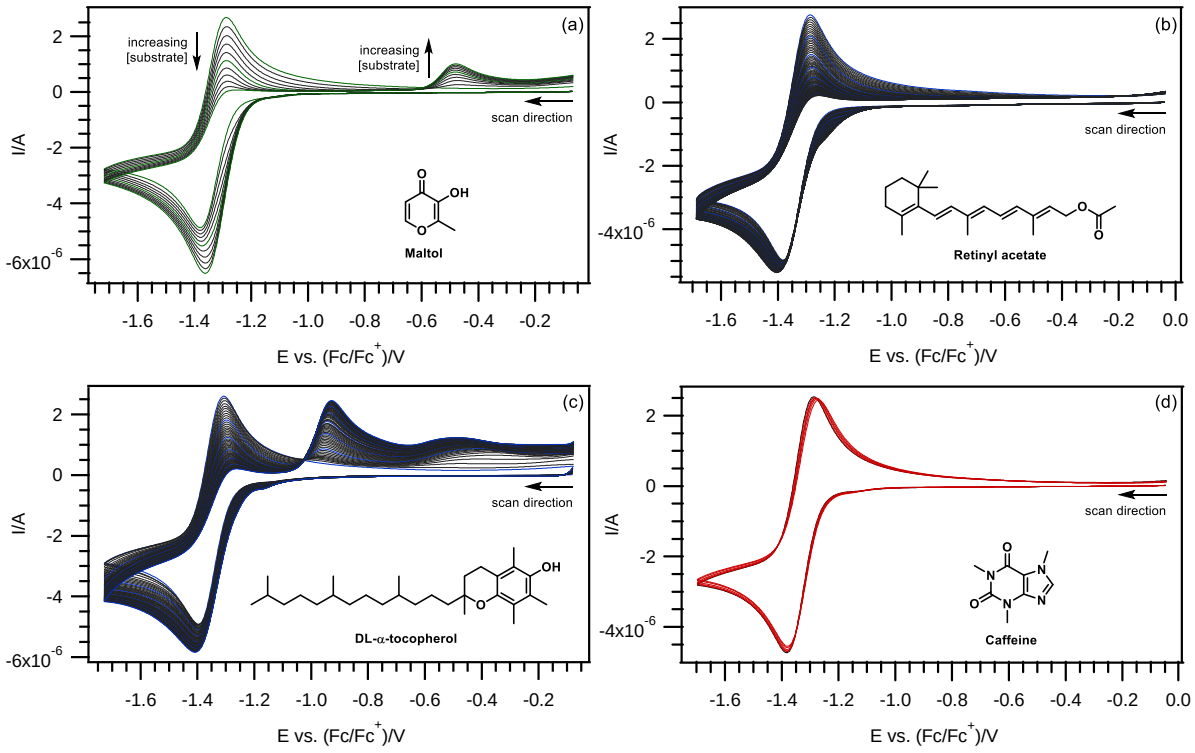

Figure 5.3. Cyclic voltammograms of the one-electron reduction of O_2 in dry, air saturated DMF containing 0.1 M Bu_4NPF_6, recorded using a 1-mm diameter planar GC disk electrode, a scan rate of 0.1 V s^{-1}, and at increasing concentrations of (a) maltol, (b) retinyl acetate, (c) dl-α-tocopherol, and (d) caffeine. (—) 0.2 mM increments. (—) 1 mM increments. (—) 2 mM increments. (—) 10 mM increments.

5.2.3. Evaluation of reactivities toward electrochemically generated superoxide

Although each compound's reactivity with $O_2^{\bullet-}$ can be broadly estimated from the graphs of O_2 reduction (Figure 5.3), more precise comparisons across different substances may be performed by utilizing a parameter such as an effective concentration index (EC); which represents the amount of analyte that is required to decrease the concentration of $O_2^{\bullet-}$ by a specific amount. As discussed briefly in the introduction section, previous studies generally estimated the relative reactivities (and EC values) of different substrates toward $O_2^{\bullet-}$ by measuring the changes in I_{pa} in the absence and presence of increasing concentrations of an analyte [11, 12]. In view of this, therefore, the EC values were obtained via a similar manner in this work, by considering the percentage change between the final and initial I_{pa} magnitudes (eq. 5.5).

$$\%\Delta I_{pa} = \left(\frac{I^{S}_{pa} - I^{0}_{pa}}{I^{0}_{pa}}\right) \times 100\ \% \qquad (5.5)$$

where: $\%\Delta I_{pa}$ is the percentage change in anodic peak current intensity or percentage $O_2^{\bullet-}$ consumed (%); I^0_{pa} is the initial anodic peak current in the absence of any analyte; I^S_{pa} is the anodic peak current at a specified analyte concentration.

For instance, assuming a hypothetical value of $\%\Delta I_{pa}$ = -50 %, it can be interpreted that I_{pa} has decreased by 50 % from its original amount, or that half of the $O_2^{\bullet-}$ generated on the forward scan of the voltammogram has reacted. Correspondingly, the concentration of compound required to attain this $\%\Delta I_{pa}$ value is designable as the EC_{50} value, and a smaller value would thus denote a stronger reactivity of the substrate toward $O_2^{\bullet-}$. It should be noted, however, that the EC_{50} values obtained in this work do not necessarily provide a direct measure of half-maximal response [15], but are more valid for comparisons between molecules examined using the same methodology (e.g. experimental timeframe/conditions), and only if the reaction pathway of $O_2^{\bullet-}$ with the compound is similar.

With this in mind, the food molecules and vitamin compounds examined in this work were subsequently analyzed for their EC_{10} and EC_{50} values (concentrations of substrate required to scavenge 10 % and 50 % of $O_2^{\bullet-}$, respectively) and the data have been consolidated in Table 5.1. A more detailed illustration of the concentration effects on $O_2^{\bullet-}$ scavenging is also provided in the appendix via best fit plots of the percentage change in I_{pa} versus concentration of substrate added (Figures A5.38–A5.49 in the appendix). However, as the EC_{10} and/or EC_{50} values could not be obtained directly from the voltammograms of O_2 reduction for 6 analytes, even at relatively high concentrations, only the percentage of $O_2^{\bullet-}$ consumed at 50 mM was approximated for these cases instead, and are listed in Table 5.2.

Table 5.1. EC_{10} and EC_{50} values obtained for the food and vitamin compounds that showed medium to high reactivity with $O_2^{\bullet-}$.

Compound	**EC_{10} (mM)**	**EC_{50} (mM)**
Maltol (**5**)	0.3	1.9
Curcumin (**3**)	0.2	2.3
Vanillin (**8**)	0.7	2.9
Pyridoxine (**13**)	0.7	3.0
Diacetyl (**4**)	0.6	3.1
Retinoic acid (**10**)	0.7	3.4
D-(+)-Biotin (**14**)	1.0	3.8
Sesamol (**7**)	0.7	5.7
Retinol (**11**)	0.9	7.9
Retinyl acetate (**12**)	1.5	10.8
DL-α-tocopherol (**17**)	0.9	11.0
Retinal (**9**)	1.5	13.8

Table 5.2. Percentage of $O_2^{\bullet-}$ scavenged at 50 mM for the food and vitamin compounds that showed low reactivities with $O_2^{\bullet-}$.

Compound	**$O_2^{\bullet-}$ scavenged (%)**
Caffeine (**1**)	3.5
Cinnamaldehyde (**2**)	11.8
Piperine (**6**)	11.7
Ergocalciferol (**15**)	15.5
Cholecalciferol (**16**)	13.6
DL-α-tocopherol acetate (**18**)	11.6

Overall, the results revealed that the majority of food and vitamin compounds tested were able to react with electrochemically generated $O_2^{\bullet-}$. The data in Table 5.1 indicated, however, that the EC_{10} values were fairly similar between several compounds. As such, subsequent discussions will be more focused on the EC_{50} values instead as it provided larger variations for comparison.

Amongst the 18 substrates measured, curcumin (**3**), diacetyl (**4**), maltol (**5**), vanillin (**8**), retinoic Acid (**10**), pyridoxine (**13**), and d-(+)-biotin (**14**) were found to exhibit the highest activity with $O_2^{\bullet-}$ (EC_{50} < 4 mM), while sesamol (**7**), retinal (**9**), retinol (**11**), retinyl acetate (**12**), and dl-α-tocopherol (**17**) all presented more modest reactivities toward the aforementioned radical anion (5 mM < EC_{50} < 14 mM). In contrast, caffeine (**1**), cinnamaldehyde (**2**), piperine (**6**), ergocalciferol (**15**), cholecalciferol (**16**), and dl-α-tocopherol acetate (**18**) each appeared to display only limited interactions with $O_2^{\bullet-}$ under the present conditions.

In line with expectations, the above observations can largely be ascribed to the presence (or absence) and chemical nature of the substituents on the examined molecules [11, 12] . For example, it is apparent from the results obtained that the compounds which possessed

acidic/labile hydrogen(s) generally underwent the greatest amount of reaction with $O_2^{\bullet-}$. In particular, the excellent reactivities observed for curcumin (**3**) and pyridoxine (**13**) are likely attributable to its large degree of hydroxylation (three –OH groups), which consequentially enables them to possess a higher stoichiometric reactivity with $O_2^{\bullet-}$ (via a proton or hydrogen atom transfer; see section 5.2.4) as compared to its counterparts. On the other hand, the relatively low EC_{50} values attained for retinoic acid (**10**) and d-(+)-biotin (**14**) can be rationalized by their principally acidic characters (due to the carboxylic acid functionality) which would correspondingly also facilitate their reaction with $O_2^{\bullet-}$. Similarly, maltol (**5)**, sesamol (**7**), and vanillin **(8**), whilst only possessing a single labile hydrogen atom, also presented fairly low EC_{50} values. In these cases, it is conceivable that their ability to scavenge $O_2^{\bullet-}$ stems from their highly conjugated hydroxy/phenolic functionalities which allows for better electron delocalisation and stabilization of the resulting conjugate base following the loss of its proton.

Concerning the different forms of vitamin A examined (i.e. retinal (**9**), retinoic acid (**10**), retinol (**11**), and retinyl acetate (**12**)), retinoic acid (**10**) demonstrated the best reactivity toward the electrochemically generated $O_2^{\bullet-}$, and as discussed above, is likely as a result of its extensively conjugated and correspondingly highly acidic carboxylic acid group. Conversely, retinol (**11**), possessing only a significantly less acidic primary alcohol, showed a multifold decrease in reactivity (increase in EC_{50} value). More interestingly, retinal (**9**) and retinyl acetate (**12**) both showed moderate $O_2^{\bullet-}$ consumption in spite of lacking of any apparent acidic protons. In this regard, it is presumable that they are involved in a different reaction pathway, such as possibly undergoing an allylic hydrogen atom abstraction and/or direct nucleophilic addition reaction with $O_2^{\bullet-}$ instead due to their highly conjugated structures (see section 5.2.4).

It is also noteworthy that diacetyl (**4**) was able to very effectively remove the electrochemically generated $O_2^{\bullet-}$ despite not having any acidic protons. As alluded with retinal

(**9**) and retinyl acetate (**12**), it is possible that $O_2^{\bullet-}$ is being scavenged by reacting with diacetyl (**4**) via a nucleophilic addition reaction (see section 5.2.4).

5.2.4. Mechanistic considerations

It has previously been proposed that phenolic molecules can react with electrochemically generated $O_2^{\bullet-}$ in aprotic organic solvents via two general pathways; the Proton Transfer and Hydrogen Atom Transfer mechanisms [6, 12, 16-19]. The third possibility is that $O_2^{\bullet-}$ acts as a direct reducing agent; however, for the molecules under study in this report this mechanism is not possible as the compounds are all harder to reduce than $O_2^{\bullet-}$ itself (Figures A5.2–A5.19 in the appendix).

In the Proton Transfer (PT) mechanism, following the initial reversible one-electron reduction of O_2 (eq. 5.1), a first proton transfer can occur between $O_2^{\bullet-}$ and the compound (RH) in a Brønsted acid/base reaction to generate a hydroperoxyl radical ($HO_2^{\bullet}$) (eq. 5.6). Subsequently, the reduction of $HO_2^{\bullet}$ into a hydroperoxide anion (HO_2^{-}) take places after either a heterogeneous one-electron transfer at the electrode surface to HO_2^{-} (eq. 5.7), or a homogeneous one-electron transfer between $HO_2^{\bullet}$ and $O_2^{\bullet-}$ (eq. 5.8), since the $HO_2^{\bullet}$ is more easily reduced than $O_2^{\bullet-}$. Regardless, both scenarios (the electrochemical-chemical-electrochemical (ECE) type mechanism in eq. 5.1, 5.6, and 5.7 or the disproportionation type mechanism in eq. 5.1, 5.6, and 5.8) then lead to a second proton transfer reaction between HO_2^{-} and another molecule of RH to form hydrogen peroxide (H_2O_2) (eq. 5.9), resulting in an overall two-electron process in this pathway (eq. 5.10).

$$O_2 + e^- \rightleftharpoons O_2^{\bullet-} \quad (5.1)$$

$$O_2^{\bullet-} + RH \rightleftharpoons HO_2^{\bullet} + R^- \quad (5.6)$$

$$HO_2^{\bullet} + e^- \rightarrow HO_2^- \quad (5.7)$$

$$HO_2^{\bullet} + O_2^{\bullet-} \rightarrow HO_2^{-} + O_2 \quad (5.8)$$

$$HO_2^{-} + RH \rightarrow H_2O_2 + R^{-} \quad (5.9)$$

$$O_2 + 2e^{-} + 2RH \rightarrow H_2O_2 + 2\ R^{-} \quad (5.10)$$

On the other hand, in the Hydrogen Atom Transfer (HAT) mechanism, the initial reversible one-electron reduction of O_2 (eq. 5.1) is followed by a hydrogen atom abstraction reaction between $O_2^{\bullet-}$ and RH to generate HO_2^{-} (eq. 5.11). As the resultant radical $R^{\bullet}$ is usually highly reactive, it then rapidly undergoes conversion (e.g. dimerization) into other more stable non-radical products (eq. 5.12). Conversely, HO_2^{-} is similarly able to react with another molecule of RH in which it gets protonated to H_2O_2 (eq. 5.9). The overall reaction of $O_2^{\bullet-}$ and RH remains a one-electron process in this pathway (eq. 5.13).

$$O_2 + e^{-} \rightleftharpoons O_2^{\bullet-} \quad (5.1)$$

$$O_2^{\bullet-} + RH \rightarrow HO_2^{-} + R^{\bullet} \quad (5.11)$$

$$R^{\bullet} \rightarrow \text{Non-radical products} \quad (5.12)$$

$$HO_2^{-} + RH \rightarrow H_2O_2 + R^{-} \quad (5.9)$$

$$O_2 + e^{-} + 2RH \rightarrow H_2O_2 + R^{-} + \text{Non-radical products} \quad (5.13)$$

Because the PT mechanism is associated with an overall two-electron reduction (as compared to only one-electron for the HAT pathway), analysis of the cathodic currents in the initial reduction of O_2 and upon substrate addition may provide a form of discrimination between the predominant mechanism favored by the hydroxy/phenolic compounds surveyed [18]; that is, substrates that afford a I^{S}_{pc}/I_{pc} ratio of > 1 are likely to be involved in the PT mechanism while substrates that give a I^{S}_{pc}/I_{pc} ratio of ca. 1 are more likely follow the HAT pathway instead.

In the present study, we chose to examine the variation of cathodic peak currents at the EC_{50} and zero concentrations (I^{50}_{pc}/I^{0}_{pc}). However, it should be highlighted that several of these compounds registered obvious pre-peaks in their voltammograms, and were thus exempted from the aforementioned measurements as they are possibly implicated in a sequence of mechanistic processes which are not presently well understood [12]. In these instances, as described by René et al., an approximate classification was instead performed by considering the difference in the potential (ΔE) of the pre-peak (when its intensity was half that of O_2 reduction) and the peak of the initial O_2 reduction [12]. Mainly, the magnitude of the pre-peak current tended to be proportional to the concentration of compound added, and a large shift in potential generally correlated to a high reactivity of the substrate. Results from the measurements of the I^{50}_{pc}/I^{0}_{pc} ratios and ΔE values for the hydroxy/phenolic compounds examined in this work are summarized in Tables 5.3 and 5.4, respectively.

Table 5.3. Ratios of the cathodic peak currents at the EC_{50} and zero concentration (I^{50}_{pc}/I^{0}_{pc}).

Compound	$\mathbf{I^{50}_{pc}/I^{0}_{pc}}$
Maltol (**5**)	1.35
Sesamol (**7**)	1.39
Ergocalciferol (**15**)[a]	0.98
Cholecalciferol (**16**)[a]	0.97
DL-α-tocopherol (**17**)	1.16

[a]The I^{50}pc value was measured at the 50 mM concentration.

Table 5.4. Difference in the potential (ΔE) of the pre-peak and peak of the initial O_2 reduction.

Compound	**ΔE (V)**
Curcumin (**3**)	0.124
Vanillin (**8**)	0.163
Retinoic Acid (**10**)	0.145
Retinol (**11**)	0.101
Pyridoxine (**13**)	0.136
D-(+)-Biotin (**14**)	0.140

It was also discussed in the preceding section that the scavenging of $O_2^{\bullet-}$ by compounds without any distinct acidic/labile protons (such as retinal (**9**) and retinyl acetate (**12**)) could entail a different type of reaction instead. Although tentative, it is possible that these unsaturated molecules may undergo a hydrogen atom abstraction reaction at their allylic position(s) to produce a resonance stabilized radical or undergo a direct addition onto the polyene chain to give a radical adduct as proposed for carotenoids [20, 21]. Alternatively, an addition reaction may also take place at the ester functionality to form a carboxylate anion and alkoxide as final products (Scheme 5.3) [7, 22].

In the case of diacetyl (**4**), its reaction with $O_2^{\bullet-}$ can be expected to follow a similar mechanism that has been proposed for diketones [23, 24] (Scheme 5.4). This might initially involve $O_2^{\bullet-}$ undergoing a nucleophilic addition at the carbonyl group, followed by another molecule of $O_2^{\bullet-}$ acting as a one-electron reductant, subsequently leading to an intramolecular cyclization reaction and cleavage of the median C-C bond.

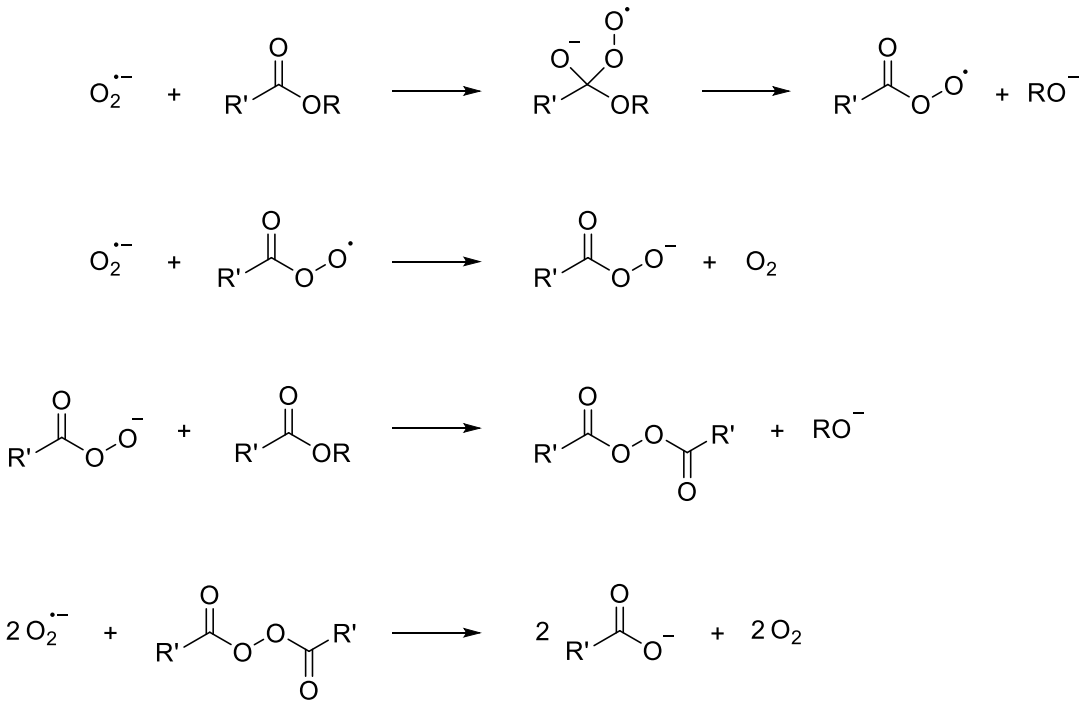

Scheme 5.3. Proposed mechanism for the nucleophilic addition reaction with $O_2^{\bullet-}$.

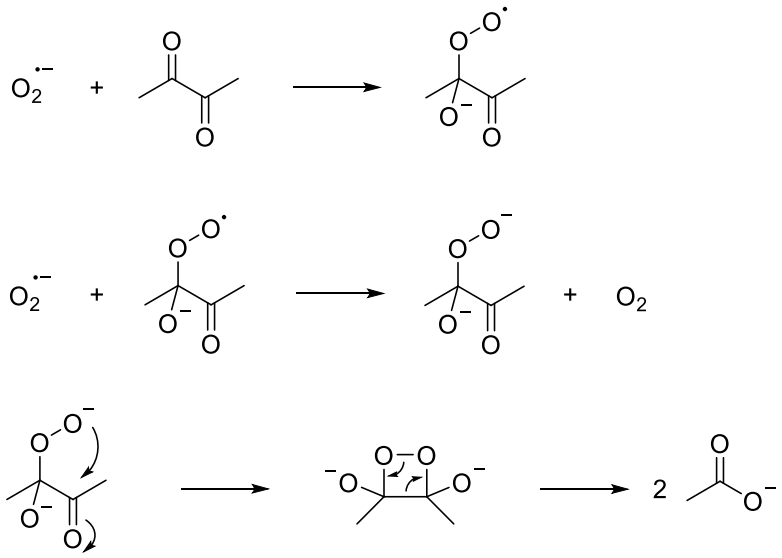

Scheme 5.4. Proposed mechanism for the reaction of diacetyl and $O_2^{\bullet-}$.

5.3. Conclusion

The comparative reactivities of 18 food molecules and vitamin analogues toward electrochemically generated $O_2^{\bullet-}$ have been investigated in DMF by monitoring the changes in the reverse anodic peak currents of O_2 reduction in the presence of increasing amounts of substrates.

The compounds that were able to bring about the largest decrease in anodic currents (smallest EC_{10} and EC_{50} values) can be inferred to possess the greatest reactivities (toward electrochemically generated $O_2^{\bullet-}$) while those that caused minimal or no change in the cyclic voltammograms of O_2 reduction (largest EC_{10} and EC_{50} values) can be interpreted to be poor scavengers of $O_2^{\bullet-}$. Overall, it was found that most analytes examined were able to interact with $O_2^{\bullet-}$ under the present conditions, and that curcumin (**3**), diacetyl (**4**), maltol (**5**), vanillin (**8**), retinoic acid (**10**), pyridoxine (**13**), and d-(+)-biotin (**14**) were revealed to the most reactive. In addition, it was also observed that their reactivity can generally be attributed to several main structural features such as: (i) the presence of labile protons, (ii) a large extent of acidity and conjugation of the labile protons, or (iii) a high degree of hydroxylation. Nevertheless, it is also worth highlighting that the reactivities of the compounds do not display a straightforward linear relationship between its reactivity and concentration added; that is, larger $\%\Delta I_{pa}$ were observed at smaller analyte concentrations as compared to higher analyte concentrations (Figures A5.38–A5.49 in the appendix). As such, more detailed analyses of the reactivities across different molecules can be performed by comparing against a calculated curve in future studies.

Lastly, it is noteworthy that the reactivities observed may differ in vivo and in vitro due to numerous factors such as solubility, metabolism, diffusion, adsorption, site binding, cell permeability, and other factors [15, 25-30]. As such, a single in vitro chemical assessment is not sufficient in uncovering the exact physiological transformations that might occur (in vivo).

Therefore, the present work may be more useful in serving as preliminary efforts to explore and showcase the general chemical reactivity patterns/trends of these compounds, rather than be used for direct correlations with the antioxidant abilities/reactions that may be manifested inside biological systems.

5.4. Materials & Methods

5.4.1. Chemicals & reagents

Unless otherwise stated, all food and vitamin compounds/analogues examined in this work were purchased from commercial sources and used as received. Curcumin (95 %, total curcuminoid content from turmeric rhizome), d-(+)-biotin (98+ %), piperine (98 %), maltol (99 %), retinoic acid (98 %), sesamol (98 %), trans-cinnamaldehyde (98+ %), and vanillin (99 %) were obtained from Alfa-Aesar. All trans-retinal (≥ 98 %), ergocalciferol (40,000,000 USP units/g), dl-α-tocopherol (97 %), dl-α-tocopherol acetate (≥ 96 %), pyridoxine (≥ 98 %), and retinyl acetate (synthetic) were obtained from Sigma-Aldrich. Caffeine (pure Ph. Eur., USP) was obtained from AppliChem. All trans-retinol (95 %) was obtained from Acros Organics. Cholecalciferol (> 98 %) and diacetyl (> 98 %) were obtained Tokyo Chemical Industry. HPLC grade acetonitrile (CH_3CN) and dimethylformamide (DMF) were obtained from Anhui Fulltime Solvents & Reagents Co. and VWR, respectively. The solvents were dried by storing over 1/16 in. rods with 3 Å pore size molecular sieves acquired from Fluka (pre-heated at 433 K under vacuum for 6 h). The supporting electrolyte, tetrabutylammonium hexafluorophosphate (Bu_4NPF_6) was prepared by reacting equimolar amounts of a 40% aqueous solution of Bu_4NOH (Alfa-Aesar) with a 65% aqueous solution of HPF_6 (Alfa-Aesar), washing the precipitate with ultra-pure water, recrystallizing three times with hot ethanol, drying in vacuo for 6 h at 433 K, and then stored in a vacuum desiccator.

5.4.2. Cyclic voltammetry instrumentation

Cyclic voltammetry (CV) measurements were conducted with a computer-controlled Eco-Chemie Autolab PGSTAT302N potentiostat using a three-electrode system. The working electrode was a 1-mm diameter planar glassy carbon (GC) disk (eDAQ Pty Ltd), used in conjunction with a Pt wire counter electrode (Metrohm), and a Ag wire miniature reference

electrode (eDAQ Pty Ltd) connected to the test solution via a salt bridge (containing 0.5 M Bu_4NPF_6 in CH_3CN). The working electrode was cleaned by polishing on a Buehler Ultra-pad polishing cloth with alumina oxide slurry (grain size = 0.3 μm), washing with acetone, and drying before introducing into the cell at the start of each experiment. Following the IUPAC convention, accurate potentials were obtained using Ferrocene (Fc), which was added to the test solutions at the end of the experiments. All cyclic voltammograms were recorded at 295 (±2) K, and inside of a Faraday cage.

5.4.3. Cyclic voltammetry procedure

CV experiments were performed in solutions of dry, air saturated DMF containing 0.1 M Bu_4NPF_6 ([H_2O] < 0.017 %; measured by Karl Fischer Titrations), inside of a glass cell that was dried in an oven at 373 K for 30 min. The test solutions were saturated by dry air (Alphagaz) for at least 15 min, and under standard laboratory conditions the solubility of O_2 is assumed to be ca. 0.94 mM; corresponding to a partial pressure of 0.2 atm [31]. Prior to the addition of each compound, a cyclic voltammogram was first registered in order to capture the initial anodic and cathodic peak currents of O_2. Following which, the substrate was added incrementally (in 0.2 or 10 mM concentrations) and the resultant cyclic voltammogram recorded after each addition. Successive additions of the 0.2 mM concentrations were carried out using aliquots of 100 mM stock solutions; while analytes added in sequential 10 mM concentrations were introduced into the solutions directly. All scans were obtained at a fixed scan rate of 0.1 V s^{-1} and in a fixed potential window of ca. between -1.70 to -0.05 vs. (Fc/Fc^+)/V to ensure a consistent timeframe for all cycles.

5.4.4. Karl Fischer titration analyses

Karl Fischer coulometric titrations were conducted with a Mettler Toledo DL32 coulometer using (Riedel-deHaën) HYDRANAL-Coulomat AG and HYDRANAL-Coulomat CG and for the anode and cathode compartments, respectively. Measurements were carried out inside a humidity controlled chamber (122 cm × 61 cm × 61 cm), maintained at a constant humidity of 30% by a dry nitrogen purge gas system from Coy Laboratory Products, after the coulometer was allowed to stabilize until a steady drift value close to 0 μg min^{-1} of water was attained. Sample solutions were kept in 5 mL vacuum syringes (SGE Analytical Science) and injected into the coulometer through a silicon/telfon septum during analyses. Each measurement was concluded within 1 min, indicating that the drift from atmospheric water was insignificant.

5.5. References

[1] R.A. Holroyd, B.H.J. Bielski, Photochemical Generation of Superoxide Radicals in Aqueous Solutions, J. Am. Chem. Soc., 100 (1978) 5796–5800.

[2] D.T. Sawyer, J.S. Valentine, How Super Is Superoxide?, Acc. Chem. Res., 14 (1981) 393–400.

[3] D. Kim, T. Oda, A. Ishimatsu, T. Muramatsu, Galacturonic Acid-Induced Increase of Superoxide Production in Red Tide Phytoplanktons *Chattonella marina* and *Heterosigma akashiwo*, Biosci., Biotechnol., Biochem., 64 (2000) 911–914.

[4] U. Stoin, A.I. Shames, I. Malka, I. Bar, Y. Sasson, In situ Generation of Superoxide Anion Radical in Aqueous Medium under Ambient Conditions, ChemPhysChem, 14 (2013) 4158–4164.

[5] A.J. Anifowose, K. Takeda, H. Sakugawa, Novel Fluorometric Method for the Determination of Production Rate and Steady-State Concentration of Photochemically Generated Superoxide Radical in Seawater Using 3',6'-(Diphenylphosphinyl)fluorescein, Anal. Chem., 87 (2015) 11998–12005.

[6] D. Vasudevan, H. Wendt, Electroreduction of Oxygen in Aprotic Media, J. Electroanal. Chem., 392 (1995) 69–74.

[7] R.D. Webster, A.M. Bond, Different Mechanisms for the Reaction of Disubstituted Aromatic Esters and Thioic *S*-Esters with Electrochemically Generated Superoxide, J. Chem. Soc., Perkin Trans. 2, (1997) 1075–1079.

[8] M. Hayyan, M.A. Hashim, I.M. AlNashef, Superoxide Ion: Generation and Chemical Implications, Chem. Rev., 116 (2016) 3029–3085.

[9] G. Feroci, A. Fini, Voltammetric Investigation of the Interactions Between Superoxide Ion and Some Sulfur Amino Acids, Inorg. Chim. Acta, 360 (2007) 1023–1031.

[10] J. Simonet, J.-F. Pilard, Electrogenerated Reagents, in: H. Lung, O. Hammerich (Eds.) Organic Electrochemistry, Marcel Dekker, New York, 2001, pp. 1163–1226.

[11] C. Le Bourvellec, D. Hauchard, A. Darchen, J.-L. Burgot, M.-L. Abasq, Validation of a New Method Using the Reactivity of Electrogenerated Superoxide Radical in the Antioxidant Capacity Determination of Flavonoids, Talanta, 75 (2008) 1098–1103.

[12] A. René, M.-L. Abasq, D. Hauchard, P. Hapiot, How Do Phenolic Compounds React toward Superoxide Ion? A Simple Electrochemical Method for Evaluating Antioxidant Capacity, Anal. Chem., 82 (2010) 8703–8710.

[13] L.L. Williams, R.D. Webster, Electrochemically Controlled Chemically Reversible Transformation of α-Tocopherol (Vitamin E) into Its Phenoxonium Cation, J. Am. Chem. Soc., 126 (2004) 12441–12450

[14] H.Y.V. Ching, E. Anxolabéhère-Mallart, H.E. Colmer, C. Costentin, P. Dorlet, T.A. Jackson, C. Policar, M. Robert, Electrochemical Formation and Reactivity of a Manganese Peroxo Complex: Acid Driven H_2O_2 Generation vs. O–O Bond Cleavage, Chem. Sci., 5 (2014) 2304–2310.

[15] R. Amorati, L. Valgimigli, Advantages and Limitations of Common Testing Methods for Antioxidants, Free Radical Res., 49 (2015) 633–649.

[16] C.P. Andrieux, P. Hapiot, J.-M. Savéant, Mechanism of Superoxide Ion Disproportionation in Aprotic Solvents J. Am. Chem. Soc., 109 (1987) 3768–3775.

[17] D.T. Sawyer, Electrochemistry of Dioxygen, in: R.J.P. Williams (Ed.) Oxygen Chemistry, Oxford University Press, Inc., New York, 1991, pp. 27.

[18] J.-M. Savéant, Elements of Molecular and Biomolecular Electrochemistry, Wiley-Interscience, New York, 2006.

[19] C. Costentin, M. Robert, J.-M. Savéant, Acceleration of the Homogeneous and Electrochemical Reductions of Dioxygen in Aprotic Media by Ammonium Ions. Is the Driving Force a Function of NH_4^+ Concentration? What Is the Mechanism of the Reaction?, J. Phys. Chem. C, 111 (2007) 12877–12880.

[20] G. Britton, Structure and Properties of Carotenoids in Relation to Function, FASEB J., 9 (1995) 1551–1558.

[21] J. Clayden, N. Greeves, S. Warren, P. Wothers, Delocalization and Conjugation, Organic Chemistry, Oxford University Press Inc., New York, 2001, pp. 151–180.

[22] M.J. Gibian, D.T. Sawyer, T. Ungermann, R. Tangpoonpholvivat, M.M. Morrison, Reactivity of Superoxide Ion with Carbonyl Compounds in Aprotic Solvents, J. Am. Chem. Soc., 101 (1979) 640–644.

[23] D.T. Sawyer, J.J. Stamp, K.A. Menton, Reactivity of Superoxide Ion with Ethyl Pyruvate, α-Diketones, and Benzil in Dimethylformamide, J. Org. Chem., 48 (1983) 3733–3736.

[24] L. Feriani, R. Kossai, K. Boujlel, Qualitative Investigation of the Oxidative Cleavage of Some Aromatic α-Diketones by Electrogenerated Superoxide Ion, Electrochim. Acta, 36 (1991) 783–789.

[25] K.L. Wolfe, R.H. Liu, Cellular Antioxidant Activity (CAA) Assay for Assessing Antioxidants, Foods, and Dietary Supplements, J. Agric. Food Chem., 55 (2007) 8896–8907.

[26] E. Niki, Assessment of Antioxidant Capacity *In Vitro* and *In Vivo*, Free Radical Biol. Med., 49 (2010) 503–515.

[27] C. López-Alarcón, A. Denicola, Evaluating the Antioxidant Capacity of Natural Products: A Review on Chemical and Cellular-Based Assays, Anal. Chim. Acta, 763 (2013) 1–10.

[28] M.C. Foti, The Use and Abuse of the DPPH• Radical, J. Agric. Food Chem., 63 (2015) 8765–8776.

[29] F. Shahidi, Y. Zhong, Measurement of Antioxidant Activity, J. Funct. Foods, 18 (2015) 757–781.

[30] R. Apak, M. Özyürek, K. Güçlü, E. Çapanoğlu, Antioxidant Activity/Capacity Measurement. 3. Reactive Oxygen and Nitrogen Species (ROS/RNS) Scavenging Assays, Oxidative Stress Biomarkers, and Chromatographic/Chemometric Assays, J. Agric. Food Chem., 64 (2016) 1046–1070.

[31] C. Dapremont-Avignon, P. Calas, A. Commeyras, C. Amatore, Synthesis of Perfluoroalkyl Carboxylic Acids by Reaction of Perfluoroalkyl Iodides with Electrogenerated Superoxide Ion, J. Fluorine Chem., 51 (1991) 357–379.

This page has been intentionally left blank

Chapter 6

Comparing the Relative Reactivities of Structurally Varied Alcohols Toward Electrochemically Generated Superoxide

This page has been intentionally left blank

6.1. Chapter Overview

It was discussed in the introduction (Chapter 1) that the reactivities of prevalent antioxidant molecules such as flavonoids [1-5] and (poly)phenols [6-11] toward electrochemically generated superoxide ($O_2^{\bullet-}$) have been successfully evaluated through of the use of voltammetry. However, because these compounds are often made up of complex chemical structures comprised of multiple functional groups, it is often challenging to unravel the exact characteristic or facet responsible for the perceived reactivity or lack thereof. This is all the more so given the many possible mechanistic pathways that $O_2^{\bullet-}$ can undergo with various types of functionalities. In light of this, and as part of continual efforts to examine the applications of electrochemically generated $O_2^{\bullet-}$, we envisaged the study of uncomplicated but structurally varied molecules such as aliphatic alcohols for the establishment of the possible relationships between a substrate's structure and its reactivity, and also to facilitate a discussion of the reactivities of these comparatively less acidic compounds (toward $O_2^{\bullet-}$) which have to date been relatively unexplored. Moreover, the understanding gained from the current work may be useful in the future design of molecules with enhanced reactivities.

With this in mind, this chapter delineates the analysis of the relative reactivities of 14 aliphatic alcohols (encompassing different steric and electronic features) toward electrochemically generated $O_2^{\bullet-}$ using cyclic voltammetry (CV) (Scheme 6.1). This was similarly performed by monitoring the decreases in the corresponding anodic peak currents (I_{pa}) in the cyclic voltammograms following the one-electron reduction of molecular oxygen/dioxygen (O_2) while methodically increasing the concentration of the test substrates in solutions of *N*,*N*-dimethylformamide (DMF). Based on the electrochemical responses gathered, best fit plots of the percentage decrease in the anodic peak current ($\%\Delta I_{pa}$) against the concentration of substrates added were obtained and compared according to the different classes

of alcohols that were examined (linear, fluorinated, branched, and multi-hydroxylated). In addition, the different parameters such as electronic effects, sterics effects, and degree of hydroxylation that affect the $O_2^{\bullet-}$ scavenging abilities of the alcohols were also discussed.

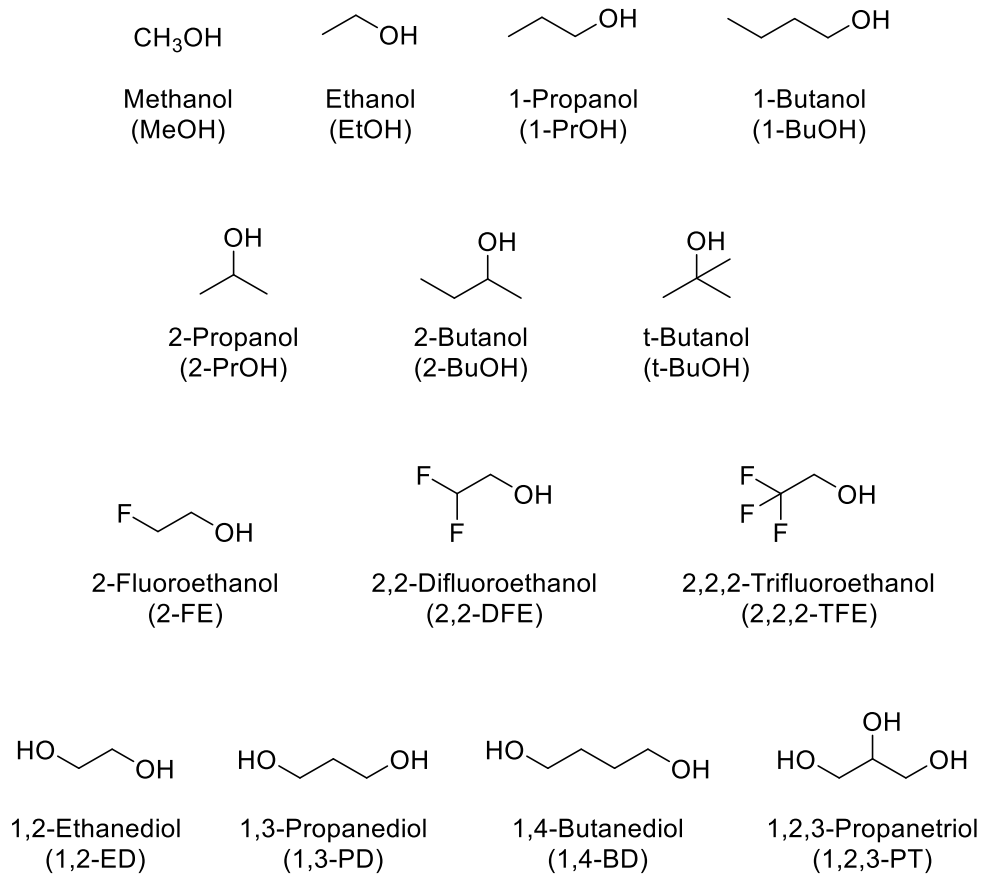

Scheme 6.1. List of alcohols examined in this study.

6.2. Results & Discussion

6.2.1. Cyclic voltammetry of molecular oxygen (O_2) reduction

As described in the preceding chapter (Chapter 5), it is notable that in many dry aprotic organic solvents such as DMF [12-14], dissolved O_2 can be electrochemically reduced by one-electron to form $O_2^{\bullet-}$ as illustrated by Figure 6.1. In addition, it is also worth mentioning that if the voltammetric scans were conducted under relatively dry conditions, then the aforementioned heterogeneous electron transfer process (to produce $O_2^{\bullet-}$) would appear to be chemically reversible in the sense that an anodic/oxidation (I_{pa}) to cathodic/reduction (I_{pc}) peak current ratio of close to unity can be obtained, which essentially suggests that the singly reduced species ($O_2^{\bullet-}$) can be fully converted back into the starting material (O_2) following its production (at least in the timeframe of the CV).

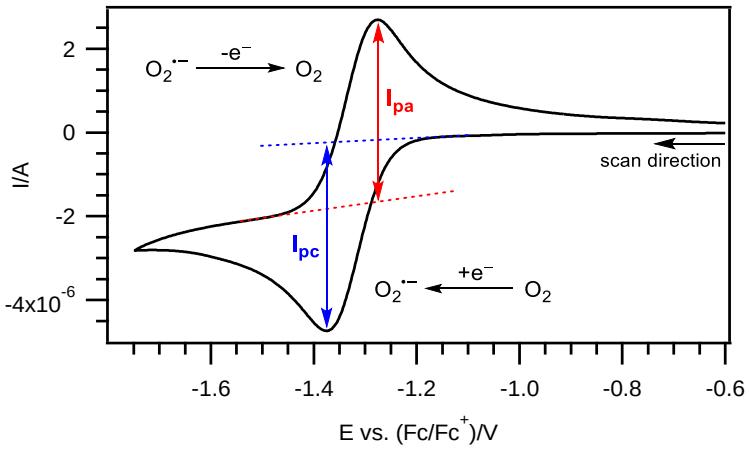

Figure 6.1. Cyclic voltammogram of the one-electron reduction of O_2 in dry, air saturated DMF containing 0.1 M Bu_4NPF_6, recorded using a 1-mm diameter planar GC disk electrode and a scan rate of 0.1 V s^{-1}. I_{pa}: Anodic peak current. I_{pc}: Cathodic peak current.

As such, akin to experiments conducted using electrochemically generated $O_2^{\bullet-}$ and the food and vitamin molecules (Chapter 6), the solvents used (DMF) in this study were pre-dried

prior usage in order to minimize the interferences that may occur from the interactions of $O_2^{\bullet-}$ with water during the voltammetric measurements [12, 15].

6.2.2. Cyclic voltammetry of O_2 reduction in the presence of alcohols

Similarly, to ensure that there was no interferences arising from the electrochemical signals of the alcohols during the measurements, their voltammetric behaviors were first examined in the scan range employed for the one-electron reduction of O_2. This demonstrated that all 14 substrates were redox inactive within the potential window of interest and their associated cyclic voltammograms are given in the appendix (Figure A6.1–A6.14).

With the above information at hand, attention was turned to probing the scavenging effects of the alcohols on $O_2^{\bullet-}$. At the start, a cyclic voltammogram of the electrochemical reduction of O_2 in dry, air saturated DMF solution containing 0.1 M Bu_4NPF_6 was first collected in order to obtain the initial currents for the $O_2/O_2^{\bullet-}$ redox couple. Following which, the alcohols were added incrementally and the resultant cyclic voltammogram recorded after each accumulation. If the electrochemically generated $O_2^{\bullet-}$ is able to undergo a reaction with the alcohol substrate that was introduced, the radical anion ($O_2^{\bullet-}$) would then no longer be available for oxidation back into O_2 (on the return sweep of the CV) and thereby lead to a corresponding decrease in the magnitude of I_{pa} (Figure 6.2) [2, 8].

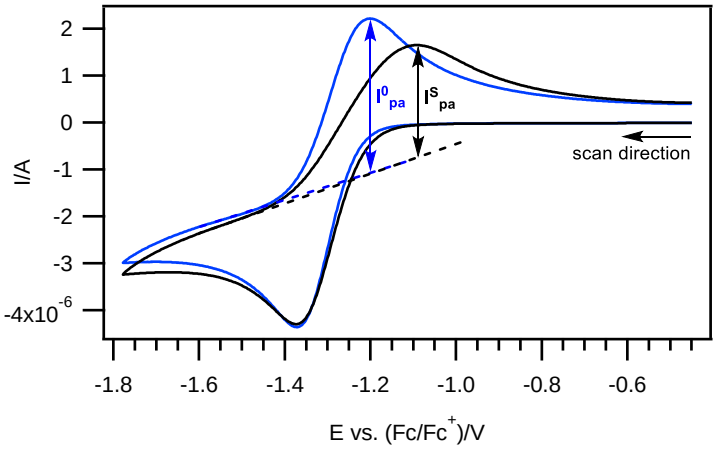

Figure 6.2. Cyclic voltammograms of the one-electron reduction of O_2 in dry, air saturated DMF containing 0.1 M Bu_4NPF_6, at a 1-mm diameter planar GC disk electrode, a scan rate of 0.1 V s^{-1}, and in the (—) absence and (—) presence of a typical alcohol analyte. I^0_{pa}: Initial anodic peak current in the absence of any analyte. I^S_{pa}: Anodic peak current after addition of the alcohol substrate.

Four representative examples (methanol (MeOH), ethanol (EtOH), 1-propanol (1-PrOH), and 1-butanol (1-BuOH)) of a series of cyclic voltammograms where increasing concentrations of substrates were added are shown in Figure 6.3, and it can be observed that the sequential additions of the alcohols into the test solution brought about corresponding decreases in the anodic currents (on the return scan of the CV) indicating therefore that some $O_2^{\bullet-}$ has been irreversibly consumed. More importantly, however, because the drop in current intensity corresponds to the amount of $O_2^{\bullet-}$ that has been removed, this provides a measure of the extent of radical inhibition [2, 8]. That is, alcohols which bring about larger decreases in I_{pa} (at a fixed substrate concentration) can be interpreted to have reacted in greater quantities with $O_2^{\bullet-}$, while alcohols which undergo little reaction with $O_2^{\bullet-}$ would result in smaller changes in I_{pa} instead. Similar experiments were also carried out for the remaining 10 compounds and their corresponding voltammograms are provided in the appendix (Figures A6.15–A6.28).

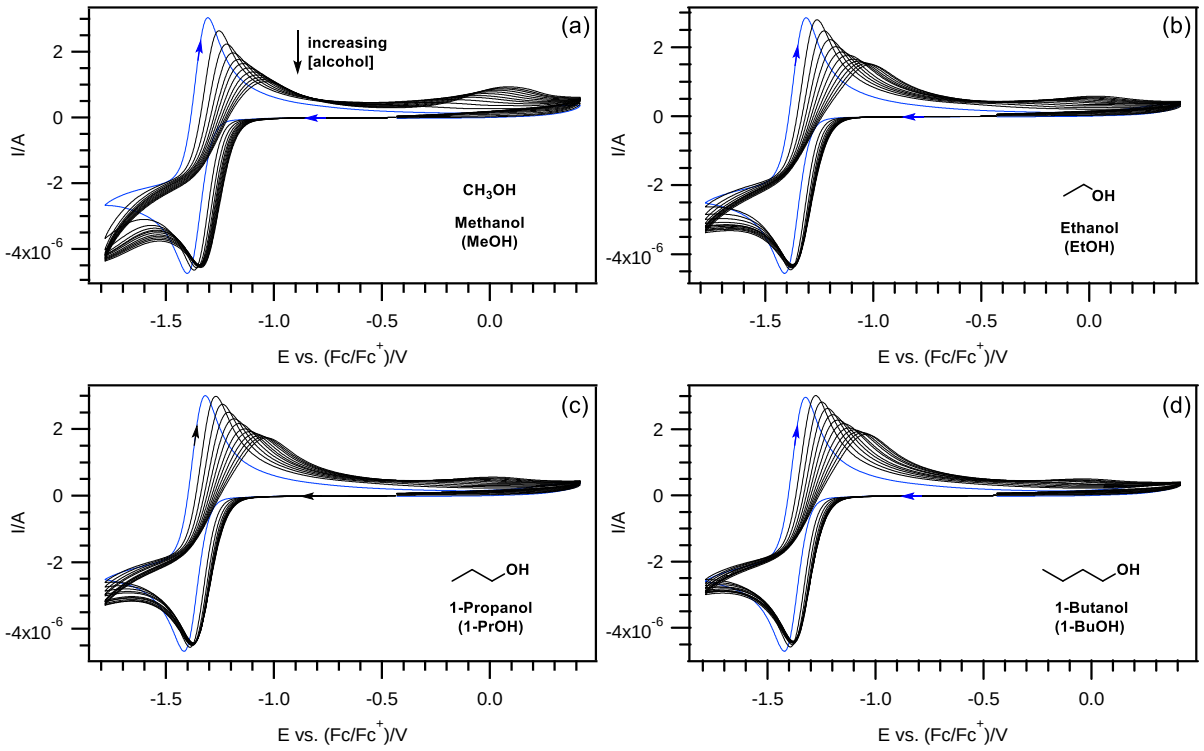

Figure 6.3. Cyclic voltammograms of the one-electron reduction of O_2 in dry, air saturated DMF containing 0.1 M Bu_4NPF_6, recorded using a 1-mm diameter planar GC disk electrode, a scan rate of 0.1 V s^{-1}, and at increasing concentrations of (a) methanol, (b) ethanol, (c) 1-propanol, and (d) 1-butanol. (—) Initial scan registered in the absence of any alcohol. (—) Scans measured at 200 mM increments in concentration of the respective alcohols.

6.2.3. Mechanistic considerations

The reactions of phenols with electrochemically generated $O_2^{\bullet-}$ have been extensively studied and is generally proposed to involve two main classes of reaction: The Proton Transfer (PT) and/or the Hydrogen Atom Transfer (HAT) mechanisms (see Chapter 5.2.4) [8, 12, 16-19].

Since the PT mechanism involves an overall two-electron reduction process (as compared to a total of one-electron involved in the HAT pathway), an increase in the cathodic currents (I_{pc}) of the $O_2/O_2^{\bullet-}$ redox couple is often registered as increasing concentrations of ROH are added [8]. Taking the above into consideration, the main pathway by which the

alcohols under study in this report follow can likely be distinguished by analyzing the ratios of the new and initial cathodic current (I^S_{pc}/ I^0_{pc}). More specifically, it can be rationalized that the substrates which afforded I^S_{pc}/ I^0_{pc} values of > 1 are more likely to favor the PT pathway (instead of the HAT mechanism) in contrast to the alcohols which furnished I^S_{pc}/ I^0_{pc} ratios of ≤ 1. In the present study, we chose to analyze the variation of I_{pc} in the absence of any alcohol and at the final concentrations that were used. The majority of the alcohols gave I^S_{pc}/I^0_{pc} values of ≤ 1 suggesting therefore that the alcohols appeared to follow the HAT pathway and the results from these measurements have been summarized in Table A6.1 in the appendix.

Additionally, it is also noteworthy to highlight that the possibility of $O_2^{\bullet-}$ acting as a direct reducing agent is negated by the fact that the alcohols examined in this study are all harder to reduce than $O_2^{\bullet-}$ (Figures A6.1–A6.14 in the appendix).

6.2.4. Comparisons of the relative reactivities of the alcohols toward superoxide

It was discussed in the previous section that the changes in I_{pa} in the cyclic voltammograms of O_2 reduction can be used to infer the reactivity of each substrate, whereby the extent of decrease is directly proportional to the amount of $O_2^{\bullet-}$ scavenged. Hence, the percentage changes in I_{pa} after each successive addition of alcohol were subsequently calculated by considering the ratios of the difference between the initial and final I_{pa} values over its original I_{pa} magnitude (eq. 6.1) [2, 8]. Thereafter, the results were plotted into best-fit curves (percentage change in I_{pa} against the concentration of alcohol added (Figures A6.29–A6.42 in the appendix) to facilitate easy comparisons of the activities across the different compounds.

$$\%\Delta I_{pa} = \left(\frac{I^{S}_{pa} - I^{0}_{pa}}{I^{0}_{pa}}\right) \times 100\ \% \quad (6.1)$$

where: $\%\Delta I_{pa}$ refers to the percentage change in anodic peak current; I^{0}_{pa} is the initial anodic peak current in the absence of any alcohol; I^{S}_{pa} represents the anodic peak current at a specified alcohol concentration.

6.2.4.1. Linear alcohols

The linear alcohols MeOH, EtOH, 1-PrOH, and 1-BuOH were first compared in order to determine if a change in the chain length of the alcohol would result in an appreciable difference in their relative reactivities. As illustrated by Figure 6.4, this revealed that the plots of $\%\Delta I_{pa}$ versus [alcohol] for the aforementioned substrates varied substantially from one another, and that $\%\Delta I_{pa}$ can be used to distinguish between the alcohols as it appears to be sensitive to the number of carbon atoms attached to the hydroxy group. For instance, it is noteworthy that for a given [alcohol], MeOH was found to exhibit the largest change in $\%\Delta I_{pa}$ whereas 1-BuOH displayed the least. These observations (MeOH (most reactive) > EtOH > 1-PrOH > 1-BuOH (least reactive)) are likely attributable to the presence of larger and more unfavorable electron-donating inductive effects on the hydroxy group as the chain length of the alcohols increases [20, 21]. More specifically, because 1-BuOH possesses the longest alkyl chain amongst its counterparts, it is presumable that the corresponding alkoxyl radical (formed after the initial hydroxyl hydrogen atom abstraction reaction by $O_2^{\bullet-}$) experiences the greatest destabilization, which in turn discourages 1-BuOH's capacity to scavenge $O_2^{\bullet-}$.

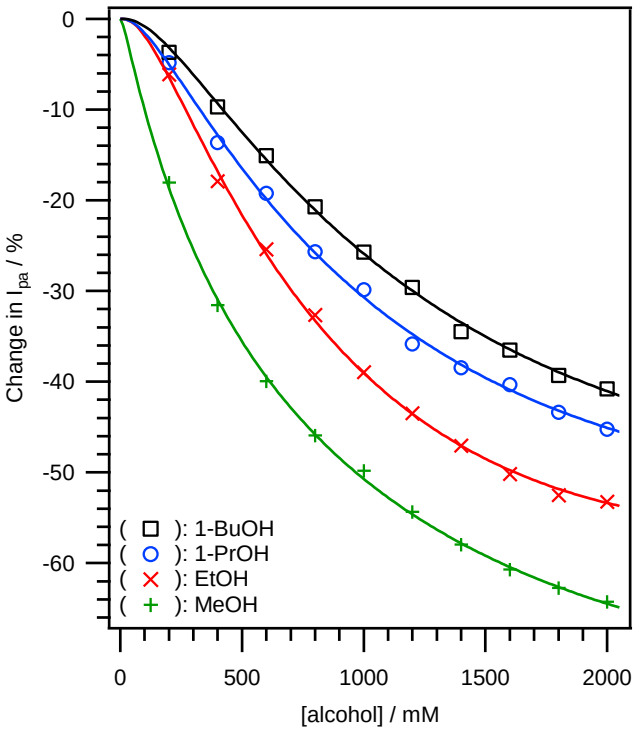

Figure 6.4. Best fit plots of the percentage change in anodic peak currents (%ΔI_{pa}) against the concentration of alcohol added as measured from the cyclic voltammograms of the one-electron reduction of O_2 in dry, air saturated DMF containing 0.1 M Bu_4NPF_6, recorded using a 1-mm diameter planar GC disk electrode, a scan rate of 0.1 V s^{-1}, and at increasing concentrations of methanol (MeOH), ethanol (EtOH), 1-propanol (1-PrOH), and 1-butanol (1-BuOH).

The reactions of increasingly fluorinated alcohols (2-fluoroethanol (2-FE), 2,2-difluoroethanol (2,2-DFE) and 2,2,2-trifluoroethanol (2,2,2-TFE)) were also studied in order to inspect the impact of electronic effects on the reactions of these compounds toward $O_2^{\bullet-}$ in more detail. It can be seen from Figure 6.5 that the reactivities differed according to the level of fluorination, whereby 2,2,2-TFE showcased the largest change in %ΔI_{pa}, indicating therefore that it is the most capable of quenching $O_2^{\bullet-}$ (followed by 2,2-DFE and 2-FE). This is in line with expectations as the strong electron-withdrawing inductive effects exerted by the highly electronegative F atoms would cause a polarization of the O–H bond (thereby increasing its acidity) and also provide greater delocalization and stabilization of the electron density on the

alkoxyl radical/alkoxide that is formed after the scavenging reactions with the fluoroethanols [22, 23]. More interestingly, however, when comparing the reactivities of the fluorinated and non-fluorinated EtOHs, it was noted that the presence of the F atoms resulted in a multi-fold increment in the reactivities observed.

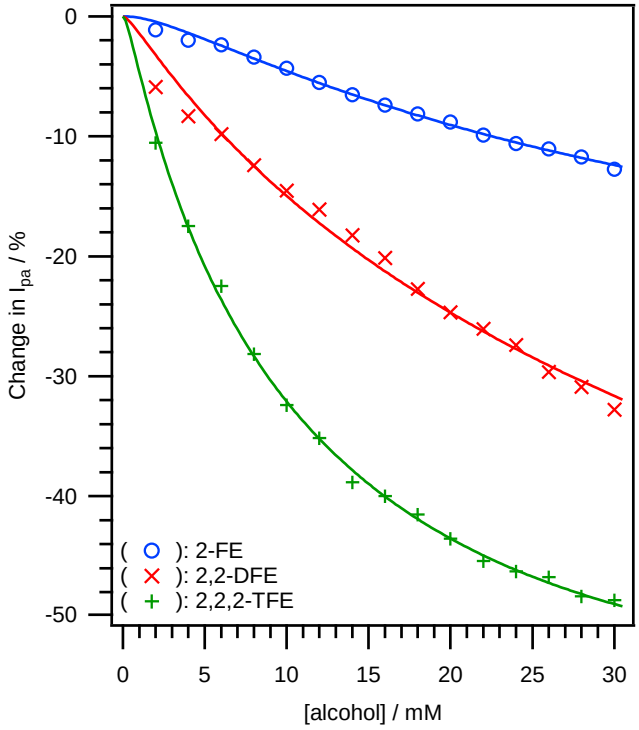

Figure 6.5. Best fit plots of the percentage change in anodic peak currents (%ΔI_{pa}) against the concentration of alcohol added as measured from the cyclic voltammograms of the one-electron reduction of O_2 in dry, air saturated DMF containing 0.1 M Bu_4NPF_6, recorded using a 1-mm diameter planar GC disk electrode, a scan rate of 0.1 V s^{-1}, and at increasing concentrations of 2-fluoroethanol (2-FE), 2,2-difluoroethanol (2,2-DFE), and 2,2,2-trifluoroethanol (2,2,2-TFE).

6.2.4.2. Branched alcohols

Having established the dependence of electronic effects on the relative reactivities of the alcohols toward the electrochemically generated $O_2^{\bullet-}$, we next sought to investigate the effects of steric hindrance on the aforementioned reaction. This was carried out through the use of

MeOH, EtOH, 2-propanol (2-PrOH), and t-butanol (t-BuOH), which were chosen to represent the unsubstituted, primary, secondary, and tertiary alcohols, respectively. Based on the results obtained (Figure 6.6), it can be discerned that the order of reactivities for the alcohols are as follows: MeOH > EtOH > 2-PrOH > t-BuOH, which indicate that the possession of increasing steric bulk leads to reduced $O_2^{\bullet-}$ scavenging abilities [24]. These observations are unsurprising as less steric effects imply that the alcohol in question would encounter correspondingly smaller amounts of hindrance when attempting to approach $O_2^{\bullet-}$ for reaction. On the other hand, the ownership of a bulky functionality such as the tert-butyl group would prevent the substrate from from having easy access to $O_2^{\bullet-}$.

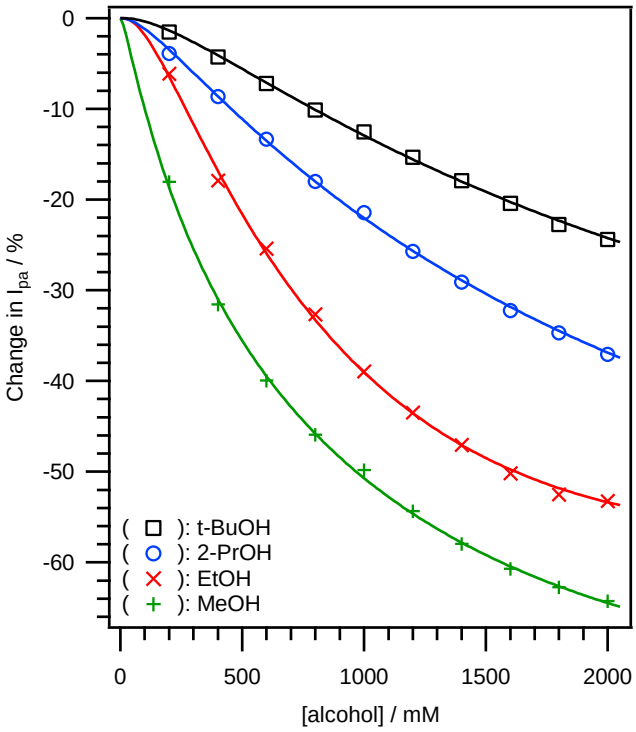

Figure 6.6. Best fit plots of the percentage change in anodic peak currents ($\%\Delta I_{pa}$) against the concentration of alcohol added as measured from the cyclic voltammograms of the one-electron reduction of O_2 in dry, air saturated DMF containing 0.1 M Bu_4NPF_6, recorded using a 1-mm diameter planar GC disk electrode, a scan rate of 0.1 V s^{-1}, and at increasing concentrations of methanol (MeOH), ethanol (EtOH), 2-propanol (2-PrOH), and t-butanol (t-BuOH).

However, it is noted that the possibility of some influence from inductive effects on the alcohols' reactivities cannot be completely ruled out since there is an increase in the number of electron-donating methyl group ($-CH_3$) substituents (on the α-position) going from MeOH to t-BuOH (Figure 6.7). Nevertheless, an analogous inverse relationship between steric impediment and substrate reactivity was also demonstrated when comparing the plots of $\%\Delta I_{pa}$ versus [alcohol] for the different structural isomers of PrOH and BuOH. In these cases, it is likewise evident that the possession of increasingly bulkier groups (n-butyl < sec-butyl < tert-butyl) resulted in the distinctive decreases in the reactivities of 1-BuOH, 2-BuOH, and t-BuOH, respectively; a similar trend that was attained when juxtaposing 1-PrOH and 2-PrOH. In addition, it is noteworthy that the relative reactivities of 2-PrOH and 2-BuOH did not appear to be well differentiated from each other – suggesting that steric effects emanating from the β-position of the alcohol probably play a comparatively minor role in influencing the alcohol's ability to scavenge electrochemically generated $O_2^{\bullet -}$.

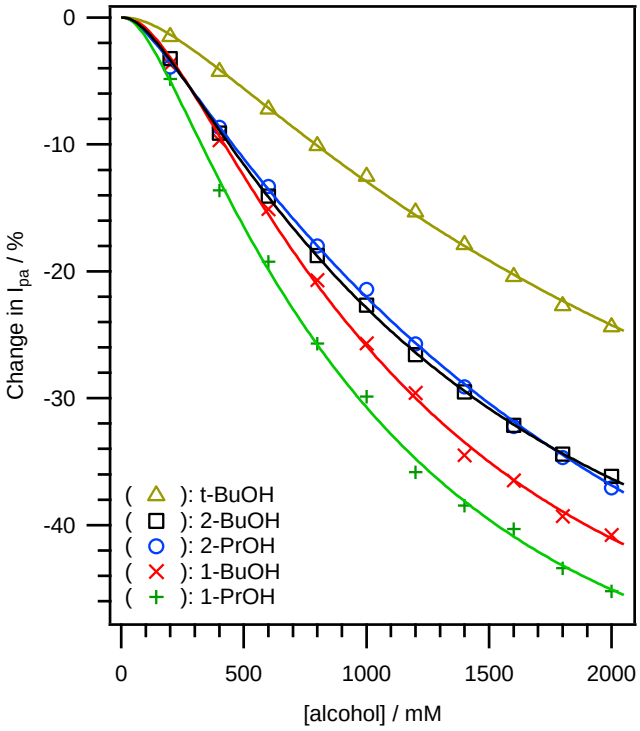

Figure 6.7. Best fit plots of the percentage change in anodic peak currents ($\%\Delta I_{pa}$) against the concentration of alcohol added as measured from the cyclic voltammograms of the one-electron reduction of O_2 in dry, air saturated DMF containing 0.1 M Bu_4NPF_6, recorded using a 1-mm diameter planar GC disk electrode, a scan rate of 0.1 V s^{-1}, and at increasing concentrations of 1-Propanol (1-PrOH), 1-Butanol (1-BuOH), 2-Propanol (2-PrOH), 2-Butanol (2-BuOH), and t-Butanol (t-BuOH).

6.2.4.3. Polyols

Since a larger degree of hydroxylation is reasoned to be able to provide a greater amount of labile hydrogens for reaction, the substrate scope was expanded to include a series of polyols so as to assess the significance of the number of hydroxy group(s) on reactivitiy. Consistent with earlier findings (Figure 6.4), the relative reactivities of the diols toward the electrochemically generated $O_2^{\bullet-}$ decreased as the alkyl chain lengths increased (1,2-ethanediol (1,2-ED) > 1,3-propanediol (1,3-PD) > 1,4-butanediol (1,4-BD)). In this regard, it is probable that this trend can similarly be rationalized by the formation of a more chemically unstable intermediate (after reaction with $O_2^{\bullet-}$) due to the increase in electron-donating inductive effects that are imposed by a longer alkyl functionality. Noteworthily, due to the presence of an additional hydroxy group, it is unsurprising the diols were generally found to afford greater changes in $\%\Delta I_{pa}$ (at a fixed substrate concentration) as compared to the mono-ols. The higher reactivities of the diols may also be attributable to their ability to form intramolecular hydrogen bonds, which would provide added stability to its conjugate base (following the loss of a proton after reaction with $O_2^{\bullet-}$) [25]. Lastly, the relationship between a larger number of hydroxy groups and increased reactivity (toward $O_2^{\bullet-}$) is also exemplified by 1,2,3-Propanetriol (1,2,3-PT), which demonstrated the steepest gradient (greatest $O_2^{\bullet-}$ quenching ability) amongst all the alcohols that were examined (Figure 6.8).

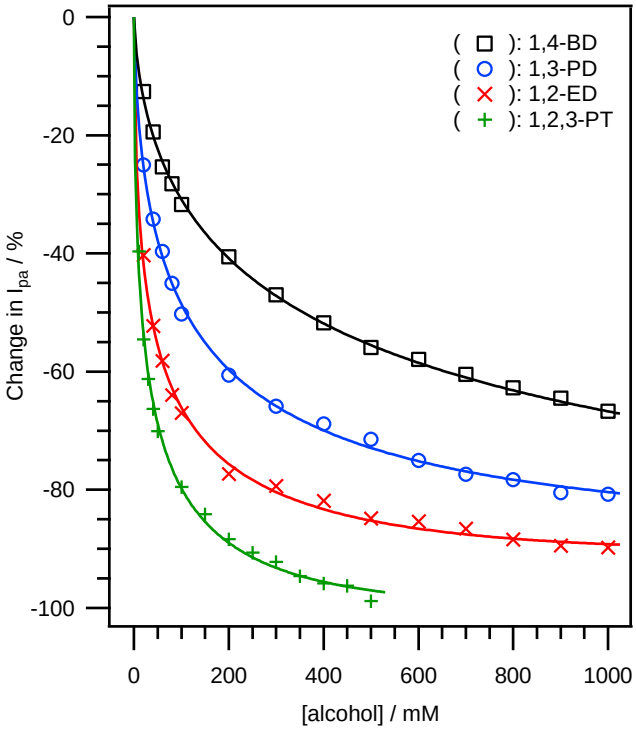

Figure 6.8. Best fit plots of the percentage change in anodic peak currents (%ΔI_{pa}) against the concentration of alcohol added as measured from the cyclic voltammograms of the one-electron reduction of O_2 in dry, air saturated DMF containing 0.1 M Bu_4NPF_6, recorded using a 1-mm diameter planar GC disk electrode, a scan rate of 0.1 V s^{-1}, and at increasing concentrations of 1,2-ethanediol (1,2-ED), 1,3-propanediol (1,3-PD), 1,4-butanediol (1,4-BD), and 1,2,3-propanetriol (1,2,3-PT).

6.3. Conclusion

Using cyclic voltammetry to generate $O_2^{\bullet-}$ in situ, the relative reactivities of 14 structurally diverse aliphatic alcohols (Scheme 6.1) were determined in DMF solutions and compared based on the plots of the percentage change in anodic peak currents ($\%\Delta I_{pa}$) against the amount of substrate added. The alcohols which displayed higher scavenging capabilities generally effected greater changes in $\%\Delta I_{pa}$ (at a specified concentration) as compared to the substrates which showed poorer reactivities.

Notably, by taking advantage of the seemingly simplistic frameworks of the aliphatic alcohols examined, the correlation between their structures and reactivities with $O_2^{\bullet-}$ were able to be determined and assigned according to the likely factors (such as electronic effects or steric effects) influencing their radical scavenging ability. For instance, the presence of an electron-donating functionality such as a long-chain alkyl group resulted in the observations of reduced reactivities due to the unfavorable destabilization of the intermediate formed after the alcohol's reaction with $O_2^{\bullet-}$. Conversely, the possession of electron-withdrawing substituents such as F atoms led to the increase in scavenging abilities. Besides the effects of electronics, it was also established that steric hindrance conferred by bulky substituents such as the tert-butyl functional group generally resulted in poorer reactivity toward $O_2^{\bullet-}$, and that an alcohol's capacity to quench $O_2^{\bullet-}$ seemed to be in accordance with the increase in hydroxylation of the substrate.

Incidentally, it was also found that the trends recorded for the relative reactivities of the mono-ols toward $O_2^{\bullet-}$ generally appeared to correlate well their relative hydrogen-bonding strengths [26], and with the ease in which they are able to donate its proton (acidity) (Table A6.2 in the appendix). Hence, it might be interesting to develop the current method for the estimation or evaluation of an alcohols' acidity in aprotic solvents. Nevertheless, as the present work only provides qualitative insights, the mathematical treatment of the experimental data,

use of a universal reference molecule for comparison, and/or gathering of information regarding the kinetic parameters associated with the mechanism may be necessitated in future studies.

6.4. Materials & Methods

6.4.1. Chemicals & reagents

Unless otherwise stated, all chemicals and reagents were purchased from commercial sources and used as received. Methanol (HPLC grade) was obtained from Anhui Fulltime Solvents & Reagents Co., Ltd. Ethanol (AR grade) and 1-propanol (AR grade) were acquired from Fisher Chemical. 1-Butanol (99 %), 2-butanol (99 %), t-butanol (99 %), 2,2-difluoroethanol (97 %), 2,2,2-trifluoroethanol (99+ %), 1,2-ethanediol (99 %), and 1,3-propanediol (99 %) were attained from Alfa-Aesar. 2-Propanol (HPLC grade) was bought from J. T. Baker. 2-Fluoroethanol (95 %) and 1,4-butanediol (99 %) were procured from Sigma-Aldrich. 1,2,3-Propanetriol (Ultrapure, MB grade) was purchased form Affymetrix USB and *N*,*N*-dimethylformamide (HPLC grade) from VWR. DMF was dried by storing over 1/16 in. rods with 3 Å pore size molecular sieves acquired from Fluka (pre-heated at 433 K under vacuum for 6 h). The supporting electrolyte, tetrabutylammonium hexafluorophosphate (Bu_4NPF_6) was prepared by reacting equimolar amounts of a 40 % aqueous solution of Bu_4NOH (Alfa-Aesar) with a 65 % aqueous solution of HPF_6 (Alfa-Aesar), washing the precipitate with ultra-pure water, recrystallizing three times with hot ethanol, drying in vacuo for 6 h at 433 K, and then stored in a vacuum desiccator.

6.4.2. Cyclic voltammetry instrumentation

Cyclic voltammetry (CV) measurements were conducted using a computer-controlled Eco-Chemie Autolab PGSTAT302N potentiostat using a three-electrode system. The working electrodes were 1-mm diameter planar glassy carbon (GC) disks (eDAQ Pty Ltd), used in conjunction with a platinum (Pt) wire counter electrode (Metrohm), and a silver (Ag) wire miniature reference electrode (eDAQ Pty Ltd) connected to the test solution via a salt bridge (containing 0.5 M Bu_4NPF_6 in CH_3CN). The working electrode was cleaned by polishing on a

Buehler Ultra-pad polishing cloth with alumina oxide slurry (grain size = 0.3 μm), washing with acetone, and drying before introducing into the cell at the start of each experiment. Following the IUPAC convention, accurate potentials were obtained using ferrocene (Fc), which was added to the test solutions at the end of the experiments. All cyclic voltammograms were recorded at 295 (±2) K, and inside of a Faraday cage.

6.4.3. Cyclic voltammetry procedure

CV experiments were performed in solutions of dried, air saturated DMF containing 0.1 M Bu_4NPF_6 ([H_2O] < 0.018 %; measured by Karl Fischer Titrations), inside of a glass cell that had been dried in an oven at 373 K for 30 min. The test solutions were saturated by dry air (Alphagaz) for at least 15 min, and under standard laboratory conditions (0.2 atm) the solubility of O_2 is assumed to be ca. 0.94 mM in DMF [27]. Prior to the addition of each alcohol, a cyclic voltammogram was first registered in order to capture the initial anodic and cathodic peak currents of O_2. Alcohol additions followed a stepwise manner that differed for different classes of alcohols.

The concentrations per addition were chosen to ensure a steady drop in the peak oxidation currents and were as follows: mono-ols at 200 mM per addition from 0 mM to 2000 mM; fluorinated ethanols at 2 mM per addition from 0 mM to 30 mM; diols at 20 mM per addition from 0 mM to 100 mM and subsequently 100 mM per addition to 1000 mM; and 1,2,3-PT at 10 mM per addition from 0 mM to 50 mM, and subsequently 50 mM per addition to 500 mM. All scans were obtained at a fixed scan rate of 0.1 V s^{-1} and in a fixed potential window of between ca. -1.78 to -0.42 vs. (Fc/Fc^+)/V to ensure a consistent timeframe for all cycles.

6.4.4. Karl Fischer titration analyses

Karl Fischer coulometric titrations were conducted with a Mettler Toledo DL32 coulometer using (Riedel-deHaën) HYDRANAL-Coulomat AG and HYDRANAL-Coulomat CG and for

the anode and cathode compartments, respectively. Measurements were carried out inside a humidity controlled chamber (122 cm × 61 cm × 61 cm), maintained at a constant humidity of 30% by a dry nitrogen purge gas system from Coy Laboratory Products, after the coulometer was allowed to stabilize until a steady drift value close to 0 μg min^{-1} of water was attained. Sample solutions were kept in 5 mL vacuum syringes (SGE Analytical Science) and injected into the coulometer through a silicon septum during analyses. Each measurement was concluded within 1 min, indicating that the drift from atmospheric water was insignificant.

6.5. References

[1] J.P. Hu, M. Calomme, A. Lasure, T. De Bruyne, L. Pieters, A. Vlietinck, D.A. Vanden Berghe, Structure-Activity Relationship of Flavonoids with Superoxide Scavenging Activity, Biol. Trace Elem. Res., 47 (1995) 327–331.

[2] C. Le Bourvellec, D. Hauchard, A. Darchen, J.-L. Burgot, M.-L. Abasq, Validation of a New Method Using the Reactivity of Electrogenerated Superoxide Radical in the Antioxidant Capacity Determination of Flavonoids, Talanta, 75 (2008) 1098–1103.

[3] S. Ahmed, F. Shakeel, Antioxidant Activity Coefficient, Mechanism, and Kinetics of Different Derivatives of Flavones and Flavanones Towards Superoxide Radical, Czech J. Food Sci., 30 (2012) 153–163.

[4] E.I. Korotkova, O.A. Voronova, E.V. Dorozhko, Study of Antioxidant Properties of Flavonoids by Voltammetry, J. Solid State Electrochem., 16 (2012) 2435–2440.

[5] J.M. Dimitrić Marković, D. Milenković, D. Amić, M. Mojović, I. Pašti, Z.S. Marković, The Preferred Radical Scavenging Mechanisms of Fisetin and Baicalein Towards Oxygen-Centred Radicals in Polar Protic and Polar Aprotic Solvents, RSC Adv., 4 (2014) 32228–32236.

[6] T. Araki, H. Kitaoka, Antioxidative Properties of Probucol Estimated by the Reactivity with Superoxide and by Electrochemical Oxidation, Chem. Pharm. Bull. (Tokyo), 49 (2001) 943–947.

[7] G.K. Ziyatdinova, D.M. Gil'metdinova, G.K. Budnikov, Reactions of Superoxide Anion Radical with Antioxidants and Their Use in Voltammetry, J. Anal. Chem., 60 (2005) 49–52.

[8] A. René, M.-L. Abasq, D. Hauchard, P. Hapiot, How Do Phenolic Compounds React toward Superoxide Ion? A Simple Electrochemical Method for Evaluating Antioxidant Capacity, Anal. Chem., 82 (2010) 8703–8710.

[9] T. Nakayama, B. Uno, Importance of Proton-Coupled Electron Transfer from Natural Phenolic Compounds in Superoxide Scavenging, Chem. Pharm. Bull., 63 (2015) 967–973.

[10] G.K. Ziyatdinova, S.P. Zakharova, H.C. Budnikov, Reactions of Phenolic Antioxidants with Electrogenerated Superoxide Anion Radical and their Analytical Application, Uch. Zap. Kazan. Univ., Ser. Estestv. Nauki, 157 (2015) 129–142.

[11] T. Nakayama, B. Uno, Concerted Two-proton–coupled Electron Transfer From Catechols To Superoxide Via Hydrogen Bonds, Electrochim. Acta, 208 (2016) 304–309.

[12] D. Vasudevan, H. Wendt, Electroreduction of Oxygen in Aprotic Media, J. Electroanal. Chem., 392 (1995) 69–74.

[13] R.D. Webster, A.M. Bond, Different Mechanisms for the Reaction of Disubstituted Aromatic Esters and Thioic *S*-Esters with Electrochemically Generated Superoxide, J. Chem. Soc., Perkin Trans. 2, (1997) 1075–1079.

[14] M. Hayyan, M.A. Hashim, I.M. AlNashef, Superoxide Ion: Generation and Chemical Implications, Chem. Rev., 116 (2016) 3029–3085.

[15] G. Feroci, A. Fini, Voltammetric Investigation of the Interactions Between Superoxide Ion and Some Sulfur Amino Acids, Inorg. Chim. Acta, 360 (2007) 1023–1031.

[16] C.P. Andrieux, P. Hapiot, J.-M. Savéant, Mechanism of Superoxide Ion Disproportionation in Aprotic Solvents J. Am. Chem. Soc., 109 (1987) 3768–3775.

[17] D.T. Sawyer, Electrochemistry of Dioxygen, in: R.J.P. Williams (Ed.) Oxygen Chemistry, Oxford University Press, Inc., New York, 1991, pp. 27.

[18] J.-M. Savéant, Elements of Molecular and Biomolecular Electrochemistry, Wiley-Interscience, New York, 2006.

[19] C. Costentin, M. Robert, J.-M. Savéant, Acceleration of the Homogeneous and Electrochemical Reductions of Dioxygen in Aprotic Media by Ammonium Ions. Is the Driving Force a Function of NH_4^+ Concentration? What Is the Mechanism of the Reaction?, J. Phys. Chem. C, 111 (2007) 12877–12880.

[20] F. De Proft, W. Langenaeker, P. Geerlings, Acidity of Alkyl Substituted Alcohols: Are Alkyl Groups Electron-Donating or Electron-Withdrawing?, Tetrahedron, 51 (1995) 4021–4032.

[21] M. Mohammad, A.Y. Khan, M.S. Subhani, N. Bibi, S. Ahmad, S. Saleemi, Kinetics and Electrochemical Studies on Superoxide, Res. Chem. Intermed., 27 (2001) 259–267.

[22] O. Schrems, H.M. Oberhoffer, W.A.P. Luck, Hydrogen Bonding in Low-Temperature Matrices: 1. Proton Donor Abilities of Fluoroalcohols. Comparative Infrared Studies of ROH•••$O(CH_3)_2$ Complex Formation in the Gas Phase, in CCI_4 Solution, and in Solid Argon, J. Phys. Chem., 88 (1984) 4335–4342.

[23] D. Pines, S. Keinan, P.M. Kiefer, J.T. Hynes, E. Pines, Effect of Solvent Dielectric Constant and Acidity on the OH Vibration Frequency in Hydrogen-Bonded Complexes of Fluorinated Ethanol, J. Phys. Chem. B, 119 (2015) 9278–9286.

[24] N.S. Venkataramanan, S. Premsingh, S. Rajagopal, K. Pitchumani, Electronic and Steric Effects on the Oxygenation of Organic Sulfides and Sulfoxides with Oxo(salen)chromium(V) Complexes, J. Org. Chem., 68 (2003) 7460–7470.

[25] Z. Tian, A. Fattahi, L. Lis, S.R. Kass, Single-Centered Hydrogen-Bonded Enhanced Acidity (SHEA) Acids: A New Class of Brønsted Acids, J. Am. Chem. Soc., 131 (2009) 16984–16988.

[26] M.E. Tessensohn, M. Lee, H. Hirao, R.D. Webster, Measuring the Relative Hydrogen-Bonding Strengths of Alcohols in Aprotic Organic Solvents, ChemPhysChem, 16 (2015) 160–168.

[27] C. Dapremont-Avignon, P. Calas, A. Commeyras, C. Amatore, Synthesis of Perfluoroalkyl Carboxylic Acids by Reaction of Perfluoroalkyl Iodides with Electrogenerated Superoxide Ion, J. Fluorine Chem., 51 (1991) 357–379.

Chapter 7

Summary

This page has been intentionally left blank

7.1. Summary

The molecular analysis of compounds that are commonly found or used in food or food-related consumer products (which would inevitably be introduced into human biological systems) can serve as an alternative approach to in vivo studies because such strategies can avoid complications that commonly arise due to the use of complex biological matrices – such as by minimizing/precluding the requirement of complex sample preparation steps or the occurrence of undesirable interferences.

More importantly, since many biological processes involve electron transfer processes, electrochemistry can be highly valuable in uncovering critical information which can aid in the unravelling of essential redox reactions that may transpire inside biological systems. For example, electroanalytical techniques are useful in obtaining information regarding the number of oxidation and/or reduction processes that can take place, the number of electrons involved, as well as the order in which they occur. Additionally, information regarding the associated electrode potentials and chemical stabilities of different substances can easily be obtained, and sometimes the observation of transient intermediates/secondary products that are formed following an electron transfer reaction can also be achieved.

Overall, the present thesis can be broadly classified into two major themes. With the above mentioned in mind, the first part of the thesis was directed toward the electroanalytical study of some biologically active carbonyl compounds (i.e. biotin, cinnamaldehyde, and di-(2-ethylhexyl) phthalate (DEHP)) in aprotic organic media using a combination of electrochemical methods such as cyclic voltammetry (CV), linear sweep voltammetry, rotating disk electrode voltammetry, controlled potential electrolysis (CPE), and digital simulations techniques (Chapters 2–4). In particular, this study was initiated to provide a complementary model of the

aforementioned compounds' electrochemical behavior which has to date (and to the best of our knowledge) been mainly focused toward aqueous solutions and polarographic techniques.

On the other hand, the second focus of this thesis encompassed the study of electrochemically generated superoxide ($O_2^{\bullet-}$) and its reactions against a variety of consumable food and vitamin molecules as well as structurally varied aliphatic alcohols (Chapters 5 and 6). $O_2^{\bullet-}$ (and its inhibition reactions) is an area of significant interest because this anionic free radical is inevitably produced in the human body during normal cellular processes such as respiration and metabolism, and has been routinely found to elicit many adverse health effects. In this work, the formation of $O_2^{\bullet-}$ was carried out using voltammetry because it enabled this biologically active compound to be generated under mild conditions, with little to no by-products, and simultaneously allowed its coupled homogeneous reactions to be monitored in situ.

As part of the initial theme of the present work, Chapter 2 disclosed the electrochemical study of biotin, which revealed a single cathodic reaction that could be detected at fairly large negative potentials. Although the reduction of biotin was found to be chemically reversible only over the time-frames of CV ($t \leq s$) but not CPE ($t \geq min$), preparative scale functionalization of the substrate with iodomethane (following bulk reductive CPE) was able to furnish a biotin methyl ester product in high yield of 91%. Characterizations of the compounds present before electrolysis, after electrolysis, and after the methylation reaction were also performed using attenuated total reflectance–Fourier transform infrared (ATR–FTIR) spectroscopy.

In Chapter 3, in-depth investigations of the redox chemistry of cinnamaldehyde was conducted and observed to exhibit a similar reduction behavior to retinal (an aldehyde form of vitamin A), with both molecules displaying two sequential one-electron cathodic peaks on the forward scan, as well as secondary oxidation processes detectable on the return sweep of CV.

As a result of its radical anionic form possessing a tendency to undergo a heterodimerization reaction with the starting material, voltammetry and CPE experiments also revealed that the electrochemical reduction of cinnamaldehyde critically depends on the amount of starting material used. Additionally, digital simulations enabled the estimation of all the electrochemical and kinetic parameters affiliated with the heterogeneous electron transfer and homogeneous reaction steps.

In Chapter 4, the electrochemical behavior of DEHP, a well-documented toxicant, was examined. Generally, DEHP was found to be reducible by two one-electron processes, which occurred at moderately large negative potentials, corresponding to the formation of its radical anion and dianion. Following the generation of its reduced forms, DEHP was also found to be susceptible to several other coupled homogeneous reactions such as dimerization and decomposition. The gathered voltammetric data were likewise modeled using digital simulations.

In the second part of this thesis, Chapter 5 outlined the interaction of 18 naturally occurring and consumable compounds (food and vitamin molecules) toward electrochemically generated $O_2^{\bullet-}$ (formed by the one-electron reduction of molecular oxygen, O_2) and was monitored using CV. The relative reactivity of each substrate was assessed based on their ability to quench $O_2^{\bullet-}$ and quantified using effective concentration indexes, EC_{10} and EC_{50}, which corresponds to the amount of compound required to reduce the concentration of $O_2^{\bullet-}$ by 10 % and 50 %, respectively. Where possible, the likely $O_2^{\bullet-}$ scavenging mechanistic pathways are also discussed.

In a similar manner, Chapter 6 examined the $O_2^{\bullet-}$ quenching ability of 14 structurally-varied alcohols (comprising of different steric and electronic features) by evaluating the decreases in the anodic peak currents (I_{pa}) of O_2 reduction (into $O_2^{\bullet-}$). Based on the collected

results, best fit plots of the percentage decrease in the anodic peak current ($\%\Delta I_{pa}$) against the concentration of substrates added were obtained and compared according to the different classes of alcohols that were examined (linear, fluorinated, branched, and multi-hydroxylated). Overall, it was found that presence of electron-withdrawing substituents and/or the lack of steric bulk generally resulted in enhanced reactivities for the alcohols examined.

Lastly, it is worth mentioning that even though the compounds under study in this thesis have been examined using a combination of several techniques such as cyclic voltammetry, controlled potential electrolysis, and digital simulations, which were performed under a variety of conditions including different scan rates, temperatures, or concentrations, other complementary electrochemical methods (e.g. differential pulse voltammetry, square wave voltammetry, impedance spectroscopy) or chemical approaches (e.g. chemical oxidants/reductants) may also be helpful for further in-depth mechanistic analyses. In addition, the employment of in-situ spectroscopic methods such as electron paramagnetic resonance or UV-vis spectroscopy, which are often coupled with electrochemical techniques, can be useful in future studies for the detection and possibly characterization of the proposed intermediate species and final products.

Appendix (Chapter 2)

The Electrochemical Reduction of Biotin (Vitamin B_7) and Conversion to its Ester

This page has been intentionally left blank

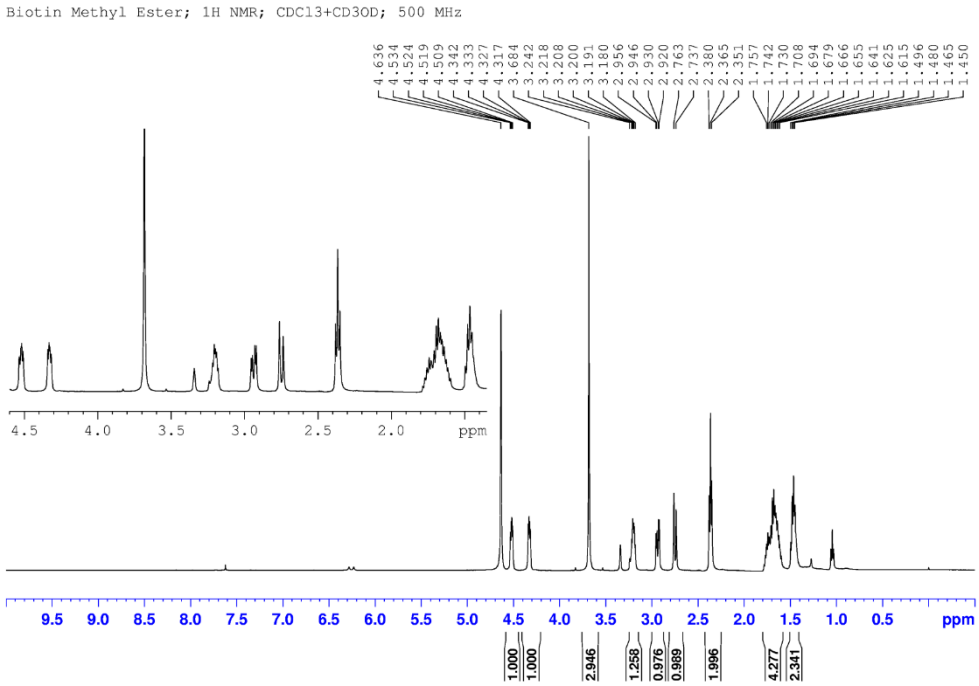

Figure A2.1. ^{1}H NMR Spectra of biotin methyl ester.

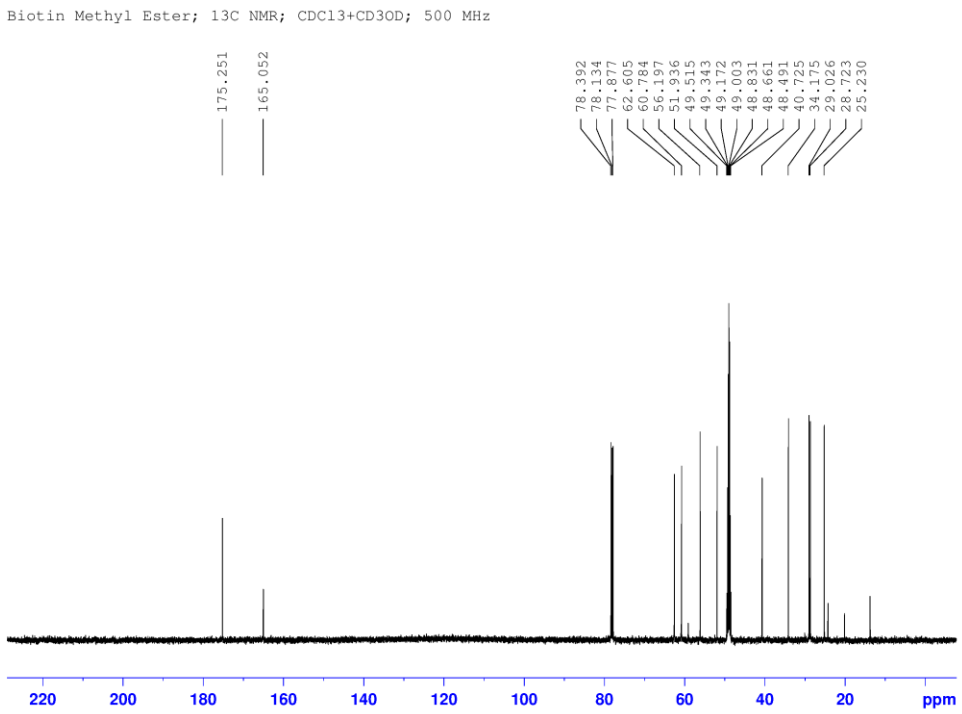

Figure A2.2. ^{13}C NMR Spectra of biotin methyl ester.

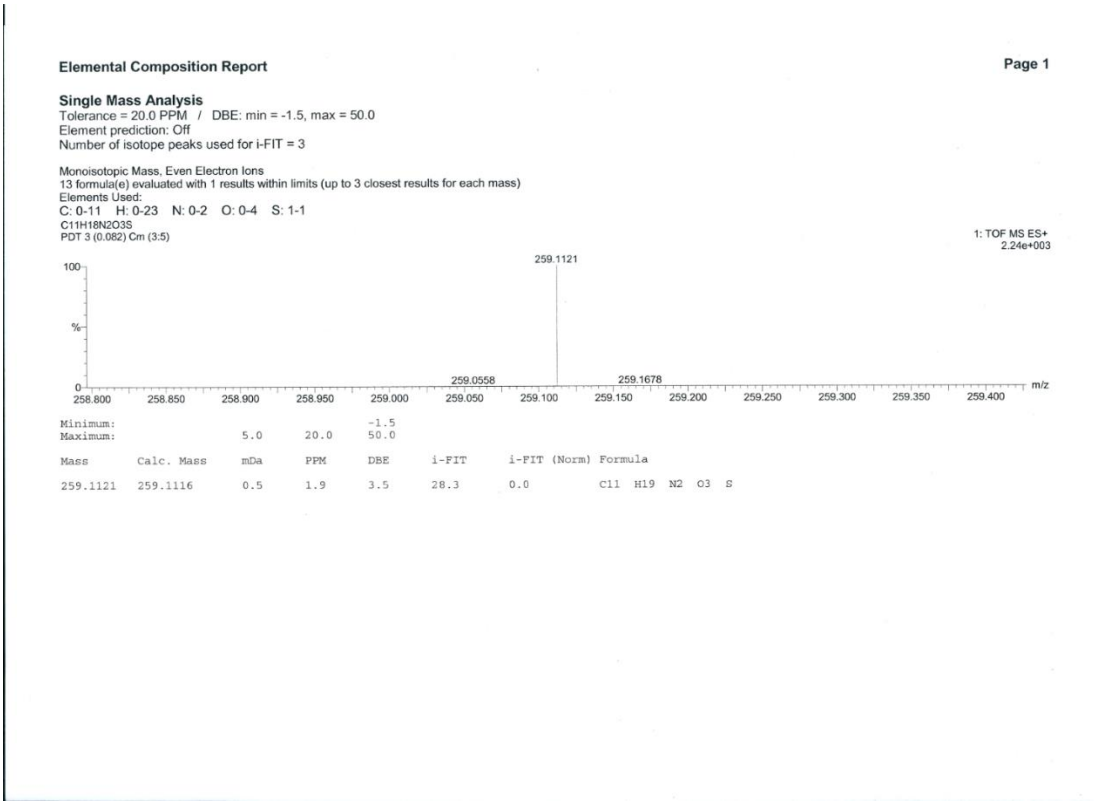

Figure A2.3. HRMS Spectra of biotin methyl ester.

Crystal structure report for biotin methyl ester

A colorless plate-like specimen of $C_{11}H_{18}N_2O_3S$, approximate dimensions 0.020 mm x 0.160 mm x 0.400 mm, was used for the X-ray crystallographic analysis. The X-ray intensity data were measured.

The total exposure time was 1.76 hours. The frames were integrated with the Bruker SAINT software package using a narrow-frame algorithm. The integration of the data using an orthorhombic unit cell yielded a total of 9796 reflections to a maximum θ angle of 28.38° (0.75 Å resolution), of which 2653 were independent (average redundancy 3.692, completeness = 89.2%, R_{int} = 5.96%, R_{sig} = 8.84%) and 2100 (79.16%) were greater than $2\sigma(F^2)$. The final cell constants of a = 4.663(6) Å, b = 7.687(10) Å, c = 35.30(5) Å, volume = 1265.(3) $Å^3$, are based upon the refinement of the XYZ-centroids of 2518 reflections above 20 σ(I) with 5.424° < 2θ < 41.36°. Data were corrected for absorption effects using the multi-scan method (SADABS). The ratio of minimum to maximum apparent transmission was 0.832. The calculated minimum and maximum transmission coefficients (based on crystal size) are 0.9049 and 0.9949.

The structure was solved and refined using the Bruker SHELXTL Software Package, using the space group P 21 21 21, with Z = 4 for the formula unit,$C_{11}H_{18}N_2O_3S$. The final anisotropic full-matrix least-squares refinement on F^2 with 163 variables converged at R1 = 5.06%, for the observed data and wR2 =9.93% for all data. The goodness-of-fit was 1.023. The largest peak in the final difference electron density synthesis was 0.319 $e^-/Å^3$ and the largest hole was -0.343 $e^-/Å^3$ with an RMS deviation of 0.084 $e^-/Å^3$. On the basis of the final model, the calculated density was 1.356 g/cm^3 and F(000), 552 e^-.

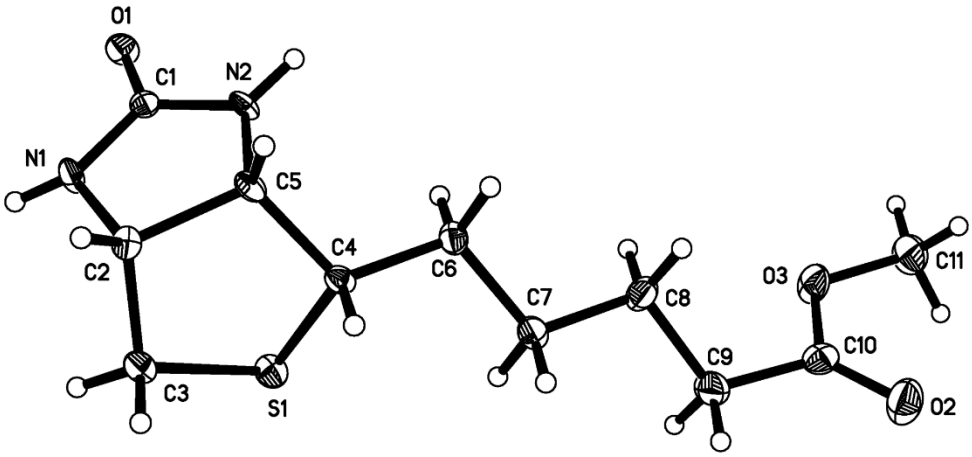

Figure A2.4. ORTEP drawing of biotin methyl ester with thermal ellipsoids at 50% probability levels.

Table A2.1. Sample and crystal data for biotin methyl ester.

Identification code	biotin methyl ester	
Chemical formula	$C_{11}H_{18}N_2O_3S$	
Formula weight	258.33	
Temperature	103(2) K	
Wavelength	0.71073 Å	
Crystal size	0.020 x 0.160 x 0.400 mm	
Crystal habit	colorless plate	
Crystal system	orthorhombic	
Space group	P 21 21 21	
Unit cell dimensions	a = 4.663(6) Å	α = 90°
	b = 7.687(10) Å	β = 90°
	c = 35.30(5) Å	γ = 90°
Volume	1265.(3) $Å^3$	
Z	4	
Density (calculated)	1.356 g/cm^3	
Absorption coefficient	0.255 mm^{-1}	
F(000)	552	

Table A2.2. Data collection and structure refinement for biotin methyl ester.

Theta range for data collection	3.17 to 28.38°	
Index ranges	-4<=h<=6, -9<=k<=10, -44<=l<=46	
Reflections collected	9796	
Independent reflections	2653 [R(int) = 0.0596]	
Coverage of independent reflections	89.2%	
Absorption correction	multi-scan	
Max. and min. transmission	0.9949 and 0.9049	
Structure solution technique	direct methods	
Structure solution program	SHELXS-97 (Sheldrick, 2008)	
Refinement method	Full-matrix least-squares on F^2	
Refinement program	SHELXL-97 (Sheldrick, 2008)	
Function minimized	$\Sigma\, w(F_o^2 - F_c^2)^2$	
Data / restraints / parameters	2653 / 0 / 163	
Goodness-of-fit on F^2	1.023	
Δ/σ_{max}	0.001	
Final R indices	2100 data; I>2σ(I)	R1 = 0.0506, wR2 = 0.0919
	all data	R1 = 0.0711, wR2 = 0.0993
Weighting scheme	$w=1/[\sigma^2(F_o^2)+(0.0436P)^2+0.0000P]$ where $P=(F_o^2+2F_c^2)/3$	
Absolute structure parameter	0.1(1)	
Largest diff. peak and hole	0.319 and -0.343 $eÅ^{-3}$	
R.M.S. deviation from mean	0.084 $eÅ^{-3}$	

Table A2.3. Atomic coordinates and equivalent isotropic atomic displacement parameters ($Å^2$) for biotin methyl ester.

U(eq) is defined as one third of the trace of the orthogonalized U_{ij} tensor.

	x/a	**y/b**	**z/c**	**U(eq)**
S1	0.63290(16)	0.82592(9)	0.862298(19)	0.0161(2)
C3	0.8766(7)	0.9738(3)	0.83844(7)	0.0152(6)
C1	0.6488(7)	0.7613(3)	0.76084(7)	0.0136(6)
C2	0.9817(6)	0.8793(3)	0.80292(7)	0.0130(7)
C4	0.8732(7)	0.6452(3)	0.85066(7)	0.0126(6)
C9	0.4630(7)	0.2525(3)	0.95225(7)	0.0241(8)
C5	0.9623(6)	0.6779(3)	0.80944(7)	0.0120(6)
C7	0.6584(7)	0.4449(3)	0.90081(7)	0.0173(7)
C11	0.0753(7)	0.8311(4)	0.95443(8)	0.0274(8)
C10	0.3741(7)	0.0739(4)	0.96547(8)	0.0186(7)
C8	0.5445(7)	0.2646(4)	0.91037(7)	0.0191(7)
C6	0.7442(6)	0.4666(3)	0.85901(7)	0.0155(7)
O1	0.4563(4)	0.7535(2)	0.73591(5)	0.0165(5)
O3	0.1723(5)	0.0034(2)	0.94308(5)	0.0247(5)
O2	0.4638(5)	0.0029(3)	0.99347(6)	0.0298(6)
N1	0.7931(5)	0.9087(3)	0.77064(6)	0.0146(6)
N2	0.7440(5)	0.6262(3)	0.78199(6)	0.0126(6)

Table A2.4. Bond lengths (Å) for biotin methyl ester.

S1-C3	1.815(3)	S1-C4	1.831(3)
C3-C2	1.530(4)	C3-H3A	0.99
C3-H3B	0.99	C1-O1	1.258(3)
C1-N2	1.354(3)	C1-N1	1.362(4)
C2-N1	1.457(4)	C2-C5	1.568(4)
C2-H2	1.0	C4-C6	1.527(4)
C4-C5	1.534(4)	C4-H4	1.0
C9-C10	1.508(4)	C9-C8	1.529(4)
C9-H9A	0.99	C9-H9B	0.99
C5-N2	1.460(4)	C5-H5	1.0
C7-C8	1.522(4)	C7-C6	1.538(4)
C7-H7A	0.99	C7-H7B	0.99
C11-O3	1.455(4)	C11-H11A	0.98
C11-H11B	0.98	C11-H11C	0.98
C10-O2	1.204(3)	C10-O3	1.343(4)
C8-H8A	0.99	C8-H8B	0.99
C6-H6A	0.99	C6-H6B	0.99
N1-H1N	0.89(3)	N2-H2N	0.85(3)

Table A2.5. Bond angles (°) for biotin methyl ester.

C3-S1-C4	89.32(15)	C2-C3-S1	106.46(19)
C2-C3-H3A	110.4	S1-C3-H3A	110.4
C2-C3-H3B	110.4	S1-C3-H3B	110.4
H3A-C3-H3B	108.6	O1-C1-N2	125.7(3)
O1-C1-N1	124.7(3)	N2-C1-N1	109.6(3)
N1-C2-C3	112.0(2)	N1-C2-C5	103.5(2)
C3-C2-C5	109.3(2)	N1-C2-H2	110.6
C3-C2-H2	110.6	C5-C2-H2	110.6
C6-C4-C5	115.9(2)	C6-C4-S1	113.4(2)
C5-C4-S1	104.72(17)	C6-C4-H4	107.5
C5-C4-H4	107.5	S1-C4-H4	107.5
C10-C9-C8	115.0(2)	C10-C9-H9A	108.5
C8-C9-H9A	108.5	C10-C9-H9B	108.5
C8-C9-H9B	108.5	H9A-C9-H9B	107.5
N2-C5-C4	113.3(2)	N2-C5-C2	102.2(2)
C4-C5-C2	108.5(2)	N2-C5-H5	110.8
C4-C5-H5	110.8	C2-C5-H5	110.8
C8-C7-C6	113.7(2)	C8-C7-H7A	108.8
C6-C7-H7A	108.8	C8-C7-H7B	108.8
C6-C7-H7B	108.8	H7A-C7-H7B	107.7
O3-C11-H11A	109.5	O3-C11-H11B	109.5
H11A-C11-H11B	109.5	O3-C11-H11C	109.5
H11A-C11-H11C	109.5	H11B-C11-H11C	109.5
O2-C10-O3	122.9(3)	O2-C10-C9	124.8(3)
O3-C10-C9	112.2(3)	C7-C8-C9	110.9(2)
C7-C8-H8A	109.5	C9-C8-H8A	109.5

C7-C8-H8B	109.5	C9-C8-H8B	109.5
H8A-C8-H8B	108.1	C4-C6-C7	112.7(2)
C4-C6-H6A	109.1	C7-C6-H6A	109.1
C4-C6-H6B	109.1	C7-C6-H6B	109.1
H6A-C6-H6B	107.8	C10-O3-C11	115.0(2)
C1-N1-C2	111.6(2)	C1-N1-H1N	120.1(18)
C2-N1-H1N	121.8(18)	C1-N2-C5	112.7(2)
C1-N2-H2N	120.8(18)	C5-N2-H2N	126.1(18)

Table A2.6. Anisotropic atomic displacement parameters ($Å^2$) for biotin methyl ester.

The anisotropic atomic displacement factor exponent takes the form: $-2\pi^2[h^2 a^{*2} U_{11} + ... + 2 h k a^* b^* U_{12}]$

	U_{11}	U_{22}	U_{33}	U_{23}	U_{13}	U_{12}
S1	0.0141(4)	0.0152(4)	0.0190(4)	-0.0007(3)	0.0018(4)	0.0008(3)
C3	0.0155(16)	0.0123(15)	0.0177(14)	-0.0012(12)	-0.0019(14)	0.0004(14)
C1	0.0144(15)	0.0129(16)	0.0135(13)	-0.0014(12)	0.0063(14)	0.0005(14)
C2	0.0105(16)	0.0136(16)	0.0148(15)	0.0016(12)	0.0004(12)	0.0013(13)
C4	0.0130(15)	0.0108(15)	0.0141(13)	-0.0016(11)	-0.0023(13)	0.0018(13)
C9	0.035(2)	0.0175(18)	0.0202(16)	-0.0009(14)	0.0072(14)	-0.0054(16)
C5	0.0093(15)	0.0093(15)	0.0175(14)	-0.0019(12)	-0.0011(12)	0.0019(13)
C7	0.0208(17)	0.0133(16)	0.0179(15)	0.0003(12)	0.0022(15)	-0.0001(14)
C11	0.033(2)	0.0208(18)	0.0288(17)	0.0027(15)	-0.0009(15)	-0.0091(16)
C10	0.0173(17)	0.0225(18)	0.0159(15)	-0.0021(12)	0.0049(16)	0.0023(16)
C8	0.0226(18)	0.0209(17)	0.0137(14)	0.0030(13)	0.0001(13)	-0.0031(14)
C6	0.0180(17)	0.0123(15)	0.0162(15)	0.0016(12)	-0.0016(13)	0.0005(12)
O1	0.0173(12)	0.0158(11)	0.0165(10)	-0.0012(9)	-0.0063(9)	0.0003(9)
O3	0.0307(13)	0.0220(12)	0.0214(11)	0.0062(9)	-0.0034(11)	-0.0127(11)
O2	0.0322(14)	0.0293(14)	0.0280(12)	0.0076(11)	-0.0080(11)	-0.0015(11)
N1	0.0172(16)	0.0083(14)	0.0183(13)	0.0023(10)	-0.0056(11)	-0.0018(12)
N2	0.0137(15)	0.0072(15)	0.0171(12)	-0.0032(11)	-0.0032(10)	-0.0014(10)

Table A2.7. Hydrogen atomic coordinates and isotropic atomic displacement parameters ($Å^2$) for biotin methyl ester.

	x/a	**y/b**	**z/c**	**U(eq)**
H3A	0.7763	1.0827	0.8315	0.018
H3B	1.0402	1.0032	0.8551	0.018
H2	1.1828	0.9144	0.7967	0.016
H4	1.0486	0.6578	0.8667	0.015
H9A	0.6288	0.2911	0.9676	0.029
H9B	0.3033	0.3343	0.9572	0.029
H5	1.1498	0.6205	0.8037	0.014
H7A	0.8277	0.4691	0.9169	0.021
H7B	0.5095	0.5321	0.9071	0.021
H11A	0.2377	-0.2498	0.9541	0.041
H11B	-0.0726	-0.2094	0.9368	0.041
H11C	-0.0044	-0.1634	0.9801	0.041
H8A	0.6928	0.1765	0.9045	0.023
H8B	0.3740	0.2395	0.8946	0.023
H6A	0.8855	0.3756	0.8523	0.019
H6B	0.5727	0.4495	0.8429	0.019
H1N	0.717(6)	1.012(4)	0.7659(7)	0.016(8)
H2N	0.692(6)	0.522(4)	0.7770(7)	0.011(8)

This page has been intentionally left blank

Appendix (Chapter 3)

The Electrochemical Reduction of Cinnamaldehyde in Acetonitrile

This page has been intentionally left blank

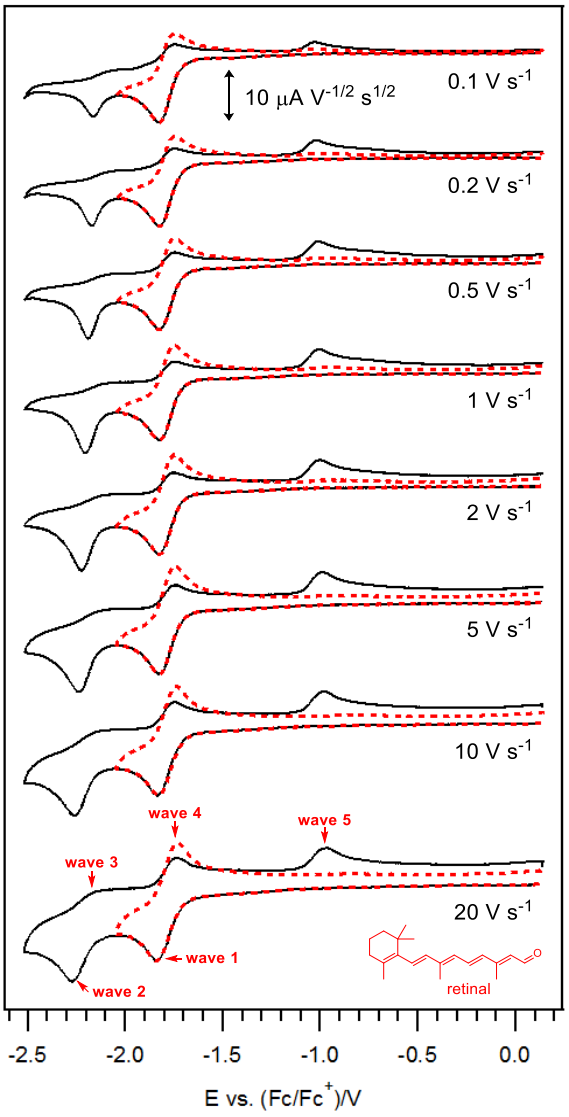

Figure A3.1. Cyclic voltammograms of 2 mM retinal in CH_3CN containing 0.2 M Bu_4NPF_6, recorded at 295 (±2) K using a 1-mm diameter planar GC disk electrode at different scan rates. (—) Switching potential ≈ -2.51 vs. $(Fc/Fc^+)/V$. (- - -) Switching potential ≈ -2.04 vs. $(Fc/Fc^+)/V$. The current data have been normalized by multiplying against $(\text{scan rate})^{-1/2}$.

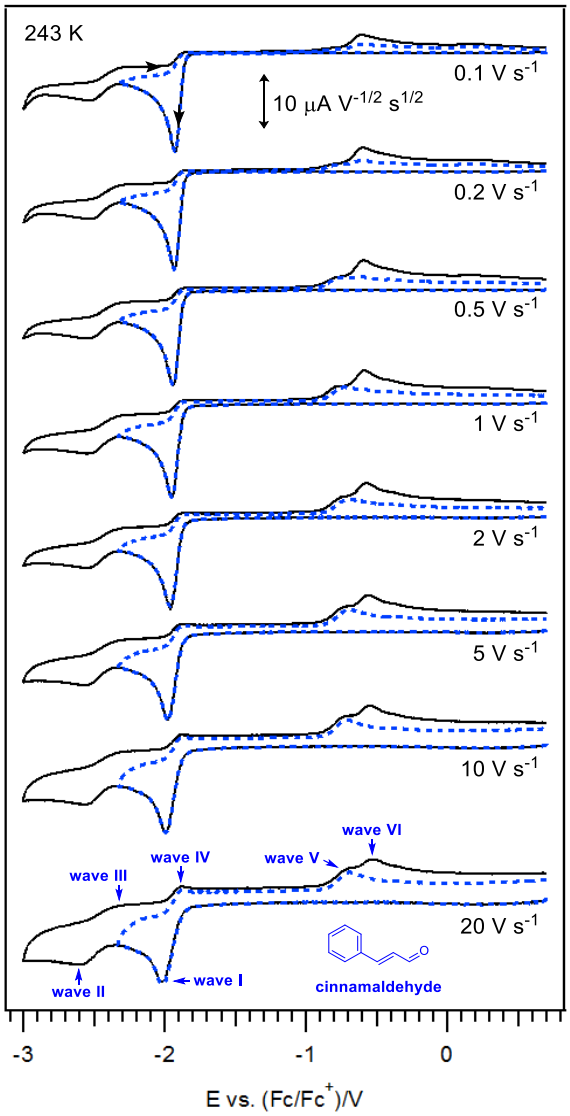

Figure A3.2. Cyclic voltammograms of 2 mM cinnamaldehyde in CH_3CN containing 0.2 M Bu_4NPF_6 recorded at 243 K using a 1-mm diameter planar GC disk electrode at different scan rates. (—) Switching potential ≈ -3.00 vs. (Fc/Fc^+)/V. (- - -) Switching potential ≈ -2.33 vs. (Fc/Fc^+)/V. The current data have been normalized by multiplying against $(\text{scan rate})^{-1/2}$.

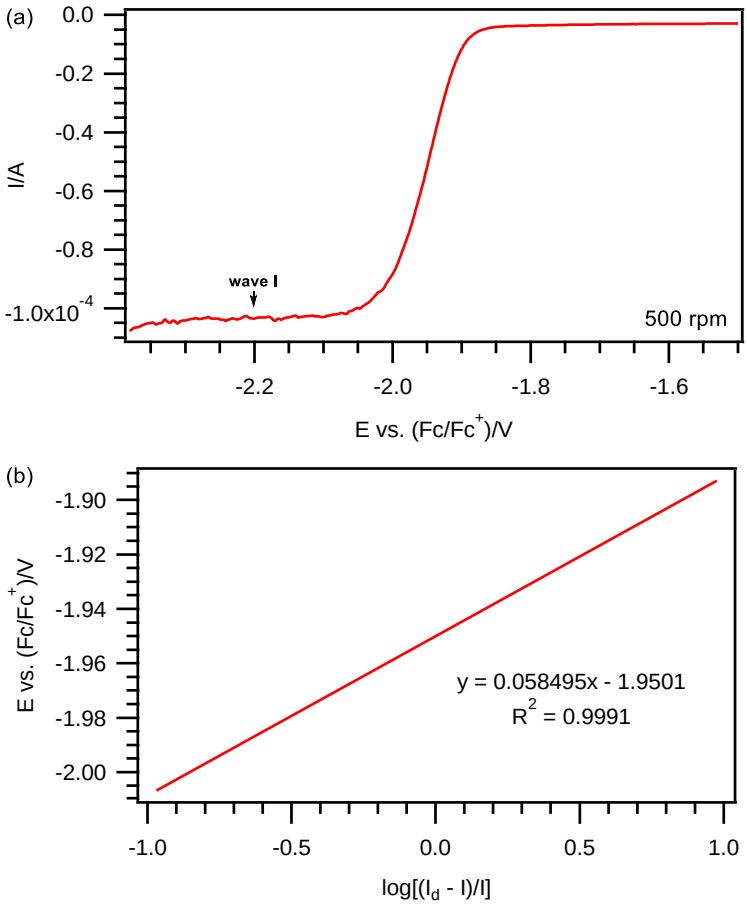

Figure A3.3. Wave slope analysis of steady state voltammogram. (a) Linear sweep voltammogram of 2 mM cinnamaldehyde in CH_3CN containing 0.2 M Bu_4NPF_6, recorded at 295 (±2) K using a 3-mm diameter planar GC rotating disk electrode, at 0.02 V s^{-1}, and at 500 rpm. (b) Plot of E vs. $\log[(I_d - I)/I]$ using the experimental data from (a).

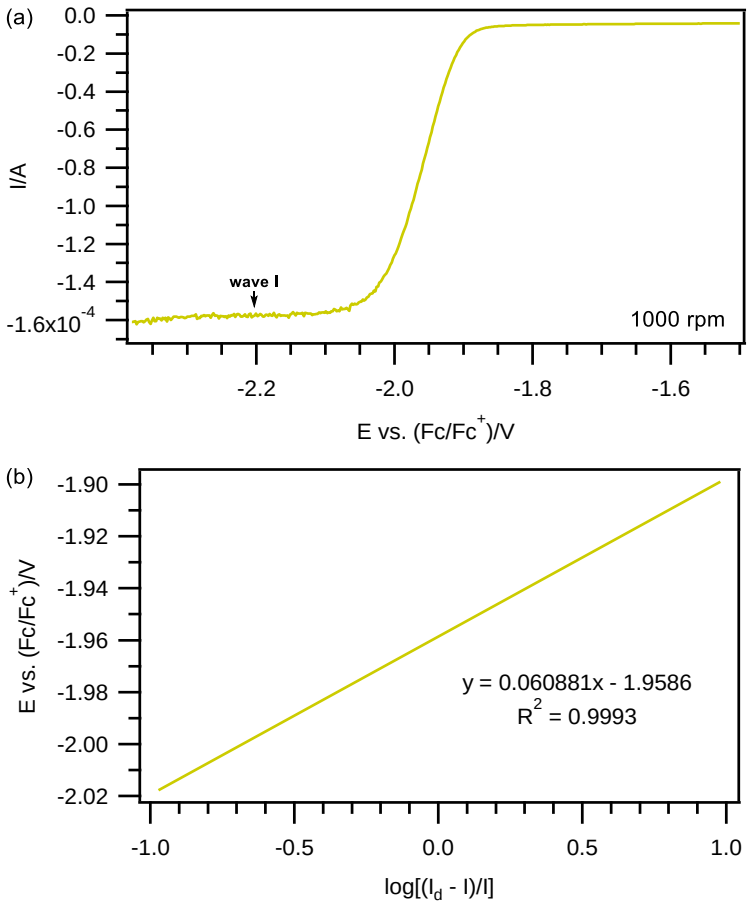

Figure A3.4. Wave slope analysis of steady state voltammogram. (a) Linear sweep voltammogram of 2 mM cinnamaldehyde in CH_3CN containing 0.2 M Bu_4NPF_6, recorded at 295 (±2) K using a 3-mm diameter planar GC rotating disk electrode, at 0.02 V s^{-1}, and at 1000 rpm. (b) Plot of E vs. $\log[(I_d - I)/I]$ using the experimental data from (a).

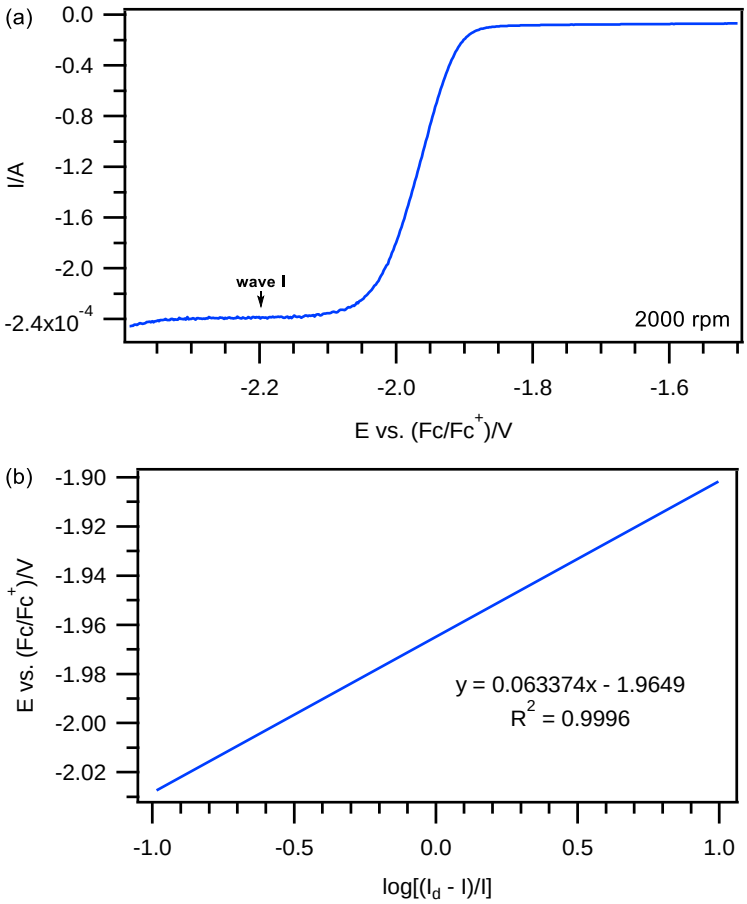

Figure A3.5. Wave slope analysis of steady state voltammogram. (a) Linear sweep voltammogram of 2 mM cinnamaldehyde in CH_3CN containing 0.2 M Bu_4NPF_6, recorded at 295 (±2) K using a 3-mm diameter planar GC rotating disk electrode, at 0.02 V s^{-1}, and at 2000 rpm. (b) Plot of E vs. log[(I_d – I)/I] using the experimental data from (a).

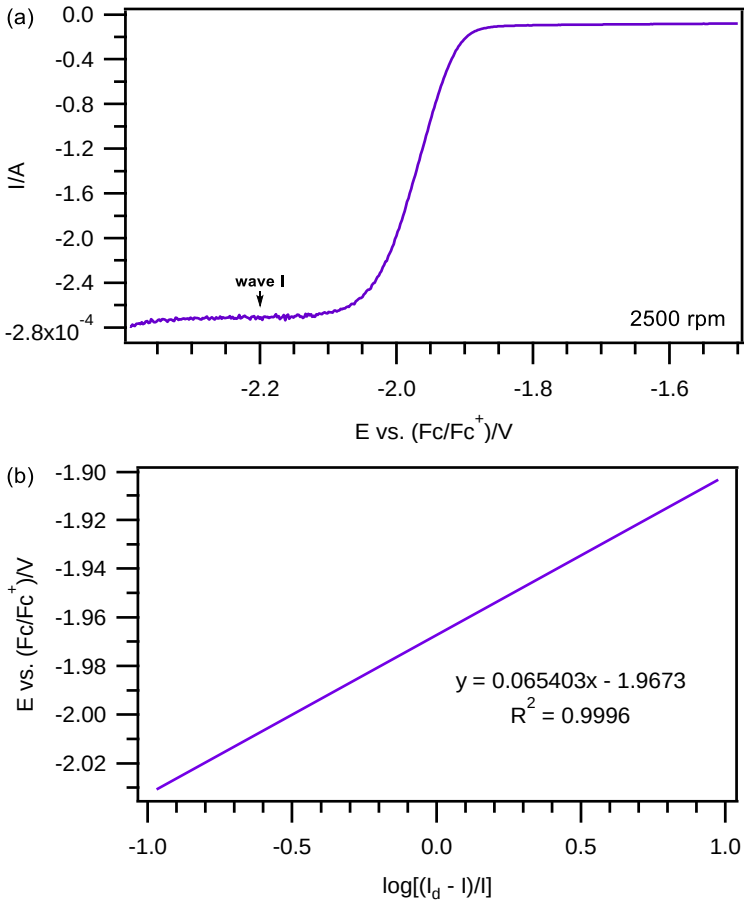

Figure A3.6. Wave slope analysis of steady state voltammogram. (a) Linear sweep voltammogram of 2 mM cinnamaldehyde in CH_3CN containing 0.2 M Bu_4NPF_6, recorded at 295 (±2) K using a 3-mm diameter planar GC rotating disk electrode, at 0.02 V s^{-1}, and at 2500 rpm. (b) Plot of E vs. $\log[(I_d - I)/I]$ using the experimental data from (a).

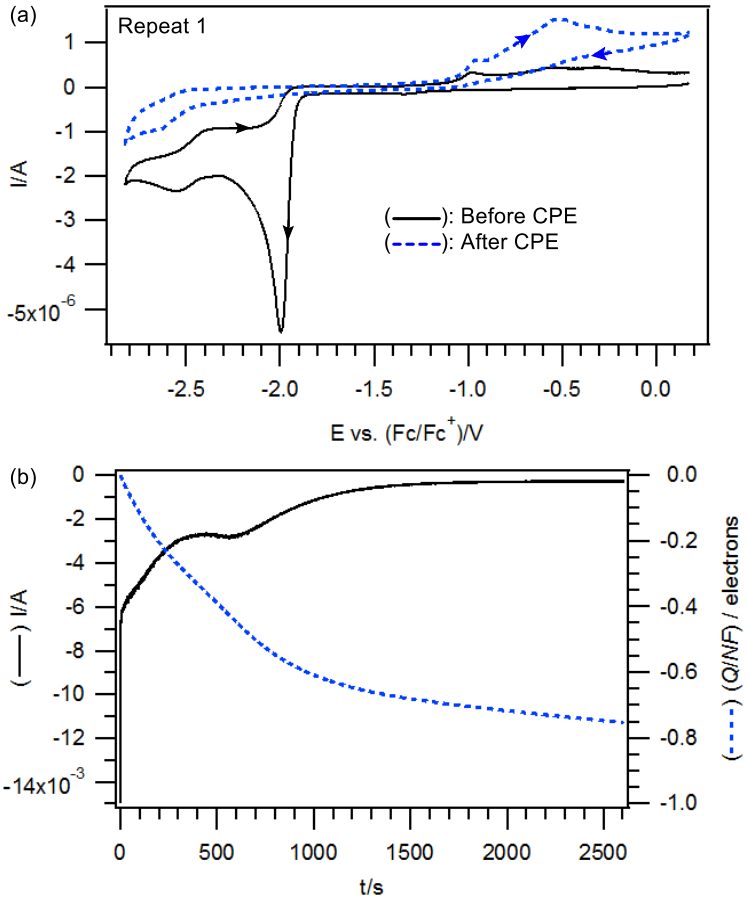

Figure A3.7. Voltammetric and coulometric data obtained during the first repeat of the reductive CPE (wave I) of 2 mM cinnamaldehyde in CH_3CN containing 0.2 M Bu_4NPF_6 at 295 (±2) K. (a) Cyclic voltammograms recorded at 0.1 V s^{-1} with a 1-mm diameter planar GC disk electrode. (b) Current/coulometry vs. time data obtained during the reductive CPE (at -2.14 vs. (Fc/Fc^+)/V). The number of electrons transferred were calculated using eq. 3.5.

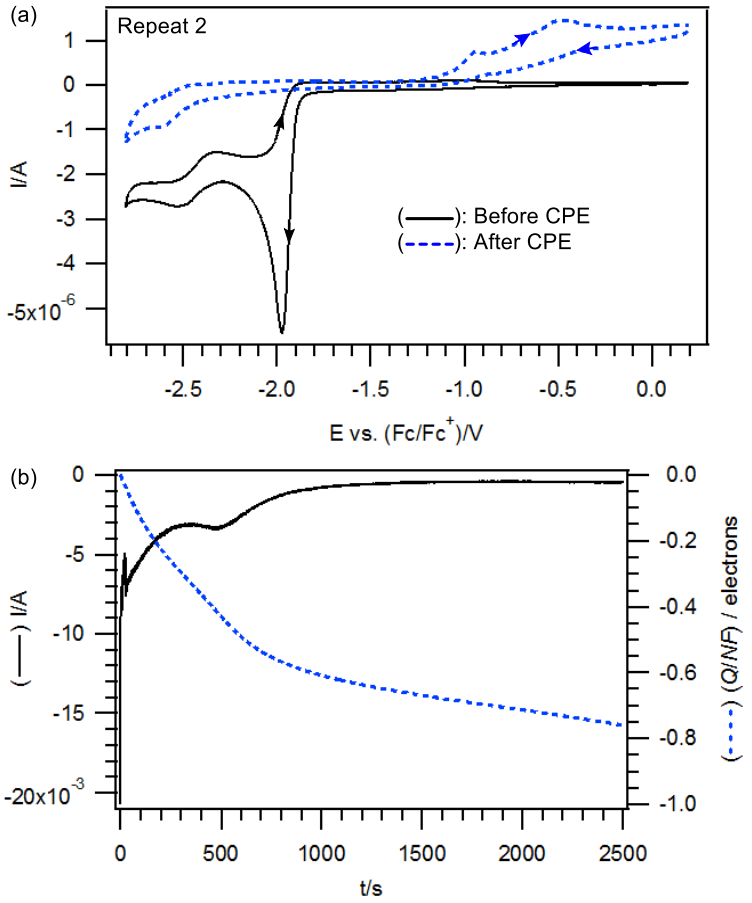

Figure A3.8. Voltammetric and coulometric data obtained during the second repeat of the reductive CPE (wave I) of 2 mM cinnamaldehyde in CH_3CN containing 0.2 M Bu_4NPF_6 at 295 (±2) K. (a) Cyclic voltammograms recorded at 0.1 V s^{-1} with a 1-mm diameter planar GC disk electrode. (b) Current/coulometry vs. time data obtained during the reductive CPE (at -2.12 vs. (Fc/Fc^+)/V). The number of electrons transferred were calculated using eq. 3.5.

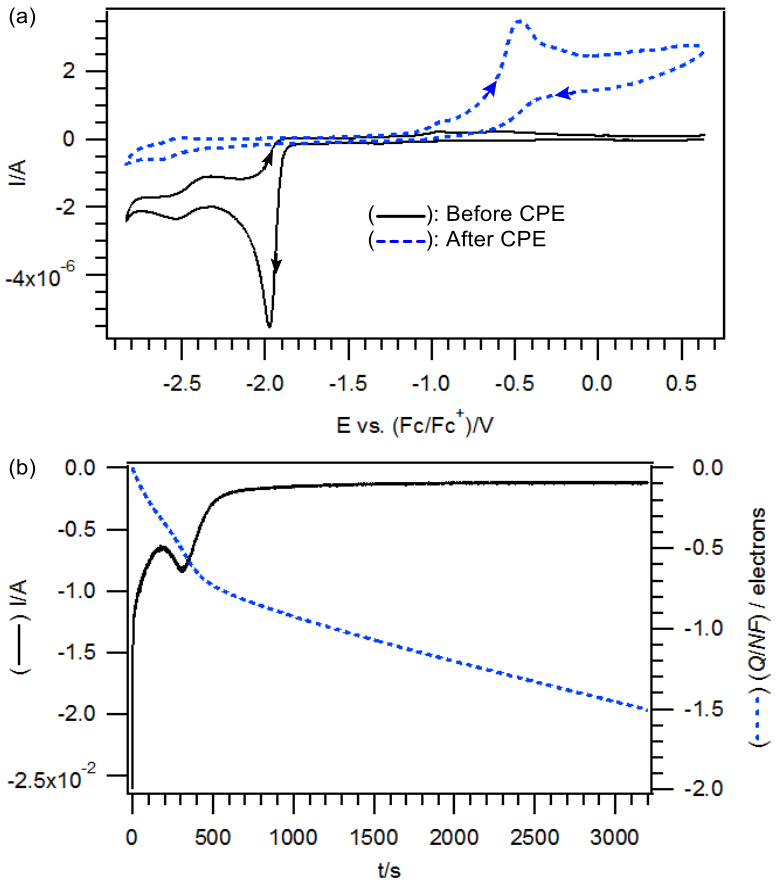

Figure A3.9. Voltammetric and coulometric data obtained during the reductive CPE (wave II) of 2 mM cinnamaldehyde in CH_3CN containing 0.2 M Bu_4NPF_6 at 295 (±2) K. (a) Cyclic voltammograms recorded at 0.1 V s^{-1} with a 1-mm diameter planar GC disk electrode. (b) Current/coulometry vs. time data obtained during the reductive CPE (at -2.71 vs. (Fc/Fc^+)/V). The number of electrons transferred were calculated using eq. 3.5.

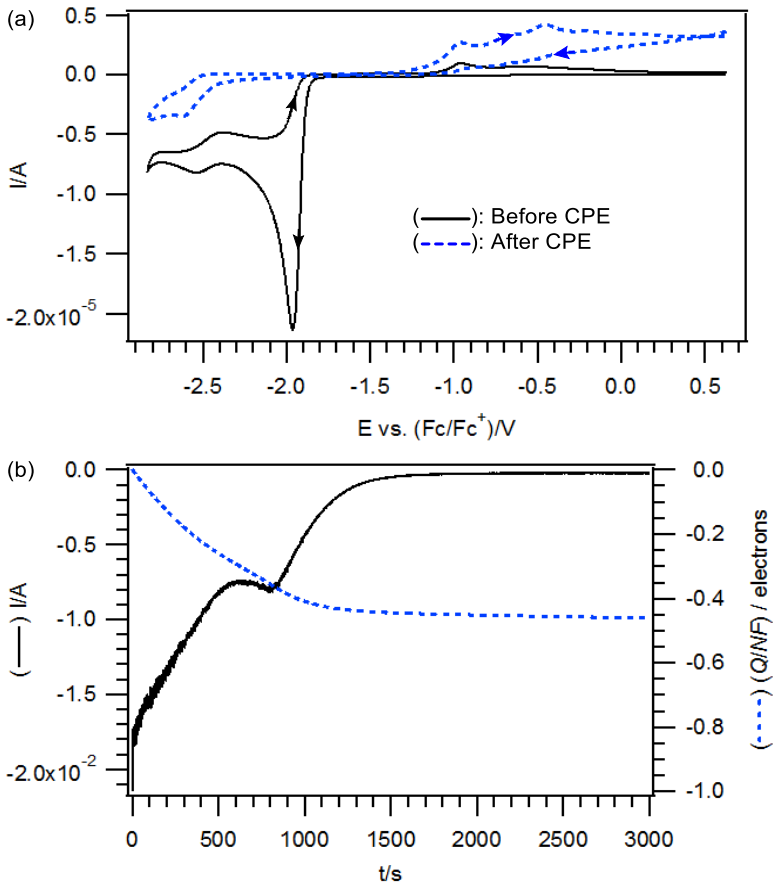

Figure A3.10. Voltammetric and coulometric data obtained during the reductive CPE (wave I) of 10 mM cinnamaldehyde in CH_3CN containing 0.2 M Bu_4NPF_6 at 295 (±2) K. (a) Cyclic voltammograms recorded at 0.1 V s^{-1} with a 1-mm diameter planar GC disk electrode. (b) Current/coulometry vs. time data obtained during the reductive CPE (at -2.12 vs. (Fc/Fc^+)/V). The number of electrons transferred were calculated using eq. 3.5.

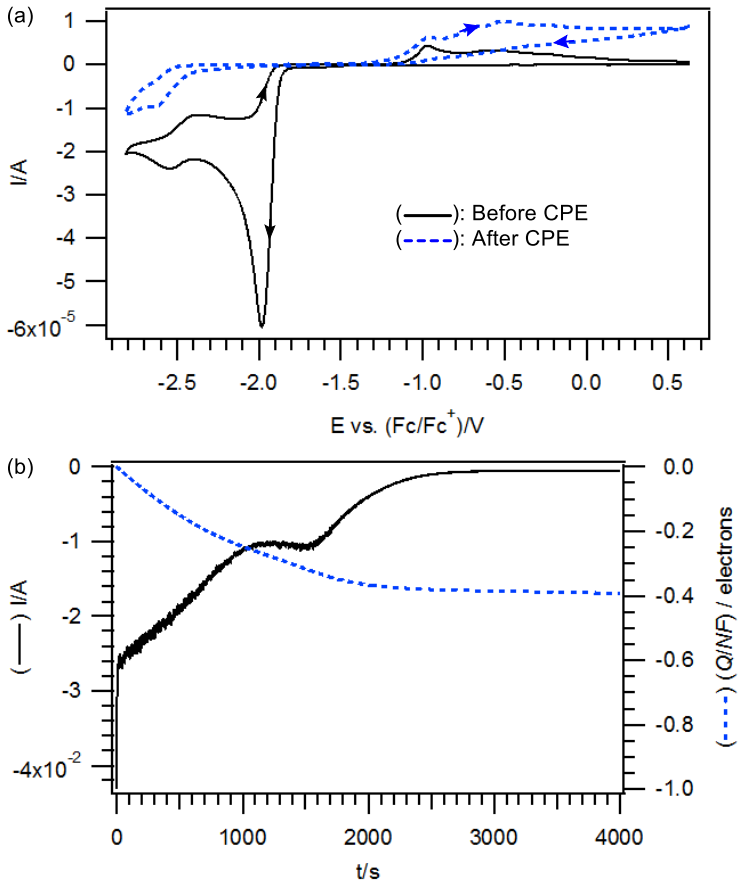

Figure A3.11. Voltammetric and coulometric data obtained during the reductive CPE (wave I) of 30 mM cinnamaldehyde in CH_3CN containing 0.2 M Bu_4NPF_6 at 295 (±2) K. (a) Cyclic voltammograms recorded at 0.1 V s^{-1} with a 1-mm diameter planar GC disk electrode. (b) Current/coulometry vs. time data obtained during the reductive CPE (at -2.14 vs. (Fc/Fc^+)/V). The number of electrons transferred were calculated using eq. 3.5.

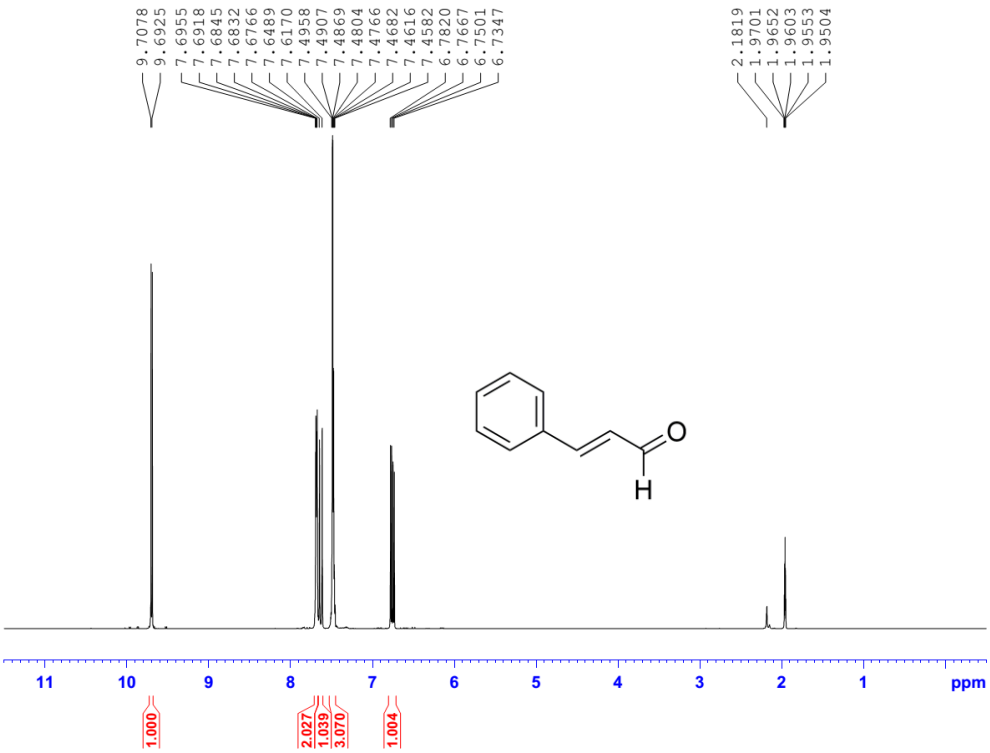

Figure A3.12. ^{1}H NMR (500 MHz) spectrum of cinnamaldehyde in CD_3CN.

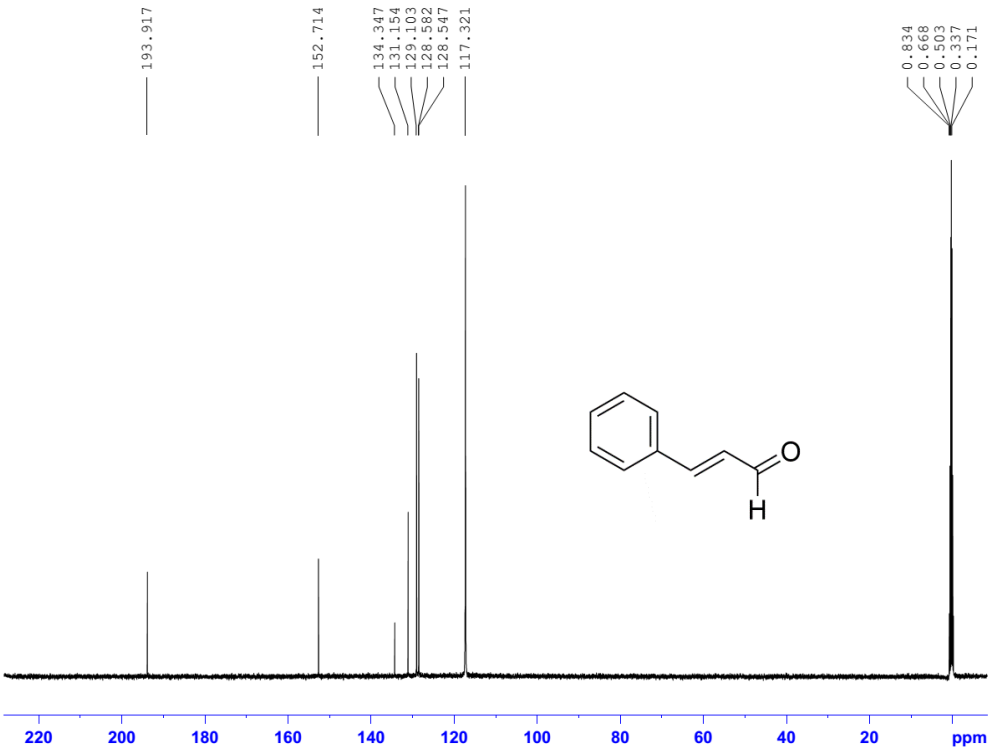

Figure A3.13. ^{13}C NMR (125 MHz) spectrum of cinnamaldehyde in CD_3CN.

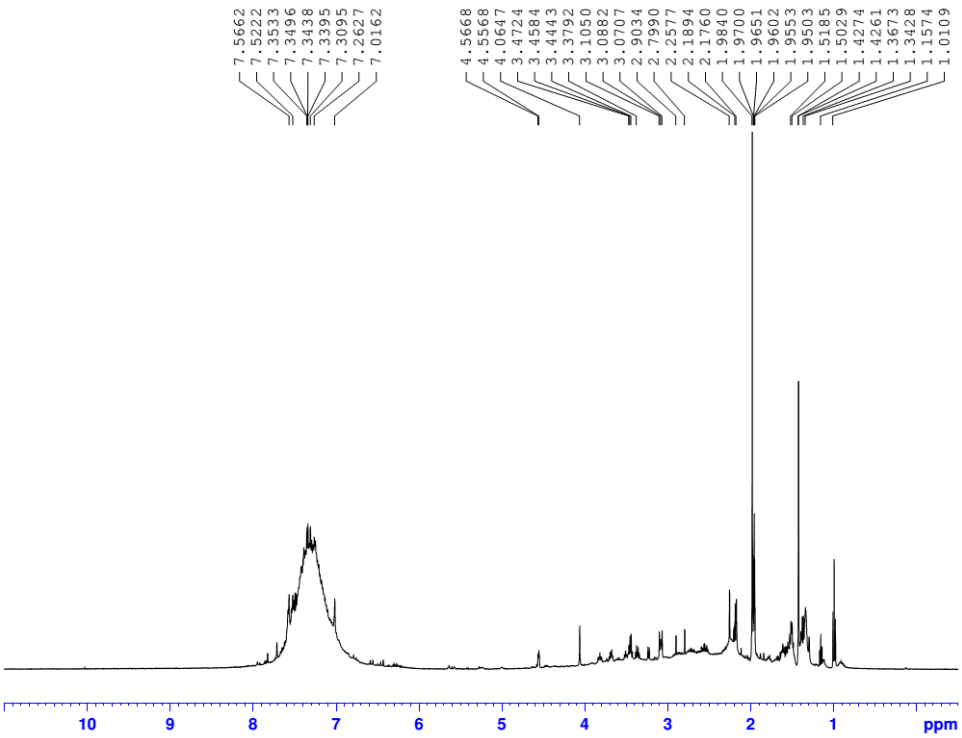

Figure A3.14. ^{1}H NMR (500 MHz) spectrum of the crude mixture obtained after a one-electron reductive electrolysis of cinnamaldehyde in CD_3CN.

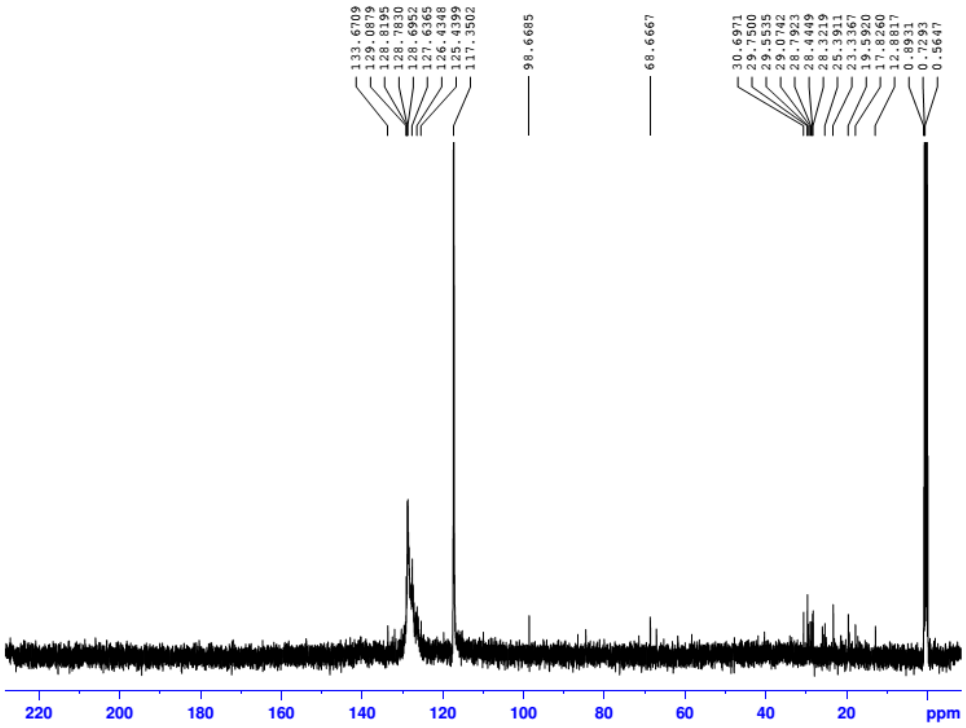

Figure A3.15. ^{13}C NMR (125 MHz) spectrum of the crude mixture obtained after a one-electron reductive electrolysis of cinnamaldehyde in CD_3CN.

This page has been intentionally left blank

Appendix (Chapter 5)

Comparing the Relative Reactivities of Food and Vitamin Molecules

Toward Electrochemically Generated Superoxide

This page has been intentionally left blank

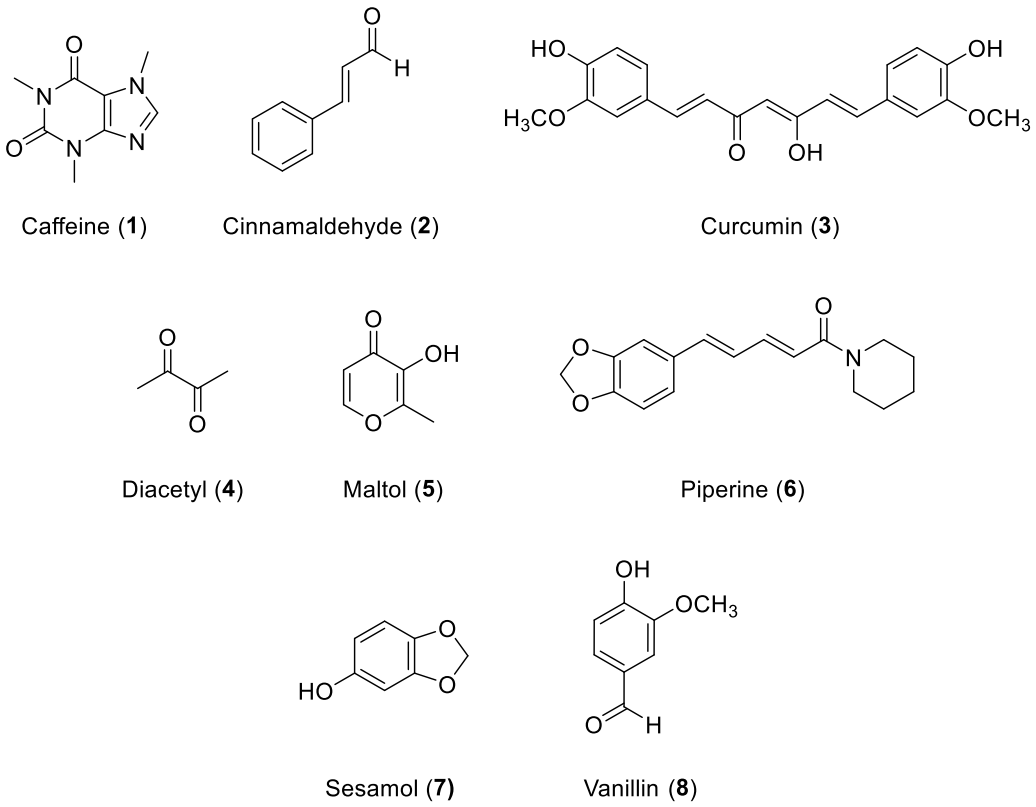

Scheme A5.1. List of food compounds examined in this study.

Vitamin A

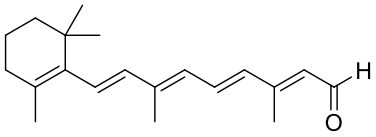

Retinal (**9**)

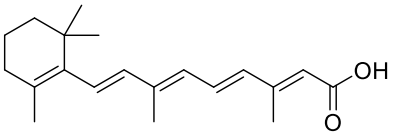

Retinoic acid (**10**)

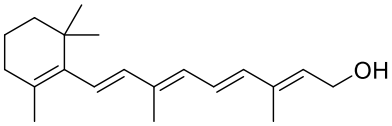

Retinol (**11**)

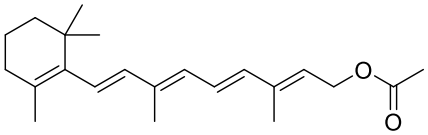

Retinyl acetate (**12**)

Vitamin B_6

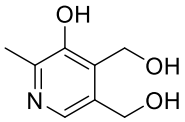

Pyridoxine (**13**)

Vitamin B_7

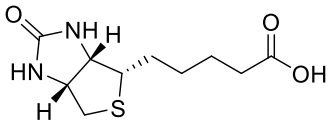

D-(+)-Biotin (**14**)

Vitamin D_2

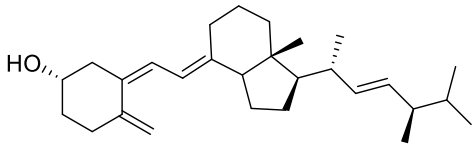

Ergocalciferol (**15**)

Vitamin D_3

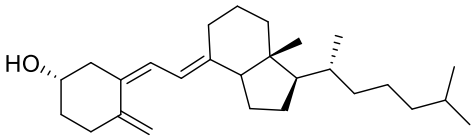

Cholecalciferol (**16**)

Vitamin E

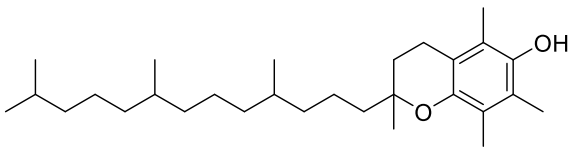

DL-α-tocopherol (**17**)

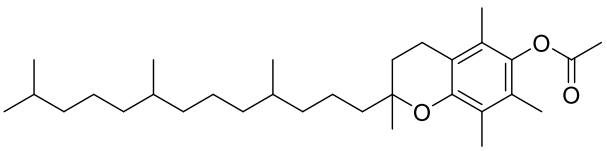

DL-α-tocopherol acetate (**18**)

Scheme A5.2. List of vitamin compounds examined in this study.

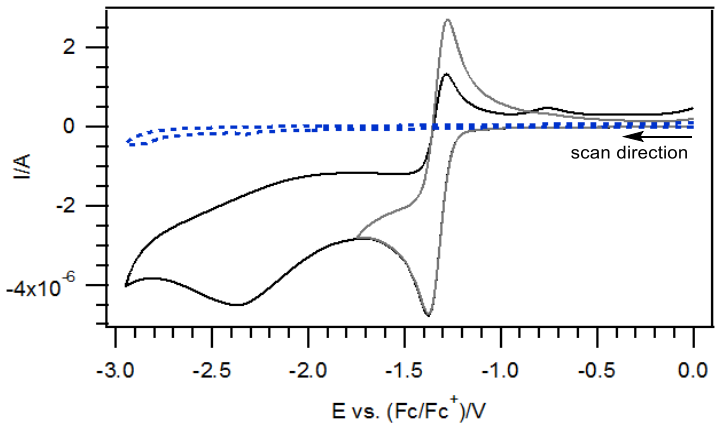

Figure A5.1. Cyclic voltammograms of the (—) one-electron and (**—**) two-electron reduction of O_2 in dry, air saturated DMF containing 0.1 M Bu_4NPF_6, recorded using a 1-mm diameter planar GC disk electrode and a scan rate of 0.1 V s^{-1}. (- - -) Cyclic voltammogram measured after the test solution was saturated with argon gas.

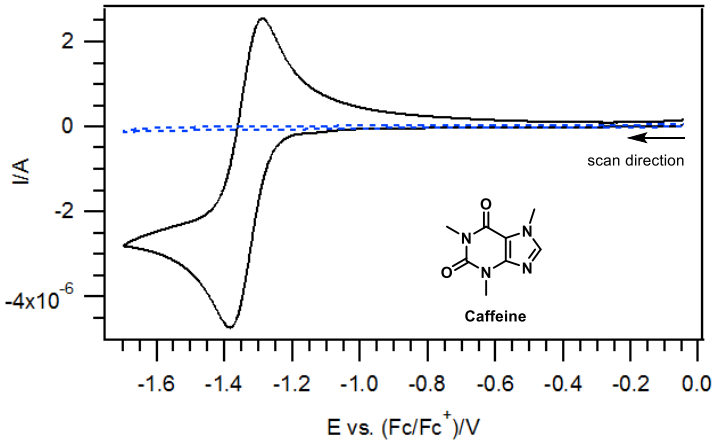

Figure A5.2. (- - -) Cyclic voltammogram of 5 mM Caffeine in dry, argon saturated DMF containing 0.1 M Bu_4NPF_6, recorded using a 1-mm diameter planar GC disk electrode and a scan rate of 0.1 V s^{-1}. (—) Overlay of the voltammogram collected for the one-electron reduction of O_2 for comparison.

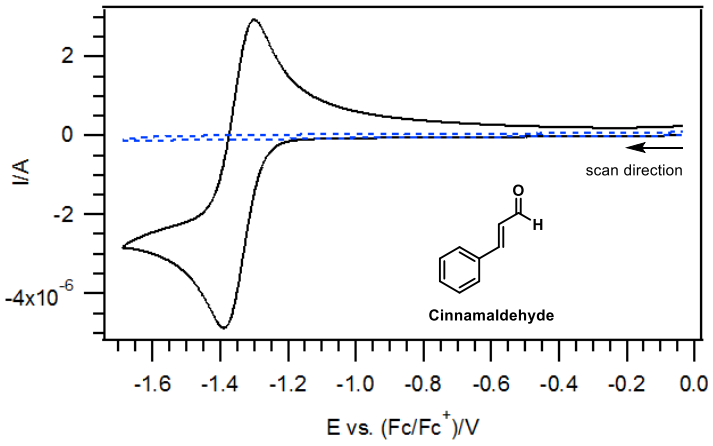

Figure A5.3. (- - -) Cyclic voltammogram of 5 mM Cinnamaldehyde in dry, argon saturated DMF containing 0.1 M Bu_4NPF_6, recorded using a 1-mm diameter planar GC disk electrode and a scan rate of 0.1 V s^{-1}. (—) Overlay of the voltammogram collected for the one-electron reduction of O_2 for comparison.

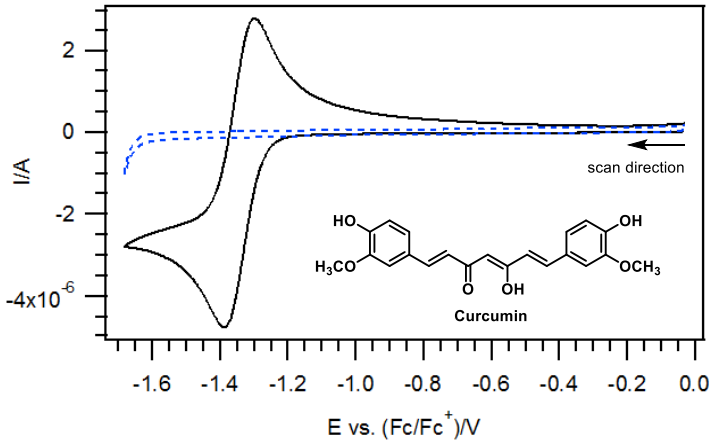

Figure A5.4. (- - -) Cyclic voltammogram of 5 mM Curcumin in dry, argon saturated DMF containing 0.1 M Bu_4NPF_6, recorded using a 1-mm diameter planar GC disk electrode and a scan rate of 0.1 V s^{-1}. (—) Overlay of the voltammogram collected for the one-electron reduction of O_2 for comparison.

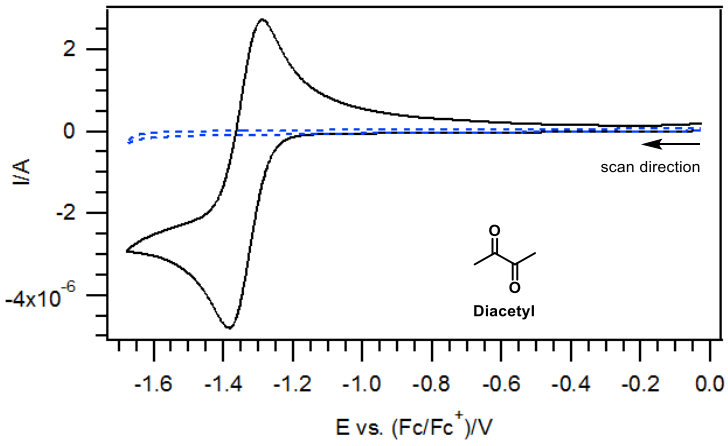

Figure A5.5. (- - -) Cyclic voltammogram of 5 mM Diacetyl in dry, argon saturated DMF containing 0.1 M Bu_4NPF_6, recorded using a 1-mm diameter planar GC disk electrode and a scan rate of 0.1 V s^{-1}. (—) Overlay of the voltammogram collected for the one-electron reduction of O_2 for comparison.

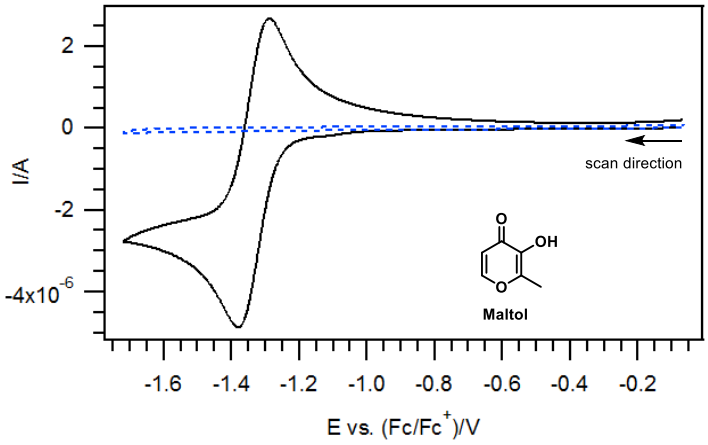

Figure A5.6. (- - -) Cyclic voltammogram of 5 mM Maltol in dry, argon saturated DMF containing 0.1 M Bu_4NPF_6, recorded using a 1-mm diameter planar GC disk electrode and a scan rate of 0.1 V s^{-1}. (—) Overlay of the voltammogram collected for the one-electron reduction of O_2 for comparison.

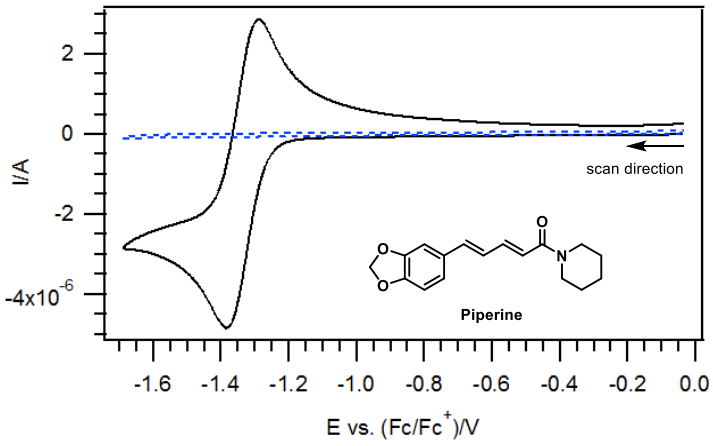

Figure A5.7. (- - -) Cyclic voltammogram of 5 mM Piperine in dry, argon saturated DMF containing 0.1 M Bu_4NPF_6, recorded using a 1-mm diameter planar GC disk electrode and a scan rate of 0.1 V s^{-1}. (—) Overlay of the voltammogram collected for the one-electron reduction of O_2 for comparison.

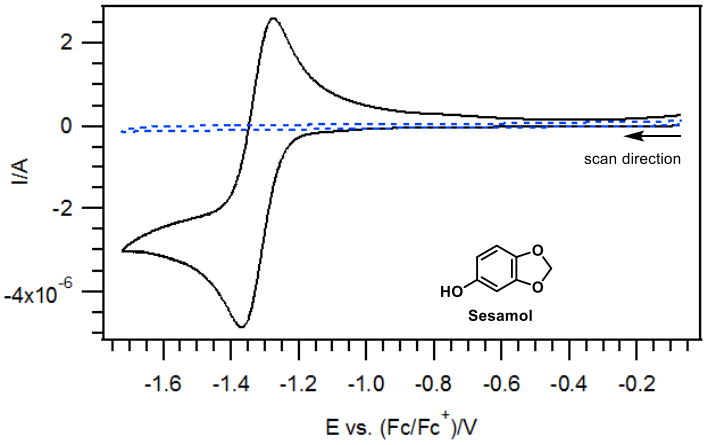

Figure A5.8. (- - -) Cyclic voltammogram of 5 mM Sesamol in dry, argon saturated DMF containing 0.1 M Bu_4NPF_6, recorded using a 1-mm diameter planar GC disk electrode and a scan rate of 0.1 V s^{-1}. (—) Overlay of the voltammogram collected for the one-electron reduction of O_2 for comparison.

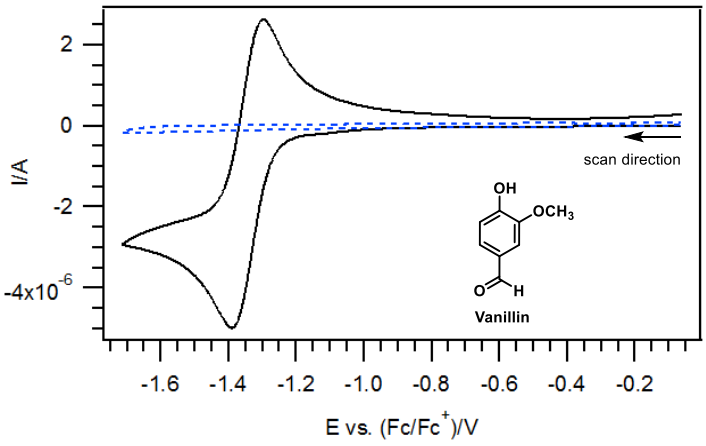

Figure A5.9. (- - -) Cyclic voltammogram of 5 mM Vanillin in dry, argon saturated DMF containing 0.1 M Bu_4NPF_6, recorded using a 1-mm diameter planar GC disk electrode and a scan rate of 0.1 V s^{-1}. (—) Overlay of the voltammogram collected for the one-electron reduction of O_2 for comparison.

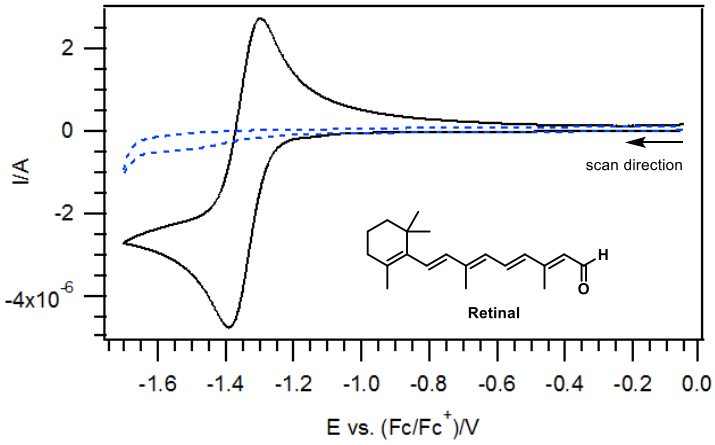

Figure A5.10. (- - -) Cyclic voltammogram of 5 mM Retinal in dry, argon saturated DMF containing 0.1 M Bu_4NPF_6, recorded using a 1-mm diameter planar GC disk electrode and a scan rate of 0.1 V s^{-1}. (—) Overlay of the voltammogram collected for the one-electron reduction of O_2 for comparison.

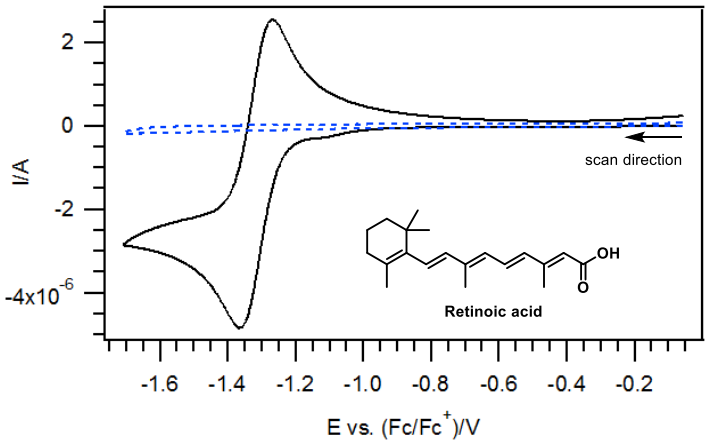

Figure A5.11. (- - -) Cyclic voltammogram of 5 mM Retinoic acid in dry, argon saturated DMF containing 0.1 M Bu_4NPF_6, recorded using a 1-mm diameter planar GC disk electrode and a scan rate of 0.1 V s^{-1}. (—) Overlay of the voltammogram collected for the one-electron reduction of O_2 for comparison.

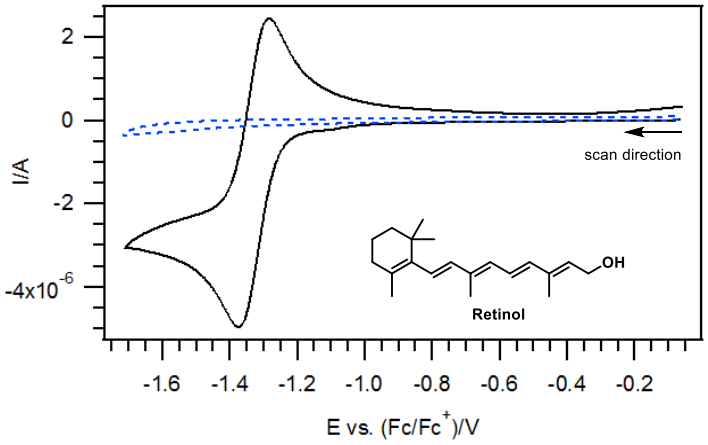

Figure A5.12. (- - -) Cyclic voltammogram of 5 mM Retinol in dry, argon saturated DMF containing 0.1 M Bu_4NPF_6, recorded using a 1-mm diameter planar GC disk electrode and a scan rate of 0.1 V s^{-1}. (—) Overlay of the voltammogram collected for the one-electron reduction of O_2 for comparison.

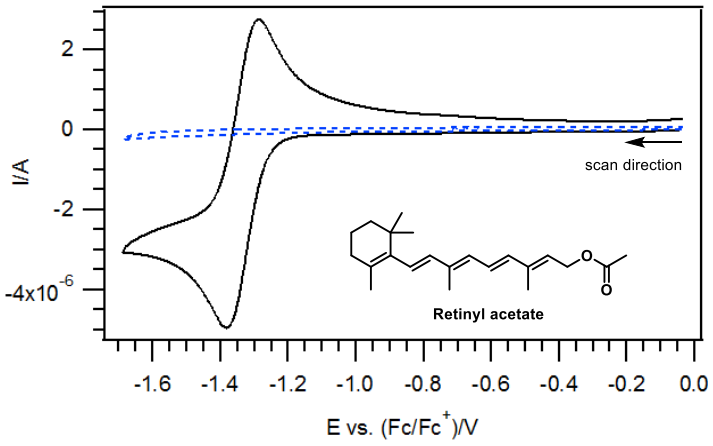

Figure A5.13. (- - -) Cyclic voltammogram of 5 mM Retinyl acetate in dry, argon saturated DMF containing 0.1 M Bu_4NPF_6, recorded using a 1-mm diameter planar GC disk electrode and a scan rate of 0.1 V s^{-1}. (—) Overlay of the voltammogram collected for the one-electron reduction of O_2 for comparison.

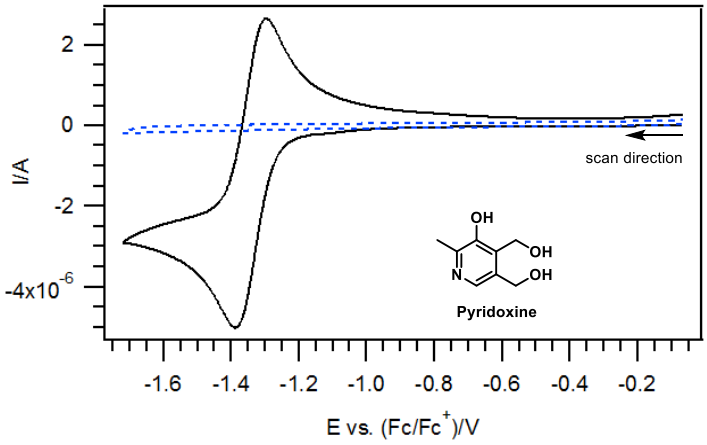

Figure A5.14. (- - -) Cyclic voltammogram of 5 mM Pyridoxine in dry, argon saturated DMF containing 0.1 M Bu_4NPF_6, recorded using a 1-mm diameter planar GC disk electrode and a scan rate of 0.1 V s^{-1}. (—) Overlay of the voltammogram collected for the one-electron reduction of O_2 for comparison.

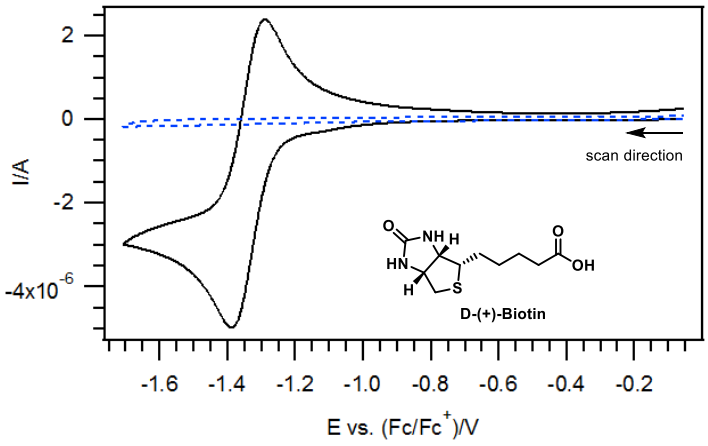

Figure A5.15. (- - -) Cyclic voltammogram of 5 mM D-(+)-Biotin in dry, argon saturated DMF containing 0.1 M Bu_4NPF_6, recorded using a 1-mm diameter planar GC disk electrode and a scan rate of 0.1 V s^{-1}. (—) Overlay of the voltammogram collected for the one-electron reduction of O_2 for comparison.

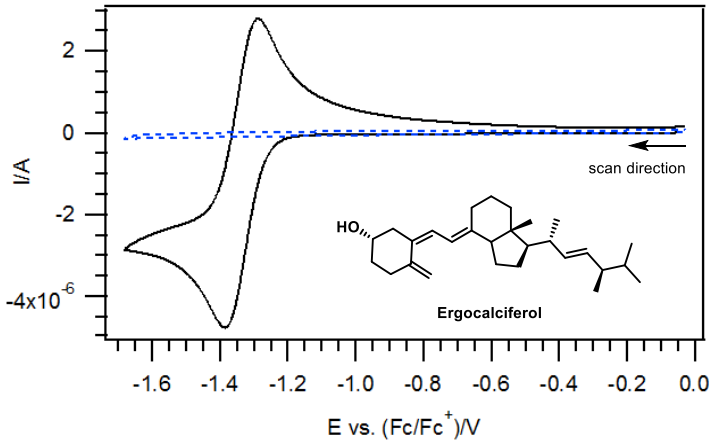

Figure A5.16. (- - -) Cyclic voltammogram of 5 mM Ergocalciferol in dry, argon saturated DMF containing 0.1 M Bu_4NPF_6, recorded using a 1-mm diameter planar GC disk electrode and a scan rate of 0.1 V s^{-1}. (—) Overlay of the voltammogram collected for the one-electron reduction of O_2 for comparison.

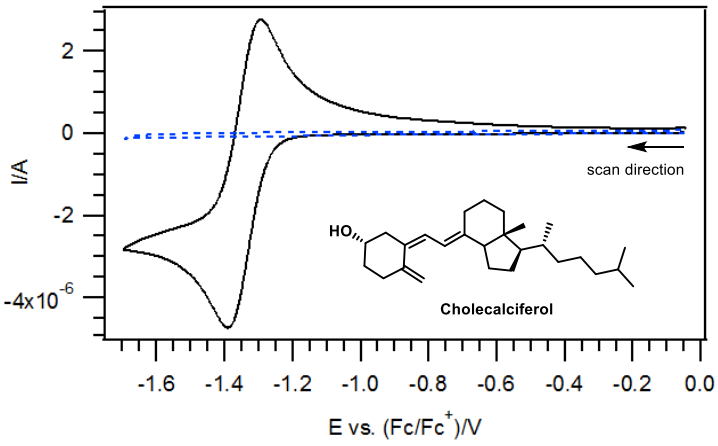

Figure A5.17. (- - -) Cyclic voltammogram of 5 mM Cholecalciferol in dry, argon saturated DMF containing 0.1 M Bu_4NPF_6, recorded using a 1-mm diameter planar GC disk electrode and a scan rate of 0.1 V s^{-1}. (—) Overlay of the voltammogram collected for the one-electron reduction of O_2 for comparison.

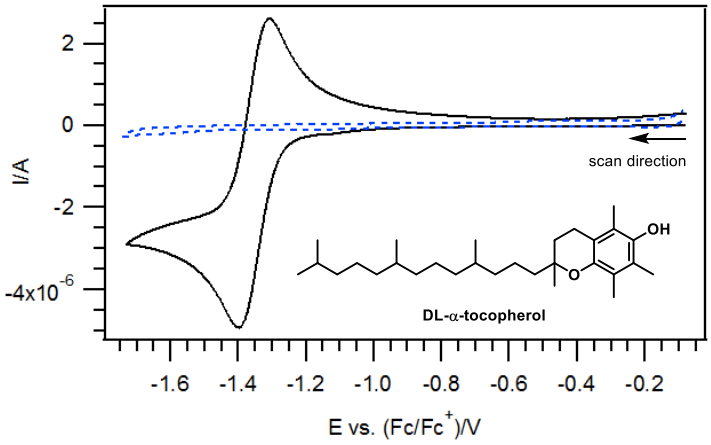

Figure A5.18. (- - -) Cyclic voltammogram of 5 mM DL-α-tocopherol in dry, argon saturated DMF containing 0.1 M Bu_4NPF_6, recorded using a 1-mm diameter planar GC disk electrode and a scan rate of 0.1 V s^{-1}. (—) Overlay of the voltammogram collected for the one-electron reduction of O_2 for comparison.

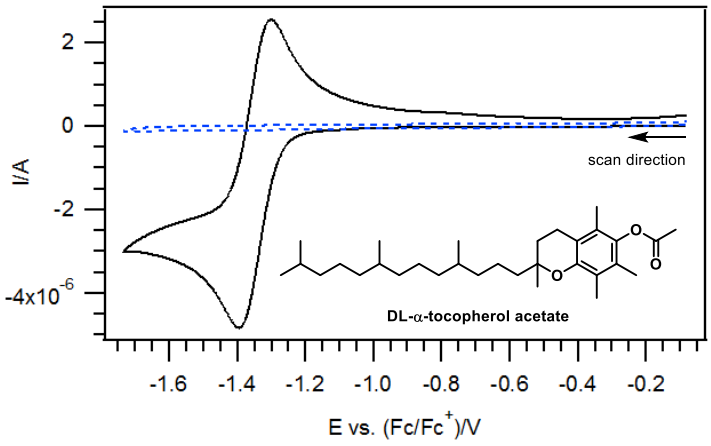

Figure A5.19. (- - -) Cyclic voltammogram of 5 mM DL-α-tocopherol acetate in dry, argon saturated DMF containing 0.1 M Bu_4NPF_6, recorded using a 1-mm diameter planar GC disk electrode and a scan rate of 0.1 V s^{-1}. (—) Overlay of the voltammogram collected for the one-electron reduction of O_2 for comparison.

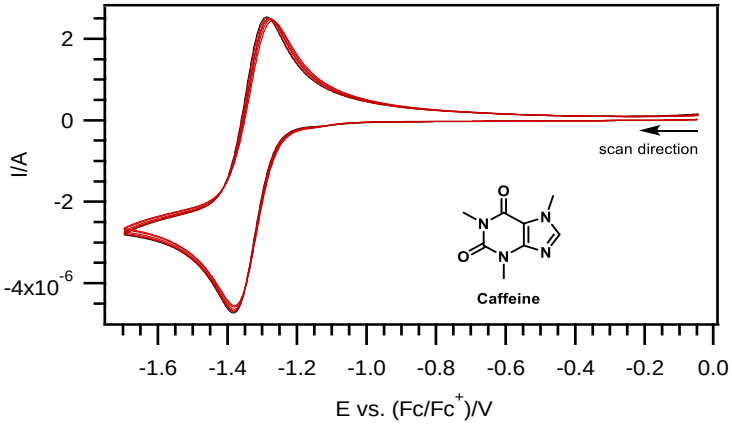

Figure A5.20. Cyclic voltammograms of the one-electron reduction of O_2 in dry, air saturated DMF containing 0.1 M Bu_4NPF_6, recorded using a 1-mm diameter planar GC disk electrode, a scan rate of 0.1 V s^{-1}, and at increasing concentrations of Caffeine. (—) No substrate added. (—) 10, 20, 30, 40, & 50 mM of Caffeine added.

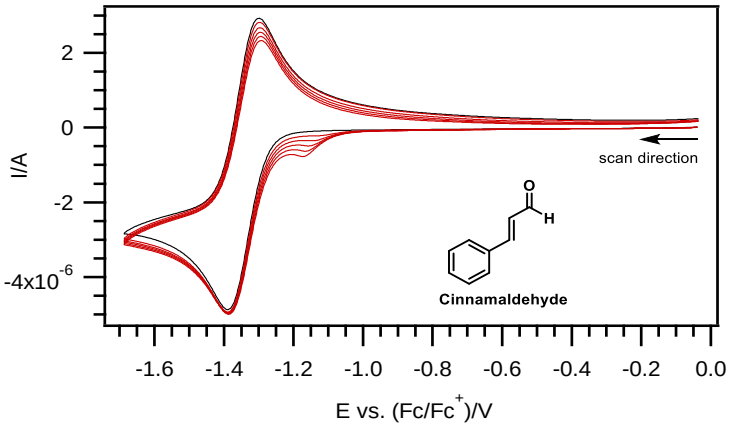

Figure A5.21. Cyclic voltammograms of the one-electron reduction of O_2 in dry, air saturated DMF containing 0.1 M Bu_4NPF_6, recorded using a 1-mm diameter planar GC disk electrode, a scan rate of 0.1 V s^{-1}, and at increasing concentrations of Cinnamaldehyde. (—) No substrate added. (—) 10, 20, 30, 40, & 50 mM of Cinnamaldehyde added.

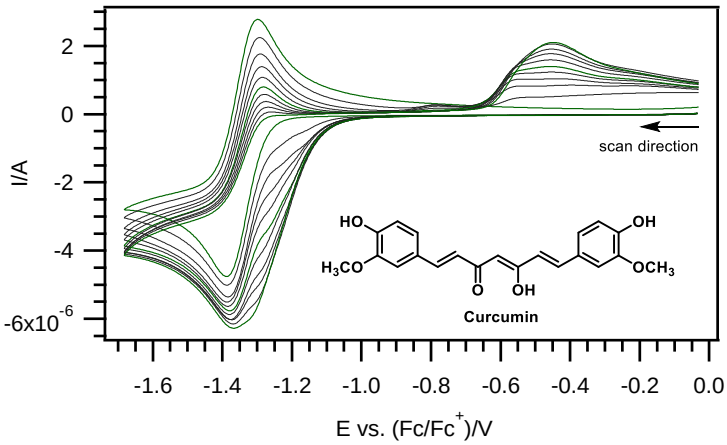

Figure A5.22. Cyclic voltammograms of the one-electron reduction of O_2 in dry, air saturated DMF containing 0.1 M Bu_4NPF_6, recorded using a 1-mm diameter planar GC disk electrode, a scan rate of 0.1 V s^{-1}, and at increasing concentrations of Curcumin. (—) 0, 1.0, & 2.0 mM of Curcumin added. (—) 0.2 mM increments in concentration.

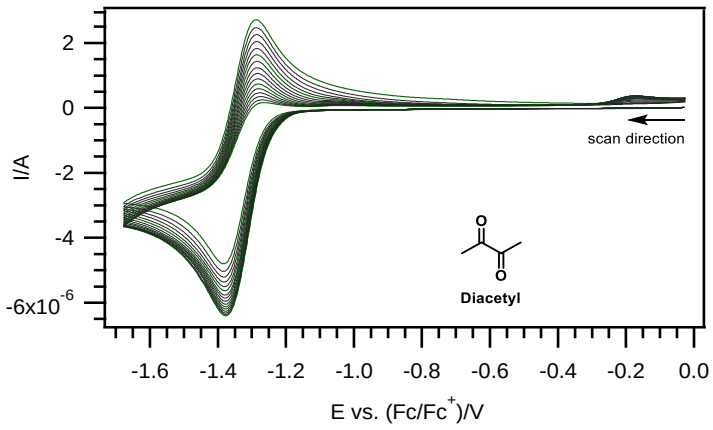

Figure A5.23. Cyclic voltammograms of the one-electron reduction of O_2 in dry, air saturated DMF containing 0.1 M Bu_4NPF_6, recorded using a 1-mm diameter planar GC disk electrode, a scan rate of 0.1 V s^{-1}, and at increasing concentrations of Diacetyl. (—) 0, 1.0, 2.0, & 3.0 mM of Diacetyl added. (—) 0.2 mM increments in concentration.

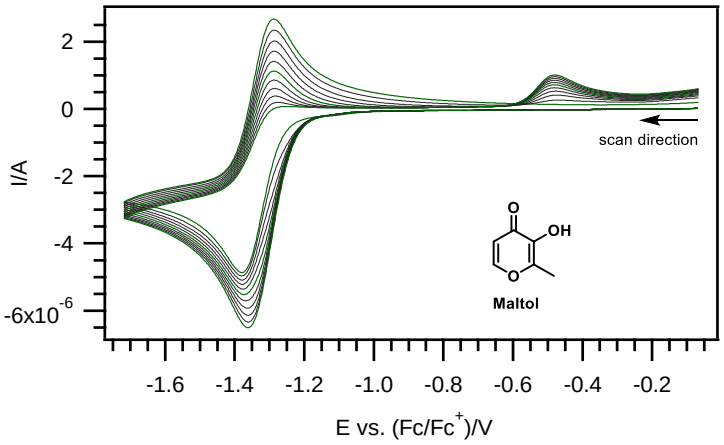

Figure A5.24. Cyclic voltammograms of the one-electron reduction of O_2 in dry, air saturated DMF containing 0.1 M Bu_4NPF_6, recorded using a 1-mm diameter planar GC disk electrode, a scan rate of 0.1 V s^{-1}, and at increasing concentrations of Maltol. (—) 0, 1.0, & 2.0 mM of Maltol added. (—) 0.2 mM increments in concentration.

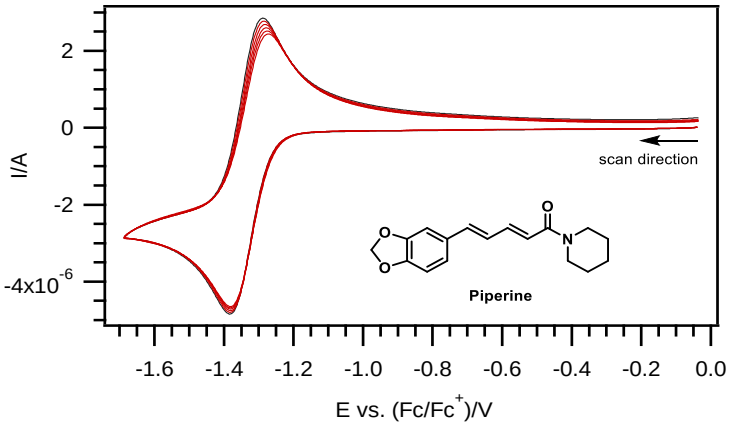

Figure A5.25. Cyclic voltammograms of the one-electron reduction of O_2 in dry, air saturated DMF containing 0.1 M Bu_4NPF_6, recorded using a 1-mm diameter planar GC disk electrode, a scan rate of 0.1 V s^{-1}, and at increasing concentrations of Piperine. (—) No substrate added. (—) 10, 20, 30, 40, & 50 mM of Piperine added.

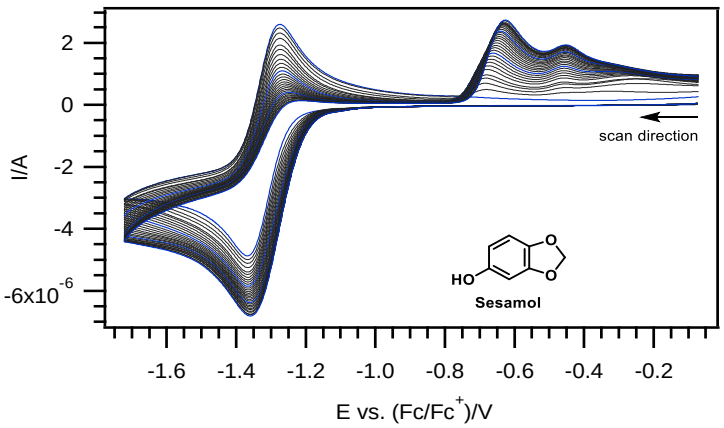

Figure A5.26. Cyclic voltammograms of the one-electron reduction of O_2 in dry, air saturated DMF containing 0.1 M Bu_4NPF_6, recorded using a 1-mm diameter planar GC disk electrode, a scan rate of 0.1 V s^{-1}, and at increasing concentrations of Sesamol. (—) 0, 2.0, 4.0, & 6.0 mM of Sesamol added. (—) 0.2 mM increments in concentration.

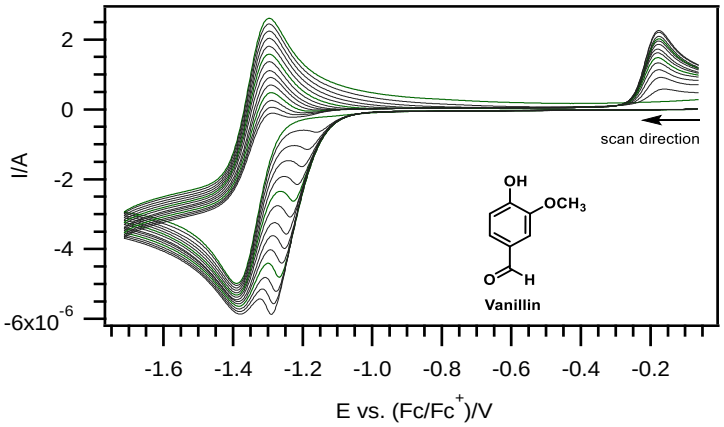

Figure A5.27. Cyclic voltammograms of the one-electron reduction of O_2 in dry, air saturated DMF containing 0.1 M Bu_4NPF_6, recorded using a 1-mm diameter planar GC disk electrode, a scan rate of 0.1 V s^{-1}, and at increasing concentrations of Vanillin. (—) 0, 1.0, 2.0 mM of Vanillin added. (—) 0.2 mM increments in concentration.

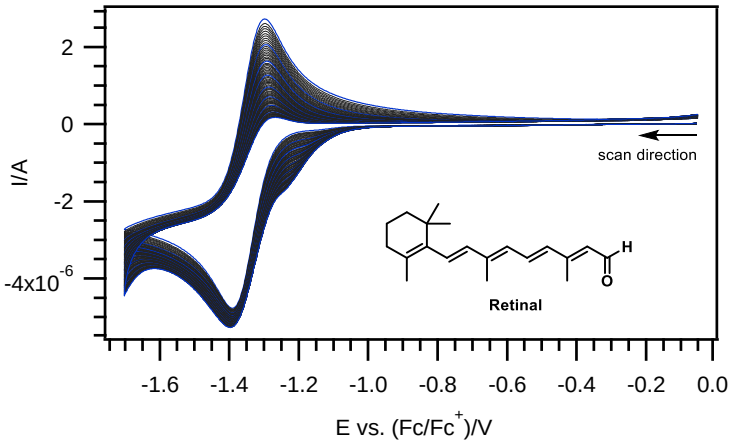

Figure A5.28. Cyclic voltammograms of the one-electron reduction of O_2 in dry, air saturated DMF containing 0.1 M Bu_4NPF_6, recorded using a 1-mm diameter planar GC disk electrode, a scan rate of 0.1 V s^{-1}, and at increasing concentrations of Retinal. (—) 0, 2.0, 4.0, 6.0, 8.0, 10.0, 12.0, 14.0 & 16.0 mM of Retinal added. (—) 0.2 mM increments in concentration.

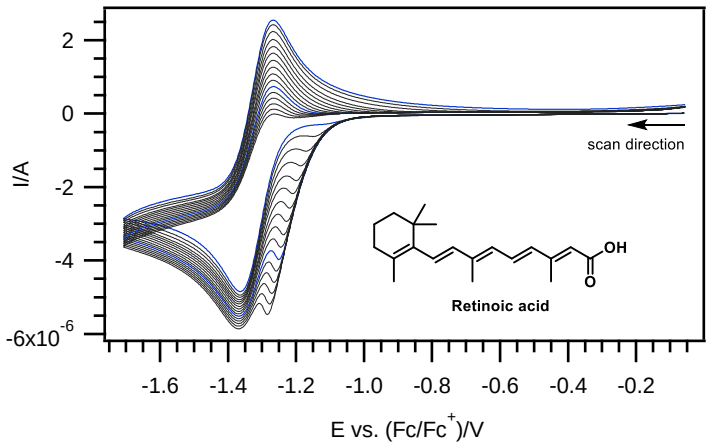

Figure A5.29. Cyclic voltammograms of the one-electron reduction of O_2 in dry, air saturated DMF containing 0.1 M Bu_4NPF_6, recorded using a 1-mm diameter planar GC disk electrode, a scan rate of 0.1 V s^{-1}, and at increasing concentrations of Retinoic acid. (—) 0, 2.0, & 4.0 mM of Retinoic acid added. (—) 0.2 mM increments in concentration.

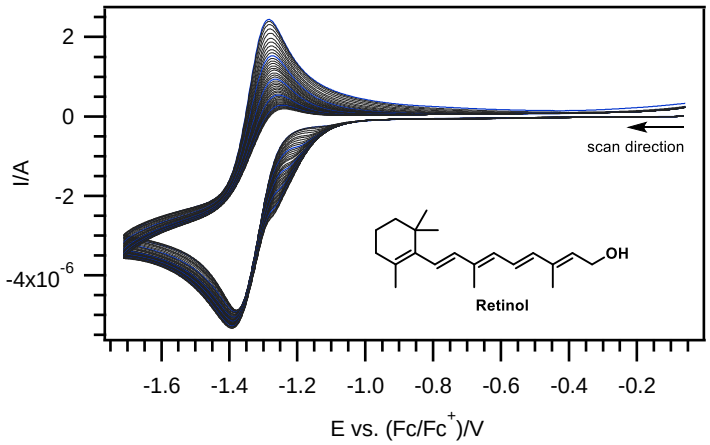

Figure A5.30. Cyclic voltammograms of the one-electron reduction of O_2 in dry, air saturated DMF containing 0.1 M Bu_4NPF_6, recorded using a 1-mm diameter planar GC disk electrode, a scan rate of 0.1 V s^{-1}, and at increasing concentrations of Retinol. (—) 0, 2.0, 4.0, 6.0, 8.0, & 10.0 mM of Retinol added. (—) 0.2 mM increments in concentration.

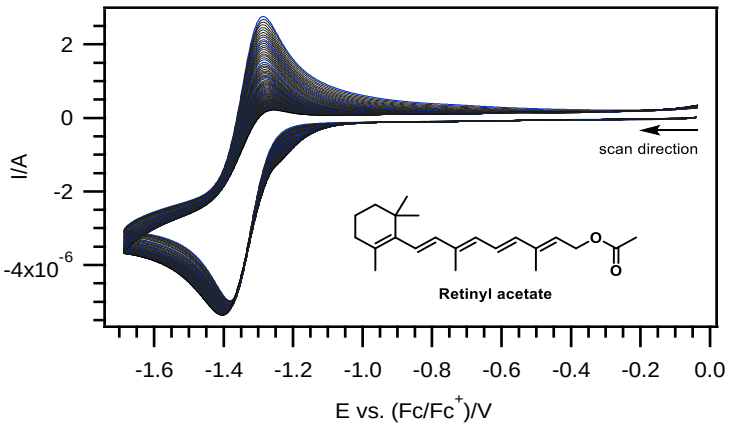

Figure A5.31. Cyclic voltammograms of the one-electron reduction of O_2 in dry, air saturated DMF containing 0.1 M Bu_4NPF_6, recorded using a 1-mm diameter planar GC disk electrode, a scan rate of 0.1 V s^{-1}, and at increasing concentrations of Retinyl acetate. (—) 0, 2.0, 4.0, 6.0, 8.0, 10.0, 12.0, 14.0 & 15.0 mM of Retinyl acetate added. (—) 0.2 mM increments in concentration.

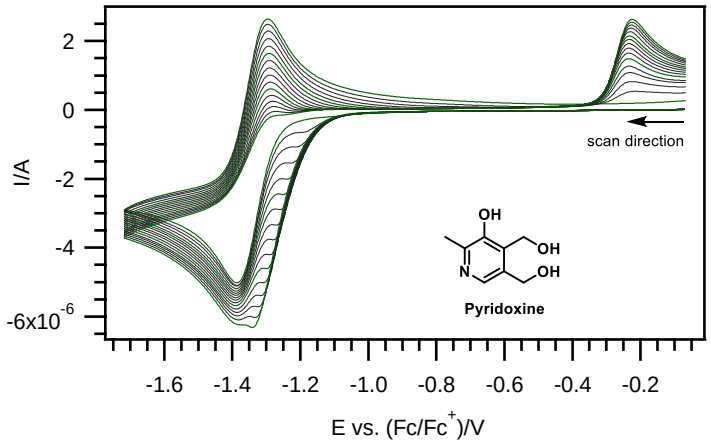

Figure A5.32. Cyclic voltammograms of the one-electron reduction of O_2 in dry, air saturated DMF containing 0.1 M Bu_4NPF_6, recorded using a 1-mm diameter planar GC disk electrode, a scan rate of 0.1 V s^{-1}, and at increasing concentrations of Pyridoxine. (—) 0, 1.0, 2.0, & 3.0 mM of Pyridoxine added. (—) 0.2 mM increments in concentration.

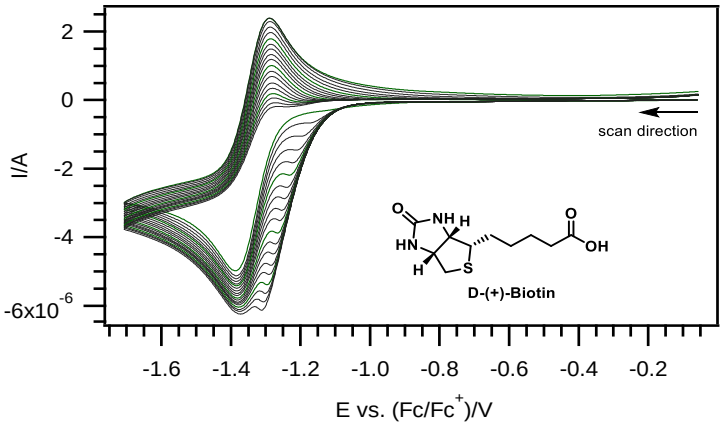

Figure A5.33. Cyclic voltammograms of the one-electron reduction of O_2 in dry, air saturated DMF containing 0.1 M Bu_4NPF_6, recorded using a 1-mm diameter planar GC disk electrode, a scan rate of 0.1 V s^{-1}, and at increasing concentrations of D-(+)-Biotin. (—) 0, 1.0, 2.0, & 3.0 mM of D-(+)-Biotin added. (—) 0.2 mM increments in concentration.

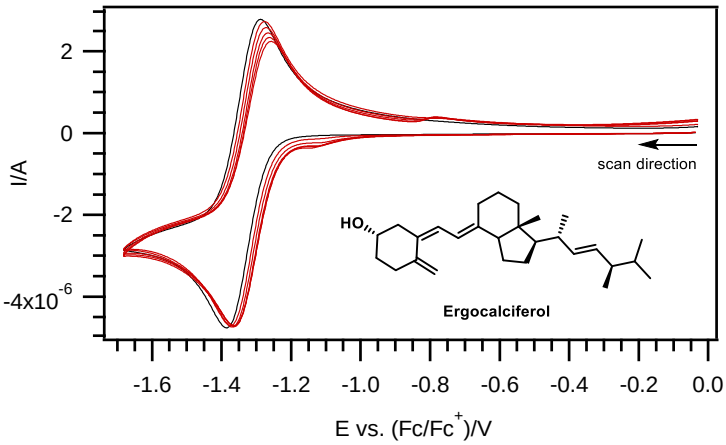

Figure A5.34. Cyclic voltammograms of the one-electron reduction of O_2 in dry, air saturated DMF containing 0.1 M Bu_4NPF_6, recorded using a 1-mm diameter planar GC disk electrode, a scan rate of 0.1 V s^{-1}, and at increasing concentrations of Ergocalciferol. (—) No substrate added. (—) 10, 20, 30, 40, & 50 mM of Ergocalciferol added.

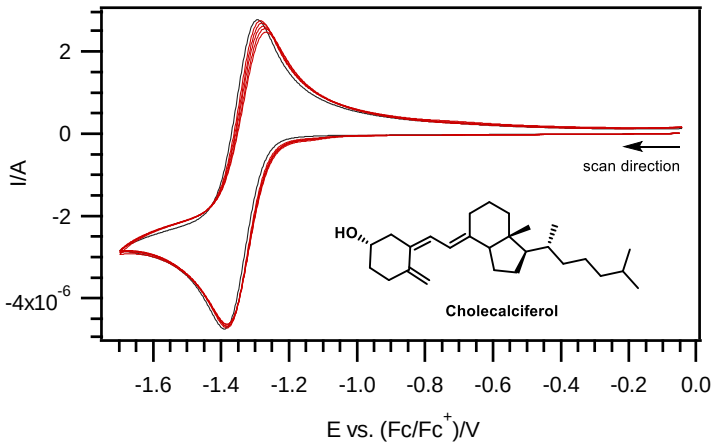

Figure A5.35. Cyclic voltammograms of the one-electron reduction of O_2 in dry, air saturated DMF containing 0.1 M Bu_4NPF_6, recorded using a 1-mm diameter planar GC disk electrode, a scan rate of 0.1 V s^{-1}, and at increasing concentrations of Cholecalciferol. (—) No substrate added. (—) 10, 20, 30, 40, & 50 mM of Cholecalciferol added.

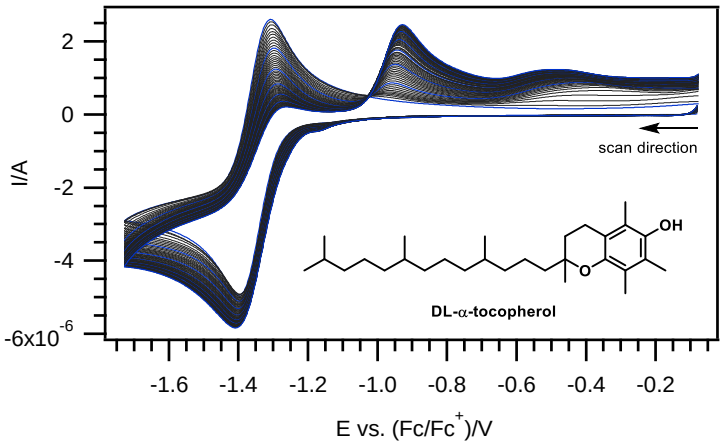

Figure A5.36. Cyclic voltammograms of the one-electron reduction of O_2 in dry, air saturated DMF containing 0.1 M Bu_4NPF_6, recorded using a 1-mm diameter planar GC disk electrode, a scan rate of 0.1 V s^{-1}, and at increasing concentrations of DL-α-tocopherol. (—) 0, 2.0, 4.0, 6.0, 8.0, 10.0, & 12.0 of DL-α-tocopherol added. (—) 0.2 mM increments in concentration.

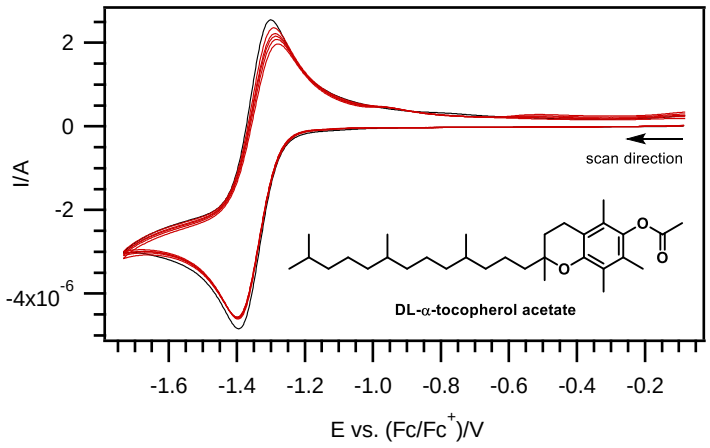

Figure A5.37. Cyclic voltammograms of the one-electron reduction of O_2 in dry, air saturated DMF containing 0.1 M Bu_4NPF_6, recorded using a 1-mm diameter planar GC disk electrode, a scan rate of 0.1 V s^{-1}, and at increasing concentrations of DL-α-tocopherol acetate. (—) No substrate added. (—) 10, 20, 30, 40, & 50 mM of DL-α-tocopherol acetate added.

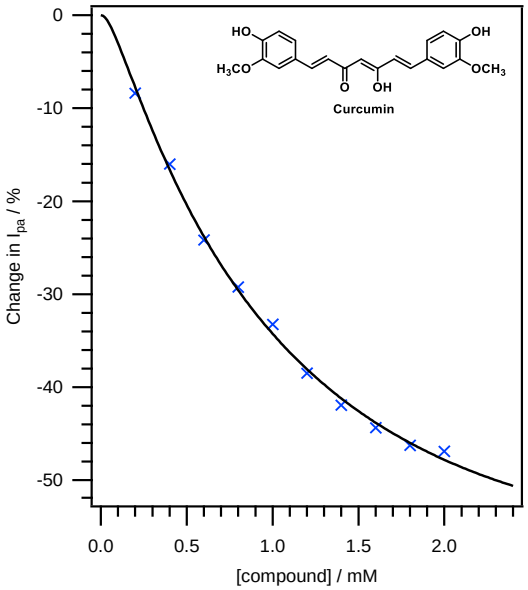

Figure A5.38. Plot of percentage change in the reverse anodic peak currents of O_2 reduction against the concentration of Curcumin added.

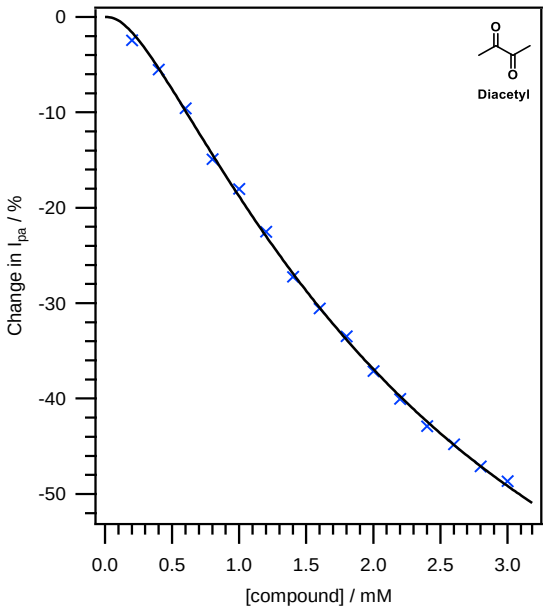

Figure A5.39. Plot of percentage change in the reverse anodic peak currents of O_2 reduction against the concentration of Diacetyl added.

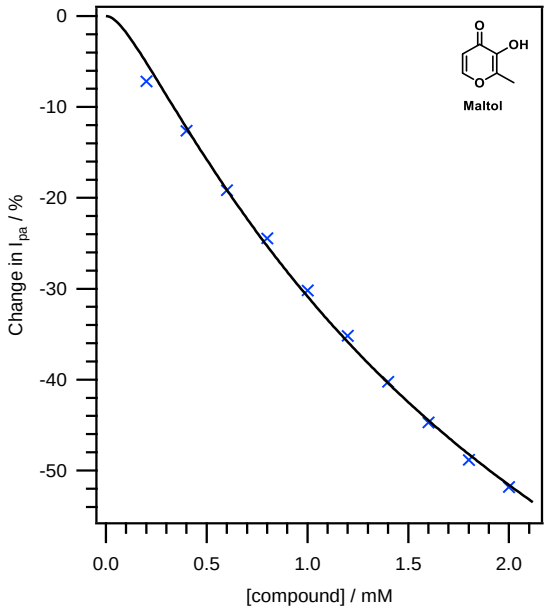

Figure A5.40. Plot of percentage change in the reverse anodic peak currents of O_2 reduction against the concentration of Maltol added.

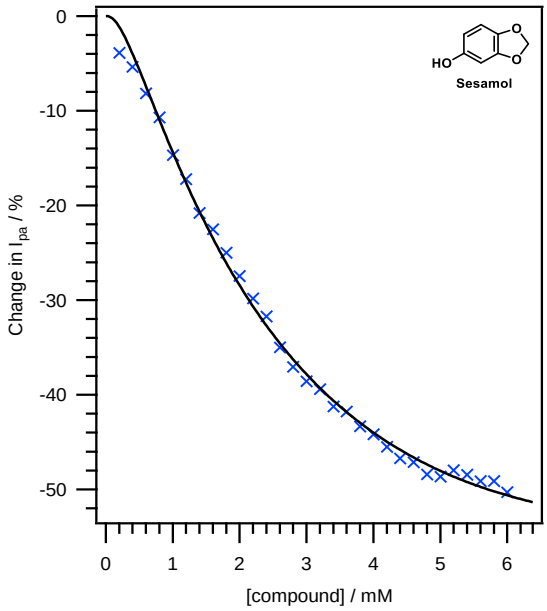

Figure A5.41. Plot of percentage change in the reverse anodic peak currents of O_2 reduction against the concentration of Sesamol added.

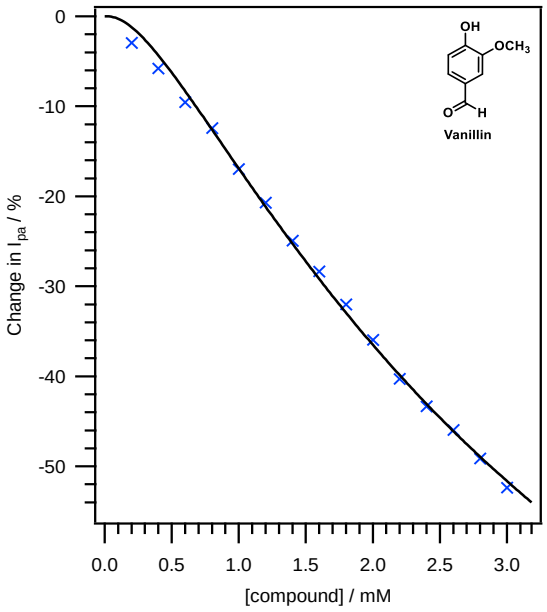

Figure A5.42. Plot of percentage change in the reverse anodic peak currents of O_2 reduction against the concentration of Vanillin added.

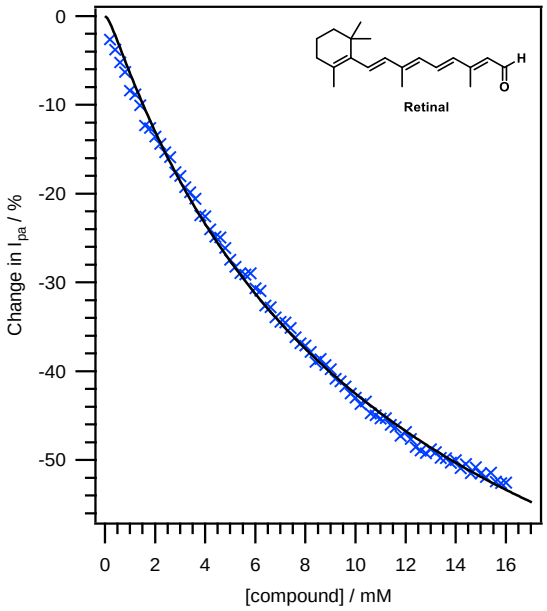

Figure A5.43. Plot of percentage change in the reverse anodic peak currents of O_2 reduction against the concentration of Retinal added.

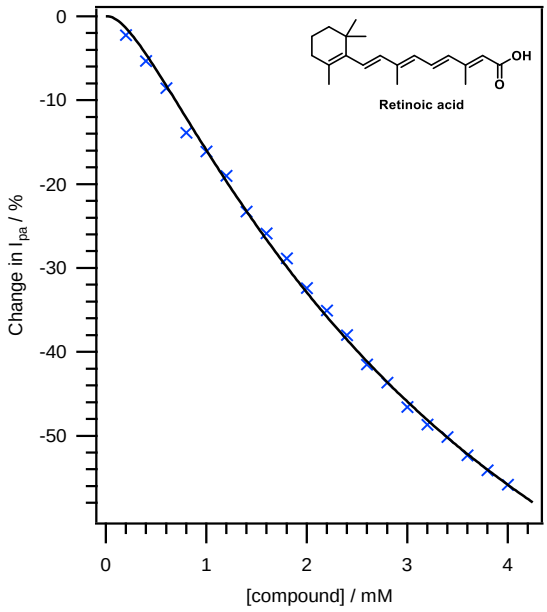

Figure A5.44. Plot of percentage change in the reverse anodic peak currents of O_2 reduction against the concentration of Retinoic acid added.

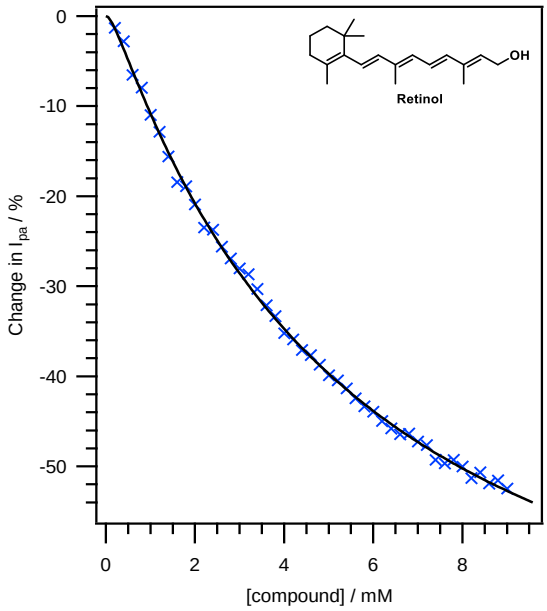

Figure A5.45. Plot of percentage change in the reverse anodic peak currents of O_2 reduction against the concentration of Retinol added.

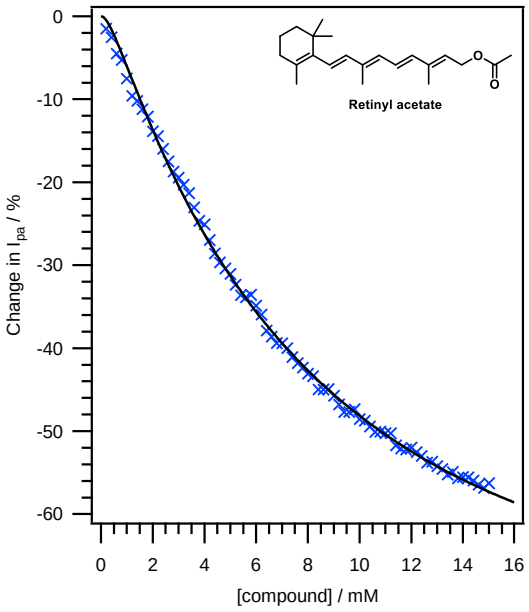

Figure A5.46. Plot of percentage change in the reverse anodic peak currents of O_2 reduction against the concentration of Retinyl acetate added.

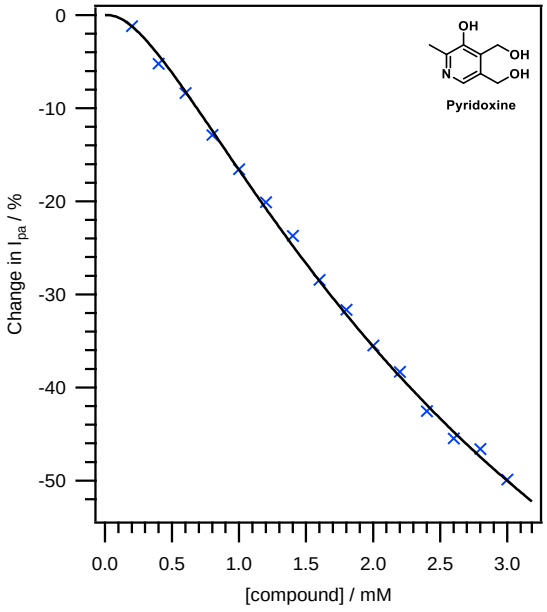

Figure A5.47. Plot of percentage change in the reverse anodic peak currents of O_2 reduction against the concentration of Pyridoxine added.

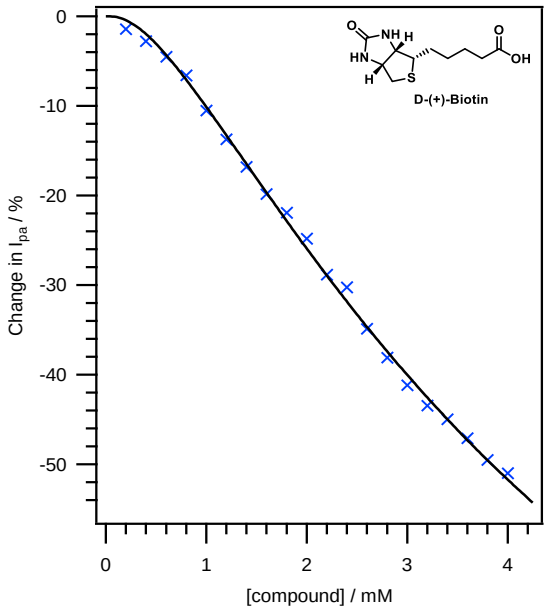

Figure A5.48. Plot of percentage change in the reverse anodic peak currents of O_2 reduction against the concentration of D-(+)-Biotin added.

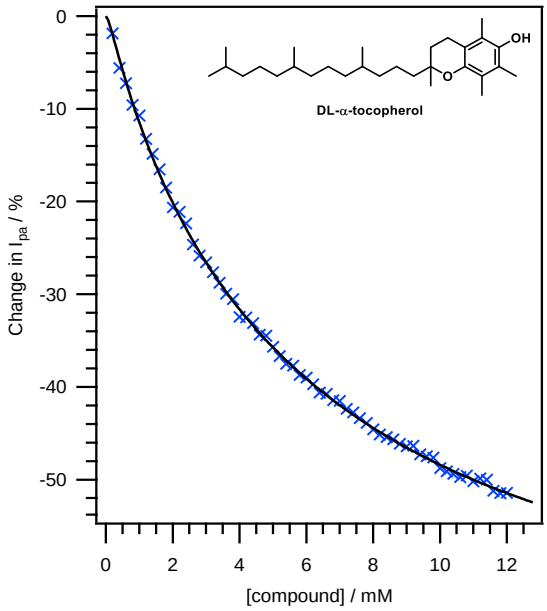

Figure A5.49. Plot of percentage change in the reverse anodic peak currents of O_2 reduction against the concentration of DL-α-tocopherol added.

This page has been intentionally left blank

Appendix (Chapter 6)

Comparing the Relative Reactivities of Structurally Varied Alcohols

Toward Electrochemically Generated Superoxide

This page has been intentionally left blank

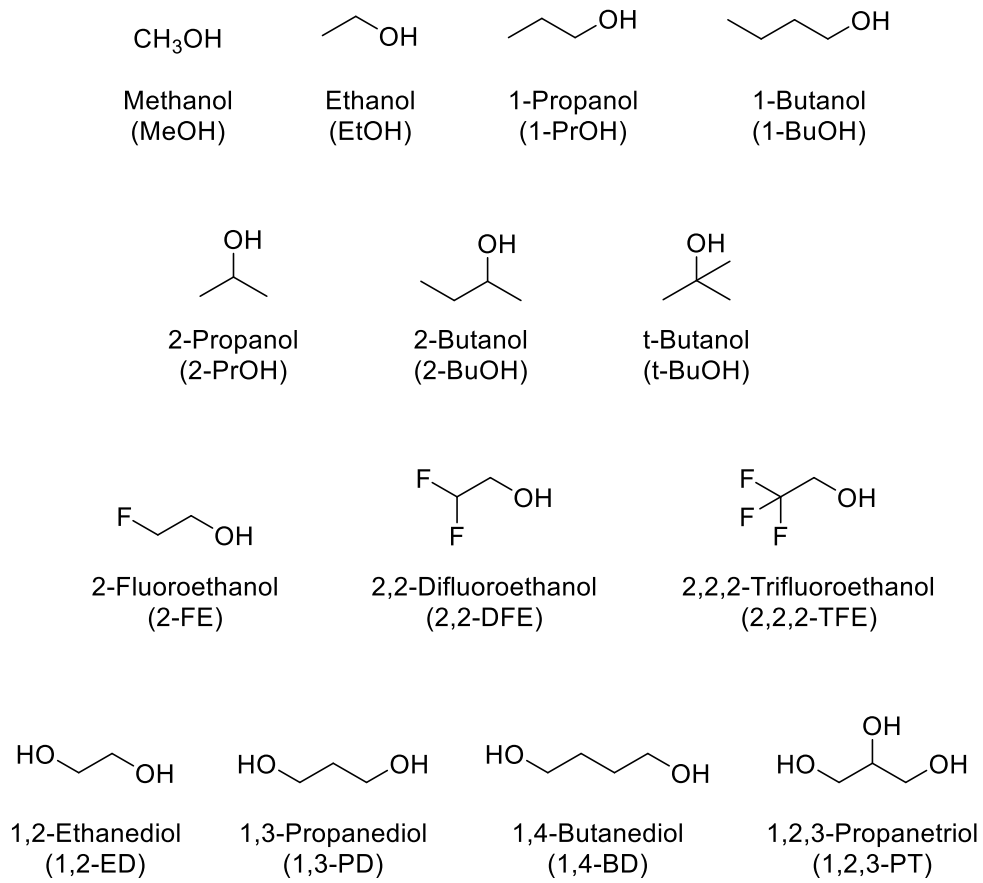

Scheme A6.1. List of alcohols examined in this study.

Table A6.1. Ratios of the cathodic peak currents at the final and initial (zero) concentrations (I^S_{pc}/I^0_{pc})[a] for the voltammograms of O_2 reduction in Figures A15–A28.

S/N	Compound	I^S_{pc}/I^0_{pc}
1.	Methanol (MeOH)	0.97
2.	Ethanol (EtOH)	0.96
3.	1-Propanol (1-PrOH)	0.96
4.	1-Butanol (1-BuOH)	0.94
5.	2-Propanol (2-PrOH)	0.94
6.	2-Butanol (2-BuOH)	0.96
7.	t-Butanol (t-BuOH)	0.95
8.	2-Fluoroethanol (2-FE)	0.97
9.	2,2-Difluoroethanol (2,2-DFE)	0.94
10.	2,2,2-Trifluoroethanol (2,2,2-TFE)	1.14
11.	1,2-Ethanediol (1,2-ED)	0.87
12.	1,3-Propanediol (1,3-PD)	0.77
13.	1,4-Butanediol (1,4-BD)	0.86
14.	1,2,3-Propanetriol (1,2,3-PT)	0.95

[a]The I^S_{pc} values were measured at the 2000 mM, 30 mM, 1000 mM, and 500 mM concentrations for alcohols 1–7, 8–10, 11–13, and 14, respectively.

Table A6.2. pK_a values (aqueous) of the mono-ols under study in this thesis.

S/N	Compound	pK_a
1.	Methanol (MeOH)	15.5[1]
2.	Ethanol (EtOH)	15.9[1]
3.	1-Propanol (1-PrOH)	16.1[2]
4.	1-Butanol (1-BuOH)	16.1[3]
5.	2-Propanol (2-PrOH)	17.1[1]
6.	2-Butanol (2-BuOH)	17.6[3]
7.	t-Butanol (t-BuOH)	18.0[4]
8.	2-Fluoroethanol (2-FE)	14.42[2]
9.	2,2-Difluoroethanol (2,2-DFE)	13.11[2]
10.	2,2,2-Trifluoroethanol (2,2,2-TFE)	12.39[2]

References

[1] P.G. Seybold, W.C. Kreye, Theoretical Estimation of the Acidities of Alcohols and Azoles in Gas Phase, DMSO, and Water, Int. J. Quantum Chem, 112 (2012) 3769–3776.

[2] M.A.K. Liton, U. Salma, M.B. Hossain, Comparative Study of Calculated and Experimental pKa Values for Some Carbon and Alcoholic Compounds, Am. J. Chem., 3 (2013) 37–43.

[3] E.P. Serjeant, B. Dempsey, International Union of Pure and Applied Chemistry. Commission on Equilibrium Data, International Union of Pure and Applied Chemistry. Commission on Electrochemical Data, Ionisation Constants of Organic Acids in Aqueous Solution., Pergamon Press, Oxford, New York, 1979.

[4] M. Breant, N. Arnaud, S. Desmettre, Spectrophotometric Determination of the pH Scale in Ethane-1,2-diol, Anal. Chim. Acta, 104 (1979) 181–183.

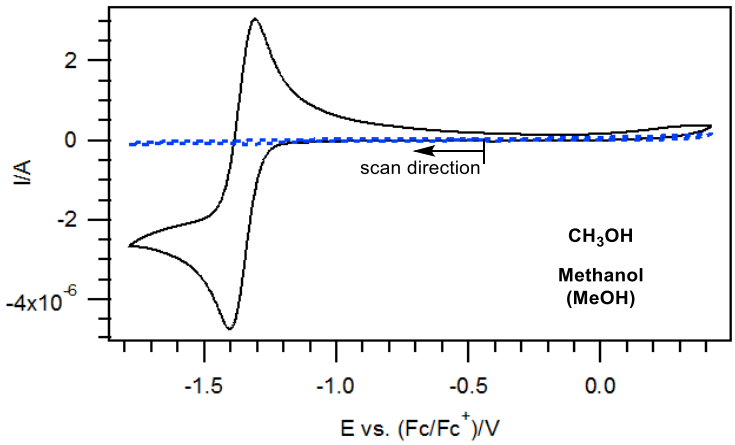

Figure A6.1. (- - -) Cyclic voltammogram of 500 mM Methanol in dry, argon saturated DMF containing 0.1 M Bu_4NPF_6, recorded using a 1-mm diameter planar GC disk electrode and a scan rate of 0.1 V s^{-1}. (—) Overlay of the voltammogram collected for the one-electron reduction of O_2 for comparison.

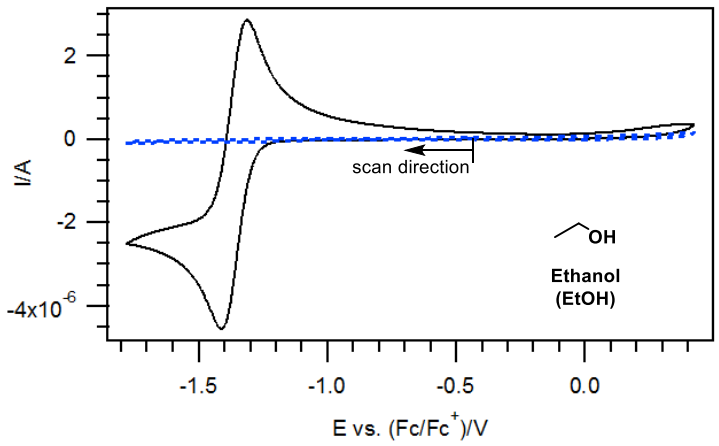

Figure A6.2. (- - -) Cyclic voltammogram of 500 mM Ethanol in dry, argon saturated DMF containing 0.1 M Bu_4NPF_6, recorded using a 1-mm diameter planar GC disk electrode and a scan rate of 0.1 V s^{-1}. (—) Overlay of the voltammogram collected for the one-electron reduction of O_2 for comparison.

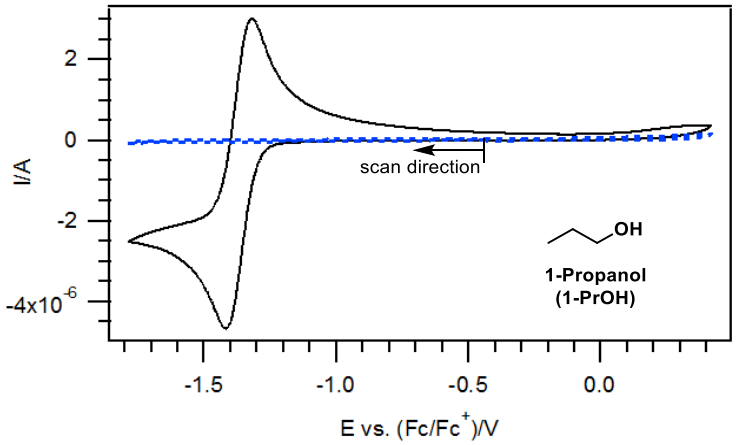

Figure A6.3. (- - -) Cyclic voltammogram of 500 mM 1-Propanol in dry, argon saturated DMF containing 0.1 M Bu_4NPF_6, recorded using a 1-mm diameter planar GC disk electrode and a scan rate of 0.1 V s^{-1}. (—) Overlay of the voltammogram collected for the one-electron reduction of O_2 for comparison.

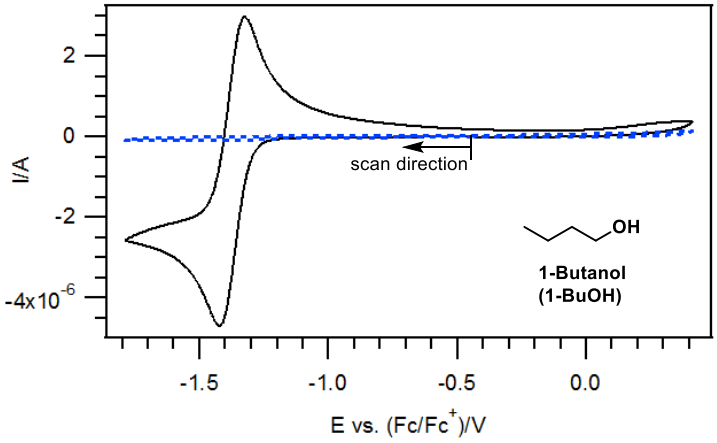

Figure A6.4. (- - -) Cyclic voltammogram of 500 mM 1-Butanol in dry, argon saturated DMF containing 0.1 M Bu_4NPF_6, recorded using a 1-mm diameter planar GC disk electrode and a scan rate of 0.1 V s^{-1}. (—) Overlay of the voltammogram collected for the one-electron reduction of O_2 for comparison.

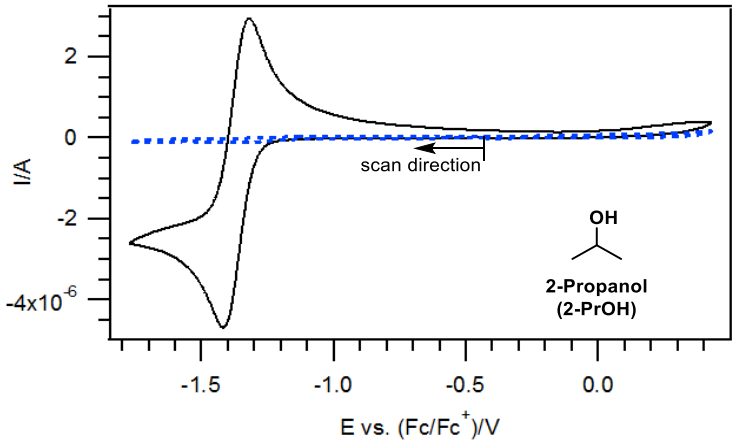

Figure A6.5. (- - -) Cyclic voltammogram of 500 mM 2-Propanol in dry, argon saturated DMF containing 0.1 M Bu_4NPF_6, recorded using a 1-mm diameter planar GC disk electrode and a scan rate of 0.1 V s^{-1}. (—) Overlay of the voltammogram collected for the one-electron reduction of O_2 for comparison.

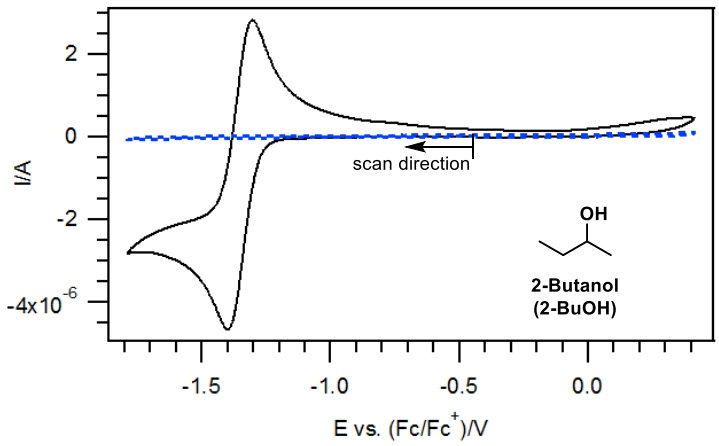

Figure A6.6. (- - -) Cyclic voltammogram of 500 mM 2-Butanol in dry, argon saturated DMF containing 0.1 M Bu_4NPF_6, recorded using a 1-mm diameter planar GC disk electrode and a scan rate of 0.1 V s^{-1}. (—) Overlay of the voltammogram collected for the one-electron reduction of O_2 for comparison.

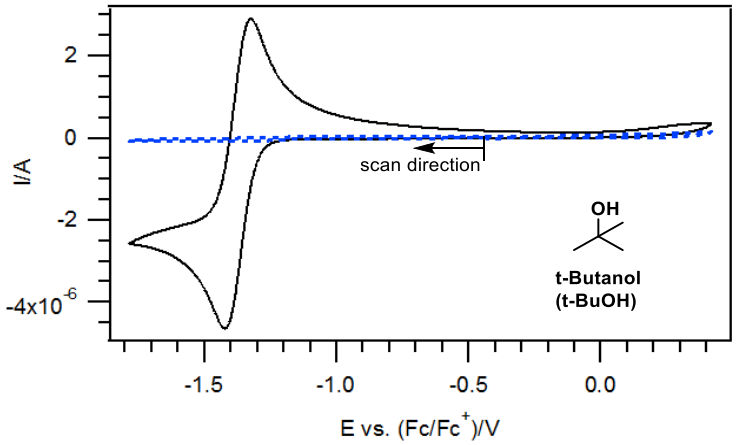

Figure A6.7. (- - -) Cyclic voltammogram of 500 mM t-Butanol in dry, argon saturated DMF containing 0.1 M Bu_4NPF_6, recorded using a 1-mm diameter planar GC disk electrode and a scan rate of 0.1 V s^{-1}. (—) Overlay of the voltammogram collected for the one-electron reduction of O_2 for comparison.

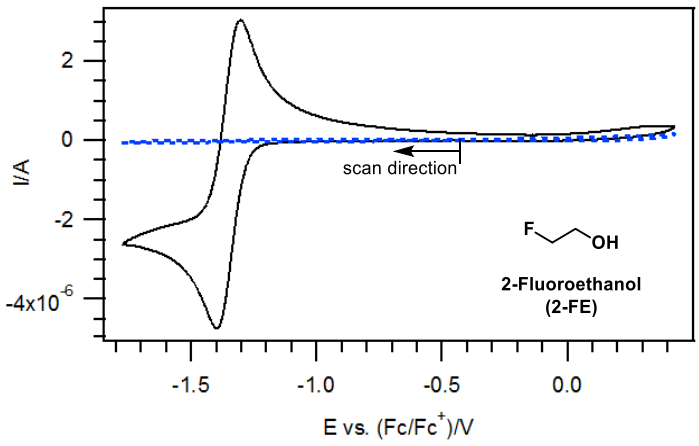

Figure A6.8. (- - -) Cyclic voltammogram of 5 mM 2-Fluoroethanol in dry, argon saturated DMF containing 0.1 M Bu_4NPF_6, recorded using a 1-mm diameter planar GC disk electrode and a scan rate of 0.1 V s^{-1}. (—) Overlay of the voltammogram collected for the one-electron reduction of O_2 for comparison.

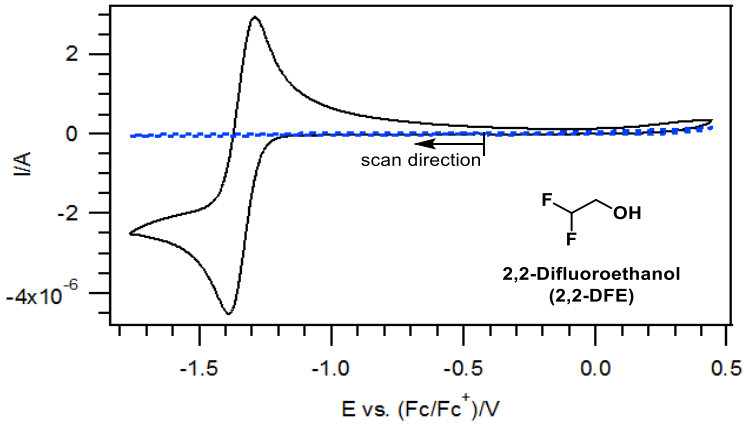

Figure A6.9. (- - -) Cyclic voltammogram of 5 mM 2,2-Difluoroethanol in dry, argon saturated DMF containing 0.1 M Bu_4NPF_6, recorded using a 1-mm diameter planar GC disk electrode and a scan rate of 0.1 V s^{-1}. (—) Overlay of the voltammogram collected for the one-electron reduction of O_2 for comparison.

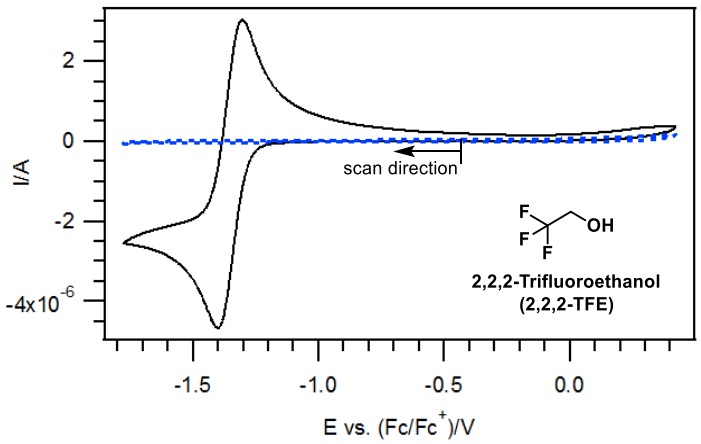

Figure A6.10. (- - -) Cyclic voltammogram of 5 mM 2,2,2-Trifluoroethanol in dry, argon saturated DMF containing 0.1 M Bu_4NPF_6, recorded using a 1-mm diameter planar GC disk electrode and a scan rate of 0.1 V s^{-1}. (—) Overlay of the voltammogram collected for the one-electron reduction of O_2 for comparison.

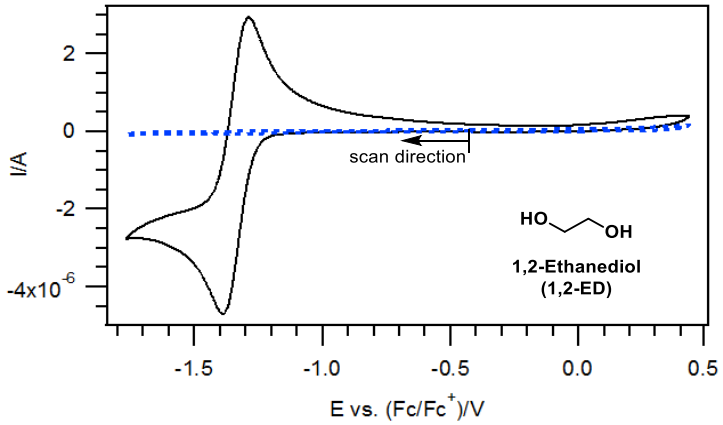

Figure A6.11. (- - -) Cyclic voltammogram of 500 mM 1,2-Ethanediol in dry, argon saturated DMF containing 0.1 M Bu_4NPF_6, recorded using a 1-mm diameter planar GC disk electrode and a scan rate of 0.1 V s^{-1}. (—) Overlay of the voltammogram collected for the one-electron reduction of O_2 for comparison.

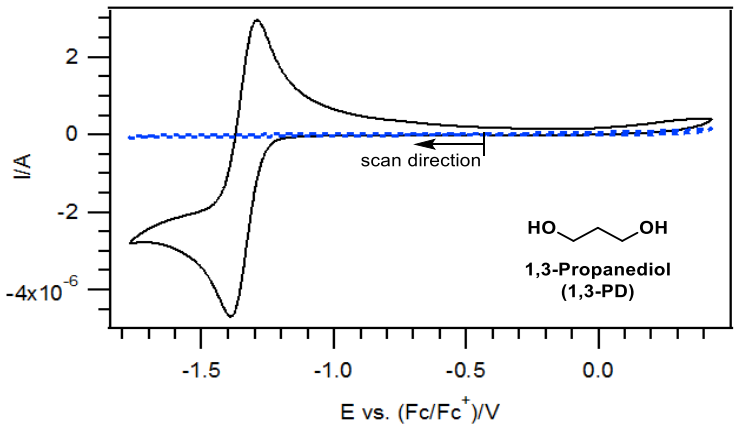

Figure A6.12. (- - -) Cyclic voltammogram of 500 mM 1,3-Propanediol in dry, argon saturated DMF containing 0.1 M Bu_4NPF_6, recorded using a 1-mm diameter planar GC disk electrode and a scan rate of 0.1 V s^{-1}. (—) Overlay of the voltammogram collected for the one-electron reduction of O_2 for comparison.

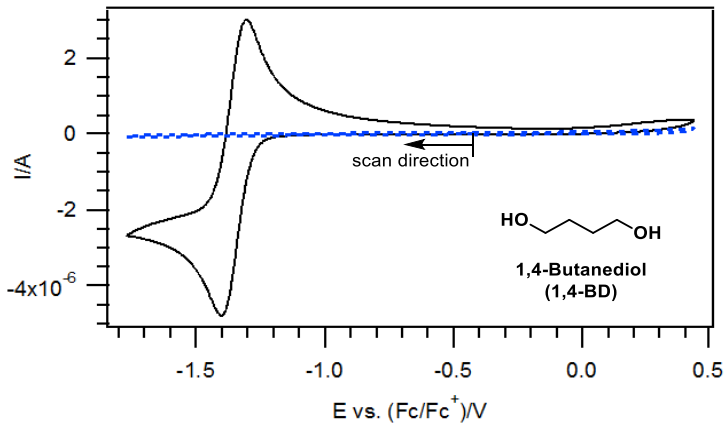

Figure A6.13. (- - -) Cyclic voltammogram of 500 mM 1,4-Butanediol in dry, argon saturated DMF containing 0.1 M Bu_4NPF_6, recorded using a 1-mm diameter planar GC disk electrode and a scan rate of 0.1 V s^{-1}. (—) Overlay of the voltammogram collected for the one-electron reduction of O_2 for comparison.

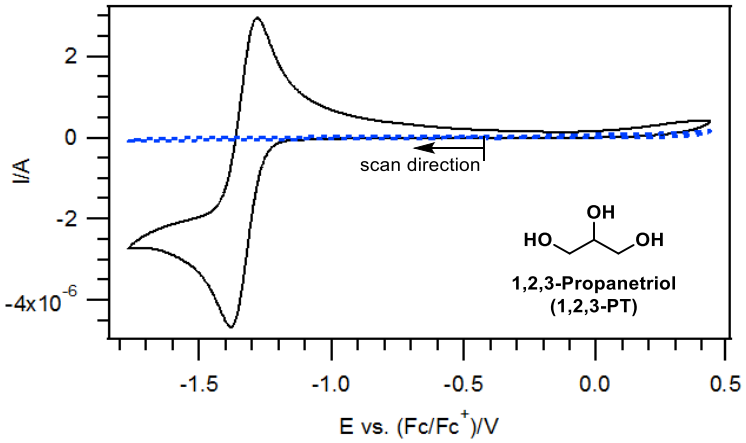

Figure A6.14. (- - -) Cyclic voltammogram of 500 mM 1,2,3-Propanetriol in dry, argon saturated DMF containing 0.1 M Bu_4NPF_6, recorded using a 1-mm diameter planar GC disk electrode and a scan rate of 0.1 V s^{-1}. (—) Overlay of the voltammogram collected for the one-electron reduction of O_2 for comparison.

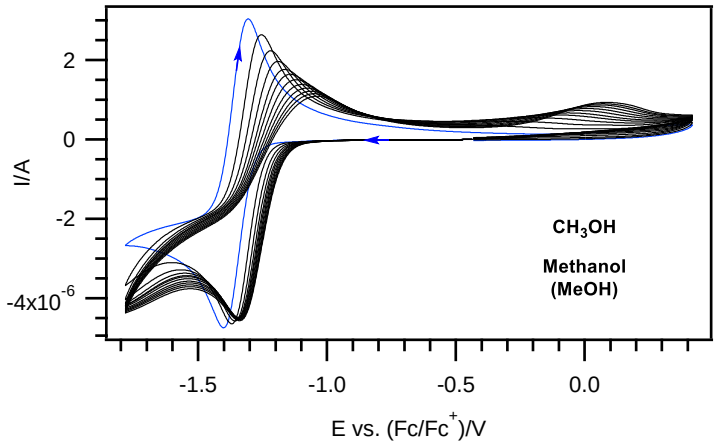

Figure A6.15. Cyclic voltammograms of the one-electron reduction of O_2 in dry, air saturated DMF containing 0.1 M Bu_4NPF_6, recorded using a 1-mm diameter planar GC disk electrode, a scan rate of 0.1 V s^{-1}, and at increasing concentrations of Methanol. (—) No alcohol added. (—) Increasing concentrations of Methanol added.

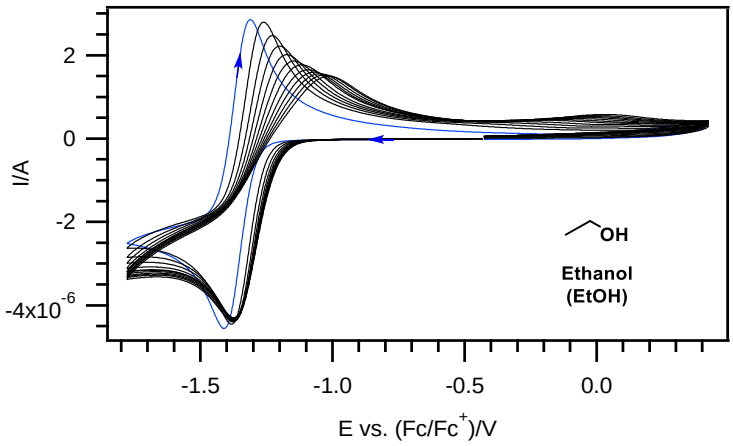

Figure A6.16. Cyclic voltammograms of the one-electron reduction of O_2 in dry, air saturated DMF containing 0.1 M Bu_4NPF_6, recorded using a 1-mm diameter planar GC disk electrode, a scan rate of 0.1 V s^{-1}, and at increasing concentrations of Ethanol. (—) No alcohol added. (—) Increasing concentrations of Ethanol added.

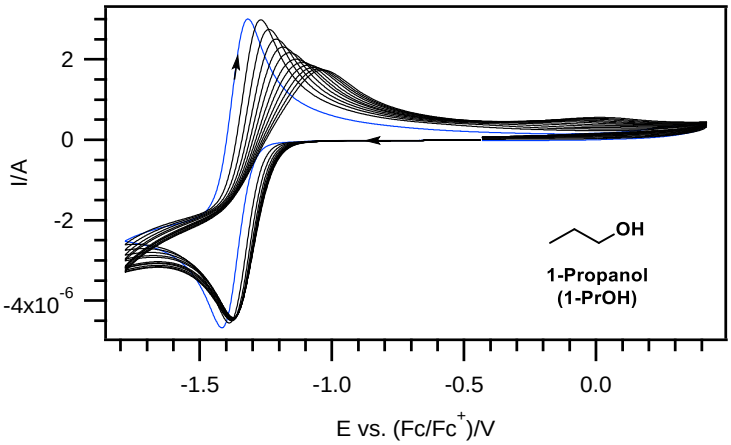

Figure A6.17. Cyclic voltammograms of the one-electron reduction of O_2 in dry, air saturated DMF containing 0.1 M Bu_4NPF_6, recorded using a 1-mm diameter planar GC disk electrode, a scan rate of 0.1 V s^{-1}, and at increasing concentrations of 1-Propanol. (—) No alcohol added. (—) Increasing concentrations of 1-Propanol added.

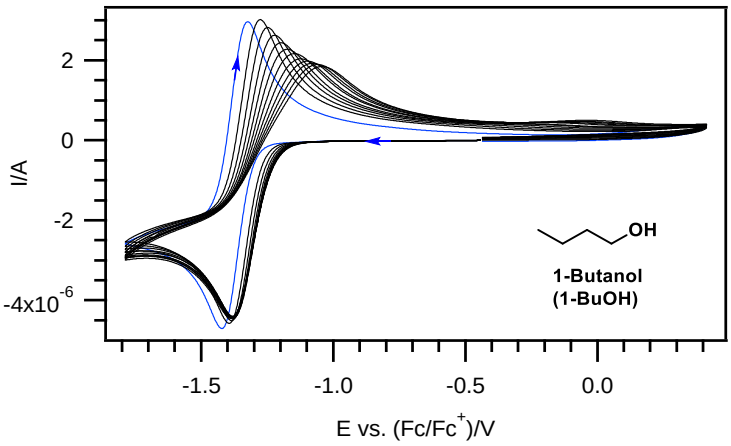

Figure A6.18. Cyclic voltammograms of the one-electron reduction of O_2 in dry, air saturated DMF containing 0.1 M Bu_4NPF_6, recorded using a 1-mm diameter planar GC disk electrode, a scan rate of 0.1 V s^{-1}, and at increasing concentrations of 1-Butanol. (—) No alcohol added. (—) Increasing concentrations of 1-Butanol added.

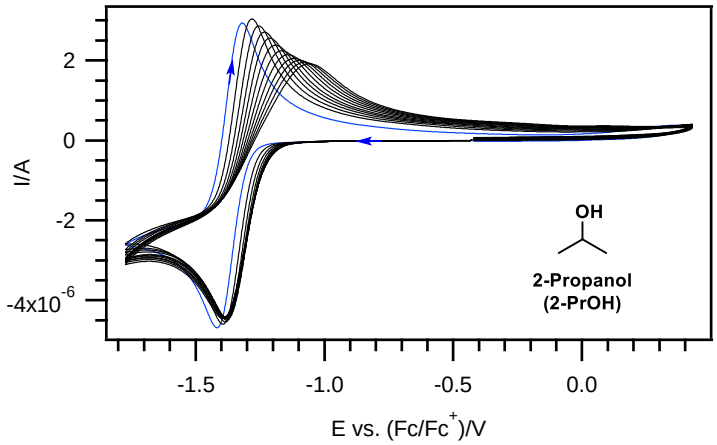

Figure A6.19. Cyclic voltammograms of the one-electron reduction of O_2 in dry, air saturated DMF containing 0.1 M Bu_4NPF_6, recorded using a 1-mm diameter planar GC disk electrode, a scan rate of 0.1 V s^{-1}, and at increasing concentrations of 2-Propanol. (—) No alcohol added. (—) Increasing concentrations of 2-Propanol added.

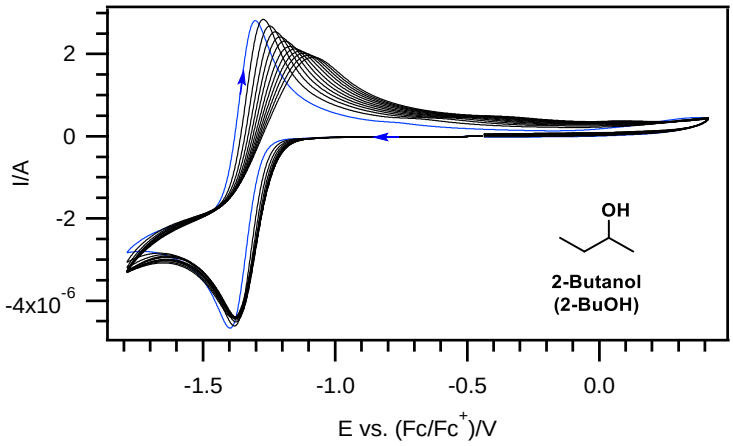

Figure A6.20. Cyclic voltammograms of the one-electron reduction of O_2 in dry, air saturated DMF containing 0.1 M Bu_4NPF_6, recorded using a 1-mm diameter planar GC disk electrode, a scan rate of 0.1 V s^{-1}, and at increasing concentrations of 2-Butanol. (—) No alcohol added. (—) Increasing concentrations of 2-Butanol added.

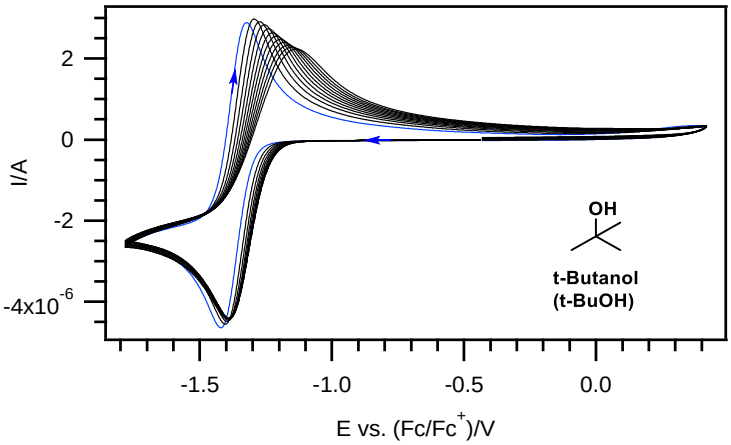

Figure A6.21. Cyclic voltammograms of the one-electron reduction of O_2 in dry, air saturated DMF containing 0.1 M Bu_4NPF_6, recorded using a 1-mm diameter planar GC disk electrode, a scan rate of 0.1 V s^{-1}, and at increasing concentrations of t-Butanol. (—) No alcohol added. (—) Increasing concentrations of t-Butanol added.

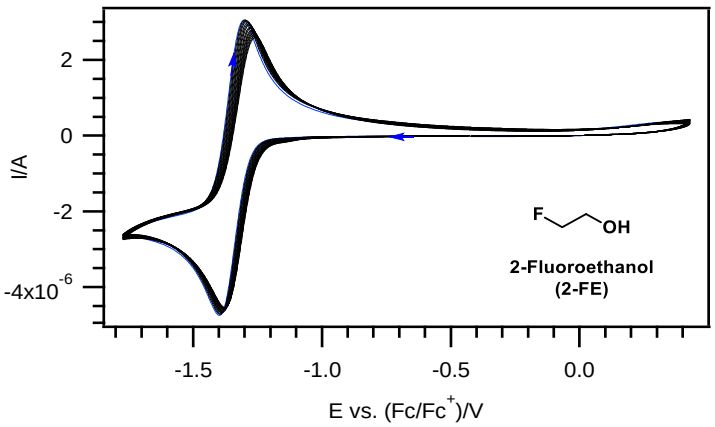

Figure A6.22. Cyclic voltammograms of the one-electron reduction of O_2 in dry, air saturated DMF containing 0.1 M Bu_4NPF_6, recorded using a 1-mm diameter planar GC disk electrode, a scan rate of 0.1 V s^{-1}, and at increasing concentrations of 2-Fluoroethanol. (—) No alcohol added. (—) Increasing concentrations of 2-Fluoroethanol added.

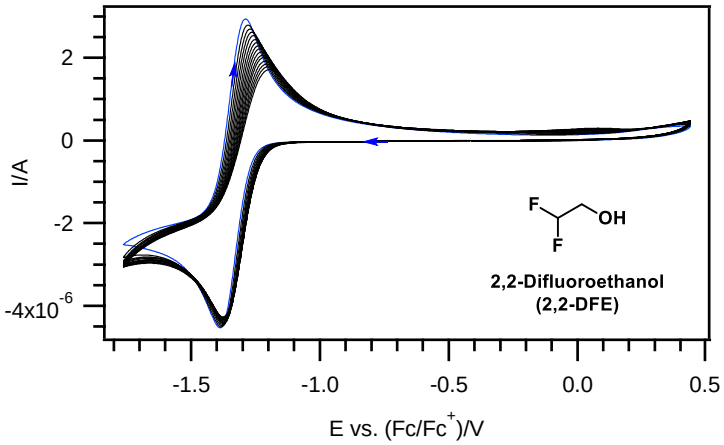

Figure A6.23. Cyclic voltammograms of the one-electron reduction of O_2 in dry, air saturated DMF containing 0.1 M Bu_4NPF_6, recorded using a 1-mm diameter planar GC disk electrode, a scan rate of 0.1 V s^{-1}, and at increasing concentrations of 2,2-Difluoroethanol. (—) No alcohol added. (—) Increasing concentrations of 2,2-Difluoroethanol added.

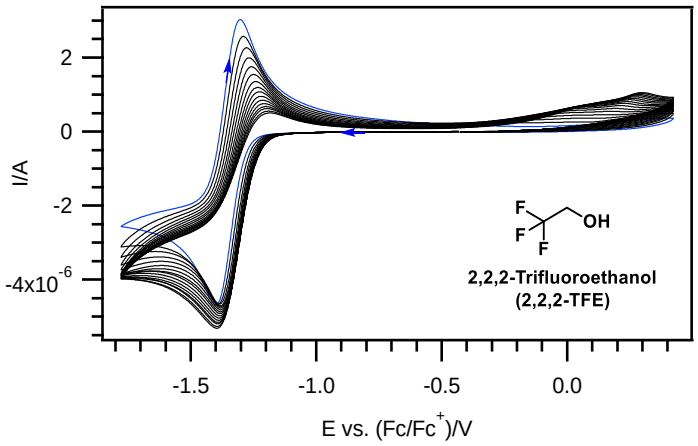

Figure A6.24. Cyclic voltammograms of the one-electron reduction of O_2 in dry, air saturated DMF containing 0.1 M Bu_4NPF_6, recorded using a 1-mm diameter planar GC disk electrode, a scan rate of 0.1 V s^{-1}, and at increasing concentrations of 2,2,2-Trifluoroethanol. (—) No alcohol added. (—) Increasing concentrations of 2,2,2-Trifluoroethanol added.

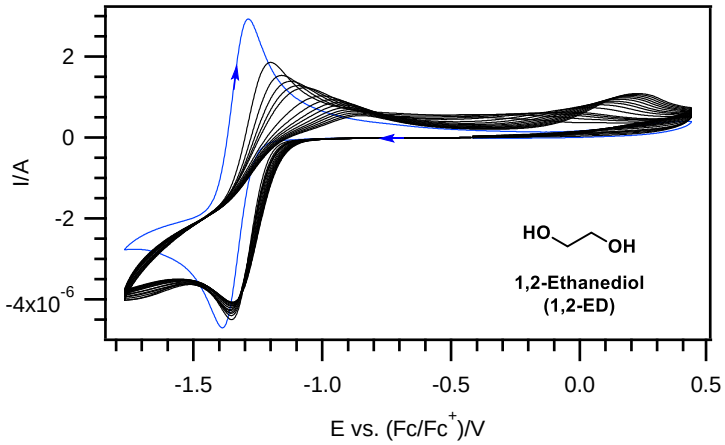

Figure A6.25. Cyclic voltammograms of the one-electron reduction of O_2 in dry, air saturated DMF containing 0.1 M Bu_4NPF_6, recorded using a 1-mm diameter planar GC disk electrode, a scan rate of 0.1 V s^{-1}, and at increasing concentrations of 1,2-Ethanediol. (—) No alcohol added. (—) Increasing concentrations of 1,2-Ethanediol added.

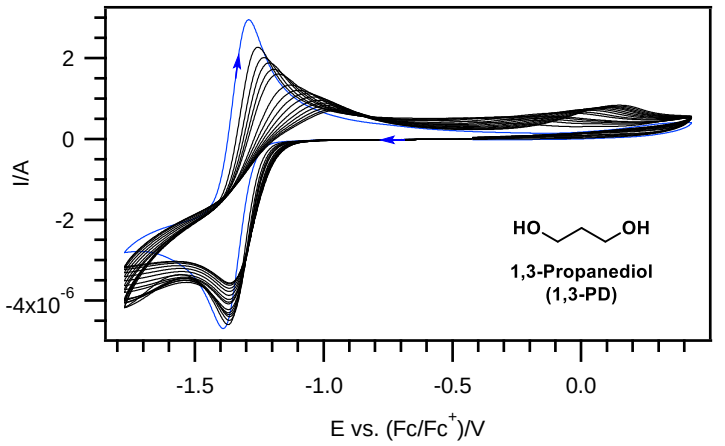

Figure A6.26. Cyclic voltammograms of the one-electron reduction of O_2 in dry, air saturated DMF containing 0.1 M Bu_4NPF_6, recorded using a 1-mm diameter planar GC disk electrode, a scan rate of 0.1 V s^{-1}, and at increasing concentrations of 1,3-Propanediol. (—) No alcohol added. (—) Increasing concentrations of 1,3-Propanediol added.

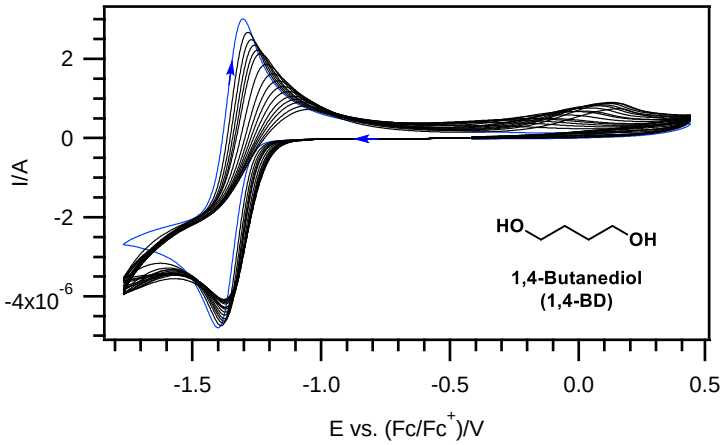

Figure A6.27. Cyclic voltammograms of the one-electron reduction of O_2 in dry, air saturated DMF containing 0.1 M Bu_4NPF_6, recorded using a 1-mm diameter planar GC disk electrode, a scan rate of 0.1 V s^{-1}, and at increasing concentrations of 1,4-Butanediol. (—) No alcohol added. (—) Increasing concentrations of 1,4-Butanediol added.

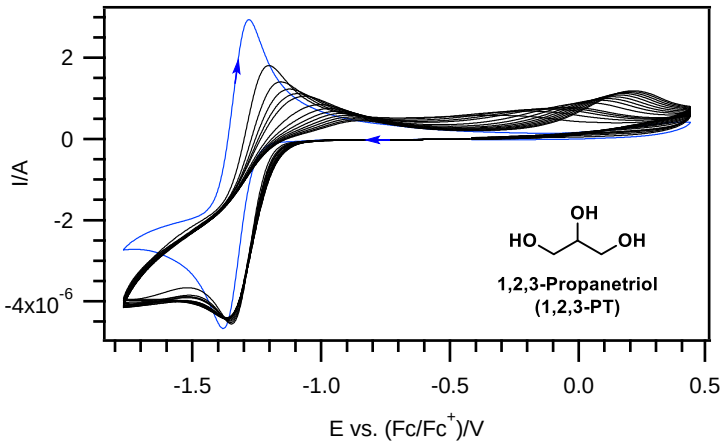

Figure A6.28. Cyclic voltammograms of the one-electron reduction of O_2 in dry, air saturated DMF containing 0.1 M Bu_4NPF_6, recorded using a 1-mm diameter planar GC disk electrode, a scan rate of 0.1 V s^{-1}, and at increasing concentrations of 1,2,3-Propanetriol. (—) No alcohol added. (—) Increasing concentrations of 1,2,3-Propanetriol added.

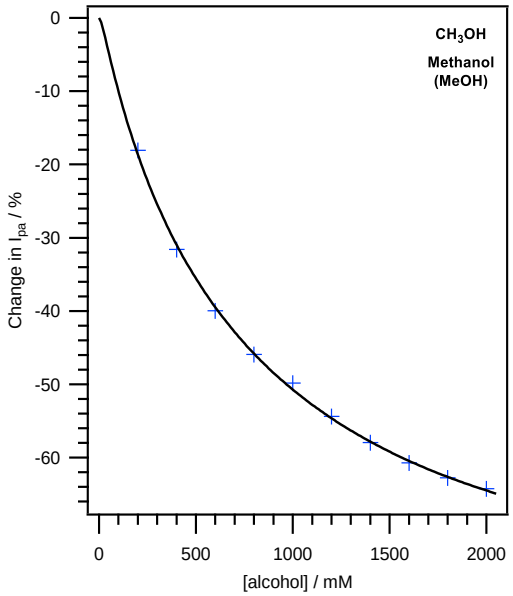

Figure A6.29. Plot of percentage change in the reverse anodic peak currents of O_2 reduction against the concentration of Methanol added.

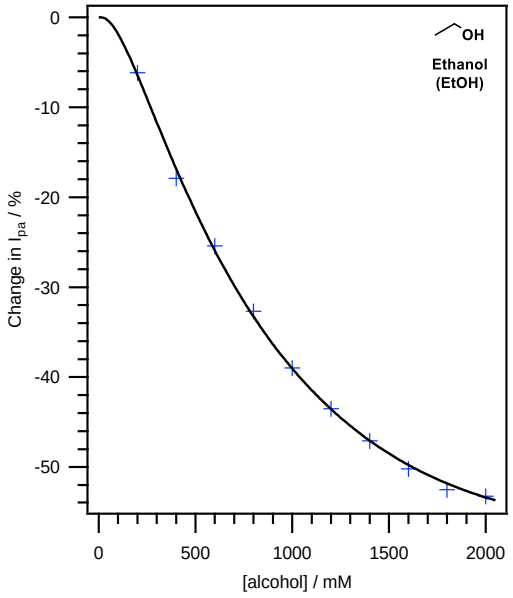

Figure A6.30. Plot of percentage change in the reverse anodic peak currents of O_2 reduction against the concentration of Ethanol added.

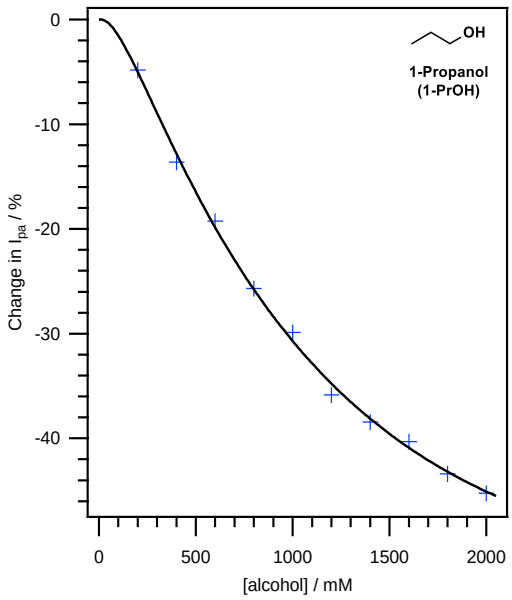

Figure A6.31. Plot of percentage change in the reverse anodic peak currents of O_2 reduction against the concentration of 1-Propanol added.

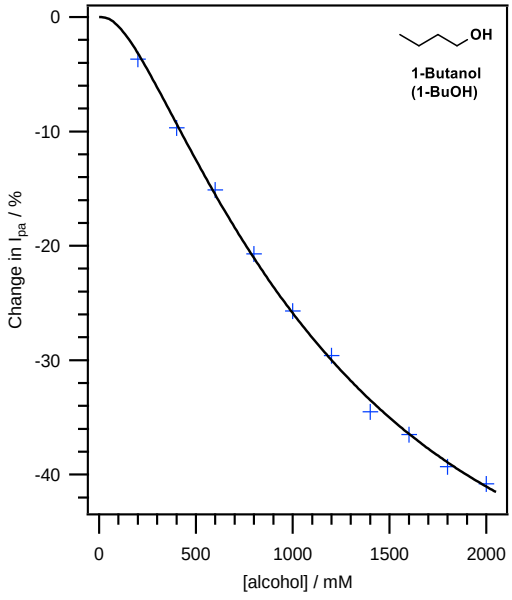

Figure A6.32. Plot of percentage change in the reverse anodic peak currents of O_2 reduction against the concentration of 1-Butanol added.

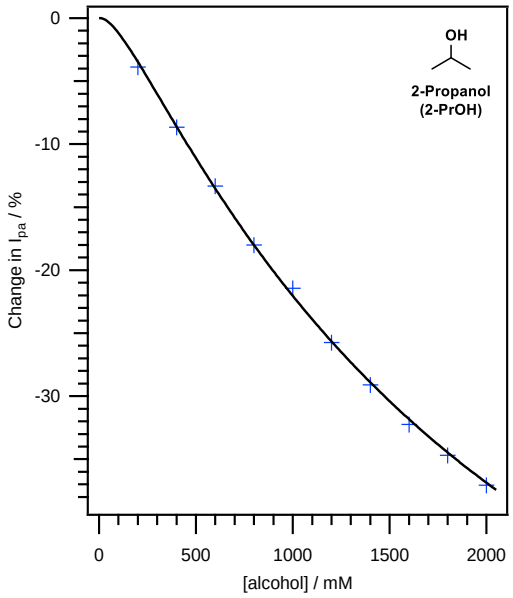

Figure A6.33. Plot of percentage change in the reverse anodic peak currents of O_2 reduction against the concentration of 2-Propanol added.

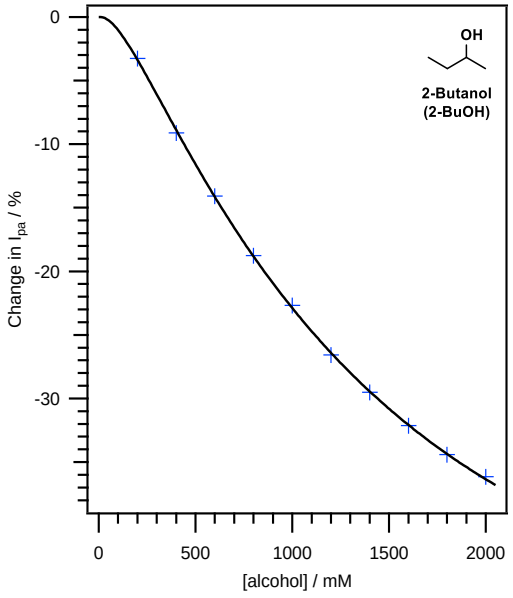

Figure A6.34. Plot of percentage change in the reverse anodic peak currents of O_2 reduction against the concentration of 2-Butanol added.

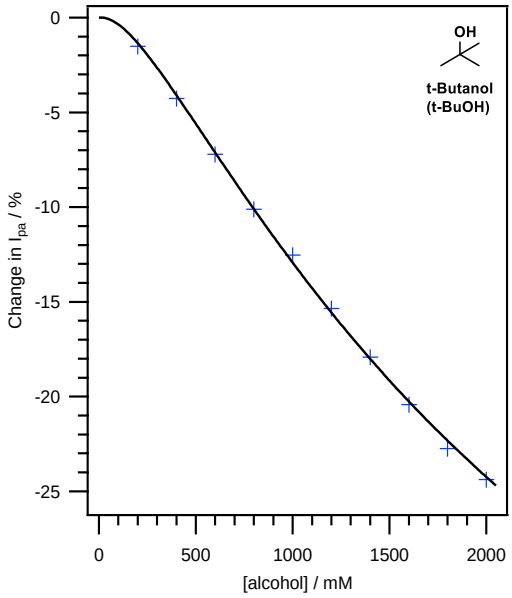

Figure A6.35. Plot of percentage change in the reverse anodic peak currents of O_2 reduction against the concentration of t-Butanol added.

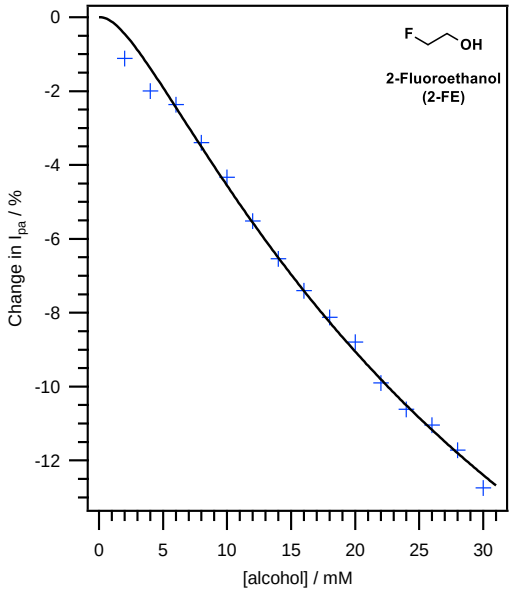

Figure A6.36. Plot of percentage change in the reverse anodic peak currents of O_2 reduction against the concentration of 2-Fluoroethanol added.

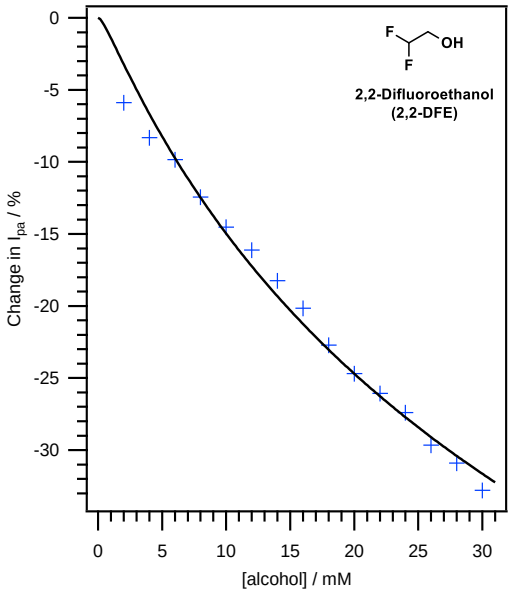

Figure A6.37. Plot of percentage change in the reverse anodic peak currents of O_2 reduction against the concentration of 2,2-Difluoroethanol added.

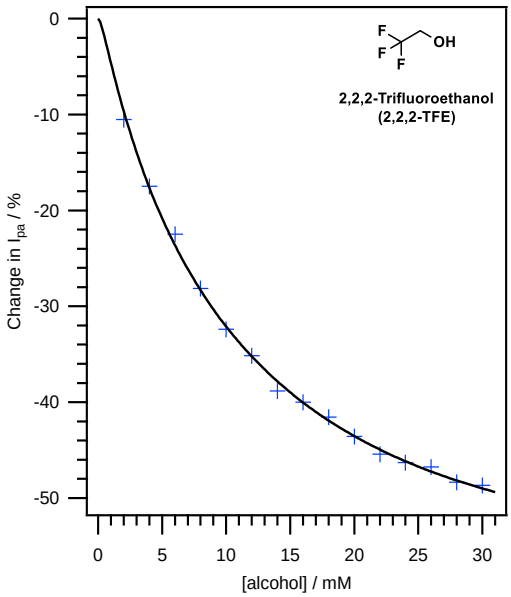

Figure A6.38. Plot of percentage change in the reverse anodic peak currents of O_2 reduction against the concentration of 2,2,2-Trifluoroethanol added.

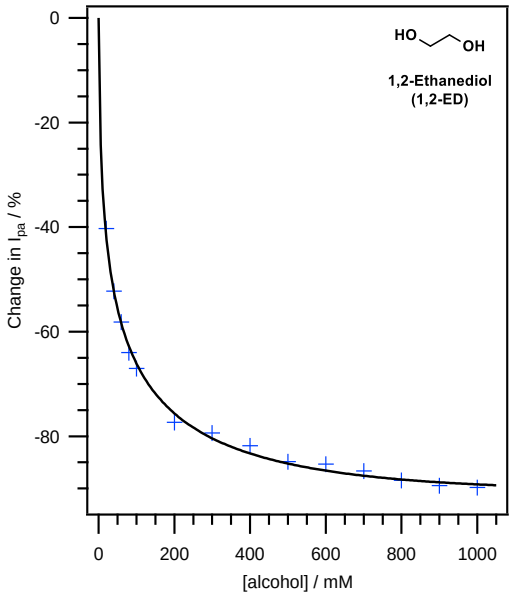

Figure A6.39. Plot of percentage change in the reverse anodic peak currents of O_2 reduction against the concentration of 1,2-Ethanediol added.

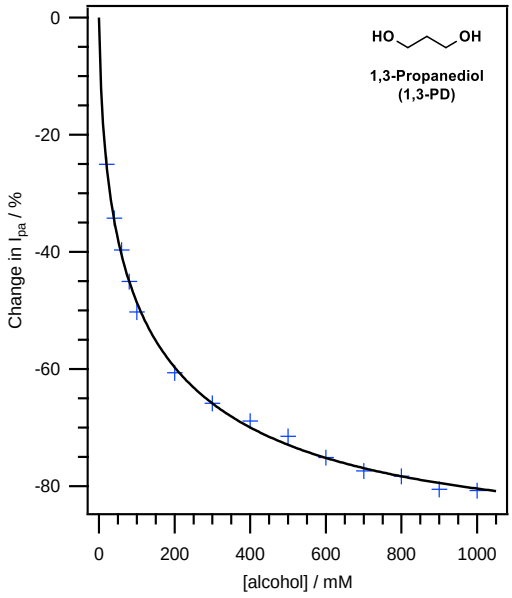

Figure A6.40. Plot of percentage change in the reverse anodic peak currents of O_2 reduction against the concentration of 1,3-Propanediol added.

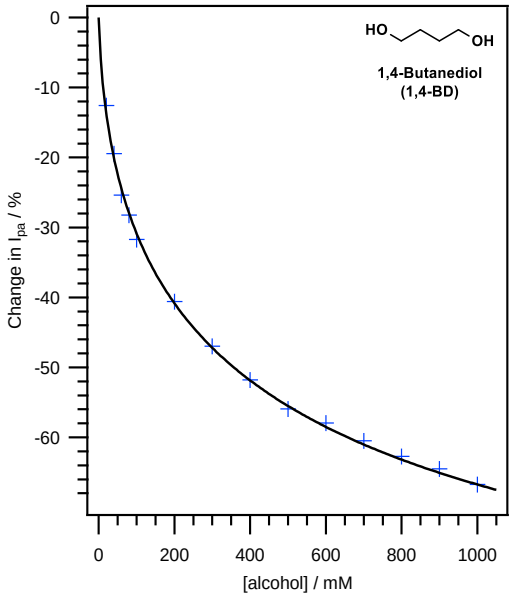

Figure A6.41. Plot of percentage change in the reverse anodic peak currents of O_2 reduction against the concentration of 1,4-Butanediol added.

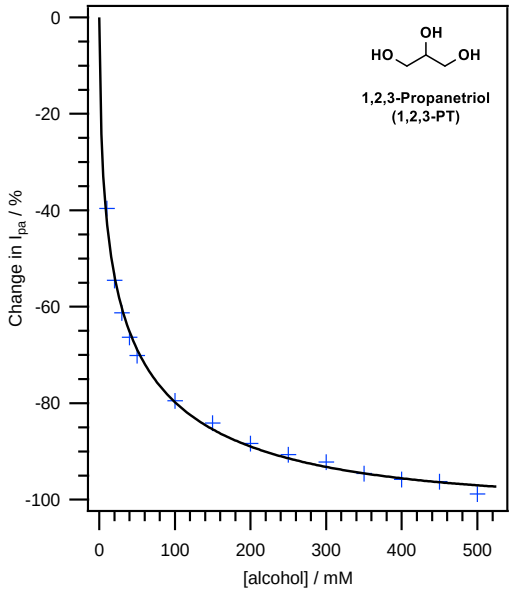

Figure A6.42. Plot of percentage change in the reverse anodic peak currents of O_2 reduction against the concentration of 1,2,3-Propanetriol added.

End of Thesis